VNiVERSiDAD D SALAMANCA

CAMPUS DE EXCELENCIA INTERNACIONAL

DEPARTAMENTO DE INGENIERÍA CARTOGRÁFICA Y DEL TERRENO

TESIS DOCTORAL

DESARROLLO DE METODOLOGÍAS MULTIDISCIPLINARES PARA LA GENERACIÓN DE MODELOS NUMÉRICOS EN PUENTES HISTÓRICOS DE ARCO

Álvaro Bautista De Castro

2019

Departamento de Ingeniería Cartográfica y del Terreno
Escuela Politécnica Superior de Ávila
Universidad de Salamanca

Autor:
Álvaro Bautista De Castro

Directores:

Dr. Luis Javier Sánchez Aparicio
Dr. Diego González Aguilera

2019

Título

Desarrollo de metodologías multidisciplinares para la generación de modelos numéricos en puentes históricos de arco

Programa de Doctorado:

Geotecnologías aplicadas a la Construcción, Energía e Industria (artículo 6 del R.D. 99/2011 de 28 de enero)

Universidad de Salamanca

LISTADO DE ARTÍCULOS PUBLICADOS

La presente Tesis Doctoral está compuesta por un compendio de tres artículos científicos que han sido publicados en revistas científicas internacionales con alto factor de impacto. A continuación, se exponen los mismos:

1. INTEGRATING GEOMATIC APPROACHES, OPERATIONAL MODALANALYSIS, ADVANCED NUMERICAL AND UPDATING METHODS TO EVALUATE THE CURRENT SAFETY CONDITIONS OF THE HISTORICAL BÔCO BRIDGE

Álvaro Bautista-De Castro[1], Luis Javier Sánchez-Aparicio[1*], Luís F. Ramos[2], José Sena-Cruz[2], Diego González-Aguilera[1]

[1]Departamento de Ingeniería Cartográfica y del Terreno. Universidad de Salamanca, Escuela Politécnica Superior de Ávila, C/ Hornos Caleros, 50, 05003, Ávila (Spain), alvarobautistadecastro@usal.es, luisj@usal.es, daguilera@usal.es Tlf: +34 920353500

[2]ISISE, Department of Civil Engineering, University of Minho, Campus de Azurém, 4800-058 Guimarães, Portugal; lramos@civil.uminho.pt, jsena@civil.uminho.pt

Construction and building materials, 2018

DOI: *https://doi.org/10.1016/j.conbuildmat.2017.10.084*

2. NON-DESTRUCTIVE MEANS AND METHODS FOR STRUCTURAL DIAGNOSIS OF MASONRY ARCH BRIDGES

Luis Javier Sánchez-Aparicio[1*], Álvaro Bautista-De Castro[1], Borja Conde-Carnero[2], Pedro Carrasco-García[1], Luís F. Ramos[3], Diego González-Aguilera[1]

[1]Departamento de Ingeniería Cartográfica y del Terreno. Universidad de Salamanca, Escuela Politécnica Superior de Ávila, C/ Hornos Caleros, 50, 05003, Ávila (Spain), alvarobautistadecastro@usal.es, luisj@usal.es, daguilera@usal.es Tlf: +34 920353500

[2]Departamento de Ingeniería de Materiales. Universidad de Vigo, Escuela de Ingeniería Industrial, Mecánica Aplicada y Construcción, Vigo (Spain); bconde@uvigo.es

[3]ISISE, Department of Civil Engineering, University of Minho, Campus de Azurém, 4800-058 Guimarães, Portugal; lramos@civil.uminho.pt.

Automation in Construction, 2019

DOI: *https://doi.org/10.1016/j.autcon.2019.04.021*

3. A MULTIDISCIPLINARY APPROACH TO CALIBRATE ADVANCED NUMERICAL SIMULATIONS OF MASONRY ARCH BRIDGES

Álvaro Bautista-De Castro[1], Luis Javier Sánchez-Aparicio[1*], Pedro Carrasco-García[1], Luís F. Ramos[2], Diego González-Aguilera[1]

[1]Departamento de Ingeniería Cartográfica y del Terreno. Universidad de Salamanca, Escuela Politécnica Superior de Ávila, C/ Hornos Caleros, 50, 05003, Ávila (Spain),

alvarobautistadecastro@usal.es, luisj@usal.es, daguilera@usal.es Tlf: +34 920353500

[2]ISISE, Department of Civil Engineering, University of Minho, Campus de Azurém, 4800-058 Guimarães, Portugal; lramos@civil.uminho.pt.

Mechanical Systems and Signal Processing, 2019

DOI: *https://doi.org/10.1016/j.ymssp.2019.04.043*

DEPARTAMENTO DE INGENIERÍA CARTOGRÁFICA Y DEL TERRENO

Hornos Caleros, nº 50 - Ávila

Tel. (34) 920 35 35 00 Fax. (34) 920 35 35 05 ict@usal.es

INFORME DE LA TESIS DOCTORAL

"Desarrollo de metodologías multidisciplinares para la generación de modelos numéricos en puentes históricos de arco"

La presente Tesis Doctoral elaborada por compendio de artículos por el Doctorando D. Álvaro Bautista De Castro reúne todas las condiciones exigidas por la Universidad de Salamanca. Los artículos presentados en este documento se adaptan de forma óptima a dichas condiciones, validando así las metodologías, resultados y conclusiones.

Como resultado de la actividad investigadora desarrollada por el Doctorando durante el periodo de realización de la Tesis Doctoral, estos artículos científicos han sido publicados en revistas internacionales de alta reputación que están indexadas en el Journal Citation Report (JCR) y pertenecen, además, al primer decil de su categoría: (i) construcción (*Construction and Building Materials Journal*); (ii) tecnologías de información en diseño e ingeniería, tecnologías de construcción, y mantenimiento y gestión de instalaciones construidas (*Automation in Construction Journal*); y (iii) técnicas de detección, instrumentación, procesamiento de señales, modelado y control de sistemas dinámicos (*Mechanical Systems and Signal Processing Journal*).

A continuación, se detalla el orden de publicación de cada uno ellos:

- La publicación: *Integrating geomatic approaches, operational modal analysis, advanced numerical and updating methods to evaluate the current safety conditions of the historical Bôco bridge*. Publicada en la revista *Construction and Building Materials Journal***,** indexada en el JCR y situada en el Q1 (primer cuartil y primer decil) de la categoría *engineering, civil*. Además, actualmente ocupa el puesto 11 de 128 revistas.
  DOI: *https://doi.org/10.1016/j.conbuildmat.2017.10.084*

- El trabajo publicado: *Non-destructive means and methods for structural diagnosis of masonry arch bridges*. Publicado en la revista *Automation in Construction Journal*, indexada en el JCR donde ocupa el primer cuartil y decil de la categoría *engineering, civil,* estando situada en el puesto 6 de 128 revistas.

DOI: *https://doi.org/10.1016/j.autcon.2019.04.021*

- El artículo publicado: *A multidisciplinary approach to calibrate advanced numerical simulations of masonry arch bridges*. Publicado en la revista *Mechanical Systems and Signal Processing Journal,* indexada en el JCR y colocada en el primer cuartil y decil de la categoría *mechanical engineering*, donde en la actualidad ocupa el puesto 7 de 128 revistas.
  DOI: *https://doi.org/10.1016/j.ymssp.2019.04.043*

Los resultados obtenidos durante la realización de la Tesis Doctoral han demostrado importantes progresos en diferentes disciplinas de la ingeniería fuertemente vinculadas con la materia desarrollada: (i) aplicación de técnicas geomáticas, láser escáner terrestre, en la caracterización geométrica de puentes históricos de arco; (ii) desarrollo de metodologías para el paso de la nube de puntos a modelos geométricos aptos para el análisis numérico por el Método de los Elementos Finitos; (iii) empleo de técnicas geofísicas, el georradar y el Análisis Multicanal de Ondas Superficiales, en puentes de arco de mampostería para la caracterización geométrica y mecánica de su estructura interna y sus materiales de relleno; (iv) uso de técnicas basadas en el análisis de la propagación de las onda, impacto-eco y ensayos sónicos, para la caracterización geométrica y mecánica de los materiales constituyentes en los puentes de arco; (v) uso de técnicas dinámicas basadas en el Análisis Modal Operacional para la caracterización de las propiedades modales de puentes de arco históricos; (vi) empleo de simulaciones numéricas avanzadas, por el Método de los Elementos Finitos, para el análisis de seguridad de puentes históricos; y (v) desarrollo de protocolos óptimos de calibración y análisis sensible de modelos numéricos basados en metamodelos y superficies de respuesta (método Douglas-Reid)

Finalmente, la presente Tesis Doctoral termina con el correspondiente apartado de conclusiones, donde las principales contribuciones son expuestas de forma rigurosa y específica, representando un sólido cimiento para el desarrollo de nuevos trabajos de investigación.

Por todo lo anteriormente descrito, emitimos un informe con todos nuestros pronunciamientos favorables y autorizamos su presentación como Tesis Doctoral en el Departamento de Ingeniería Cartográfica y del Terreno de la Universidad de Salamanca.

En Ávila, a 14 de Mayo de 2019

Dr. Luis Javier Sánchez Aparicio Dr. Diego González Aguilera

AGRADECIMIENTOS

Al finalizar esta Tesis Doctoral se cumple uno de los objetivos más importantes de mi vida académica, el cual ha sido posible alcanzar gracias al apoyo de varias personas. A todas ellas que han contribuido a la realización de esta Tesis Doctoral, mi más sincero agradecimiento.

En primer lugar, en un ámbito más personal, quiero agradecer a mis padres el sacrificio que han hecho para poder proporcionarme esta formación y a mis hermanos por su apoyo incondicional durante estos años.

En segundo lugar, me gustaría agradecer a los directores de esta Tesis Doctoral, los doctores Diego González Aguilera y Luis Javier Sánchez Aparicio la confianza, el apoyo y el aprendizaje brindado a lo largo de estos años para poder alcanzar este objetivo importante.

Finalmente, debo agradecer también la colaboración prestada de los doctores Pedro Carrasco García de la Universidad de Salamanca, Luís F. Ramos de la Universidad de Minho (Portugal), José Sena Cruz de la Universidad de Minho (Portugal), y Borja Conde Carnero de la Universidad de Vigo, la cual ha hecho posible alcanzar los objetivos marcados en esta Tesis Doctoral.

RESUMEN

La generación de modelos numéricos avanzados de puentes históricos supone un gran desafío desde el punto de vista de las simulaciones numéricas para realizar diagnósticos estructurales precisos. Fundamentalmente, esto se debe por los siguientes aspectos: (i) la presencia de una gran variedad de patologías que definen su estado actual, destacando las fisuras, deformaciones y pérdidas materiales; (ii) las formas geométricas complejas e irregulares, tanto internas como externas que están presentes en la mayoría de ellos y que en ocasiones dificultan su accesibilidad; (iii) la variedad de materiales utilizados para su construcción; y (iv) la variedad de sus condiciones de contorno.

Teniendo en cuenta estos aspectos, para poder crear estos modelos numéricos avanzados de puentes históricos con gran precisión, es necesario desarrollar metodologías que permitan obtener simulaciones numéricas con resultados fiables para poder realizar un diagnóstico estructural preciso en estas construcciones.

Para lograr este objetivo, la presente Tesis Doctoral está enfocada en obtener modelos numéricos avanzados de puentes históricos mediante la combinación de métodos no destructivos, ensayos cuasi-no destructivos, el desarrollo de una metodología para crear modelos CAD posicionados en el sistema de coordenadas correcto y finalmente, el desarrollo de estrategias de modelización numérica que permiten obtener simulaciones con resultados fiables. Además, cabe destacar que la combinación de estos métodos no destructivos y ensayos cuasi-no destructivos permiten caracterizar puentes históricos a tres niveles: (i) a nivel geométrico; (ii) a nivel material; y (iii) a nivel estructural.

En una primera fase, se realizó un modelo CAD y dos modelos numéricos de un puente de arco histórico compuesto por dos capas de hormigón armado con el propósito de llevar a cabo un análisis de seguridad con respecto a su estado actual. Por una parte, para obtener el modelo CAD de este puente, su geometría externa fue caracterizada por medio del sensor geomático láser escáner terrestre, donde el eje longitudinal de la nube de puntos de este puente fue posicionado con el eje *x* del sistema de coordenadas global por medio de una metodología basada en el Análisis de Componentes Principales (PCA), permitiendo así integrar correctamente los diferentes datos capturados (por ejemplo, Ensayos de Vibración Ambiental-AVT). Por otra parte, fueron realizados ensayos cuasi-no destructivos para extraer muestras que se sometieron a ensayos de compresión para obtener las propiedades mecánicas y físicas de cada capa de hormigón. Además, para caracterizar este puente desde el punto de vista de su comportamiento estructural, se llevó a cabo una campaña experimental basada en ensayos de vibración ambiental (AVT) para obtener

las frecuencias, desplazamientos modales y coeficientes de amortiguamiento. Una vez caracterizado este puente a los tres niveles (geométrico, material y estructural), se generó un primer modelo numérico con un hormigón homogéneo equivalente a las dos capas de hormigón para realizar una simulación, desarrollando una estrategia de calibración con el fin de reducir discrepancias. Además, en este modelo numérico se llevó a cabo una evaluación basada en el criterio de Aseguramiento Modal de Coordenadas (COMAC) para identificar el origen de estas discrepancias. Con el propósito de reducir todavía más estas discrepancias, se creó un segundo modelo numérico, que al igual que el primer modelo, se realizó con un hormigón homogéneo equivalente, añadiéndole más parámetros que representan las zonas dañadas en el puente. Así, al igual que en el primer modelo, este segundo modelo fue calibrado con otra estrategia diferente con respecto al primer modelo, obteniendo discrepancias más pequeñas. Por lo tanto, este segundo modelo numérico fue utilizado para llevar a cabo un análisis de seguridad del puente, evaluando su Estado Límite Último (ULS) de acuerdo con las recomendaciones del Eurocódigo.

En una segunda fase, se propone un método multidisciplinar no destructivo aplicado a un puente de arco histórico que presenta una mezcla compleja de materiales: (i) una mampostería de granito gris; (ii) una mampostería de granito ocre; (iii) una capa de relleno de material cohesivo; (iv) una capa de relleno de material romano *opus caementicium*; y (v) hormigón armado. Este método multidisciplinar propuesto permite caracterizar este puente a los tres niveles: (i) a nivel geométrico mediante la integración del láser escáner terrestre para definir su geometría exterior y el uso del georradar combinado con ensayos de impacto-eco para definir su geometría interior; (ii) a nivel material mediante ensayos sónicos indirectos con el propósito de obtener los parámetros mecánicos de sus dos mamposterías y el uso del método de Análisis Multicanal de Ondas Superficiales (MASW) con el fin de caracterizar las propiedades mecánicas y físicas de sus materiales de relleno además de identificar los límites de las capas de estos materiales de relleno ; y (iii) a nivel estructural mediante AVT con el propósito de identificar las propiedades dinámicas de este puente. Además, todos los datos obtenidos de estas técnicas son combinados con una estrategia de modelado sólida basada en el análisis de componentes principales (PCA), superficies Lofts y operadores Booleanos capaz de crear un modelo CAD adecuado para llevar a cabo simulaciones numéricas. El modelo numérico generado de este modelo CAD es calibrado manualmente con el propósito de reducir discrepancias para realizar un análisis de seguridad del puente teniendo en cuenta el comportamiento no-lineal de las dos mamposterías y el pavimento.

Finalmente, en una tercera fase, se desarrolla un método multidisciplinar aplicado en un puente histórico de arco de mampostería. Esta metodología propuesta combina las siguientes técnicas no destructivas: (i) el láser escáner terrestre e ingeniería inversa para definir su geometría externa;

(ii) el georradar para caracterizar su geometría interna; (iii) el Análisis Multicanal de Ondas Superficiales (MASW) para caracterizar las propiedades mecánicas y físicas de sus materiales de relleno, así como la identificación de los límites de las capas que componen estos materiales de relleno; (iv) ensayos sónicos indirectos para obtener las propiedades mecánicas de su mampostería; (v) ensayos de impacto-eco para corroborar los espesores de sus paredes de mampostería obtenidos previamente con el georradar; y (vi) Ensayos de Vibración Ambiental (AVT) para obtener los parámetros modales de este puente (frecuencias, desplazamientos modales y coeficientes de amortiguamiento). Por lo tanto, estas técnicas no destructivas permitieron caracterizar este puente histórico de arco de mampostería a nivel geométrico, material y estructural. Además de estos métodos no destructivos, la metodología propuesta está complementada con el desarrollo de una estrategia basada en el análisis sensible global de metamodelos y un método robusto de calibración, con el fin reducir discrepancias entre las frecuencias y desplazamientos modales obtenidos de la simulación numérica con respecto a los resultados experimentales de los AVT realizados en el puente.

ABSTRACT

The generation of advanced numerical models of historical bridges supposes a great challenge from the point of view of numerical simulations to perform structural diagnosis. Fundamentally, this is due to the following aspects: (i) the presence of a great variety of pathologies that define their current state, highlighting cracks, deformations and material losses; (ii) irregular and complex shapes, both internal and external which are present in the most of them; (iii) variety of materials used for their construction and; (iv) variety of their boundary conditions.

Taking into account these aspects, to be able to create these advanced numerical models of historical bridges with high accuracy, is necessary to develop methodologies that allow to obtain numerical simulations with reliable results to be able to perform an accurate structural diagnostic in these constructions.

To achieve this aim, this Doctoral Thesis is focused on obtaining advanced numerical models of historical bridges through the combination of non-destructive methods, quasi-non-destructive tests, the development of a methodology to create positioned CAD models in the correct coordinate system and finally, the development of numerical modelling strategies that allow to obtain simulations with reliable results. Furthermore, it is worth highlighting that the combination of these non-destructive methods and quasi-non-destructive tests allow to characterize historical bridges at three levels: (i) at geometrical level; (ii) at material level and; (iii) at structural level.

In a first phase, a CAD model and two numerical models of a historical arch bridge composed by two layers of armored concrete were performed with the purpose of carrying out a safety analysis regarding its current state. On the one hand, to obtain the CAD model of this bridge, its external geometry was characterized by means of the geomatic sensor terrestrial laser scanner, where the longitudinal axis of the point cloud of this bridge was placed with the *x*-axis of the global coordinate system by means of a methodology based on the Principal Component Analysis (PCA), and thus to successfully integrate the different captured data (e .g. Ambient Vibration Tests-AVT). On the other hand, quasi-non-destructive tests were performed to extract samples that were submitted to compression efforts to obtain the mechanical and physical properties of each concrete layer. Furthermore, to characterize this bridge from the point of view of its structural behaviour, an experimental campaign based on ambient vibration tests (AVT) was carried out to obtain the frequencies, modal displacements and damping ratios. Once characterized this bridge to the three levels (geometrical, material and structural), a first model with a homogeneous concrete equivalent to the two concrete layers was generated to perform a simulation, developing a calibration strategy in order to reduce discrepancies. Furthermore, on

this numerical model it wascarried out an assessment based on the Coordinate Modal Assurance Criterion (COMAC) to identify the origin of these discrepancies. With the purpose of reducing even more these discrepancies, a second numerical model was created, that as the first model, it was performed with an equivalent homogeneous concrete, adding it more parameters that represent the damaged areas in the bridge. Thus, as in the first model, this second model was calibrated with other different strategy regarding the first model, obtaining lower discrepancies. Therefore, this second numerical model was used to carry out a safety analysis of the bridge, assessing its Ultimate Limit State (ULS) according with the Eurocode recommendations.

In a second phase, it is proposed a non-destructive multidisciplinary method applied to a historical arch bridge that presents a complex mixture of materials: (i) a masonry of grey granite; (ii) a masonry of ochre granite; (iii) an infill layer of cohesive material; (iv) an infill layer of roman material *opus caementicium* and; (v) armored concrete. This proposed multidisciplinary method allows to characterize this bridge to the three levels: (i) at geometrical level through the integration of the terrestrial laser scanner to define its external geometry and the use of the ground penetrating radar combined with impact-echo tests to define its internal geometry; (ii) at material level through indirect sonic tests with the purpose of obtaining the mechanical parameters of its two masonries and the use of the Multichannel Analysis of Surface Waves (MASW) method in order to characterize the mechanical and physical properties of its infill materials in addition to identify the limits of the layers of these infill materials and; (iii) at structural level through AVT with the purpose of identifying the dynamic properties of this bridge. Furthermore, all data obtained from these techniques are combined with a solid modelling strategy based on the principal component analysis (PCA), Lofts surfaces and Boolean operators able to create a suitable CAD model to carry out numerical simulations. The numerical model generated from this CAD model, is manually calibrated with the purpose of reducing discrepancies to perform a safety analysis taking into account the non-linear behaviour of the two masonries and the pavement.

Finally, in a third phase, a multidisciplinary method applied in a historical masonry arch bridge is developed. This proposed methodology combines the next non-destructive techniques: (i) the terrestrial laser scanner and reverse engineering to define its external geometry; (ii) the ground penetrating radar to characterize its internal geometry; (iii) the Multichannel Analysis of Surface Waves (MASW) to characterize the mechanical and physical properties of its infill materials as well as the identification of the limits of the layers that compose these infill materials; (iv) indirect sonic tests to obtain the mechanical properties of its masonry; (v) impact-echo tests to corroborate the thicknesses of its spandrel walls previously obtained with the ground penetrating radar and; (vi) Ambient Vibration Tests (AVT) to obtain the modal parameters of this bridge (frequencies, modal displacements and damping ratios). Therefore, these non-destructive techniques allowed

to characterize this historical masonry arch bridge at geometrical, material and structural level. Apart from these non-destructive methods, the proposed methodology is complemented with the development of a strategy based on the global sensitivity analysis of metamodels and a robust calibration method in order to reduce discrepancies between the frequencies and modal displacements obtained from the numerical simulation regarding the experimental results from the AVT performed in the bridge.

A mis padres y mis hermanos que me han dado todo su apoyo.

A mis abuelos que los tengo siempre presentes en mi memoria.

ÍNDICE

Contenido

CAPÍTULO I

INTRODUCCIÓN

La necesidad de conservar construcciones de nuestro legado histórico ha ido aumentando en los últimos años [1], al ser estas una parte fundamental de nuestra identidad como sociedad y una característica integral del entorno en el que vivimos [2, 3]. De ahí la preocupación de las Administraciones y organismos públicos y privados por la conservación de las mismas. Hecho que queda agravado por el elevado número de construcciones históricas de edad muy avanzada que requieren unos trabajos de mantenimiento, acondicionamiento, rehabilitación y reparación continuos.

De entre la gran variedad de tipologías existentes en la actualidad, desde grandes catedrales hasta pequeñas construcciones vernáculas, los puentes constituyen una pieza esencial, al permitir salvar accidentes geográficos, tales como ríos, cañones o valles, estando en la actualidad muchos de ellos en servicio [4, 5]. Asimismo, muchas de estas infraestructuras todavía desempeñan un papel importante dentro de las redes de comunicación y comercio entre diferentes lugares. Ejemplo de ello lo tenemos en Europa, donde el 40% de la infraestructura de su red ferroviaria queda constituida por puentes históricos con una edad superior a los 100 años [6, 7]. Además, se debe tener en cuenta que estas infraestructuras son unas de las construcciones más vulnerables, debido a que en la actualidad muchas de ellas están soportando condiciones de cargas más elevadas que las consideradas en su fase de diseño [8]. Sin olvidar, tampoco, la presencia de agentes de deterioro extrínsecos tales como los factores climáticos (temperaturas extremas, humedad del entorno, precipitaciones y viento), enraizamiento de árboles y arbustos, o acciones accidentales (e. g. seísmos) entre otros. Todo este conjunto de casuísticas promueve en estas infraestructuras la presencia de deformaciones, agrietamientos o incluso pérdidas de material a lo largo de su vida útil [9, 10].

En lo que respecta a la tipología, estas infraestructuras se pueden clasificar en cuatro clases principales [11]: (i) puentes atirantados, tales como el Viaducto de Millau (Francia) [12], el puente Quincy Bayview (Estados Unidos) [13], el puente Rande (España) o el puente del Centenario (España) [14]; (ii) puentes colgantes, tales como el puente Humber (Reino Unido) [15], el puente Golden Gate (Estados Unidos) [16] o el puente de Innoshima (Japón) [17]; (iii) puentes viga, tales como el puente del río Sororó (Brasil) [18] o el puente del río Sorraia (Portugal) [19]; y (iv) puentes de arco, tales como el puente de Monforte de Lemos (España) [20], el puente de Bibei (España) [4] o el puente de Alcántara [5].

De estas tipologías mencionadas previamente, cabe señalar los puentes de arco, cuyo uso se remonta a las civilizaciones etruscas y griegas. De hecho, el puente arco más antiguo del que se tiene constancia y que continúa hoy en día en servicio es el puente Arkadiko (Grecia), que data de alrededor del año 1300 a.C. [21]. Posteriormente, la civilización romana aportó mejoras en

esta clase de puentes, destacando principalmente en la mayoría de ellos el uso de bóvedas de cañón a base de arcos de medio punto. Además, muchos de estos puentes han sobrevivido hasta nuestros días, donde todavía siguen siendo operativos [4, 5]. Sin embargo, cuando el Imperio Romano desapareció, sus conocimientos para la construcción de estas antiguas infraestructuras se perdieron durante siglos. No obstante, en los siglos XI y XII, se produjeron cambios sociales y se incrementaron las actividades económicas, promoviendo así el retorno de este tipo de infraestructuras [22].

En cuanto a la variedad de materiales utilizados en su construcción, los puentes de arco más antiguos que actualmente siguen operativos están construidos con mampostería, datando la mayoría de ellos de las épocas romana y medieval (tales como el puente de Bibei, el puente de Cernadela o el puente de Traba) [4, 23, 24]. Técnica constructiva que continuó utilizándose hasta finales del siglo XVIII, época en la que las fundiciones tomaron parte del relevo en la construcción de estas infraestructuras (puente Iron) [25]. Posteriormente, en la primera mitad del siglo XIX, la fundición fue reemplazada por el hierro, ya que presentaba una resistencia a tracción superior, permitiendo así mejorar esta clase de infraestructuras (puente Mythe) [26], mientras que en la segunda mitad del siglo XIX y primera mitad del siglo XX el hierro fue sustituido por el acero, haciendo posible la construcción de puentes de arco con luces mayores (puente de Requejo) [27]. Además, cabe destacar que en esta misma época, finales del siglo XIX y principios del siglo XX, se empezó a utilizar el hormigón reforzado para la construcción de esta clase de puentes. Ejemplo de ello son los puentes de Golbardo y Canalejas en España o el puente Luz Bandeira en Portugal [9, 28, 29]. En su mayoría, estas infraestructuras fueron construidas mediante el uso de patentes de construcción ideadas por Hennebique [30] y Monier [31]. La popularidad de estos sistemas de construcción se debió fundamentalmente a la alta disponibilidad de este material, a sus excelentes propiedades mecánicas como resultado de la sinergia entre acero y hormigón, a su fácil maleabilidad, y a su menor coste de mantenimiento en comparación con otras técnicas constructivas.

Este conjunto de infraestructuras viarias, bien sean estas erigidas en mampostería, acero u hormigón armado, forman un importante grupo desde el punto de vista cuantitativo, siendo justificado por su número. De acuerdo a la longitud de la Red de Carreteras del Estado (estimada en 26,392.56 km) el 12% del total de los puentes son puentes de arco [32]. Cifras donde el hormigón armado y la mampostería constituyen el grueso del mismo (Tabla 1) [32, 33]:

Tabla 1: número de puentes de arco en función del material utilizado en su construcción.

Hormigón reforzado	Acero	Mampostería
2165	13	2925

Por otra parte, cabe destacar que esta clase de puentes son de los más robustos, ya que el diseño curvado de sus arcos aporta un punto de fuerza extraordinario en la mitad de sus vanos, ofreciendo así un mayor nivel de resistencia a los esfuerzos de flexión que intentan deformarlos. Asimismo, las cargas móviles (tráfico, personas, etc.) que cruza estos puentes van directamente hacia abajo en aquellos que están construidos con hormigón reforzado y acero, mientras que son dispersadas en su totalidad en aquellos que están construidos con mampostería por medio de sus materiales de relleno, permitiendo así que ninguna de las partes de estas infraestructuras sufra esfuerzos de compresión muy elevados.

Sin embargo, hay que tener en cuenta que los puentes de arco presentan una serie de inconvenientes, destacando principalmente [34]: (i) la necesidad de uso de soportes más fuertes que las otras clases de puentes, ya que su integridad estructural depende en gran medida de la firmeza de sus pilares y su asentamiento en el suelo; (ii) la limitación de sus vanos, ya que a diferencia de las otras tipologías, necesitan detenerse en un punto concreto, sino serán infraestructuras demasiado débiles para soportar las cargas; (iii) el terreno donde están construidos debe de ser lo suficientemente fuerte y compacto para poder soportar los esfuerzos distribuidos a lo largo de estas infraestructuras; y (iv) requieren un mantenimiento y reparaciones más frecuentes que las otras clases de puentes, ya que su diseño flexible los hace más propensos a sufrir agrietamientos y deformaciones cuando están expuestos a merced de los elementos.

Fruto de las interacciones entre este tipo de infraestructuras y el medioambiente (bien en forma de agentes de deterioro o cargas muertas y vivas), aparecen un conjunto de indicadores visuales de deterioro (tales como pandeo, coqueras, desprendimientos, fisuras o erosiones entre otros), que sin las debidas acciones de conservación y/o restauración pueden promover la pérdida parcial de la capacidad portante de estas infraestructuras. Esta pérdida pone en riesgo la seguridad y comportamiento de las mismas, pudiendo llegar a producirse el colapso de éstas [35]. Por esta razón, casos de desastre recientes, tales como el puente histórico de Keritis (2019) [36] o el puente histórico de Plaka (2015) [37], llevan a plantearse que la seguridad estructural no puede darse por supuesta en infraestructuras envejecidas. Por consiguiente, con la finalidad de evitar su colapso y aportar una operatividad de forma ininterrumpida, la evaluación del estado de estas históricas infraestructuras vulnerables, es hoy en día una cuestión de gran importancia. Esta cuestión requiere el uso de estrategias avanzadas de simulación numérica a fin de someter a la estructura a diferentes estados de carga, tales como tráfico, seísmos o la simple degradación del material. De entre las posibilidades existentes a día de hoy para la evaluación de la estabilidad de estructuras de puentes de arco, el Método de los Elementos Finitos se ha convertido en una de las preferidas dada su versatilidad, pudiendo así ser empleado para evaluar estados límites, el comportamiento de nuevas soluciones de refuerzo e incluso la degradación del material [9, 10]. Este conjunto de

estrategias requiere de forma ineludible un conocimiento amplio de la estructura a diferentes niveles, desde las propiedades mecánicas de cada uno de los materiales constituyentes hasta la posible interacción de la infraestructura con el terreno [10, 38].

Por consiguiente, resulta requisito indispensable el desarrollo de metodologías multidisciplinares, bajo un contexto mínimamente intrusivo y en concordancia con la Moderna Teoría de la Restauración promulgada por la Carta Internacional del Restauro de Cracovia [3], que sean capaces de caracterizar a tres niveles la construcción: (i) a nivel material, (ii) a nivel geométrico y (iii) a nivel estructural, permitiendo así crear modelos numéricos avanzados por el Método de los Elementos Finitos. Caracterización que ha de ser capaz de detectar de forma adecuada las condiciones actuales del puente, generalmente con presencia de daños, y poder llevar a cabo un análisis estructural preciso.

Bajo este contexto es posible encontrar en la literatura un amplio número de trabajos científicos enfocados al desarrollo de metodologías multidisciplinares para la generación de simulaciones numéricas avanzadas por medio del Método de los Elementos Finitos. Dentro de estos trabajos, cabe mencionar los realizados por Conde et al. [10] en puentes de mampostería o los efectuados por Sena-Cruz et al. [9] en puentes de hormigón armado. Además, dentro de este conjunto de métodos multidisciplinares es posible encontrar un conjunto de limitaciones comunes: (i) la escasa explotación de las ventajas que ofrecen los métodos más recientes de ingeniería inversa, los cuales son capaces de simular formas no paramétricas (e. g. deformaciones existentes), por parte de la nube de puntos obtenida de los sensores geomáticos (láser escáner terrestre y cámaras digitales); y (ii) la necesidad de extracción de muestras por medio de técnicas invasivas con el fin de caracterizar los parámetros mecánicos y físicos de los materiales de estas infraestructuras históricas. Dichas limitaciones han de ser solventadas a fin de obtener simulaciones numéricas robustas que aseguren diseñar procesos de conservación adecuados.

Con el objetivo de mejorar estas simulaciones numéricas, y por ende las metodologías multidisciplinares destinadas a la evaluación de la seguridad en puentes de arco, la presente Tesis Doctoral abre su investigación con un **primer artículo científico** titulado "*Integrating geomatic approaches, operational modal analysis, advanced numerical and updating methods to evaluate the current safety conditions of the Historical Bôco Bridge*" (sección 3.1 del capítulo III). En esta publicación, se propone una metodología multidisciplinar aplicada al puente de arco histórico de hormigón reforzado de Bôco, construido en Portugal sobre el río Cávado donde comunica las localidades de Amares y Vieira do Minho, con el fin de evaluar sus actuales condiciones de seguridad. Este puente fue erigido en 1909 utilizando el sistema de construcción Hennebique y posteriormente, en 1962 las secciones de sus elementos estructurales fueron aumentadas para soportar tráfico más pesado. Sin embargo, la baja calidad del hormigón utilizado en las obras de

1962 ha generado un proceso acelerado de degradación en la mayoría de sus elementos estructurales, produciéndose principalmente fisuras y pérdidas materiales, así como la presencia de corrosión en las barras de acero añadidas durante estas obras. Eco de ello, así como de las cargas actuales a las que está sometido resulta indispensable desarrollar modelos numéricos avanzados capaces de ofrecer una imagen fidedigna de su actual capacidad portante. Los avances científicos logrados en esta primera investigación parecen solventar parte de las limitaciones detectadas y mostradas con anterioridad, en especial en lo referente a la integración de datos procedentes de diferentes sensores (e. g. láser escáner terrestre y ensayos de vibración ambiental), la creación de modelos CAE as-built a partir de b-splines y los últimos desarrollos en ingeniería inversa [10], así como el desarrollo de un método de calibración robusto y eficaz en términos de coste computacional basado en la superficie respuesta de Douglas-Reid [39] y el empleo de algoritmos evolutivos para la optimización de la función de coste.

Si bien la metodología multidisciplinar propuesta con anterioridad parece situarse como un potente enfoque en el análisis numérico de puentes de arco, son múltiples las cuestiones abiertas en el caso de la otra tipología más común de puentes de arco: los puentes de mampostería (Tabla 1), en especial en lo concerniente a la caracterización de rellenos (tanto a nivel geométrico como mecánico) o incluso en el desarrollo de métodos matemáticos para el análisis de la influencia de las variables de entrada en la respuesta del puente. Eco de ello, las secciones 3.2 y 3.3 del capítulo III de la presente Tesis Doctoral centrarán su mirada en desarrollar metodologías multidisciplinares para la evaluación de puentes de arco en mampostería.

A diferencia de los puentes erigidos en hormigón armado, esta tipología de puentes cuenta fundamentalmente con dos elementos estructurales: (i) la fábrica pétrea; y (ii) el relleno. Por una parte, la fábrica pétrea ha sido utilizada para construir las partes principales de soporte de carga de estas construcciones históricas, tales como las bóvedas, los tímpanos y las pilastras, así como otros elementos complementarios, tales como los contrafuertes o tajamares. Por otra parte, los materiales de relleno de estos puentes desempeñan un papel importante en su comportamiento estructural teniendo en cuenta los siguientes aspectos: (i) su peso propio en la dirección vertical, donde añade esfuerzos de compresión adicionales en las bóvedas, dando como resultado un incremento en su estabilidad; (ii) la proporción de una mejor dispersión de las cargas dinámicas (personas y tráfico rodado) que son transmitidas desde el pavimento hasta la parte interna de las bóvedas (extradós); y (iii) la limitación de los movimientos laterales de las bóvedas mediante la movilización de la presión pasiva del terreno. Es, este último componente, el que suscita mayores problemáticas para su evaluación.

Desde el punto de vista geométrico, la evaluación de la estructura interna de estos puentes (el ancho de tímpanos, el espesor de bóvedas o la distribución del relleno) suelo ser llevada a cabo a través del georradar [10]. Esta técnica geofísica, basa su éxito en el análisis del cambio morfológico sufrido por un conjunto de ondas electromagnéticas que son emitidas por un receptor y posteriormente recibidas por una antena emisora. Dentro de las problemáticas de dicha técnica, cabe destacar la limitada información aportada, siendo ampliamente dependiente de la humedad y de la porosidad del terreno, así como la imposibilidad de penetrar con la presencia de materiales metálicos al reflejar éstos las ondas [40].

Desde el punto de vista mecánico, los enfoques actuales suelen asumir los valores aportados por la literatura [10, 41], los cuales pueden llegar a diferir significativamente de la realidad, o incluso los valores aportados por ensayos de laboratorio (previa extracción de muestras) o de ensayos invasivos como el Presurómetro Ménard [42].

Teniendo en cuenta los antecedentes descritos previamente, el **segundo artículo** de la presente Tesis Doctoral "*Non-destructive means and methods for structural diagnosis of masonry arch bridges*" (sección 3.2 del capítulo III) propone una innovadora metodología multidisciplinar totalmente no invasiva capaz de dar un salto cualitativo en la caracterización geométrica y mecánica de la disposición interna de este tipo de infraestructuras. Para tal fin, introduce dentro del marco multidisciplinar desarrollado en el primer artículo, una nueva tipología de ensayo: el análisis multicanal de ondas superficiales. Este método sísmico se basa en la detección de un frente de ondas elásticas (ondas sísmicas superficiales y ondas primarias) que son propagadas a través del subsuelo que es investigado, siendo posteriormente detectadas en la superficie mediante sensores (geófonos) con el fin de obtener una imagen 1D, 2D o 3D del terreno en base a las propiedades elásticas de sus materiales [43]. La validación de esta metodología toma como caso de estudio el puente Romano de Ávila. Esta infraestructura histórica de amplia complejidad alberga una amplia variedad de materiales y técnicas constructivas, desde el uso de *Opus Quadratum* o el *Opus Caementicium* hasta el empleo del hormigón armado. Los resultados arrojados por dicha investigación abren un nuevo horizonte de posibilidades en la caracterización estructural de puentes históricos de fábrica.

Tal y como se pone de manifiesto en las investigaciones llevadas a cabo en el primer y segundo artículo, una evaluación precisa de la seguridad estructural de estas infraestructuras requiere contrastar los resultados numéricos con unos datos experimentales (generalmente los proporcionados por los ensayos de vibración ambiental). Contraste que a menudo deriva en la necesidad de calibrar dichas simulaciones numéricas. Dentro de este contexto, son muchas las investigaciones centradas en desarrollar metodologías de calibración de modelos numéricos

avanzados [10, 44, 45], donde destacan, entre otras cuestiones, dos problemáticas fundamentales [10, 46]: i) la elección adecuada de las variables de entrada y; ii) el elevado número de iteraciones requeridas, gran parte de ellas con amplio coste computacional, necesarias para minimizar las discrepancias entre el modelo numérico y el modelo experimental. Sin bien dentro de este contexto ha sido posible realizar un avance plausible en el primer artículo, las técnicas empleadas (matriz de correlación de Spearman y superficie de Douglas-Reid) puede ser insuficientes para una evaluación adecuada de las variables en modelos con fuertes no-linealidades input-output.

Eco de esta necesidad, en el **tercer artículo** de la presente Tesis Doctoral "*A multidisciplinary approach to calibrate advanced numerical simulations of masonry arch bridges*" (sección 3.3 del capítulo III). Partiendo del avance logrado en la segunda investigación, se propone una innovadora metodología de calibración basada en la combinación del metamodelo de la expansión del caos polinomial (PCE) con los índices de Sobol para el análisis sensible, así como el método de optimización no lineal de mínimos cuadrados [46]. El uso de técnicas de subrogación o metamodelos permite bajar considerablemente los costes computacionales de cada interacción, lo cual posibilita el uso de un amplio número de muestras para el análisis sensible de variables y con ello una elección objetiva, basada en la influencia de las variables de entrada (e. g. Módulo de Young o densidades del material) en la respuesta del modelo numérico. Como caso particular, esta metodología es aplicada en el puente Arco de Burgohondo (Ávila), que data del siglo XVI de acuerdo con las características constructivas descritas por el arqueólogo e historiador Emilio Rodríguez Almeida [47].

1.1 Estructura de la Tesis Doctoral

La presente Tesis Doctoral se expone siguiendo el procedimiento de la presentación en el formato de compendio de artículos/publicaciones establecido por la Universidad de Salamanca donde se transfieren los conocimientos científicos por medio de tres artículos que han sido publicados en revistas científicas internacionales de prestigio con alto factor de impacto.

La estructura de esta Tesis Doctoral se basa en cuatro capítulos conforme al desarrollo de las tareas de investigación que han sido realizadas con el fin de alcanzar los objetivos marcados, y un anexo añadido donde se muestra información que resulta de interés. A continuación, se exponen estos capítulos y el anexo añadido:

- **Capítulo I. Introducción:** este capítulo proporciona una visión general de la tipología de los puentes de arco, continuando con las técnicas constructivas empleadas para erigirlos y una breve exposición de los métodos multidisciplinares empleados para su

caracterización, prosiguiendo con una presentación de las metodologías multidisciplinares innovadoras, fruto de la investigación, que han sido desarrolladas y aplicadas a casos particulares a lo largo de la presente Tesis Doctoral. Este capítulo finaliza describiendo la estructura del presente documento.

- **Capítulo II. Hipótesis de trabajo y objetivos:** en este capítulo se describen las hipótesis de trabajo y los objetivos principales a superar con el fin de desarrollar las líneas de investigación que se han llevado a cabo en esta Tesis Doctoral.

- **Capítulo III. Artículos publicados:** este capítulo muestra un resumen extendido de cada uno de los artículos publicados junto con los propios artículos publicados:

  - "*Integrating geomatic approaches, operational modal analysis, advanced numerical and updating methods to evaluate the current safety conditions of the Historical Bôco Bridge*".
  - "*Non-destructive means and methods for structural diagnosis of masonry arch bridges*".
  - "*A multidisciplinary approach to calibrate advanced numerical simulations of masonry arch bridges*".

- **Capítulo IV. Conclusiones y perspectivas futuras:** en este apartado se exponen las conclusiones y los resultados que han sido obtenidos a medida que se ha ido desarrollando esta Tesis Doctoral y, además son reveladas las líneas de investigación que permitirán la continuidad de futuros trabajos.

- **Anexo I. Indexación y factor de impacto de los artículos publicados:** en este anexo se detalla información que hace referencia a parámetros de calidad de las revistas científicas donde se han publicado los artículos de esta Tesis Doctoral.

CAPÍTULO II

HIPÓTESIS DE TRABAJO Y OBJETIVOS

2.1 Hipótesis de trabajo

Con el fin de poder alcanzar los objetivos establecidos en la presente Tesis Doctoral, se exponen las siguientes hipótesis de trabajo:

- ¿Qué utilidad ofrecen las técnicas cuasi no-destructivas y no-destructivas en la caracterización de puentes de arco históricos desde los puntos de vista geométrico, material y estructural?

- ¿Son los procedimientos de ingeniería inversa herramientas capaces de generar modelos CAD precisos de puentes de arco históricos adecuados para llevar a cabo simulaciones numéricas?

- ¿Existe algún método alternativo no invasivo que permita extraer los parámetros mecánicos y físicos de los materiales de relleno de puentes de arco de mampostería?

- ¿Existe otro método no invasivo alternativo al georradar que permita caracterizar los espesores de los tímpanos y las bóvedas de los puentes de arco de mampostería?

- ¿Permite el Método de los Elementos Finitos la integración de datos obtenidos por medio de diferentes disciplinas?

- ¿Es el Método de los Elementos Finitos una herramienta de gran potencial a la hora de llevar a cabo diagnósticos estructurales en simulaciones numéricas avanzadas de puentes de arco históricos?

- ¿Es posible optimizar los costes computacionales de los métodos de calibración a través del empleo de modelos subrrogados o metamodelos?

2.2 Objetivos

Teniendo en cuenta las bases expuestas en el Capítulo I, para poder generar de forma precisa modelos numéricos avanzados de puentes de arco históricos que permitan evaluar su comportamiento estructural global, la presente Tesis Doctoral ha sido desarrollada considerando un **objetivo principal** y unos **objetivos específicos**:

2.2.1 Objetivo principal

- Desarrollar metodologías multidisciplinares con el fin de poder evolucionar modelos numéricos avanzados de puentes de arco históricos de hormigón reforzado y de mampostería.

2.2.2 Objetivos específicos

- Evaluar las ventajas del uso de sensores geomáticos (láser escáner terrestre) en puentes históricos para caracterizar la geometría de sus componentes estructurales.

- Desarrollar metodologías que permitan hacer coincidir la nube de puntos obtenida mediante técnicas de escaneado láser con los ejes longitudinal y transversal de puentes de arco históricos, con el fin de integrar de forma correcta los datos obtenidos de la campaña experimental (Ensayos de Vibración Ambiental).

- Desarrollar metodologías que permitan construir modelos CAD precisos a partir de la nube de puntos obtenida mediante sensores geomáticos (láser escáner terrestre), con el fin de que sean adecuados para realizar simulaciones numéricas avanzadas.

- Evaluar las ventajas e inconvenientes de la aplicación de diferentes enfoques geofísicos (georradar y análisis multicanal de ondas superficiales) para la caracterización del relleno en puentes de arco de mampostería.

- Analizar la aplicabilidad de métodos no-destructivos basados en ondas (ensayos sónicos e impacto-eco) para la caracterización de los materiales que constituyen los tímpanos y las bóvedas de puentes de arco de mampostería, así como sus espesores.

- Aplicar técnicas basadas en ensayos de vibración ambiental (AVT) para evaluar el comportamiento dinámico de los puentes de arco históricos en función de su estado actual de conservación.

- Desarrollar estrategias de calibración robusta de modelos numéricos de puentes de arco históricos que permitan reducir las discrepancias entre los resultados experimentales y los resultados obtenidos mediante simulaciones numéricas.

CAPÍTULO III

ARTÍCULOS PUBLICADOS

3.1 Integración de enfoques geomáticos, análisis modal operacional, métodos numéricos avanzados y de calibración para evaluar las condiciones de seguridad actuales del puente histórico de Bôco.

El artículo científico publicado en este apartado simboliza el primer paso para avanzar en el desarrollo de esta Tesis Doctoral. Esta publicación científica describe de forma detallada una nueva metodología multidisciplinar que permite crear modelos numéricos avanzados precisos de puentes de arco de hormigón reforzado históricos con el fin de poder evaluar sus condiciones de seguridad actuales, ya que a día de hoy muchos de ellos están soportando nuevas demandas de tráfico.

Esta metodología multidisciplinar propuesta se basa en la combinación del sensor geomático láser escáner terrestre, en ensayos de vibración ambiental (AVT) y ensayos cuasi no-destructivos, la cual es aplicada para la caracterización del puente de arco de hormigón reforzado histórico de Bôco (Portugal). Todos los métodos son complementados por simulaciones numéricas avanzadas y una estrategia de calibración que va desde un refinamiento "basto" a otro más "fino", combinando el método de Douglas-Reid (estrategia de aproximación) y la minimización no-lineal por Mínimos Cuadrados (estrategia de minimización local). Los resultados obtenidos demuestran la robustez de esta metodología propuesta, donde se obtiene un error relativo en las frecuencias de 1.22 % y un valor medio MAC (Modal Assurance Criterion) de 0.91. Considerando este modelo, se lleva a cabo una evaluación de las condiciones de seguridad, obteniendo un factor de seguridad mínimo de 2.1.

Cabe destacar que la nube de puntos obtenida mediante el láser escáner terrestre es alineada respecto a los ejes longitudinal y transversal de este puente histórico con el fin de poder incorporar correctamente los diferentes datos capturados de la campaña experimental (e. g. AVT), permitiendo así realizar simulaciones numéricas precisas para su evaluación. Este método innovador se basa en el siguiente flujo de trabajo: (i) la evaluación de la matriz de covarianza de la nube de puntos; (ii) el análisis de los autovalores y autovectores de la matriz de covarianza; y (iii) la rotación de la nube de puntos considerando el ángulo entre el eje de la dirección X y el tercer autovector (dirección de la dispersión máxima del puente).

Palabras clave: Puente histórico; Hormigón reforzado; Daño estructural; Láser escáner terrestre; Ensayos de vibración ambiental; Actualización del modelo de elementos finitos.

Construction and Building Materials 158 (2018) 961–984

Contents lists available at ScienceDirect

Construction and Building Materials

journal homepage: www.elsevier.com/locate/conbuildmat

Integrating geomatic approaches, Operational Modal Analysis, advanced numerical and updating methods to evaluate the current safety conditions of the historical Bôco Bridge

Álvaro Bautista-De Castro [a], Luis Javier Sánchez-Aparicio [a,*], Luís F. Ramos [b], José Sena-Cruz [b], Diego González-Aguilera [a]

[a] Department of Cartographic and Land Engineering, University of Salamanca, High Polytechnic School of Ávila, Hornos Caleros, 50, 05003 Ávila, Spain
[b] ISISE, Department of Civil Engineering, University of Minho, Campus de Azurém, 4800-058 Guimarães, Portugal

HIGHLIGHTS

- A multidisciplinary method was used to assess the safety conditions of the bridge.
- The bridge's model was placed in its longitudinal axis following a PCA analysis.
- The calibration strategy improved the results of the numerical simulations.
- The methodology can be applied to verify the load bearing capacity of bridges.

ARTICLE INFO

Article history:
Received 30 June 2017
Received in revised form 12 October 2017
Accepted 19 October 2017
Available online 5 November 2017

Keywords:
Historical bridge
Reinforcement concrete
Structural damage
Terrestrial laser scanner
Ambient vibration tests
Finite element model updating

ABSTRACT

This paper proposes a multidisciplinary approach, combining the terrestrial laser scanner, ambient vibration tests and minor destructive tests, to characterize an early reinforced concrete bridge in Portugal: the Bôco Bridge. All methods are complemented by advanced numerical simulations and a coarse to fine calibration strategy, based on the Douglas-Reid and the non-linear least squares approaches. Results obtained corroborate the robustness of the proposed approach, with an average relative error in frequencies of 1.2% and an average modal assurance criterion of 0.91. Considering this model, its current safety conditions were evaluated, obtaining a minimum safety factor of 2.1.

1. Introduction

Transportation networks are fundamental elements in the economic development of countries, facilitating the communication and trade between different places. Inside the wide diversity of infrastructures that compose these networks, bridges are necessary elements to overpass topographic accidents, such as rivers or gullies, being considered, as ones of the most common, expensive and vulnerable infrastructures [1].

Among the variety of materials utilized in the construction of bridges, from masonry to steel [2], reinforced concrete (RC) has been one of the most used construction material, especially after the development and popularization of the Hennebique [3] and Monier [4] systems in the beginning of the XXth century. This popularity has been mainly due to its high availability, good mechanical properties, (caused by the synergy between steel and concrete), moldability and relatively low maintenance costs among other factors [5]. However, the aggressive environments on which the concrete bridges are constructed (usually with presence of chlorides, melting salts and carbon dioxide), tend to degrade this structural material. This degradation is mainly governed by the destruction of the passivation layer (protection layer created between the concrete and steel bars promoted by the alkaline environment created into the concrete) due to the presence of chlorides from melting salts and carbonation from atmospheric CO_2 among other factors. Promoting the penetration of the water and the oxygen, the oxidation and volumetric expansion of the steel bars will

* Corresponding author.
E-mail addresses: alvarobautistadecastro@usal.es (Á. Bautista-De Castro), luisj@usal.es (L.J. Sánchez-Aparicio), lramos@civil.uminho.pt (L.F. Ramos), jsena@civil.uminho.pt (J. Sena-Cruz), daguilera@usal.es (D. González-Aguilera).

https://doi.org/10.1016/j.conbuildmat.2017.10.084
0950-0618/

be developed. Consequently, concrete cracking and concrete spalling and reduction on the mechanical adhesion between concrete and steel rebars will take place [6]. As a result, the bearing capacity of these infrastructures and their working life can be considerably reduced, being necessary to carry out accurate safety verifications in order to evaluate the response of existing structures to the current and new demands of traffic loads [7].

Added to this, the limited knowledge of the construction technology, the use of semi-empirical rules or the theoretical background of the engineering analysis, lead to a challenging topic in the study and preservation of historic RC bridges. Rigorous multidisciplinary approaches able to characterize the structures at different levels, mainly (i) at geometrical level; (ii) at structural level and; (iii) at material level, are required.

Regarding the geometry, geomatic sensors (e.g. terrestrial laser scanner or digital cameras) have been placed in a privileged position in the geometrical characterization of bridges, being possible the digitalization of these structures in a fast and accurate way [8,9]. However, the product of this digitalization, the point cloud, is limited to the extraction of sections and individual measurements through which the 3D model is created [9]. Not exploiting all the advantages offered by the new methods emerged into the reverse engineering field [10].

Concerning the structural and material characterizations, the use of the ambient vibration tests (AVT) as well as the use of in-situ and minor-destructive tests have been placed as the most feasible strategies to characterize bridges at these levels [7,9,11,12]. The results of these tests are later used into set-up advanced numerical simulations by means of the finite element method (FEM), allowing the evaluation of the structure under different casuistic (e.g. traffic loads or seismic actions) [12–14]. However, and behind the advantages offered by the FEM, the incorrect modelling of its geometry, boundary conditions, and mechanical properties may lead to erroneous results [14,15]. To avoid these unreliable results, different global optimization strategies can be applied, such as the particle swarm or the genetic algorithms [12], in order to minimize the discrepancies between the experimental and the numerical results, requiring in most of the cases, a large number of iterations in order to get reliable results and thus, large computational times [15]. In contrast with this limitation, different authors have been proposed the use local optimization strategies [9,14]. These methods use lower number of iterations to converge in a minimum, but needing a good initial approximation to ensure accurate results.

Considering the limitations previously detailed, the present paper proposes a multidisciplinary method, based on the combination of terrestrial laser scanning procedures, ambient vibration tests, laboratory tests, advanced numerical simulations, by means of FEM, and a robust cost-optimized calibration strategy based on the Douglas-Reid (approximation strategy) and non-linear least squares (local minimization approach) methods, with the aim of creating accurate numerical simulations. Simulations able to reproduce accurately the current safety conditions of these structures. Particularly, this methodology has been validated in the historical RC bridge constructed over the Cávado river: the Bôco Bridge located in Braga region, Portugal. This infrastructure was built in its origin according to the guidelines imposed by the Hennebique system in the year 1909 and later expanded, in order to withstand heavy traffic, in the year 1962. The low quality of the used concrete during this intervention has caused the degradation of its structural elements (mainly concrete spalling and steel corrosion), being necessary the evaluation of its current carrying capacity under the actual loading demand.

Within this context, the paper is organized as follows: after is initial Introduction, Section 2 briefly describes the study case, its historical background, constructive system and current state of conservation; Section 3 shows the experimental campaign carried out on the bridge; Section 4 presents the calibration of the numerical model; Section 5 details the safety analysis carried out; and finally, in Section 6 the conclusions are drawn.

2. The Bôco Bridge

2.1. Historical background

Located along the road EM595-1, connecting the regions of Amares and Vieira do Minho, the Bôco Bridge is the actual oldest RC bridge in use in Portugal. Erected between the years 1909 and 1910 by the company Moreira de Sá & Malevez, following the project designed by the architect Sebasião Lopes (Fig. 1a). In the year 1950, the bridge was analyzed by engineers of different institutions reporting its bad state of conservation. The main damages found were concrete spalling and corrosion of the reinforcements, specially on the arches and deck. Furthermore, the traffic was limited to a load of 5 tons per vehicle without crossing the bridge at the same time until the retrofitting took place. In September 1961, the rehabilitation works started, following the project designed by the engineer J. Duarte Carrilho. Project that was ended in 1962 and consisted on concrete jacketing by increasing the concrete sections and adding additional reinforcement to the different structural elements (Fig. 2) (Table 1) with amild steel S400-B [7], in contrast with the original steel that could be considered identical to the steel used in the Luiz Bandeira bridge (erected by the same company and following the same construction method) [11]: a Bessemer mild steel.

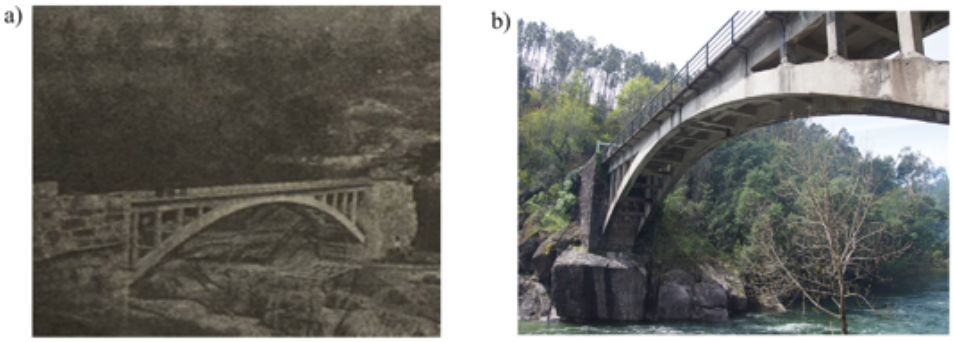

Fig. 1. General views of the RC bridge evaluated: a) Bôco bridge in the year 1910 [7] (original project); and b) current state of the Bôco Bridge.

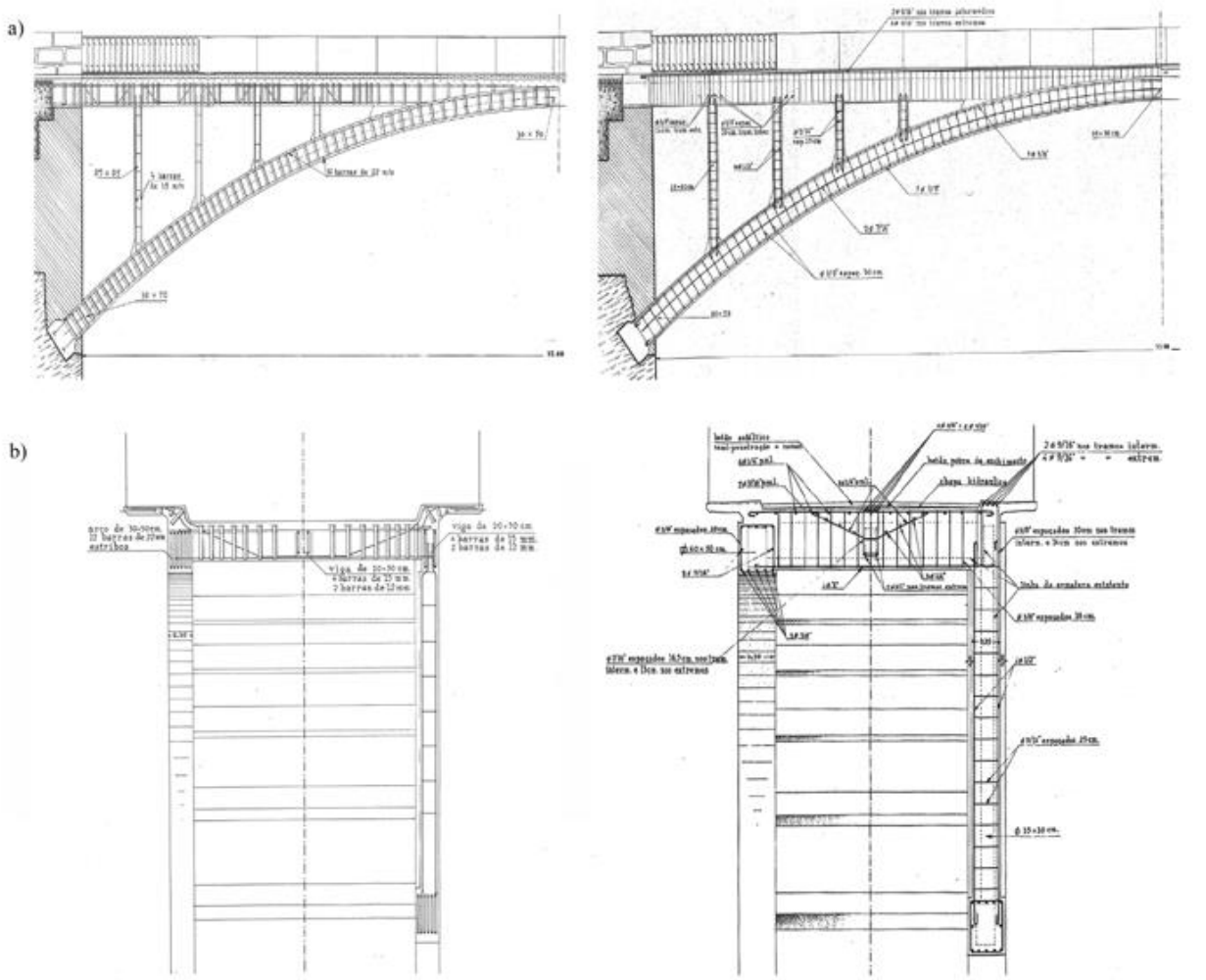

Fig. 2. Geometry and steel reinforcements of the Bôco Bridge [16]: a) downstream elevation before and after of the rehabilitation works; and b) cross-section of the deck before and after of the rehabilitation works.

2.2. Description of the bridge

The bridge is composed of seven different structural elements (Fig. 3): i) two arch girders with an average cross-section of 500 × 725 mm^2 (variable from their ends to the mid-span) and 35 m length, embedded its extreme in mansory walls; ii) 16 pillars spaced from each other 2 m with a cross-section of 350 × 320 mm^2, passing the loads from the lateral longitudinal girders to the arch girders; iii) 10 rectangular girders of 2.5 m length between the arch girders, making the bridge more rigid in the transversal direction; iv) 16 transverse girders with 2.7 m length that are connected to the lateral longitudinal girders and the central girder, with a cross-section of 300 × 550 mm^2, performing the same role that the rectangular girders connected to the arch girders; v) one central girder with 33 m length and a cross-section of 300 × 350 mm^2, with the ends supported on the masonry wall; vi) two lateral and longitudinal girders of 33 m length with a cross-section of 300 × 550 mm^2, embedded into the vertical masonry walls (Fig. 2a); and, vii) a deck, composed by a concrete shell with 120 mm of thickness. Furthermore, the non-structural elements used in the bridge (Fig. 3) (Fig. 4) are: i) an overlay of dry joints granite blocks of 150 × 150 mm^2 with 130 mm of thickness placed on the concrete deck; ii) two pedestrian sidewalks of 750 mm wide; and iii) metallic parapets of 900 mm high placed on the pedestrian sidewalks.

As stated in Section 2.1, the current structural elements of the Bôco Bridge have been the result of two stages, showing each one two concrete layers, namely (Fig. 5): i) old concrete, from the original desing; and ii) new concrete, added during the rehabilitations works.

2.3. Visual inspection

Results derived from the visual inspection carried out in 2016 corroborated the presence of different visual indicators of alteration, namely (Figs. 6 and 7): i) concrete spalling in the new concrete layer of the most of the structural components; ii) salt crusts in the arch girders and some pillars due to the aggressiveness of the environment; iii) presence of moisture, promoted by the infiltration of water from the pavement and the vertical masonry walls to the structural elements; iv) corrosion of the steel bars on the arch girders, pillars and rectangular girders connected

Table 1
Original and current dimensions, reinforcement bars and stirrups of the different structural elements of the Bôco Bridge [7].

Structural element	Original dimensions (mm)	Original reinforcement bars (mm)	Hennebique curved plates (mm)	Current dimensions (mm)	Added reinforcement bars (inches)	Added stirrups (inches)
Longitudinal arch girders (mid-span)	300 × 500	12 Ø 22	12	500 × 600	10 Ø 5/8 + 2 Ø 7/16	Ø 3/8
Longitudinal arch girders (at the abutments)	300 × 700	12 Ø 22	12	500 × 850	10 Ø 5/8 + 2 Ø 7/16	Ø 3/8
Pillars	250 × 250	4 Ø 15	12	350 × 320	4 Ø 1/2	Ø 5/16
Transverse girders	200 × 350	4 Ø 15	12	300 × 550	4 Ø 1	Ø 3/8
Central girder	200 × 300	4 Ø 15	12	300 × 350	2 Ø 3/4	Ø 7/16
Lateral longitudinal girders	200 × 500	4 Ø 15	12	300 × 550	–	–

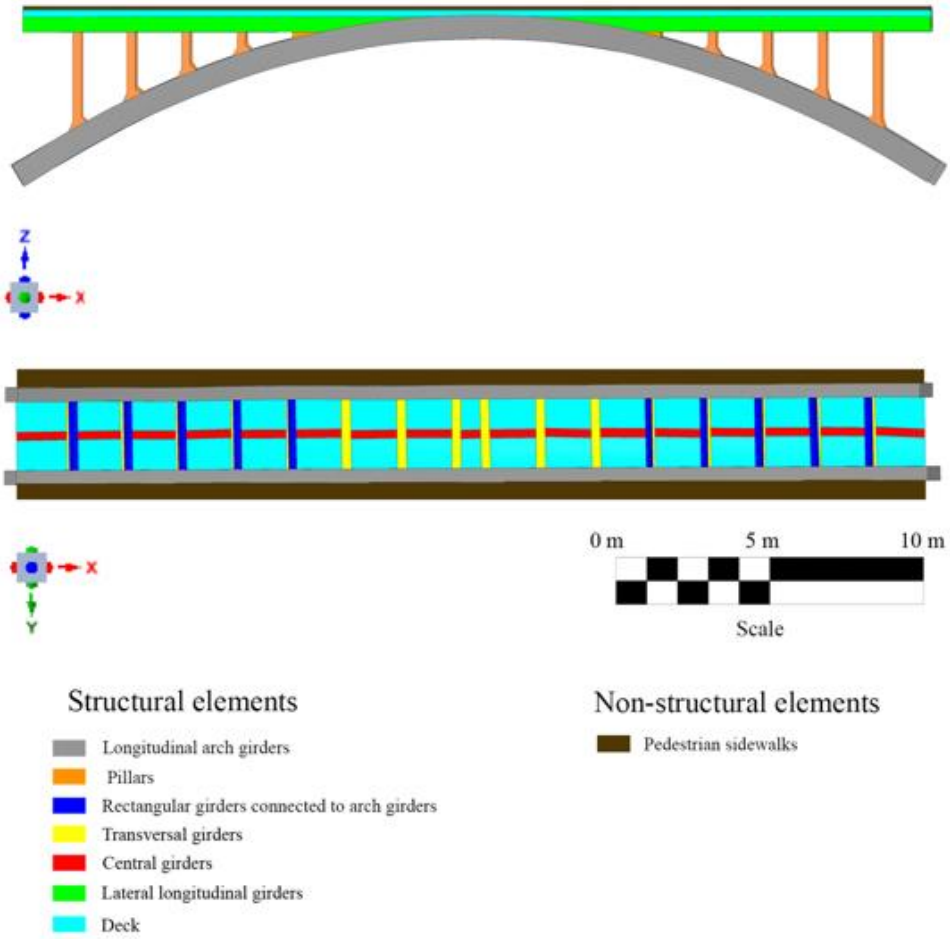

Fig. 3. Structural elements and non-structural elements of the Bôco Bridge.

to the arch girders; v) cracks on the connections between the arch girders and the vertical masonry walls; vi) algae in the arch girders and rectangular girders connected to the arch girders; vii) plants on the vertical masonry walls; viii) presence of lichen on a rectangular girder connected to the arch girders; and ix) moss on the arch girders, on a rectangular girder connected to the arch girders and on the vertical masonry walls. Part of these damages, more specifically the concrete spalling and steel bars corrosions, can be attributed to the high porosity (9.8% in contrast with the 3.2% of the old concrete layer) and the carbonation of the new concrete layer [7].

3. Experimental program: geometrical, dynamic and material characterization of the bridge

3.1. Geometrical characterization: Terrestrial laser scanner

Among the different digitalization strategies that can be used to reconstruct historical bridges [8,9], the terrestrial laser scanner (TLS) has been one of the more used, mostly due to it fast data acquisition, data processing, high accuracy and the absence of specific light conditions to acquire the data. Taking into account

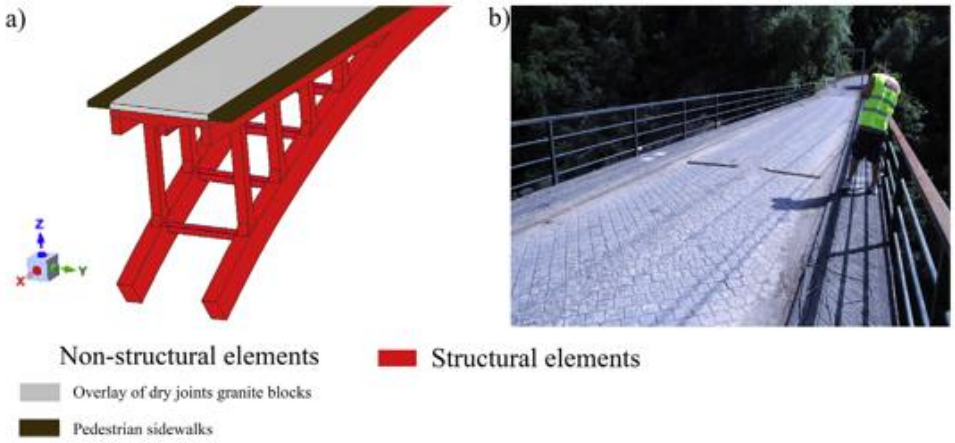

Fig. 4. Non-structural elements of the Bôco Bridge: a) Deck overlay composed by dry joints granite blocks and pedestrian sidewalks; and b) General view of the non-structural elements, overlay, pedestrian sidewalks and metallic parapets.

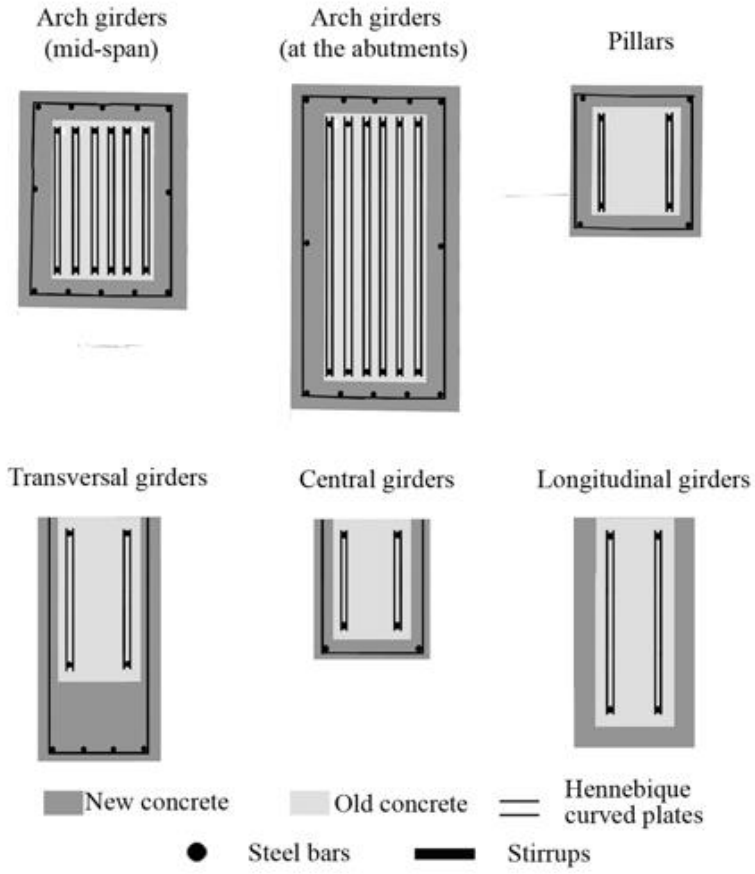

Fig. 5. Cross-sections with concrete layers and reinforcement (steel bars, stirrups and Hennenbique curved plates) of the structural components. Adapted from [7].

this, the lightweight Faro Focus 3D 120 TLS system (Table 2) (Fig. 8), based on the phase shift physical principle [17], was used to assess the geometry of the bridge.

Additionally to the TLS system, several registration spheres, with 20.0 cm and 14.5 cm of diameter (Fig. 8a), were used to align the different scans stations following the algorithm defined by [18].

As a result, 18 scan stations were needed to record the whole structure: i) 12 scans under the bridge; and ii) 6 scans on the bridge's deck, obtaining an alignment error of 0.003 ± 0.002 m. The huge amount of data captured, with a total of 672,316,191 points, required an optimization of the point cloud for further evaluations. In order to better manipulate the data, the following

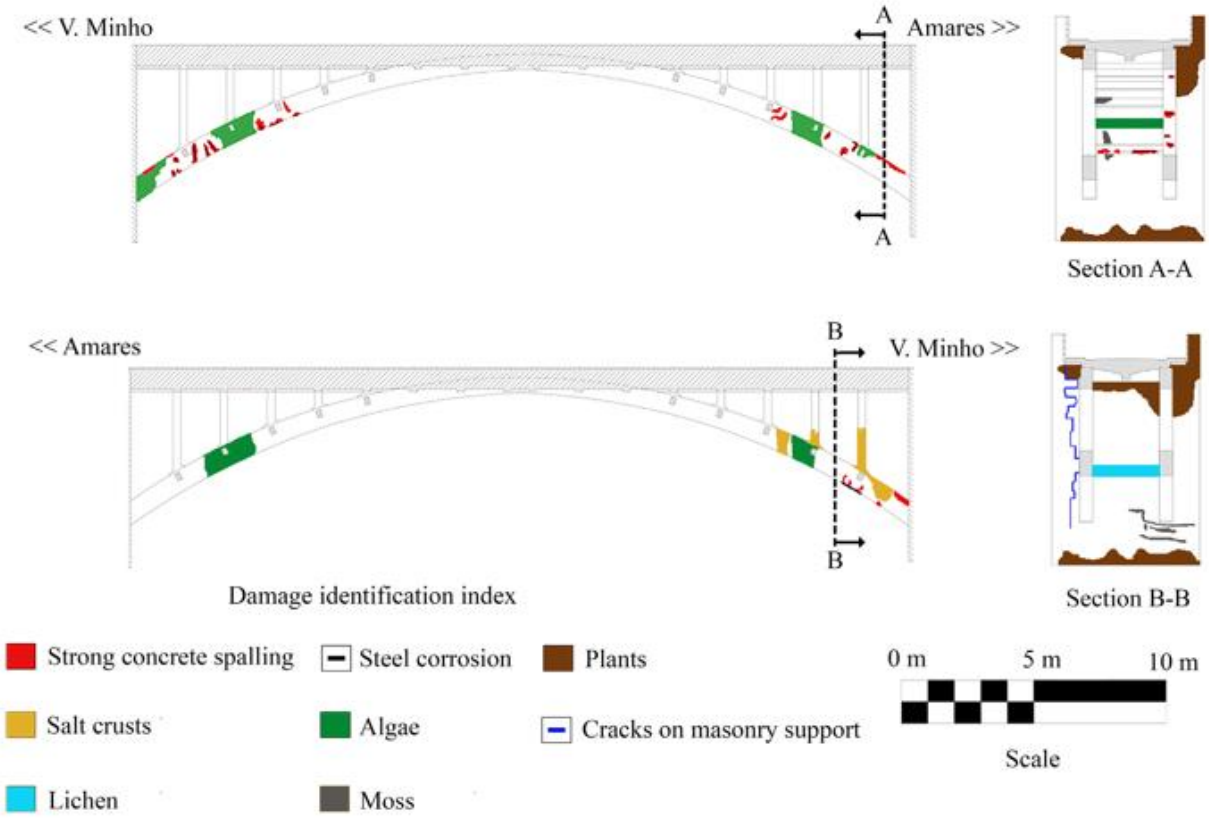

Fig. 6. Damage mapping obtained from the visual inspection carried out.

Fig. 7. Current state of conservation: a) extreme of an arch girder; b) concrete spalling on an arch girder; c) concrete spalling on a pillar; and d) cracks on the V. Minho vertical masonry wall.

Table 2
Technical specifications of the TLS Faro Focus 3D 120.

Faro Focus 3D 120	
Measurement principle	Phase shift
Measurement range	0.6–120 m
Accuracy nominal value	2 mm to 25 m in normal conditions of illumination and reflectivity
Field of view	360° Horizontal 305° Vertical
Capture rate	122,000/976,000 points
Beam divergence	0.19 mrad

decimation filters were applied: i) a distance filter with an average threshold of 40.0 m; and ii) a curvature-based decimation filter [19], with a threshold of 0.01 m, with the aim of simplifying flat areas while maintains relevant details, such as beam edges. As a result, an optimized 3D representation of the bridge was obtained made up by 9,853,819 points (1.47% of the original point cloud) (Fig. 9).

3.1.1. From the point cloud to the as-built CAD model

In the present dynamic identification and numerical evaluation of bridges the *x* and *y* axis were assumed as the longitudinal and transversal axis of the structure, respectively [7,15]. Being necessary the use of an additional procedure to place the bridge's point cloud in the correct coordinate system (Fig. 10). To this end, the following workflow was used: i) the evaluation of the covariance matrix of the point cloud; ii) the analysis of the Eigen-values and Eigen-vectors of the covariance matrix; and iii) the rotation of the point cloud considering the angle between *x* axis and third eigenvector (direction of maximum dispersion of the bridge).

With the aim of creating an accurate CAD model suitable for subsequent numerical evaluations, the multistep geometrical modelling strategy, proposed by [10] was considered which includes the following steps: i) Delaunay triangulation of the point cloud; ii) hole filling based on radial basis functions [20]; iii) topological noise removal by means of a local re-triangulation [21]; iv) segmentation of the different structural components and; v) adjustment of segmented elements into basic primitives based

Fig. 8. TLS and registration spheres used during the data acquisition: a) during the recording of the deck; and b) TLS surveying at the lower part of the bridge.

Fig. 9. 3D representation of the bridge resulting of the point cloud optimization.

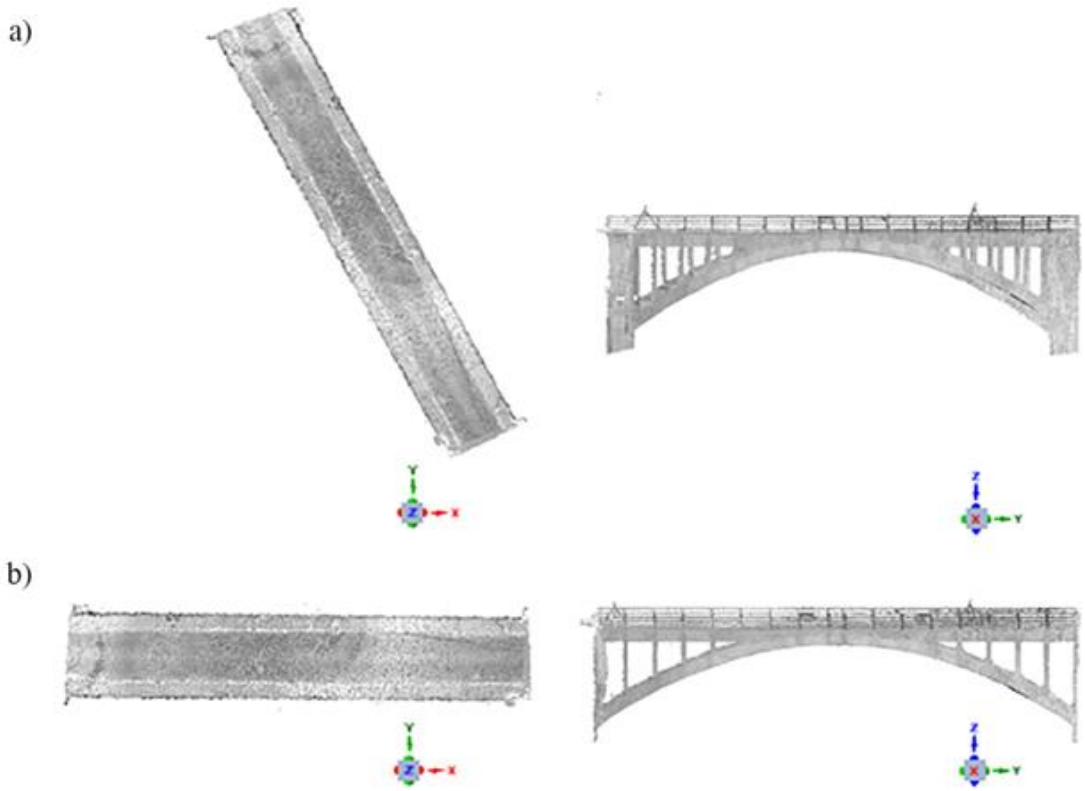

Fig. 10. Results derived from the methodology proposed: a) original point cloud; and b) rotated point cloud.

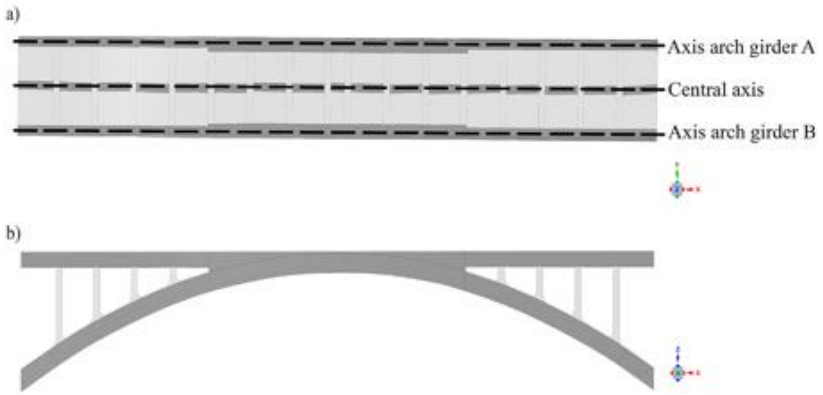

Fig. 11. As-built CAD model obtained by the proposed method: a) plant view (arches A and B); and b) elevation view.

on linear and non-linear (b-splines) extrusions. As a result, an as-built CAD model was obtained (Fig. 11), on which the geometrical deviations during the bridge construction were taken into account (Fig. 12).

3.2. Ambient vibration tests

A dynamical identification campaign, based on the Operational Modal Analysis (OMA) approach, was performed with the purpose of identifying the modal properties of the bridge (such as the frequencies, damping ratios and modal shapes). For a better results achievement, several numerical and previous dynamic analyses with different boundary conditions (Y-axis translation free and fixed) and mechanical properties were performed. These simulations allowed the proper configuration of the OMA tests (acquisition time and sampling rate) as well as the most suitable areas to place the accelerometers.

According to the obtained results, two setups with a total acquisition time of 20 min and a sampling rate of 256 Hz, were used. On each setup, a total of 14 uniaxial piezoelectric accelerometers, with a sensitivity of 10 V/g, range of ±0.5 g and 8 μg rms broadband resolution, were placed along the bridge's deck, being

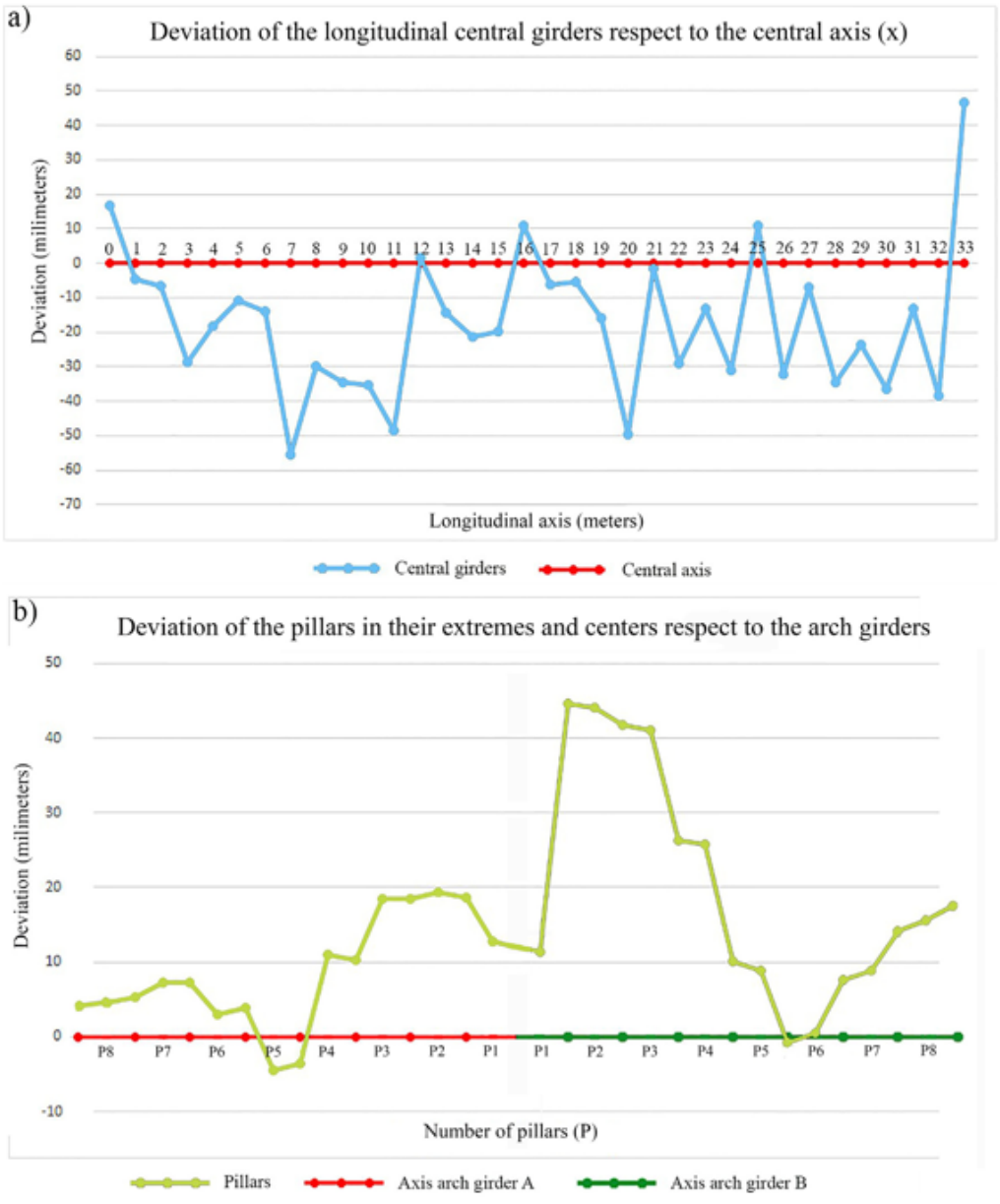

Fig. 12. Deviations of structural elements with respect to their theoretical positions: a) longitudinal central girders; and b) pillars.

5 of them considered as references (Fig. 13), namely accelerometers (3), (11), and (6) in the Z direction, and accelerometers (4) and (6) in the Y direction.

Finally, to extract the dynamic properties the Enhanced Frequency Domain Decomposition algorithm (EFDD), based on the power spectral density, was used to extract the mode shapes, natural frequencies and damping ratios [22]. As a result, 12 modes were identified with a range of frequencies between 4.15 Hz and 27.13 Hz (Table 3) (Fig. 14). The low coefficient of variation (CoV) for frequencies and damping ratios show the quality of the identified modal properties. On average, the damping ratio was equal to 1.67%.

3.3. Material characterization

Built in reinforced concrete, the Bôco Bridge shows in each structural component a total of two layers of concrete, namely: i) old concrete and ii) new concrete. According with this distribution, several mechanical and chemical tests were carried out in a previous experimental campaign to characterize the concrete and the steel of the bridge [7], by extracting samples from different locations as shown Fig. 15.

The average values for the elastic modulus of the new and old concrete (E_c) as well as their corresponding compressive strength ($f_{is,cyl}$) (Table 4) were obtained following the recommendations

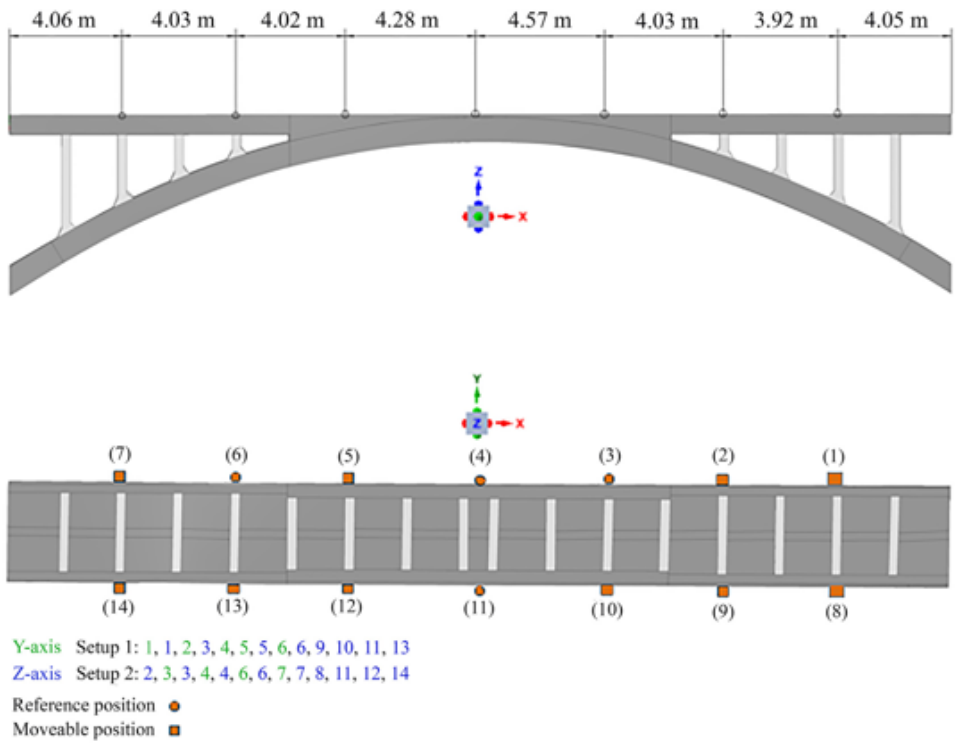

Fig. 13. Accelerometers positions and setups used during the ambient vibration tests.

Table 3
Natural frequencies and damping ratios obtained.

Mode shape	Frequencies (Hz)	CoV (%)	Damping ratios (%)	CoV (%)	Description
1	4.15	0.02	1.91	1.70	1st symmetrical translational (Y-axis)
2	6.51	<0.01	2.13	2.60	1st symmetrical vertical bending (Z-axis)
3	9.88	0.01	0.62	1.75	2nd asymmetrical vertical bending (Z-axis)
4	11.53	0.02	1.54	2.57	3rd asymmetrical vertical bending (Z-axis)
					2nd asymmetrical torsional (X-axis)
5	11.75	0.02	1.36	2.99	3rd asymmetrical torsional (X-axis)
6	12.34	0.01	2.47	2.41	2nd asymmetrical translational (Y-axis)
					4th asymmetrical torsional (X-axis)
7	14.11	0.04	2.43	6.15	5th asymmetrical torsional (X-axis)
8	18.71	0.03	3.95	3.13	4th asymmetrical vertical bending (Z-axis)
9	19.95	0.01	1.29	1.18	6th asymmetrical torsional (X-axis)
10	21.67	0.01	2.11	1.27	7th asymmetrical torsional (X-axis)
11	26.56	0.02	4.69	0.59	5th asymmetrical vertical bending (Z-axis)
12	27.13	0.01	1.70	0.98	8th asymmetrical torsional (X-axis)

exposed in LNEC E397:1993 [23] and NP EN 12390-3:2003 [24] respectively. From normalized cylinder of 150 mm of diameter and 300 mm of height, the following values were obtained: i) 41.30 GPa (with a coefficient of variation of 24.73%) and 52.1 MPa (with a coefficient of variation of 22.66%) for the old concrete; and ii) 27.25 GPa (with a coefficient of variation of 12.71%) and 21.1 MPa (with a coefficient of variation of 41.32%) for the new concrete.

In general the results derived from the physical, chemical and mechanical tests of the concrete used in the Bôco Bridge corroborated the low quality of the new concrete layer. In fact, this material shows a low compression resistance (Table 4) as well as a high porosity (around 9.8% with a coefficient of variation of 8.6%). This physical property, the porosity, has accelerated the carbonation effects and thus, steel corrosion and consequently concrete spalling along the different structural components of the bridge took place (Fig. 7) [7]. In contrast with this, the high elastic modulus and compressive strength and low level of porosity (3.2%) obtained for the old concrete layer suggests a high-quality concrete.

Regarding the steel used in the reinforcement bars, four samples were extracted and characterizing in laboratory using the following tests: i) scanning electron microscope with X-ray fluorescent spectrometer; and ii) carbon element tests. As a result, was possible to conclude that the steel used in the bridge was mild steel (presenting inclusions of manganese sulphide) [7].

4. Modelling the current state of the Bôco Bridge

Negative effects that bridges present, without a proper maintenance plan, can increase when time elapses, reducing its load capacity [26]. It is for this reason that is necessary not only to carry

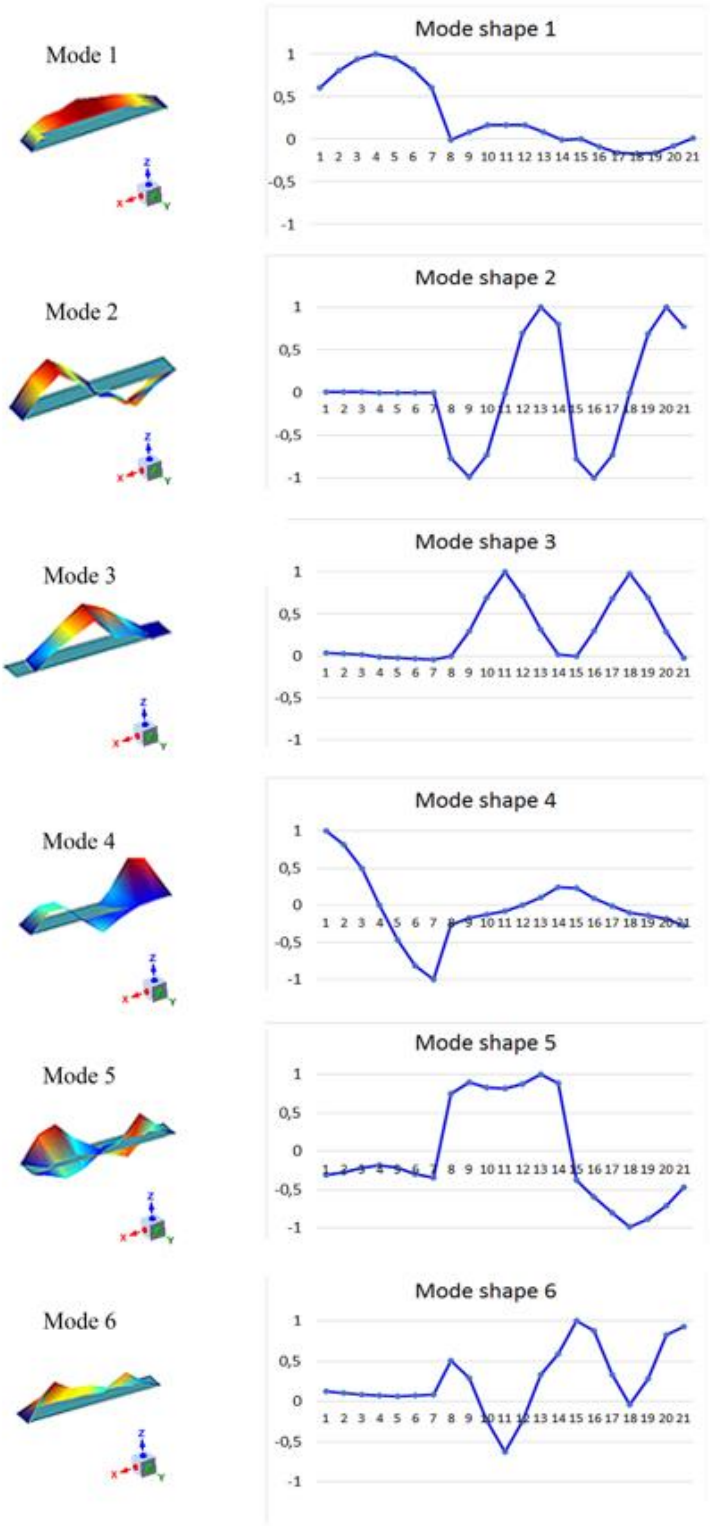

Fig. 14. Graphical representation of the first six vibrational modes extracted by the EFDD algorithm. In blue the experimental modal displacements. The horizontal axis of the graphs represent the degree of freedoms and the vertical axis the normalized modal displacements. (For interpretation of the references to colour in this figure legend, the reader is referred to the web version of this article.)

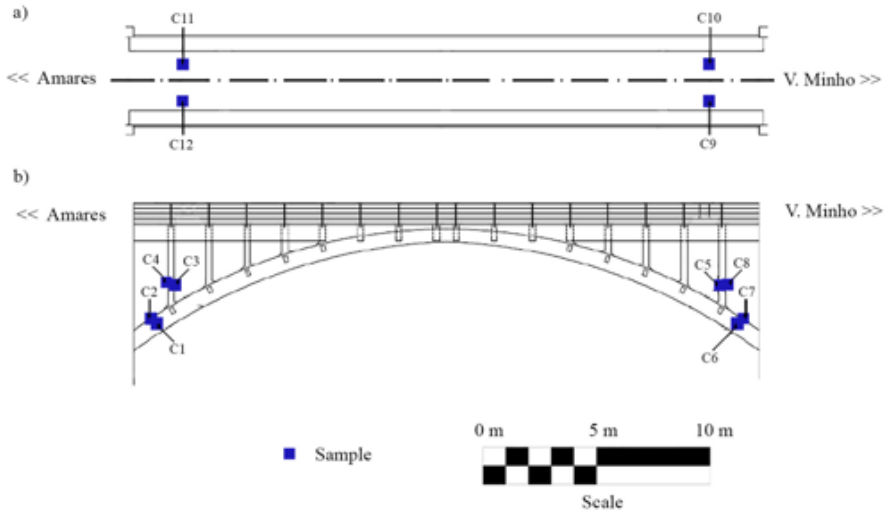

Fig. 15. Locations of the samples taken from the bridge by [7]: a) top view; and b) elevation view.

Table 4
Results obtained from the compression tests carried out by [7]. Young Modulus (E_c) of the new concrete have been estimated through the relation proposed by [25].

	Old concrete		New concrete	
Structural element	E_c (GPa)	$f_{is,cyl}$ (MPa)	E_c (GPa)	$f_{is,cyl}$ (MPa)
Arch (C1)	–	–	24.8	14.9
Deck (C10)	–	–	29.7	27.2
Pillar (C3)	54.1	58.8	–	–
Pillar (C4)	45.7	48.0	–	–
Pillar (C5)	–	59.2	–	–
Arch (C6.2)	43.2	58.0	–	–
Deck (C9)	36.6	29.9	–	–
Deck (C11)	–	64.8	–	–
Deck (C12.2)	26.7	46.1	–	–

out extensive experimental campaigns, focused on the characterization of the different structural components, damages or mechanical properties, but also numerical simulations to evaluate the current safety conditions of the bridge. These models need to be contrasted with experimental data, such as ambient vibration tests, to validate them.

4.1. Construction of the numerical model

According with the exposed above, a numerical simulation by means of FEM was carried out. To this end, the software TNO Diana ® [27] was used together with a numerical mesh composed of 193,814 elements (Fig. 16): i) 193,546 solid elements for the structural components and ii) 268 interface elements for the simulation of the interaction of the structure with its supports. The following constrains were considered: i) maximum size of the element 0.20 m; ii) minimum size of 0.05 m to represent properly the complexity of the as-built CAD model as well as to ensure a good quality of the different elements and; iii) at least 2 elements in the different structural components, with 4 elements in the z direction of the arch and longitudinal girders in order to capture possible non-linearities in further non-linear evaluations.

As it was described in Section 2, the different structural components of the bridge were retrofitted, showing each element two layers composed by concretes with different mechanical properties (Table 4). With the aim of reducing the complexity of the numerical simulation and thus, the computational effort, a homogenous concrete section was considered on each structural element. Therefore, the numerical model was divided in 5 groups of elements according with the similarity, in terms of concrete properties and structural components (Figs. 5 and 17).

To pass from the heterogeneous section (sections with two concrete layers) to the equivalent homogeneous section, the following variables were calculated: i) equivalent density; and ii) equivalent Young Modulus.

On one hand, the equivalent density of each group was calculated through the weighted arithmetic mean (considering as weight the percentage in volume of the two concrete in the structural element evaluated) (Fig. 3), taking into account as base values those obtained in the previous experimental campaign [7] (Table 5). On the other hand, the equivalent Young modulus of each group was obtained according following workflow depicted in Fig. 18.

The updated equivalent Young's modulus was computed as follows:

$$E_{updated} = E_{initial} \times \left(\frac{f_{i,j}^{ref}}{f_{i,j}^{num}} \right)^2 \quad (1)$$

where $E_{updated}$ is the calibrated equivalent Young Modulus; $E_{initial}$ is the initial value of the equivalent Young Modulus (homogenous section); $f_{i,j}^{ref}$ is the reference frequency (homogeneous section)

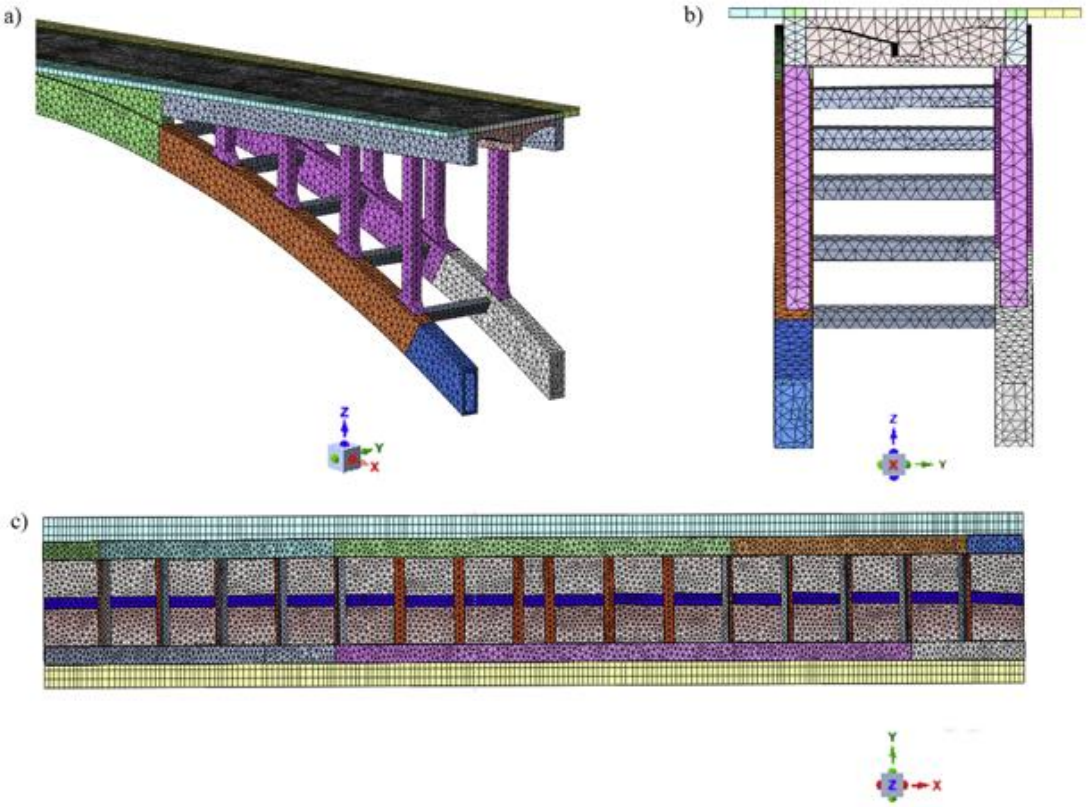

Fig. 16. Mesh of numerical model utilized: a) isometric view; b) front view and c) plant view.

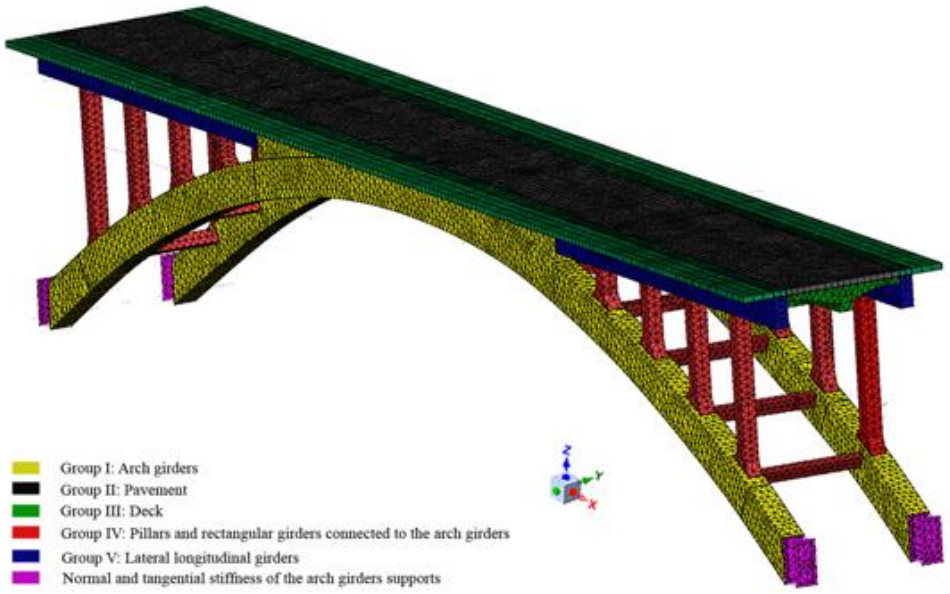

Fig. 17. Elements' groups considered during the calibration stage.

Table 5
Average, upper and lower Young Modulus and density values considered during the homogenization stage.

	Young modulus (GPa)		Density (kg/m^3)	
	Old concrete	New concrete	Old concrete	New concrete
Upper bound	62	34	2607	2217
Average	41	27	2418	2144
Lower bound	21	20	2229	2071

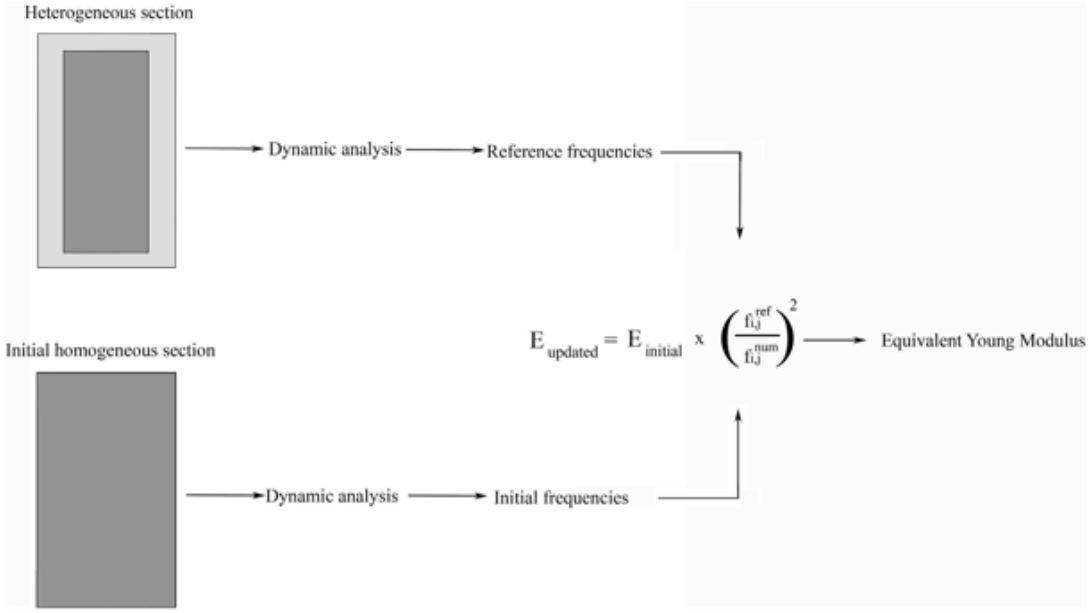

Fig. 18. Proposed workflow to obtain the equivalent Young modulus.

Table 6
Average, upper and lower equivalent Young Modulus and equivalent density values obtained during the homogenization stage.

		Upper bound	Average	Lower bound
Group I	*E* (GPa)	45	33	21
	Density (kg/m^3)	2412	2281	2150
Group III	*E* (GPa)	39	31	22
	Density (kg/m^3)	2500	2307	2114
Group IV	*E* (GPa)	30	22	13
	Density (kg/m^3)	2410	2297	2184
Group V	*E* (GPa)	33	24	15
	Density (kg/m^3)	2434	2310	2186

Table 7
Comparison between experimental and numerical frequencies and MAC values from the initial model.

Vibration modes	f_{exp} (Hz)	f_{num} (Hz)	Relative error (%)	MAC
1	4.15	5.52	32.96	0.85
2	6.52	6.31	3.07	0.97
3	9.88	10.77	8.97	0.97
4	11.53	13.61	18.06	0.75
5	11.81	26.07	120.76	0.85
6	12.34	13.69	10.92	0.81

obtained from the eigenvalue analysis of the group *i* (heterogeneous section) for the mode *j*; and $f_{i,j}^{num}$ is the frequency (homogeneous section) derived from the eigenvalue analysis of the group *i* for the mode *j*. As a result, the following equivalent values were obtained (Table 6) for the different groups considered. Concerning the Group II, the pavement ((granite blocks without mortar), the Young's modulus provided by [28] was considered equal to $E = 0.2 \pm 0.14$ GPa.

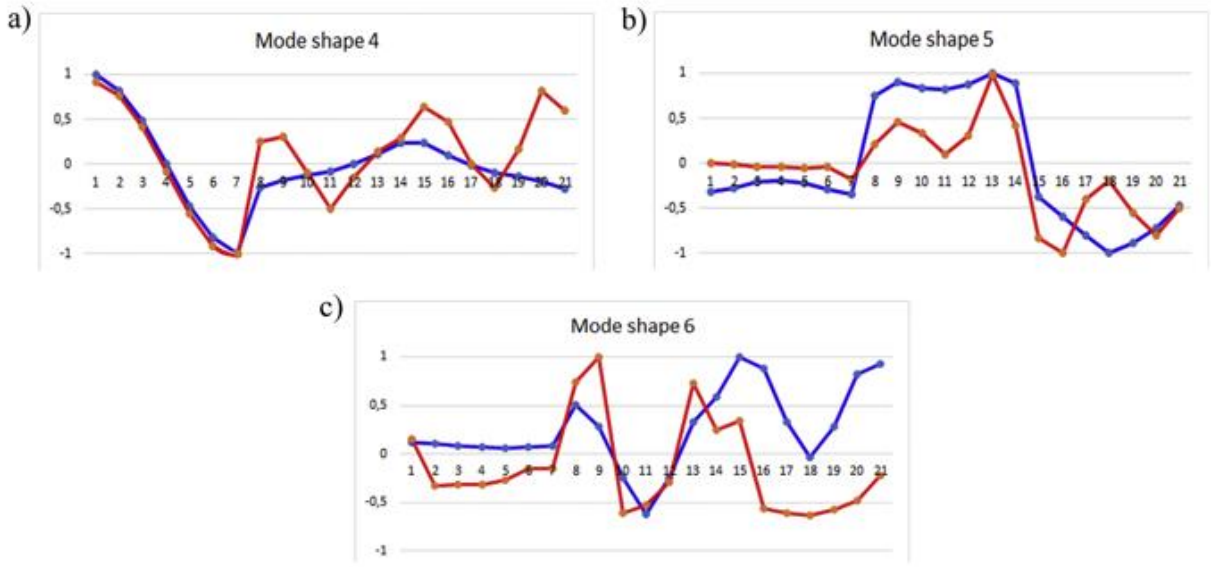

Fig. 19. Comparison between experimental and numerical modal displacements: a) mode shape 4; b) mode shape 5; and c) mode shape 6. In red the numerical modal displacements and in blue the experimental ones. The horizontal axis of the graphs represent the degree of freedoms and the vertical axis the normalized modal displacements. (For interpretation of the references to colour in this figure legend, the reader is referred to the web version of this article.)

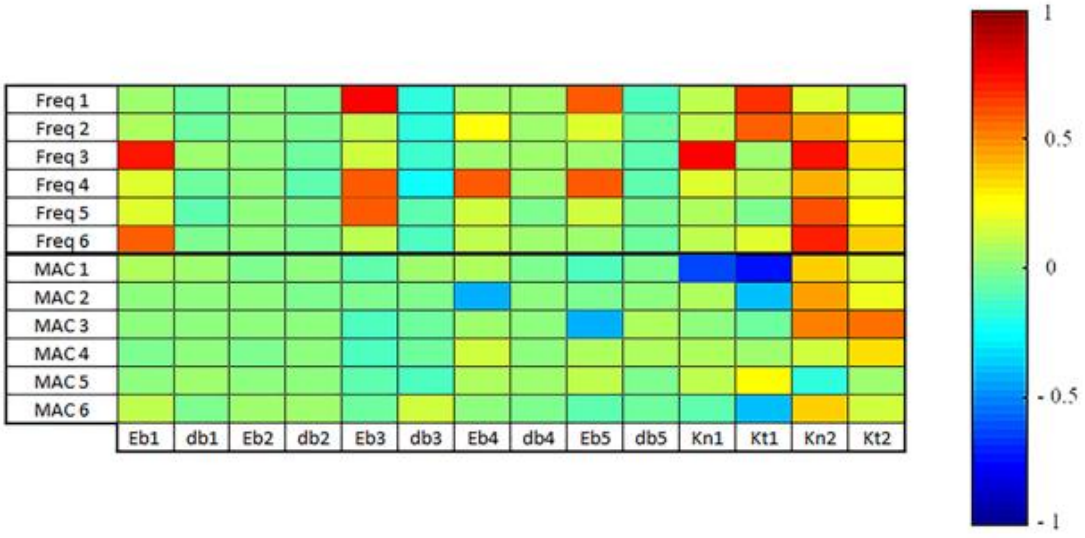

Fig. 20. Linear Spearman correlation matrix obtained during the first calibration (A).

Table 8
Updated values obtained during the DR and LS calibration.

Parameter	Upper bounds	Lower bounds	DR	LS
Eb1 (GPa)	47.95	20.59	31.08	29.96
Eb3 (GPa)	38.68	22.40	33.13	29.24
Eb4 (GPa)	29.63	22.79	29.52	28.66
Eb5 (GPa)	33.17	22.97	31.05	28.92
Kn1 (N/m^3)	1×10^{10}	1×10^{7}	1.91×10^{7}	1.36×10^{7}
Kt1 (N/m^3)	1×10^{10}	1×10^{7}	3.44×10^{8}	4.48×10^{8}
Kn2 (N/m^3)	1×10^{10}	1×10^{7}	6.14×10^{9}	6.35×10^{9}
Kt2 (N/m^3)	1×10^{10}	1×10^{7}	2.84×10^{9}	3.94×10^{9}

Table 9
Discrepancies obtained during the calibration A in terms of relative error in frequencies (f) and MAC values. In brackets, values achieved during the DR calibration.

Vibration modes	f_{exp} (Hz)	f_{num} (Hz)	Relative error (%)	MAC
1	4.15	4.19 (4.21)	1.02 (1.42)	0.93 (0.94)
2	6.51	6.42 (6.53)	1.37 (0.34)	0.97 (0.97)
3	9.88	9.53 (10.04)	3.55 (1.63)	0.97 (0.97)
4	11.53	11.71 (12.08)	1.56 (4.77)	0.83 (0.78)
5	11.81	11.57 (12.90)	2.05 (9.23)	0.88 (0.88)
6	12.34	12.64 (11.75)	2.42 (4.78)	0.82 (0.82)

4.2. Initial results

Taking into account the average equivalent Youngs' modulus obtained in Table 6, as well as the boundary conditions used during the evaluation of the Luiz Bandeira bridge erected in the same epoch and with the same construction system) [11], an initial evaluation was carried out.

To validate the accuracy of the numerical model, the relative error in frequencies and the modal assurance criterion (MAC) [29] were taken into account. Considering for these purpose, the first six frequencies and modal shapes (integrated by flexural and torsional modes). Results derived for this initial model shown a rigid structural system, especially in the transversal direction (modes 1,5,6) (Table 7), in comparison with the results obtained during the AVT.

Higher discrepancies were observer in the 4th and 6th vibrational mode (with MAC values of 0.75 and 0.81 respectively), arising from a bias, in terms of modal displacement, in the vicinity of the supports (Fig. 19). These discrepancies suggest a wrong modelling of the bridge's boundary conditions.

4.3. Finite element model updating strategy

As shown in the previous section, the first numerical simulation presented great discrepancies between the numerical and the experimental data, with an average relative error in frequencies of 32.46% and an average MAC value of 0.87, thus a calibration process able to minimize the discrepancies between the numerical and experimental modal responses was required.

From a mathematical point of view, the calibration of a numerical model can be considered as a constrained optimization problem [30], being possible to use two types of calibration methods: i) global optimization approaches or ii) local optimization algorithms. On one hand, the global optimization strategies can be used to find the global minimum of the cost function (function to be minimized), involving a high number of evaluations and thus large computational times, especially when the numerical model is complex [15]. On the other hand, local approaches can be used to find the nearest minimum of the cost function (which generally is a local minimum), using to this end a low number of evaluations, being more practical for complex simulations [14]. According with these premises, in this paper a coarse to fine calibration strategy is proposed of the following sequential stages: i) a global sensitivity analysis based on the Spearman correlation method [31] and the Latin hypercube sampling strategy [32] in order to evaluate the more sensible parameters; ii) a coarse calibration by means of the Douglas-Reid (DR) method [33] and the genetic algorithm [34]; and iii) a fine calibration through the non-linear least-squares strategy. Equation (2) define the cost function used during the calibration stage.

$$J = \frac{1}{2}\left[W_f \sum_{i=1}^{m}\left(\frac{f_i^{num} - f_i^{exp}}{f_i^{exp}}\right)^2 + W_{MAC}\sum_{i=1}^{m}(1 - MAC_i)^2\right] \quad (2)$$

where f_i^{num} and f_i^{exp} are the numerical and experimental frequencies for mode i respectively, MAC is the modal assurance criterion of the mode i, W_f is the frequency weight and W_{MAC} is the MAC weight. The values of one for the W_f and two for the W_{MAC} were considered

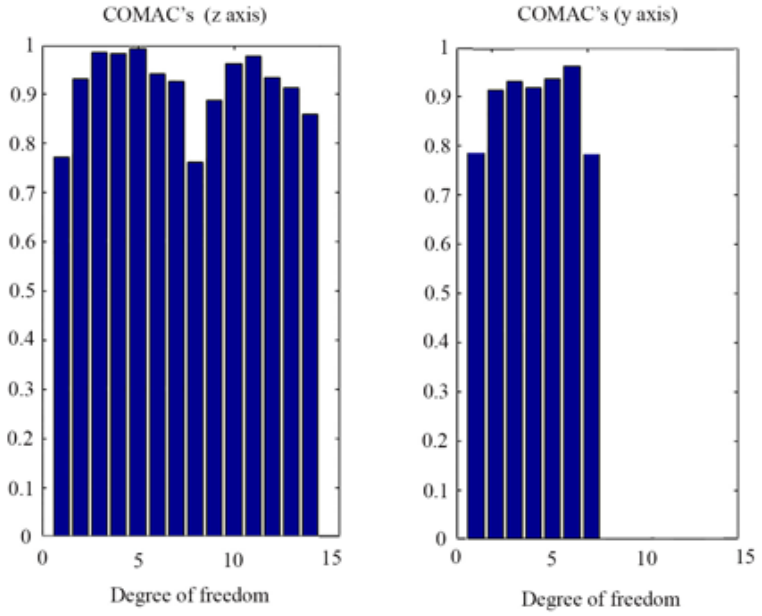

Fig. 21. COMAC values obtained during the first calibration: a) COMAC values in z axis; and b) COMAC values in y axis.

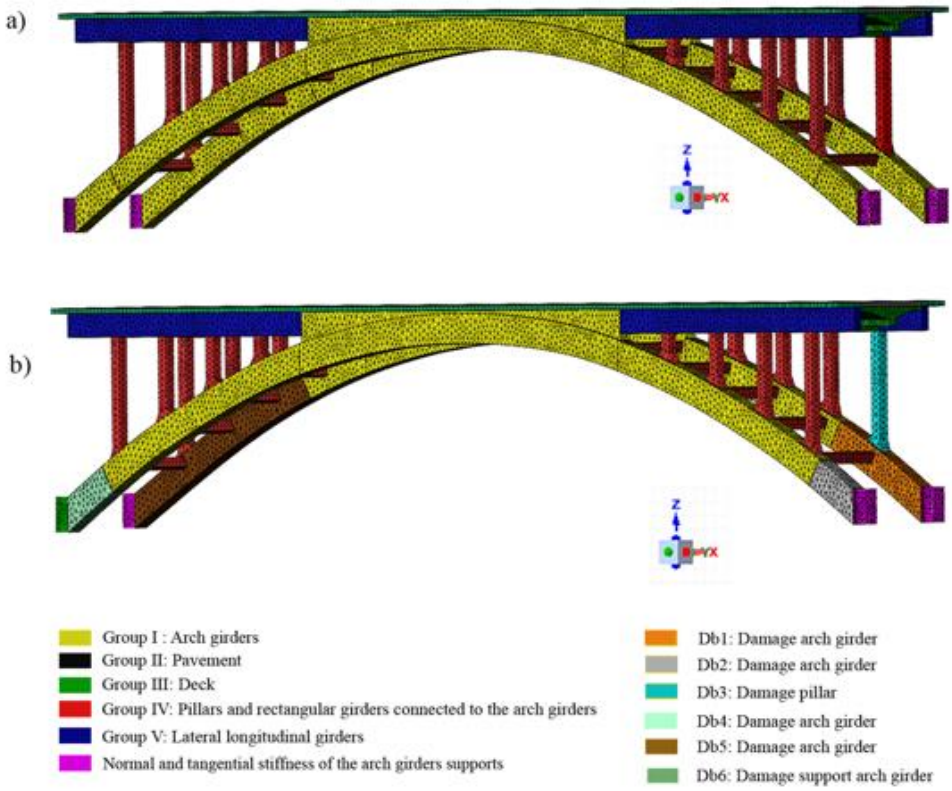

Fig. 22. Comparison between numerical models: a) numerical model 1; and b) numerical model 2.

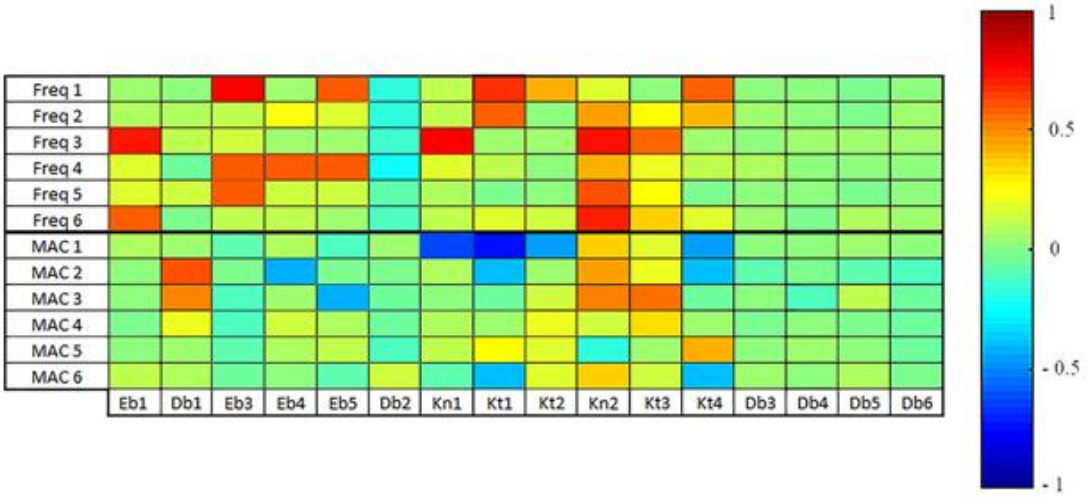

Fig. 23. Linear Spearman correlation matrix obtained during the second calibration (B).

in order to balance the contributions of the frequencies and MAC of the residuals of cost function.

With the cost function defined in (Eq. (2)), the DR algorithm was used to estimate the surface response (Eq. (3)), requiring a total of $2n + 1$ evaluations, being n the numerical variables to be calibrated.

$$R_i^{num} = \sum_{k=1}^{n}\left[A_{ik}X_k + B_{ik}X_k^2\right] + C_i \quad (3)$$

where R_i^{num} is the *ith* frequency or MAC values; A_{ik}, B_{ik} and C_i are the coefficients of the second order function; and X_k the k numerical variable applied during the calibration. Complementary to the DR algorithm, a genetic algorithm was applied to find the global minimum of the DR response surface. Finally, the global minimum of the DR response surface was refined through a the robust calibration method based on the non-linear least squares (LS), the

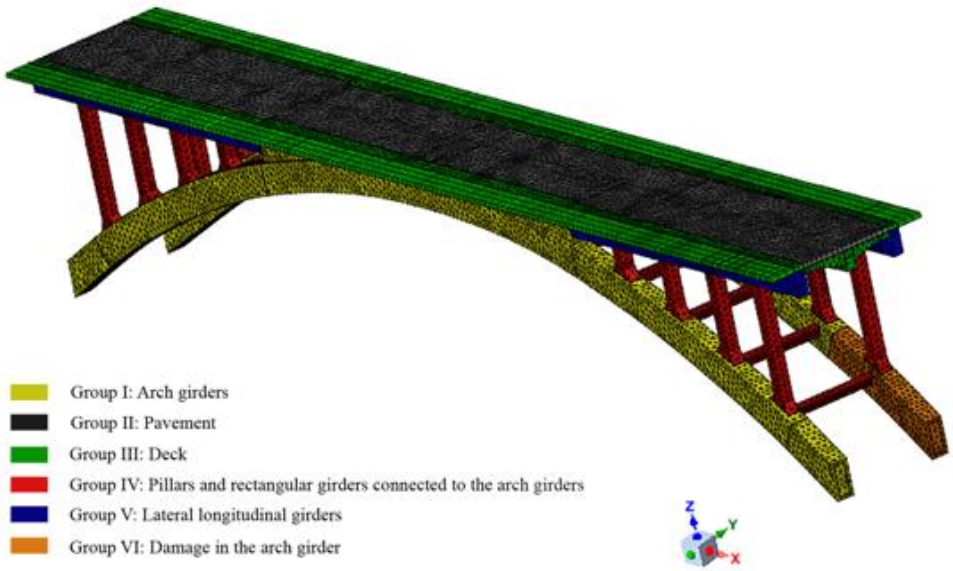

Fig. 24. Concrete groups considered during the second calibration (B).

Table 10
Discrepancies between the experimental and numerical data obtained during the second calibration stage (B). In brackets, the discrepancies of the initial model.

Vibration modes	f_{exp} (Hz)	f_{num} (Hz)	Relative error (%)	MAC
1	4.15	4.17 (5.52)	0.53 (32.96)	0.93 (0.85)
2	6.51	6.53 (6.31)	0.24 (3.07)	0.97 (0.97)
3	9.88	9.61 (10.77)	2.68 (8.97)	0.96 (0.97)
4	11.53	11.60 (13.61)	0.64 (18.06)	0.87 (0.75)
5	11.81	11.92 (26.07)	0.97 (120.76)	0.90 (0.85)
6	12.34	12.62 (13.69)	2.25 (10.92)	0.84 (0.81)

gradient-based Gauss Newton and the trust region reflective algorithms as exposed.

4.3.1. Numerical model 1: Calibration a

Considering the workflow proposed in the previous section, a global sensitivity analysis was carried out using 1500 samples (obtained through the Latin hypercube sampling method) and a total of 14 parameters, given by: i) five Young Modulus (*Eb1* to *Eb5*) and densities (*db1* to *db5*), representing the five groups previously defined (Fig. 14); ii) the normal and tangential stiffness of the deck supports (*Kn1* and *Kt1*); and iii) the normal and tangential stiffness of the arch girders supports (*Kn2* and *Kt2*).

On one hand, upper and lower bounds obtained in Table 6 were used as limits for the density and Young Modulus, respectively. On the other hand, and according with the literature [14,15,35,36], 1×10^{10} N/m^3 and 1×10^{7} N/m^3 were used as suitable upper and lower bounds, respectively, for the interface elements considered.

The sensitivity analysis (Fig. 20) revealed higher correlation coefficients, especially in the frequencies, between the dynamic response of the bridge and the support's stiffness (*Kn1, Kt1, Kn2 and Kt2*). These results corroborates the high relevance of the supports in the dynamic response of the structure in agreement with the conclusions obtained with the initial evaluation.

From the results obtained during the sensitivity analysis (Fig. 20), the following eight parameters were considered as suitable calibration variables: i) four Young Modulus, corresponding with the groups I, III, IV and V; and ii) the normal and tangential stiffness of the deck and arch girder supports.

As it was described in Section 4.3, the DR method and the genetic algorithm, with 50 individuals, 150 generations and a cross-over fraction of 0.8 according with the values used in similar works [12,37], was used to estimate the rough minimum of the cost function. The initial population used in the genetic algorithm was randomly generated by the Latin Hypercube sampling method. Finally, this minimum was refined with the LS method (Tables 8 and 9).

The average values of the calibration A (Table 8) for the relative error frequencies and MAC were 1.99% and 0.90, respectively. Comparing with the calibration performed by DR with the average values of the relative error frequencies and MAC, 3.70% and 0.89 were obtained, respectively. These results demonstrate that the LS method reduces the difference between numerical and experimental frequencies but doesn't significantly increases the MAC values.

To evaluate the possible origin of these discrepancies, the coordinate modal assurance criterion (COMAC) [29] was used. Results derived from this index show a concentration of discrepancies in the first, eighth, fifteenth and twenty-first degree of freedom (Fig. 21). These discrepancies correspond with the supports of the arch girders as well as the areas with higher concentration of damages (see Section 2.3 and Section 3.2).

4.3.2. Numerical model 2: Calibration B

Although the results obtained during the calibration A can be considered with acceptable accuracy (Table 9) (Fig. 17), a second calibration stage, named calibration B, was carried out with the aim to minimize discrepancies and to provide a more accurate numerical simulation.

Considering the results obtained during the AVT, with asymmetric modes (Fig. 14), as well as the high discrepancies observed in the first, eighth, fifteenth and twenty-first degrees of freedom (Fig. 17), additional parameters were introduced in the sensitivity analysis, namely (Fig. 22): i) damages in the arch girders, *db1, db2,*

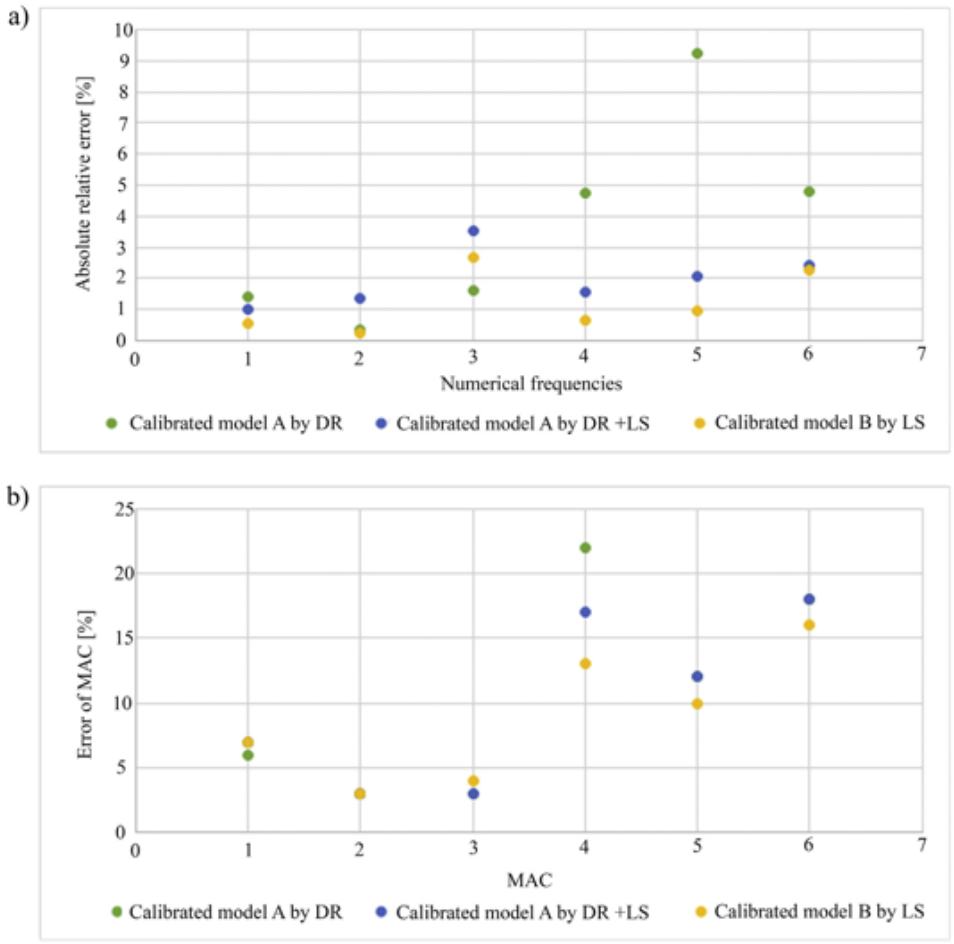

Fig. 25. Errors obtained during the different calibrations (A, B): a) Absolute relative error in frequencies; b) Relative error in MAC values.

Table 11
Updated values obtained during the different calibration stages.

Parameter	Upper bounds	Lower bounds	Calibration A	Calibration B
Eb1 (GPa)	47.95	20.59	29.96	29.79
Db1 (GPa)	47.95	20.59	29.96	27.80
Eb3 (GPa)	38.68	22.40	29.24	30.07
Eb4 (GPa)	29.63	22.79	28.66	27.92
Eb5 (GPa)	33.17	22.97	28.92	28.60
Kn1 (N/m^3)	1×10^{10}	1×10^{7}	1.36×10^{7}	1.04×10^{7}
Kt1 (N/m^3)	1×10^{10}	1×10^{7}	4.48×10^{8}	5.60×10^{8}
Kt2 (N/m^3)	1×10^{10}	1×10^{7}	4.48×10^{8}	4.22×10^{8}
Kn2 (N/m^3)	1×10^{10}	1×10^{7}	6.35×10^{9}	6.24×10^{9}
Kt3 (N/m^3)	1×10^{10}	1×10^{7}	3.94×10^{9}	4.34×10^{9}
Kt4 (N/m^3)	1×10^{10}	1×10^{7}	3.94×10^{9}	3.95×10^{9}

db4 and *db5* (Fig. 6) (Fig. 7a) (Fig. 7b); ii) damage in a support of the arch girder B, *db6* (Fig. 7d) and iii) damages in a pillar, *db3* (Fig. 7c).

From the evaluation of the Spearman correlation matrix (Fig. 23) two additional considerations were taken into account to improve the numerical calibration: i) the parameter *Db1*; and ii) an orthotropic behaviour of the supports. Therefore, in this analysis 12 calibration variables were considered (Fig. 24): i) 9 from the calibration A; ii) one variable that represent the damage on the arch girder; and iii) two additional shear stiffness on the deck and on arch girders supports. For this second calibration, only the robust calibration (LS method) was used. Using as starting values the results obtained during the calibration A. Thus, a more accurate simulation of the bridge, with an average relative error in frequencies of 1.2% and an average MAC value of 0.91 (Table 10) (Fig. 25), was obtained.

Concerning the updated parameters achieved in the different calibrations carried out (Table 11), especially the Young's Modulus variables (average value of 28.84 GPa), it is possible to corroborate a generalized damage of the new concrete layer observed during the visual inspection carried out (see Section 2.3) showed similar results that those obtained in Section 4.1 (average value of 30.81 GPa). In what regards to the calibrated stiffness, low values were obtained on the deck in the normal direction (1.04×10^7 N/m^3) with respect to the tangential stiffness (4.91×10^8 N/m^3) where obtained and higher values for the interfaces that define the interaction between the arch girders and the abutments (average value of 4.84×10^9 N/m^3).

Finally, Fig. 26 shows a graphical comparison between the experimental and numerical mode shapes. Analysing all results, one can conclude that the results derived from the second approach show a reasonable better correlation with the ones obtained from AVT (Figs. 25 and 26), especially for the

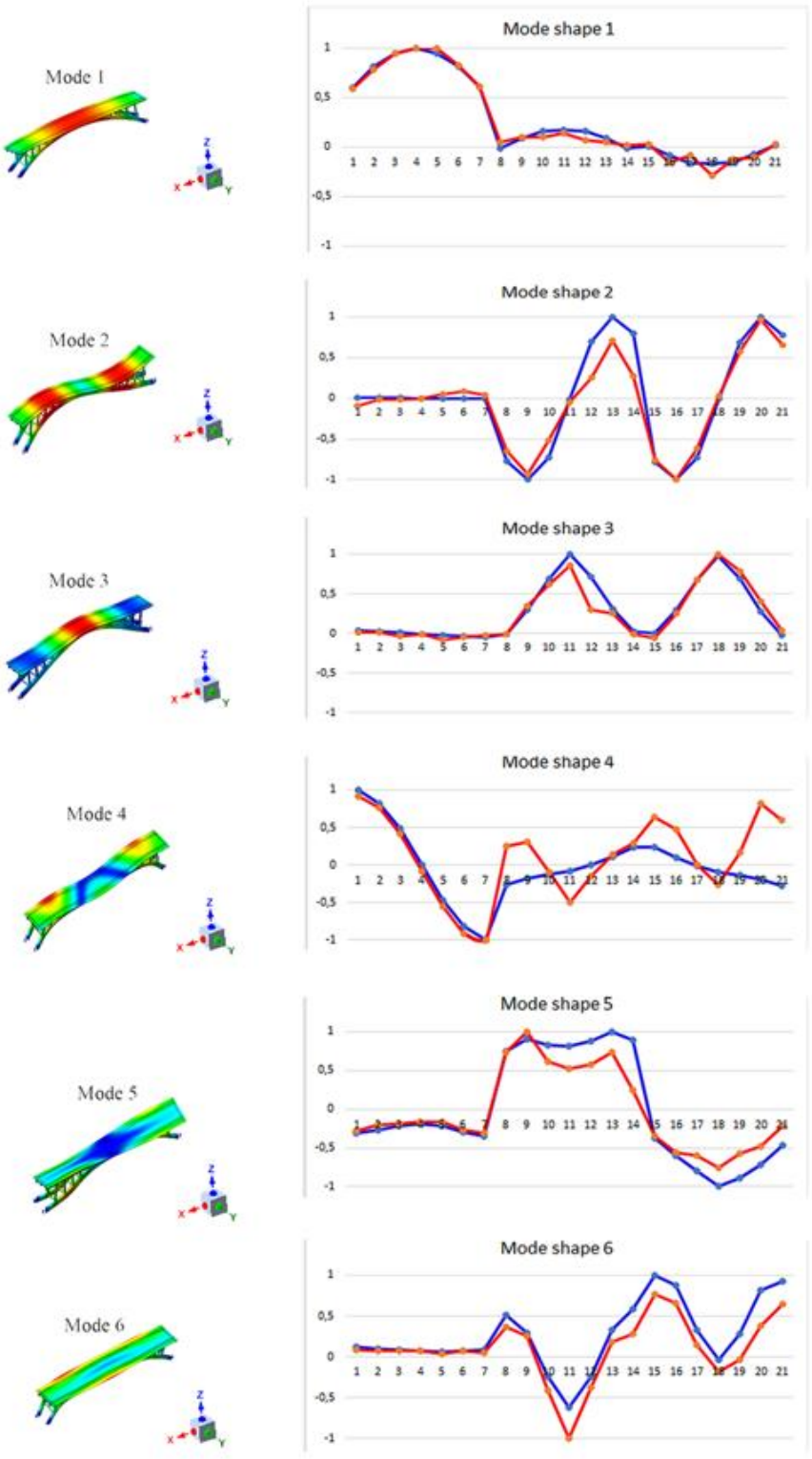

Fig. 26. Graphical comparison between experimental and numerical modal shapes obtained in the second.

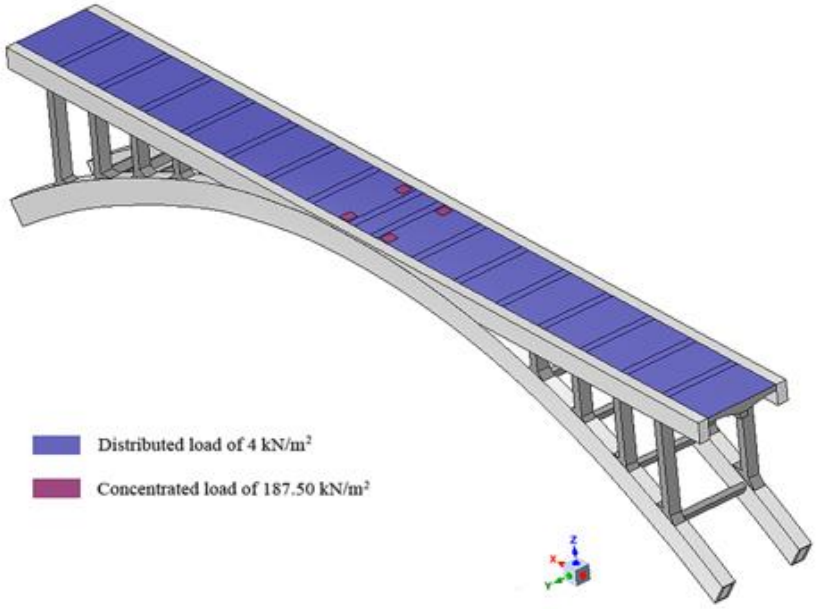

Fig. 27. Considered loads according with LM-1 of Eurocode.

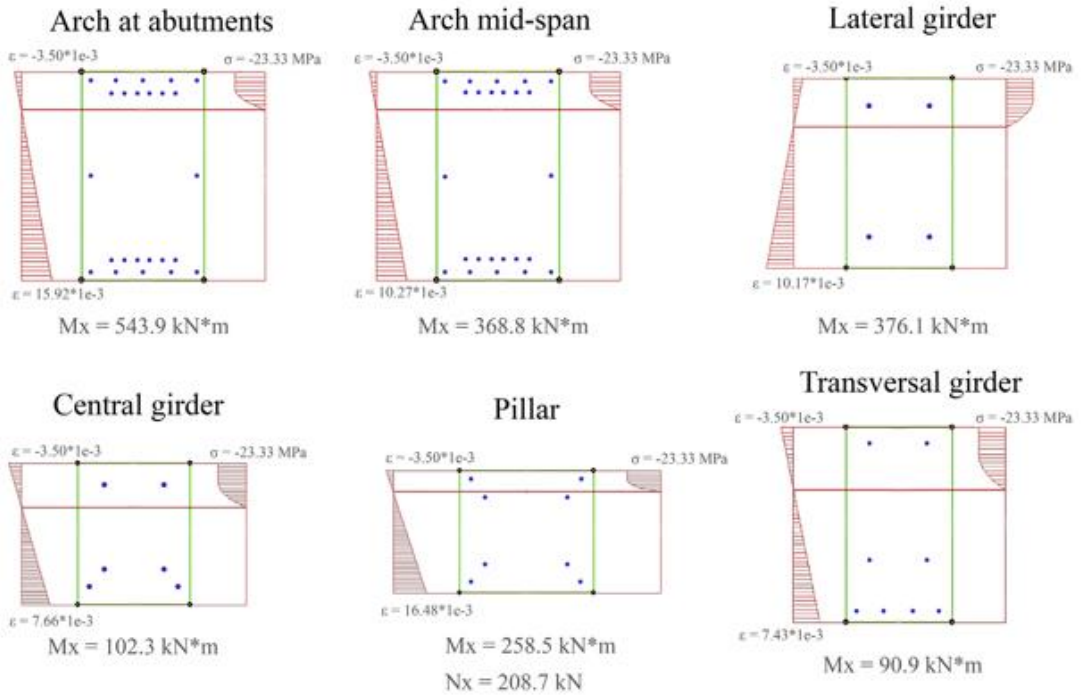

Fig. 28. Maximum flexural capacity of structural members and maximum compression axial force in the pillars. Results obtained by CSA analysis [42].

discrepancies observer in the 4th and 6th vibrational modes, corroborating the high influence of the boundary conditions in the dynamical response of the structure. It is worth mentioning that the discrepancies observed in the present numerical model that are concentred in local points (Fig. 26); can be attributed to the casting phases. These results requires further improvements of the numerical model.

5. Safety analysis

Considering the last calibrated model as the most accurate numerical representation of the bridge, an evaluation of the Ultimate Limit State (ULS) was carried out following the Eurocode recommendations [38–41]. During this evaluation, the maximum flexural capacity of each structural component and the

Table 12
Results obtained from the non-calibrated ideal model and the last calibrated numerical model during the static safety evaluation.

Structural elements	Action values of the ideal model	Action values of the calibrated model	Resistance values
$Mx_{Arch\_abutments}$	153.5 kN.m	180.3 kN.m	543.9 kN.m
$Mx_{Arch\_mid\text{-}span}$	125.3 kN.m	177.3 kN.m	368.8 kN.m
$Mx_{\_Lateral\ girder}$	64.4 kN.m	42.3 kN.m	376.1 kN.m
$Mx_{\_Central\ girder}$	18.9 kN.m	14.9 kN.m	102.3 kN.m
$Mx_{\_Pillar}$	57.6 kN.m	58.1 kN.m	258.5 kN.m
$N_{\_Pillar}$	67.6 kN	71.5 kN	208.7 kN
$Mx_{\_Transversal\ girder}$	30.3 kN.m	14.2 kN.m	90.9 kN.m

Table 13
Safety factors obtained from the ideal model and the last calibrated numerical model during the static safety evaluation.

Structural elements	Safety factors of the ideal model	Safety factors of the calibrated model
$Mx_{Arch\_abutments}$	3.5	3
$Mx_{Arch\_mid\text{-}span}$	2.9	2.1
$Mx_{\_Lateral\ girder}$	5.8	8.9
$Mx_{\_Central\ girder}$	5.4	6.9
$Mx_{\_Pillar}$	4.5	4.4
$N_{\_Pillar}$	3.1	2.9
$Mx_{\_Transversal\ girder}$	3	6.4

compression axial forces in the pillars were compared (resistance values) with the moments and the compression axial forces obtained by the numerical simulations (action values).

The static safety analysis was performed considering the current limitations of the bridge (maximum weight of 117.68 kN, maximum height of 3.50 m and 2.50 m of maximum width). A modification of the loads proposed in the Load Model 1 (LM-1) (Fig. 27) was considered [40], namely: i) gravity load; ii) LM-1 distributed load of 4.00 kN/m^2; and iii) LM-1 concentrated load of 187.50 kN/m^2 (area of the wheels of 0.16 m^2 according with LM-1 of Eurocode).

Loads were combined applying the Eurocode, where the safety factors for the most unfavourable case were considered (1.2 for gravity load and 1.5 for distributed load and concentrated load), obtaining the flexural moments of all structural elements and the compression axial force in the pillars (Fig. 28).

Results obtained from the safety evaluation shown that the most critical structural elements are the arch girders with a safety factor of 2.1 at the mid-span (Tables 12 and 13) (Fig. 29), verifying all the structural elements the ULS. These results were compared with those arose from a numerical simulation of an ideal model (model obtained from the historical plans and with the boundary conditions and material's properties considered in the first numerical simulation), showing large discrepancies, especially in the arch (17% more) and in the deck's girders (21% lower).

Regarding the seismic safety analysis, the desing ground acceleration was calculated according with the Eurocode 8 [43]. Being its value the results of the following considerations: i) a peak ground acceleration of 0.35 m/s^2; ii) a ground type A and; iii) an importance factor for buildings of 1. As a result, a desing ground acceleration of 0.35 m/s^2 was obtained, not being necessary the seismic verification of the bridge (0.35 m/s^2 < 0.04g, being g the gravity acceleration).

6. Conclusions

This paper proposed a multidisciplinary approach focused on the evaluation of the current safety conditions of historic bridges erected in reinforcement concrete. The method combines terrestrial laser scanning procedures, ambient vibration approaches, laboratory tests (e.g. scanning electron microscope and compression tests), advanced numerical simulation, by means of the FEM method, and a cost-optimized calibration strategy with the aim of characterizing the bridge at geometrical, material and structural level. With this approach several conclusions and advantages emerged when evaluating historic bridges, such as: i) the creation

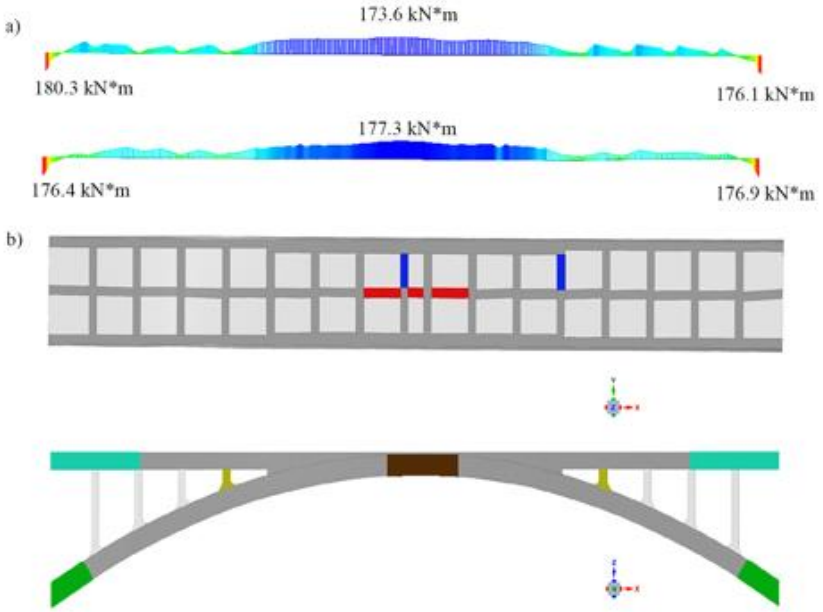

Fig. 29. Results obtained during the safety evaluation: a) graphical representation of the flexural moments (arch girders) obtained though the FEM; and b) structural components evaluated.

of as-built CAD models suitable for numerical simulations; ii) the automatic alignment between the geometrical data, the point cloud, and the data provided by the dynamic identification and; iii) the use of a cost-optimized calibration strategy.

To corroborate the robustness of the proposed method, an early reinforcement concrete bridge was chosen as study case: the Bôco Bridge in the north of Portugal. The method was able to create an accurate numerical simulation of the current state of the bridge, representing correctly the geometry of the structure, its material's properties and boundary conditions. The cost-optimized method used to calibrate the model, based on a coarse (DR and genetic algorithm) to fine (LS approach) methodology, allowed the reduction of the relative error in frequencies from an initial value of 32.46% to 1.22%, increasing the average MAC value from 0.87 to 0.91, spending a total of 5246 s (780 s in DR approximation and 4466 s during LS optimization) for the first calibration and 4704 s (only with LS method) for the second one in a processor Intel® XEON E3-1240 v3 at 3.4 Ghz and 8Gb RAM DDRII.

With respect to the safety conditions, the static analysis shown a bridge with enough capacity to bear the current solicitations on which the most critical structural part was the arch girder in mid-span with an estimated safety factor of 2.1 (value 17% lower than the safety factor obtained from a numerical simulation built with the ideal geometry, the average values of the concrete derived from the tests carried out and hypothetical support's conditions). Additionally, the studies carried out concluded that it is not necessary to take into account the seismic actions on the safety evaluation due to the low seismicity of the area.

Futures works will be focused on several fields: i) the application of additional NDT tests such as sonic and ultrasonic or rebar detector tests with the aim of improving the knowledge about the materials used in the Bôco Bridge; ii) the use of close-range aerial photogrammetry approaches (Unmanned Aerial Vehicles and Structure from Motion) to complement the TLS's point cloud with the aim of digitalizing all those areas not captured by this sensor (areas not visible from the ground); iii) the refinement of the numerical model according with the discrepancies observed in the second model calibration (punctual discrepancies), considering different the constructions and casting phases; iv) further calibrations including transient analysis with traffic actions and; v) nonlinear numerical evaluations by means of the push-over and the non-linear static analysis. Additionally, several radiometric classifications (by means of pixel-based approaches), based on the data captured by the TLS system, will be carried out to complete the damage diagnosis of the bridge.

Acknowledgments

This work was financed by ERDF funds through the V Sudoe Interreg program within the framework of the HeritageCARE project, Ref. SOE1/P5/P0258 and the Competitiveness Factors Operational Programme – COMPETE. This research has been also partially supported by CHT2 – Cultural Heritage through Time – funded by JPI CH Joint Call and supported by the Ministerio de Economia y Competitividad, Ref. PCIN-2015-071 and by national funds through FCT – Foundation for Science and Technology within the scope of the project POCI-01-0145-FEDER-007633.

References

[1] H. González-Jorge, D. Gonzalez-Aguilera, P. Rodriguez-Gonzalvez, P. Arias, Monitoring biological crusts in civil engineering structures using intensity data from terrestrial laser scanners, Constr. Build. Mater. 31 (2012) 119–128, https://doi.org/10.1016/j.conbuildmat.2011.12.053.
[2] F. Leonhardt, Bridges, 1984 ISBN: 0-262-12105-0.
[3] A. Hellebois, A. Launoy, C. Pierre, M. De Lanève, B. Espion, 100-year-old Hennebique concrete, from composition to performance, Constr. Build. Mater. 44 (2013) 149–160, https://doi.org/10.1016/j.conbuildmat.2013.03.017.
[4] J.-L. Bosc, J.-M. Chauveau, J. Clément, J. Degenne, B. Marrey, M. Paulin, Joseph Monier et la naissance du ciment armé, Ed. du Linteau 2001.
[5] M.L. Gambhir, Concrete Technology: Theory and Practice, Tata McGraw-Hill Education, 2013. ISBN: 1259062554, 9781259062551.
[6] F.P. Glasser, J. Marchand, E. Samson, Durability of concrete—degradation phenomena involving detrimental chemical reactions, Cem. Concr. Res. 38 (2) (2008) 226–246, https://doi.org/10.1016/j.cemconres.2007.09.015.
[7] J. Sena-Cruz, J.C. Araújo, F. Castro, M. Jorge, Assessment of the bôco historical RC bridge, SAHC2012–Structural Analysis of Historical Constructions (2012) 2214-2221 ISBN: 978-83-7125-216-7.
[8] M. Stavroulaki, B. Riveiro, G. Drosopoulos, M. Solla, P. Koutsianitis, G.E. Stavroulakis, Modelling and strength evaluation of masonry bridges using terrestrial photogrammetry and finite elements, Adv. Eng. Softw. 101 (2016) 136–148, https://doi.org/10.1016/j.advengsoft.2015.12.007.
[9] B. Conde, L.F. Ramos, D.V. Oliveira, B. Riveiro, M. Solla, Structural assessment of masonry arch bridges by combination of non-destructive testing techniques and three-dimensional numerical modelling: application to Vilanova bridge, Eng. Struct. 148 (2017) 621–638, https://doi.org/10.1016/j.engstruct.2017.07.011.
[10] M. Herrero-Huerta, D. González-Aguilera, P. Rodriguez-Gonzalvez, D. Hernández-López, Vineyard yield estimation by automatic 3D bunch modelling in field conditions, Comput. Electron. Agric. 110 (2015) 17–26, https://doi.org/10.1016/j.compag.2014.10.003.
[11] J. Sena-Cruz, R.M. Ferreira, L.F. Ramos, F. Fernandes, T. Miranda, F. Castro, Luiz Bandeira Bridge: assessment of a Historical Reinforced Concrete (RC) Bridge, Int. J. Archit. Heritage 7 (6) (2013) 628–652, https://doi.org/10.1080/15583058.2012.654895.
[12] D. Ribeiro, R. Calçada, R. Delgado, M. Brehm, V. Zabel, Finite element model updating of a bowstring-arch railway bridge based on experimental modal parameters, Eng. Struct. 40 (2012) 413–435, https://doi.org/10.1016/j.engstruct.2012.03.013.
[13] T. Türker, A. Bayraktar, Structural safety assessment of bowstring type RC arch bridges using ambient vibration testing and finite element model calibration, Measurement 58 (2014) 33–45, https://doi.org/10.1016/j.measurement.2014.08.002.
[14] L.J. Sánchez-Aparicio, L.F. Ramos, J. Sena-Cruz, J.O. Barros, B. Riveiro, Experimental and numerical approaches for structural assessment in new footbridge designs (SFRSCC–GFPR hybrid structure), Compos. Struct. 134 (2015) 95–105, https://doi.org/10.1016/j.compstruct.2015.07.041.
[15] T. Zordan, B. Briseghella, T. Liu, Finite element model updating of a tied-arch bridge using Douglas-Reid method and Rosenbrock optimization algorithm, J. Traffic Transp. Eng. (English Edition) 1 (4) (2014) 280–292, https://doi.org/10.1016/S2095-7564(15)30273-7.
[16] M.d.O. Publicas, "Ponte do Bôco" Direcção Geral dos Serviços de Urbanização, (1962).
[17] H. Yoon, H. Song, K. Park, A phase-shift laser scanner based on a time-counting method for high linearity performance, Rev. Sci. Instrum. 82 (7) (2011) 075108, https://doi.org/10.1063/1.3600456.
[18] A. Bienert, H.-G. Maas, Methods for the automatic geometric registration of terrestrial laser scanner point clouds in forest stands, Int. Arch. Photogramm. Remote Sens. Spatial Inf. Sci. 38 (part 3) (2009). W8.
[19] V.-S. Nguyen, A. Bac, M. Daniel, Simplification of 3D point clouds sampled from elevation surfaces, (2013) ISBN: 978-80-86943-75-6.
[20] D. Branch, L.C. Dang, N. Hall, W. Ketchum, M. Melakayil, J. Parrent, M. Troxel, D. Casebeer, D.J. Jeffery, E. Baron, Comparative direct analysis of type Ia supernova spectra. II. Maximum light, Publ. Astron. Soc. Pac. 118 (842) (2006) 560.
[21] I. Guskov, Z.J. Wood, Topological noise removal, 2001 Graphics Interface Proceedings: Ottawa, Canada, 19 (2001).
[22] R. Brincker, L. Zhang, P. Andersen, Modal identification from ambient responses using frequency domain decomposition, Proc. of the 18thInternational Modal Analysis Conference (IMAC), San Antonio, Texas, (2000).
[23] L.P. Standard, E397–1993, OPC concrete: Determination of elastic modulus in compression (1993).
[24] N. EN, 12390-3: 2003–Ensaios do betão endurecido, Resistência à compressão dos provetes. Lisboa.
[25] C.E. de Normalisation, EN 1992–1–1 Eurocode 2: Design of Concrete Structures, Part I-1: Generai Rules and Rules for Buildings, CEN, Brussels, 2004.
[26] N. Chouw, A. Pipinato, Dynamics of bridge structures, Innovative Bridge Des. Handb. (2016) 127–153.
[27] T. Diana, DIANA-finite element analysis, The Netherlands (2005).
[28] A. Kasahara, S. Matsuno, Estimation of apparent elastic modulus of concrete block layer, Proceedings of 3rd International Conference on Concrete Block Paving, 1988, pp. 142–147.
[29] R.J. Allemang, The modal assurance criterion–twenty years of use and abuse, Sound vib. 37 (8) (2003) 14–23.
[30] E. Simoen, G. De Roeck, G. Lombaert, Dealing with uncertainty in model updating for damage assessment: a review, Mech. Syst. Sig. Process. 56 (2015) 123–149, https://doi.org/10.1016/j.ymssp.2014.11.001.
[31] L. Myers, M.J. Sirois, Spearman Correlation Coefficients, Differences Between, Wiley StatsRef: Statistics Reference Online (2006), https://doi.org/10.1002/9781118445112.stat02802.

[32] M.D. McKay, R.J. Beckman, W.J. Conover, Comparison of three methods for selecting values of input variables in the analysis of output from a computer code, Technometrics 21 (2) (1979) 239–245, https://doi.org/10.1080/00401706.1979.10489755.
[33] B.M. Douglas, W.H. Reid, Dynamic tests and system identification of bridges, J. Struct. Div. 108 (ST10) (1982).
[34] D.E. Goldberg, Genetic algorithms, Pearson Education India 2006 ISBN: 817758829X, 9788177588293.
[35] X. Chen, P. Omenzetter, S. Beskhyroun, Calibration of the Finite Element Model of a Twelve-Span Prestressed Concrete Bridge Using Ambient Vibration Data, EWSHM-7th European Workshop on Structural Health Monitoring, 2014.
[36] D.-S. Jung, C.-Y. Kim, Finite element model updating on small-scale bridge model using the hybrid genetic algorithm, Struct. Infrastruct. Eng. 9 (5) (2013) 481–495, https://doi.org/10.1080/15732479.2011.564635.
[37] C. Costa, D. Ribeiro, P. Jorge, R. Silva, A. Arêde, R. Calçada, Calibration of the numerical model of a stone masonry railway bridge based on experimentally identified modal parameters, Eng. Struct. 123 (2016) 354–371, https://doi.org/10.1016/j.engstruct.2016.05.044.
[38] B.S. Institution, Eurocode 0 - Basis of structural design, BSI2004.
[39] E. STN Eurocode 1: Actions on structures, Part 1–1: General actions, Densities, self-weight, imposed loads for buildings, Slovak Office of Standards, Metrology and Testing (2007).
[40] C. Eurocode, 1: Actions on structures, Part 2: Traffic loads on bridges, Brussels: European Standard EN 2 (1991) 2003.
[41] C.R. Hendy, D.A. Smith, Designers' guide to EN 1992–2: Eurocode 2: design of concrete structures, Concr. Bridges (2007). Thomas Telford.
[42] H. Miranda, Á.F. Azevedo, J. Sena-Cruz, Cálculo orgânico de secções quaisquer em flexão desviada segundo o Eurocódigo 2, Encontro Nacional Betão Estrutural 2008: Actas (2008) 1–10.
[43] N. EN, 1 (2010) Eurocódigo 8: Projecto de estruturas para resistência aos sismos, Parte 1: Regras gerais, acções sísmicas e regras para edifícios, Lisboa: IPQ. 230p (1998).

Medios y métodos no destructivos para el diagnóstico estructural de puentes de arco de mampostería.

El artículo científico publicado en este apartado es una continuación en el desarrollo de la presente Tesis Doctoral. Dentro de las normas defendidas por la Carta Internacional del Restauro de Cracovia, esta publicación propone una innovadora metodología multidisciplinar totalmente no destructiva para caracterizar puentes de arco de mampostería desde los puntos de vista geométrico, material y estructural.

Esta metodología propuesta integra el sensor geomático láser escáner terrestre, el sensor geofísico georradar, los métodos de Impacto-Eco y ensayos sónicos indirectos, el método del Análisis Multicanal de Ondas Superficiales (MASW) y ensayos de vibración ambiental (AVT). Todos estos datos son combinados con procedimientos de ingeniería inversa, permitiendo así crear modelos CAD adecuados para llevar a cabo simulaciones numéricas avanzadas. Además, estos modelos numéricos son comparados y calibrados por medio de los datos obtenidos de los AVT. Con el fin de validar esta metodología propuesta, el puente Romano de Ávila es utilizado como caso de estudio. Este puente histórico presenta una mezcla compleja de técnicas constructivas (dos mamposterías, material de relleno cohesivo, material de relleno *Opus Caementicium*, y una losa de hormigón reforzado). De esta manera, ha sido posible llevar a cabo un análisis estructural predictivo en el modelo numérico de este puente histórico.

Cabe señalar que la integración del método no invasivo MASW demuestra su efectividad en la caracterización de los parámetros mecánicos y físicos de los dos materiales de relleno que presenta este puente, así como la estimación de la profundidad de cada uno de ellos por medio de las velocidades de las ondas de corte obtenidas con este método.

Palabras clave: Construcciones históricas; Puente de arco de mampostería; Ensayos no destructivos; Ensayos sónicos; Análisis Multicanal de Ondas Superficiales; Georadar; Ensayos de vibración ambiental; Método de los Elementos Finitos; Análisis no-lineal.

Automation in Construction 104 (2019) 360–382

Contents lists available at ScienceDirect

Automation in Construction

journal homepage: www.elsevier.com/locate/autcon

Non-destructive means and methods for structural diagnosis of masonry arch bridges

Luis Javier Sánchez-Aparicio[a,*], Álvaro Bautista-De Castro[a], Borja Conde[b], Pedro Carrasco[a], Luís F. Ramos[c]

[a] Department of Cartographic and Land Engineering, University of Salamanca, High Polytechnic School of Ávila, Hornos Caleros, 50, 05003, Ávila, (Spain)
[b] University of Vigo, School of Industrial Engineering, Department of Engineering Materials, Applied Mechanics and Construction, Vigo, Spain
[c] ISISE, Department of Civil Engineering, University of Minho, Campus de Azurém, 4800-058 Guimarães, Portugal

ARTICLE INFO

Keywords:
Historical constructions
Masonry arch bridge
Non-destructive testing
Terrestrial laser scanner
Sonic testing
Multichannel analysis of surface waves
Ground penetrating radar
Ambient vibration tests
Finite element method
Non-linear analysis

ABSTRACT

Within the precepts defended by the International Charter of Kraków, this paper aims at presenting a fully non-destructive multidisciplinary approach able to characterize masonry bridges at three different levels: i) geometrical level; ii) material level and; iii) structural level. To this end, this approach integrates the terrestrial laser scanner, the sonic and impact-echo methods, the ground penetrating radar and the multichannel analysis of surface waves. All these data are combined with reverse engineering procedures, allowing the creation of suitable as-built CAD models for advanced numerical simulations. Then, these numerical models are contrasted and updated through the data provided by the ambient vibration tests. To validate the methodology proposed in this paper, the Roman bridge of Avila was used as study case. This bridge shows a complex mixture of constructive techniques (masonry, cohesive material, *Opus Caementicium* and reinforced concrete). Thus, the numerical model was considered for performing predictive structural analysis.

1. Introduction

Among the wide variety of constructive typologies that make up our historical legacy, masonry arch bridges have been placed as one of the most important elements through history, being still an essential part within the current communication networks. Many of these ancient constructions are at present day enduring potentially destructive conditions due to new traffic loads, large vibrations, foundation settlements, extreme natural events (e.g., earthquakes, river overflows or floods) and environmental agents (e.g., the presence of high levels of moisture or melting salts) [1]. The combination of these effects progressively induces the deterioration of the materials and the development of damage phenomena such as cracks or permanent deformations [2–4]. Because of this it is necessary to carry out a comprehensive structural diagnosis in order to know the current and the future structural condition of these types of infrastructures and consequently, designing proper conservation or restoration actions.

Among the different numerical modeling strategies proposed so far to evaluate masonry arch bridges mechanical behavior, from the Limit Analysis theory to the Discrete Element Method, the Finite Element Method [4] has been considered as one of the most powerful. This approach has allowed to simulate successfully masonry bridges under different casuistic such as settlements [2], pier scours [5], seismic actions and live loads [6–10], being possible to replicate the damages that appears along the history of the construction [2,11].

Despite this potential, one of the major drawbacks of this computational modeling approach is that it requires extensive knowledge of the physical and mechanical properties of the materials present on the structure, and thus the need of using multidisciplinary approaches to collect the required input data [12]. Under this framework, several studies in the past have focused on the development of multidisciplinary strategies targeted to characterize masonry arch bridges at different levels [8,13–15]: i) at a geometrical level; ii) at a material level and; iii) at the structural system level.

Concerning the first level, i.e., the geometry, this type of construction is typically characterized by its high complexity in terms of size, location, and inner composition. To face these challenges, the most widespread sensors are the terrestrial laser scanner and digital cameras. Through the terrestrial laser scanning and the photogrammetric method, they are extensively used to determine the external envelope of this typology of bridges [13,15–21]. The product obtained from these geomatic sensors, the so-called point cloud, is then employed for the

* Corresponding author.
E-mail addresses: luisj@usal.es (L.J. Sánchez-Aparicio), alvarobautistadecastro@usal.es (Á. Bautista-De Castro), bconde@uvigo.es (B. Conde), retep81@usal.es (P. Carrasco), lramos@civil.uminho.pt (L.F. Ramos).

https://doi.org/10.1016/j.autcon.2019.04.021
Received 3 January 2019; Received in revised form 23 April 2019; Accepted 24 April 2019

creation of CAD models suitable for structural analysis by means of the following approaches [22]: i) creation of CAD models based on sections and individual measurements coming from the point cloud obtained [8,11,17,21]; ii) meshing of the point cloud and creation of the CAD model based on the mesh [22–24] and; iii) creation of non-uniform rational b-splines from the point cloud [24,25]. Additionally, it is possible to find in the recent literature procedures able to exploit the concept of the point cloud voxelization such as the Cloud2FEM procedure proposed by Castellazzi et al. [11,26,27]. These procedures are able to generate a numerical mesh from the point cloud in a semi-automatic way. However, these methods require a point cloud with few holes and tend to generate numerical meshes with a large number of elements. Besides, the presence existing permanent deformations can hardly be captured by means of these methods. In contrast to these strategies, it is possible to find approaches based on the latest advances in reverse engineering. These approaches exploit methods such as the extrusion of surfaces or b-splines to represent CAD models in which it is possible to control the level of detail [12,28]. Complementary to these techniques, the ground penetrating radar method has also been extensively used in order to characterize the inner composition of masonry arch bridges, such as the thickness of the barrel vaults or the layering of the infill materials [6,13,19,20,29].

Regarding the second level, the characterization of the constituent materials, masonry arch bridges present two main components: i) the masonry and; ii) the infill. Firstly, the masonry is used to build the main load-bearing parts of the bridge, such as the barrel vaults, spandrel walls and piers as well as other secondary elements such as buttresses or cutwaters. Masonry mechanical properties can be characterized resorting to laboratory tests (e.g., compression tests) or even in-situ tests using the flat-jack tests. On the one hand, the first approach is very time-consuming, since it requires the confection of several masonry samples. On other hand, the flat-jack tests are invasive, requiring the preparation of a slot through which a thin envelope-like bladder is inserted and pressurized with a fluid. Thus, as an alternative, the sonic testing approach has recently emerged as a suitable non-destructive testing technique aimed at determining the physical and mechanical properties of masonry [19,30]. Secondly, the infill material helps by dispersing the loads coming from the road surface down to the vaults as well as in its stabilization by providing additional lateral stiffness. The contribution of the infill material to the overall bridge strength is generally high, being an important aspect that should be taken into account in the structural assessment procedure, as it has been highlighted in previous research works [8,10]. However, the accurate characterization of the physical and mechanical parameters of infill materials poses a great challenge nowadays, requiring the use of invasive techniques to extract samples [31], or even the use of other invasive methods such as the Ménard Pressuremeter tests to locally characterize the infill properties [6,32].

Finally, with regards to the third level, i.e., the characterization of the structural system at a global level, several authors have considered the ambient vibration tests as the most suitable technique for evaluating the global response of this type of structures [10,19,32]. This approach allows obtaining the dynamic response of the structure, namely its natural frequencies and mode shapes, under operational conditions. These dynamic properties can be posteriorly considered within a constrained optimization framework. This framework's main goal is obtaining a set of input values for the Finite Element model of the structure (e.g., Young's Modulus of the masonry or infill) so that model outcomes best fit the experimentally obtained response of the structure; thus better representing its current mechanical behavior in operational conditions [8,19,32].

According to the above mentioned, the success of any numerical simulation, and hence the ability to emit an accurate structural diagnosis, strongly depends on the knowledge of the different constructive elements and the physical and mechanical properties of the materials with which they are built. Under this basis, and inside the framework of the modern restoration theory based on the precepts defended by the International Charter of Kraków [33], this paper proposes a multidisciplinary approach, fully based on non-destructive methods, aimed at generating high-fidelity numerical models. To this end, the approach combines well-known methods in the structural evaluation of masonry bridges such as the terrestrial laser scanner or the ground penetrating radar [20,21,34] with other procedures able to overcome part of the main limitations of the current multidisciplinary approaches. Among these limitations, stand out: i) the capacity of characterizing, in-situ and from a non-destructive point of view, part of the mechanical properties of the masonry and the infill; ii) the use of additional tests able to supplement the information provided by the ground penetrating radar and; iii) a method, based on the latest advances in reverse engineering, able to generate as-built CAD models, that reproduces the current deformed state of the bridge.

To validate the proposed methodology, described and highlighted in the above text, the roman bridge of Avila (Castile and León, Spain) is used as a case study. This bridge was initially erected during the age of Trajan to connect the *Decumanus Maximus* of the city with its riverside. However, the presence of anthropic and environmental agents has promoted on the bridge intense changes, currently showing a mixture of constructive systems (roman, mediaeval and modern) and materials (stone and concrete solutions). Bearing this in mind, the paper is structured as follows: after this initial introduction, Section 2 briefly describes the masonry arch bridge chosen to validate the multidisciplinary approach. Section 3 exposes the experimental campaign carried out and the obtained results. Section 4 presents the method proposed to generate an accurate numerical simulation of the bridge. Section 5 evaluates the accuracy of the developed model by comparing simulation outcomes with the experimentally obtained dynamic behavior of the bridge. Section 6 provides and discusses the results of the safety evaluation of the bridge, and finally, in Section 7 the conclusions are drawn.

2. The Roman bridge over the Adaja river

2.1. Historical background

The Roman bridge over the Adaja river is located on the road of Extremadura in the city of Avila, Spain, specifically in the western part of its Mediaeval Wall (Fig. 1). Its origin can be attributed to the Roman epoch, presumably during the Trajan period (98-117 A.C.) due to its similarity, in terms of constructive techniques and design, with other roman bridges erected in the same epoch, such as the Alcantara or the Bibey bridges [35]. The construction of this infrastructure was motivated by the necessity of communicating the *Decumanus Maximus* of the roman city *Abula* with its riverside.

In the Mediaeval age, probably during the Muslim invasion of the Iberian Peninsula in the year 711 A.C., the upper part of the bridge was demolished with the purpose of isolating the city. From this demolition, the piers, the cutwaters and the beginning of some of the vaults have remained intact [35]. During the XIth century, the spandrel walls and the missing parts of the vaults were restored with ochre granite coming from the nearby quarry of "La Colilla". This type of granite was the most used in Avila during the Mediaeval age. However, due to the premature erosion that this kind of material suffers, periodic restoration works were carried out on the bridge, being highlighted the restoration actions carried out in the XIIIth century, in which the parapets were replaced with grey granite masonry (Fig. 1).

Between 1788 and 1900 several industrial buildings were annexed to the east part of the bridge (Fig. 2). These constructions were demolished around 1996 due to their deficient state of conservation, especially after the fire that took place in 1984 [36] After the demolition of these buildings, the upstream right side of the bridge was covered with natural soil in order to restore the urban environment (Fig. 2b).

Fig. 1. General view of the bridge: a) upstream and; b) downstream.

More recently, on August 21st, 1995, a heavy rainfall damaged the bridge. The damage was amplified by the increase of the infill pressures due to its saturation, partially collapsing the upstream spandrel wall (Fig. 3a). This collapse along with the bridge's overall deficient state of conservation determined the necessity of undertaking major restoration works. These works were carried out during that year, repairing the right side, the left pier of the major vault as well as the central voussoirs of all the minor barrel vaults (Fig. 3b). Additionally, the bridge's deck was completely reconstructed, adding a weather-tightening concrete slab of 15 cm with non-structural steel bars and a granite cobblestone pavement (Fig. 3c and d).

2.2. Constructive description of the bridge

The bridge has a total length of approximately 60.00 m and a total width of 4.14 m, presenting five vaults along its trace. These vaults have a rise/span ratio near to 0.50 (Fig. 4) (Table 1). Viewing the bridge from the upstream side and from West to East (from the road of Extremadura to the Mediaeval Wall), the barrel vaults 1/2/3/5 show an average span of 6.18 m. In turn, the barrel vault 4 shows higher dimensions with a span of 9.20 m (Fig. 4d). The most relevant geometrical features are shown in Table 1.

Moreover, this bridge was built over a narrowing of the waterway produced by a rock formation of granite which was used as foundation for the piers of the bridge (Fig. 4). These piers have rectangular shape with an average height of 3.50 m and an average width of 4.66 m, thereby presenting an average pier slenderness (pier height-pier width ratio) of 1.33. All the piers at their bases have triangular cross-section starlings, or cutwaters, facing the upstream side (Fig. 4d). These cutwaters have an average height of 2.58 m and an average width of 2.11 m.

Apart from the geometrical features of the barrel vaults, piers and cutwaters, one of the most remarkable features of this historical bridge is the presence of two types of masonry (Fig. 4). On one hand, grey granite masonry from the Roman period, except for the parapets, that date from the Mediaeval period. This masonry is located in the lower part of the bridge as well as in all bridge's cutwaters and it is made up by regular masonry blocks. On the other hand, the upper part of the spandrel walls and the barrel vaults is made up by a regular ochre granite masonry with mortar joints (Fig. 4c and d).

Concerning the infill of the bridge, the archaeological samples taken in 1995 revealed the presence of two infill layers: i) a roman concrete with large aggregate size (*Opus Caementicium*) from the foundation until approximately 2/3 of the vault's rise and; ii) a compacted cohesive infill with inclusions of large aggregates from the 2/3 of the vault's rise until the deck. Over this layer rests a 0.15 m-thick concrete layer and a grey granite cobblestone pavement made up by stone blocks whose dimensions are 0.10 × 0.20 × 0.10 m. These stone blocks are with cement mortar (Fig. 3 c and d). Concerning the parapets, they have an average thickness of approximately 0.38 m and an average height of 1.36 m.

2.3. Damage indicators analysis

Before performing the in-situ non-destructive tests, a damage mapping was carried out with the aim of assessing the bridge's current state of conservation. This procedure resulted in the following visual indicators of alteration (Fig. 5) (Fig. 6): i) material losses; ii) deformations; iii) salt crusts; iv) biological colonization; v) moisture; and vi) graffiti.

It is worth mentioning the material losses observed on the barrel vaults (Fig. 6a) and the spandrel walls (Fig. 6b). These pathologies are mainly attributed to the high porosity and low frost resistance of the ochre granite [38], which in combination with the environment and the mechanical and chemical behavior of the cement mortar are causing

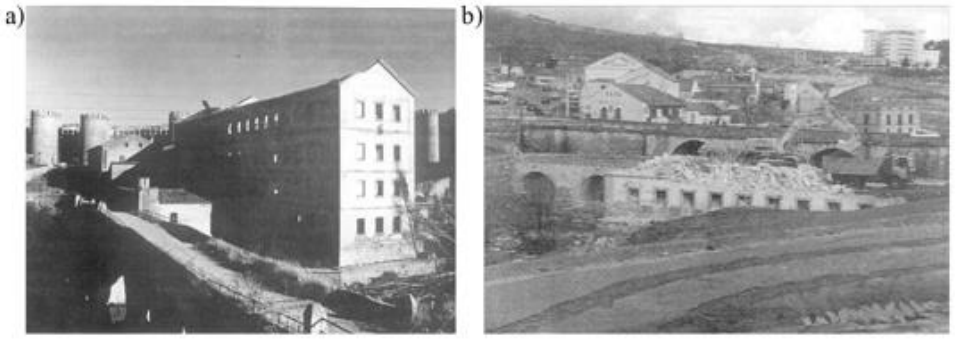

Fig. 2. Industrial buildings annexed to the upstream right side of the bridge [36]: a) view from the downstream and; b) image captured during the demolition of these buildings.

Fig. 3. State of conservation before the urgent restoration works carried out in 1995: a) general view of the east spandrel wall after the waterspout; b) state of conservation of the east barrel vault on which is possible to observe heavy material losses (in some sections around the 30% of the original thickness) and; c) and d) details of the granite cobblestone pavement added in 1995. Source: Memoria valorada para la actuación urgente en el Puente romano sobre el Río Adaja (Obras municipales 80/6).

material losses. This damage reduces the effective cross-section of the main load-bearing elements of the bridge. Also, it was possible to observe out-of-plane deformations in the upper part of the spandrel walls (Fig. 5).

3. Experimental program: geometrical, material and dynamical characterization of the bridge

Considering the necessity to determine all the structural components of the bridge, from both a geometrical and a mechanical point of view, the following multidisciplinary methodology was adopted (Fig. 7).

For the characterization of the external envelop of the bridge, it is proposed the use of the terrestrial laser scanner (TLS). Since this sensor is only able to capture the external geometry of the construction, the ground penetrating radar (GPR), the impact-echo method (IE) and the multichannel analysis of surface waves (MASW) are proposed as complementary sensors. In this case, the GPR and the IE method are employed to characterize the thicknesses of the spandrel walls and vaults. On the other hand, the MASW method is used to characterize the inner distribution of the infill. All information is later combined and used to create an as-built CAD model of the bridge by means of reverse engineering procedures.

From the material point of view, the proposed methodology uses the sonic testing for the characterization of the elastic properties of the masonry components. Meanwhile, the MASW method is used to characterize the Young Modulus as well as the density of the infill layers.

Finally, it is proposed the use of the Ambient Vibration Tests with the aim of validating the numerical simulation arose from the previous tests. Result of this combination of tests and procedures, it was possible to generate an accurate advance numerical simulation of the construction.

3.1. Geometrical characterization of the bridge

3.1.1. Terrestrial laser scanner survey

Due to the difficulty accessing some parts of the bridge, as well as to the complexity of its geometry, the use of the terrestrial laser scanning technology was the best solution, given its portability, accuracy and working range [12,39]. Accordingly, the Faro Focus 3D 120 equipment was used to characterize the geometrical envelope of the bridge (Fig. 8). This lightweight laser scanner is able to capture from 122,000 to 976,000 points per second with a nominal accuracy of 2 mm at 25 m.

Complementary to this sensor, several registration spheres, with two different diameters (200 mm and 145 mm), were used to perform an automatic alignment between the different scan stations. To this end, the target-based procedure defined by Franaszek et al. [40] was used.

As a result, a total of sixteen scans were required in order to record the whole bridge structure: i) ten scan stations to capture the downstream part of the bridge and; ii) six scan stations to represent its upper part, obtaining an alignment error of 0.005 ± 0.003 m. The huge amount of data captured was then reduced by applying a density filter with a threshold of 0.01 m. Therefore, an optimized 3D digitalization of the bridge made up by 15,631,250 points (representing the 32% of the total points captured during the experimental campaign) was finally obtained (Fig. 9).

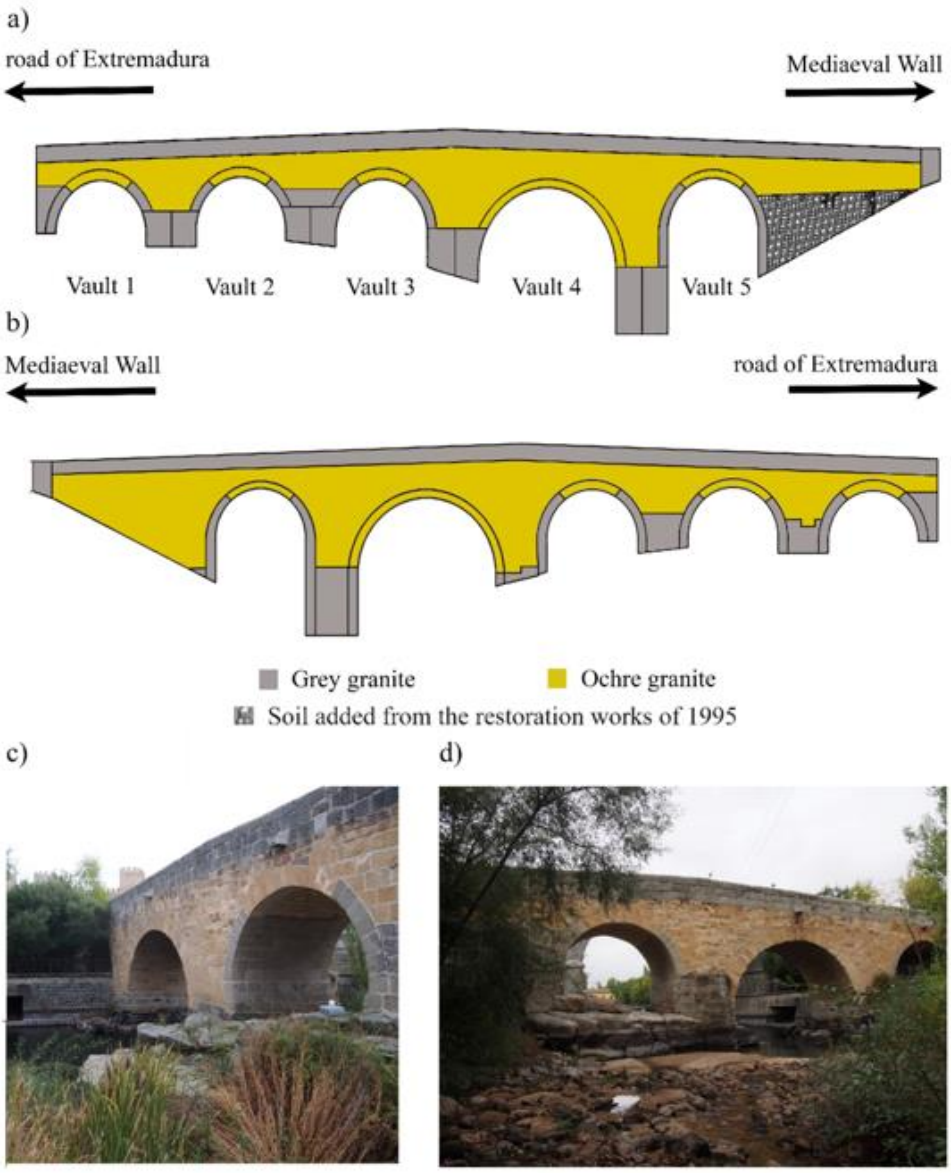

Fig. 4. Historical bridge over the Adaja river: a) downstream elevation; b) upstream elevation; c) general view of the upstream side and; d) general view of the downstream side.

Table 1
Geometrical features of the bridge barrel vaults.

Arch	Span (m)	Rise (m)	Rise/span ratio	Thickness (m)
1 (West)	6.17	3.04	0.49	0.55
2	6.19	3.03	0.49	0.54
3	6.19	3.03	0.49	0.53
4	9.20	4.86	0.53	0.85
5 (East)	6.15	3.05	0.50	0.55

3.1.2. Ground penetrating radar survey

Complementary to the TLS survey, the ground penetrating radar (GPR) method was used with the purpose to determine the inner structure of the bridge. To this end, the X3M® GPR system from MALA Geoscience was used, performing a total of five radargrams (Fig. 10): i) two horizontal profiles along the longitudinal axis of the bridge, with a central frequency of 250 MHz and a total time window of 30 ns and; ii) three profiles in the vertical direction with a central frequency of 800 MHz and a total time window of 100 ns. To scale the profiles, several marks were used during the data acquisition coinciding with the start and end points of each radargram.

On one hand, the vertical GPR profiles made it possible to determinethe cross-section of the bridge, which is made up by (Fig. 11): i) a 10.00 cm-thick granite cobblestone layer; ii) a 15.00 cm thick concrete slab; iii) a first infill layer from the concrete slab to 2/3 of the vault's rise (Mediaeval infill); iv) a second infill layer from 2/3 of the vault's rise until the foundation (Roman infill) and; v) a masonry foundation. These results were consistent with those obtained during the multichannel analysis of the surface waves test (Section 3.2.2) as well as with the archaeological samples (Section 2.2). Additionally, it

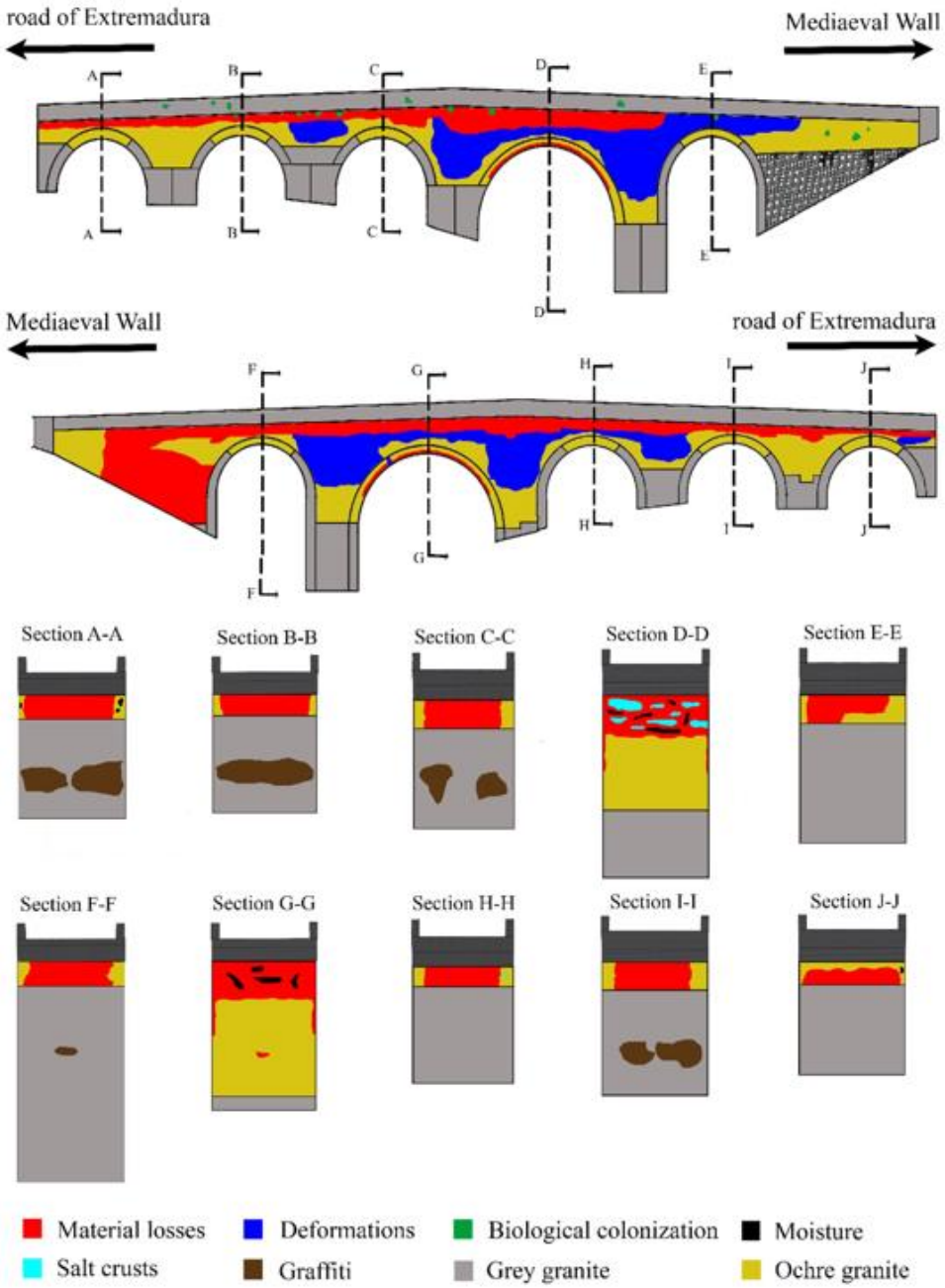

Fig. 5. Damage mapping obtained from the visual inspection performed according to the damage indicators defined within the framework of the European research project HeritageCARE [37].

was possible to estimate the thickness of the spandrel walls, with an average value of 0.45 m (Fig. 11).

On the other hand, the horizontal radargrams were characterized by the presence of a continuous reflection due to the presence of steel bars within the bridge's deck. These bars were used to avoid the presence of cracks due to the retraction of the concrete, having no influence from the structural point of view during the restoration works carried out in 1995. Thus, it was not possible to identify the infill distribution of the bridge (Fig. 12). Furthermore, it was possible to observe the presence of expansion joints equally spaced at 6.00 m along the concrete layer (Fig. 12).

3.1.3. Impact-echo tests

The impact-echo method was used to characterize the thickness of the masonry elements (spandrel walls and barrel vaults) and to verify the average thickness shown by the vertical profiles obtained from the GPR survey (Fig. 11). To perform these impact-echo tests, an equipment composed by the following elements was used: i) an instrumental hammer; ii) a data acquisition unit of 24 bit of resolution with a maximum sampling rate of 100 kHz and; iii) a transducer (piezoelectric

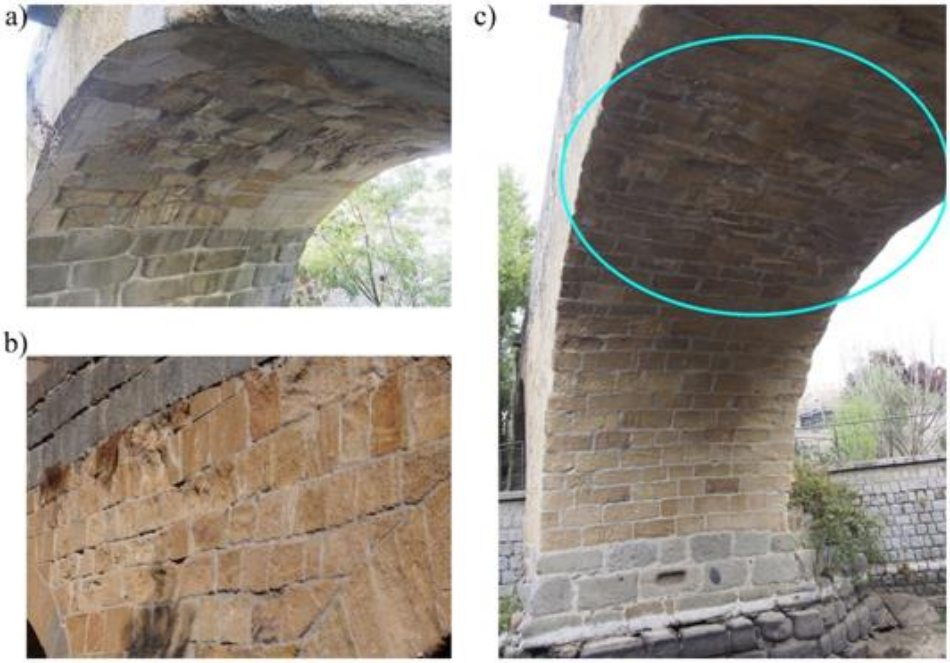

Fig. 6. Detail of the bridge's material losses caused by the aggressiveness of the environment and the cement mortar used to restore the masonry: a) keystone of the vault 5; b) upstream spandrel wall between the vaults 3 and 4 and; c) presence of white crusts on the main barrel vault keystone.

accelerometer) with a sensitivity of 10 V/g, range of ± 0.5 g and 8 μg of broadband resolution. It is worth mentioning that the instrumental hammer as well as the transducer was placed in the same position, making it possible to establish the starting and the ending point in the same location [41]. The excitation recorded by the transducer was then processed, and the frequency spectrum was then obtained through the use of the Fast Fourier Transform (FFT) [41]. The peaks detected by the FFT indicate the presence of internal heterogeneities which could be attributed to the interface between materials, in this case, masonry-infill.

Consequently, a total of six impact-echo tests were carried out on the bridge (Fig. 10b): i) three on the barrel vaults (stone 1 to stone 3) and; ii) three on the spandrel walls (stone 4 to stone 6). To extract the depth of the interface masonry-infill, the following equation was applied (Eq. 1).

$$V_p = 2df \tag{1}$$

where V_p is the P-wave velocity in m/s of the stone block and d is the distance in meters from the receptor to a point with a peak frequency f in Hz.

In order to obtain the propagation velocity of the P-waves (primary waves), several indirect sonic tests were carried out in the same position as the impact-echo tests. In this case, the hammer was placed at 0.50 m from the transducer (Fig. 10b). As expected, the propagation speeds obtained in the ochre granite were lower than the propagation speeds in the grey granite (11.82% lower) (see Table 2). This difference

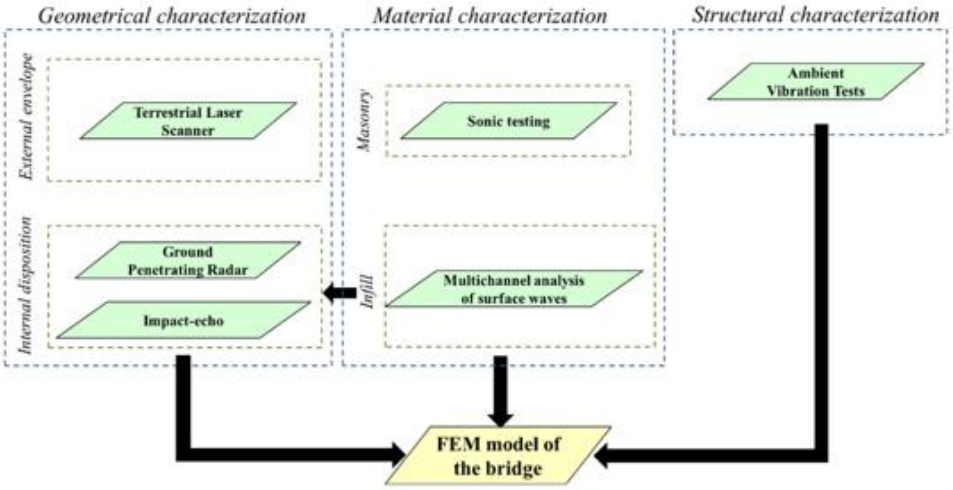

Fig. 7. The multidisciplinary methodology employed for the development of an advanced numerical simulation of the bridge.

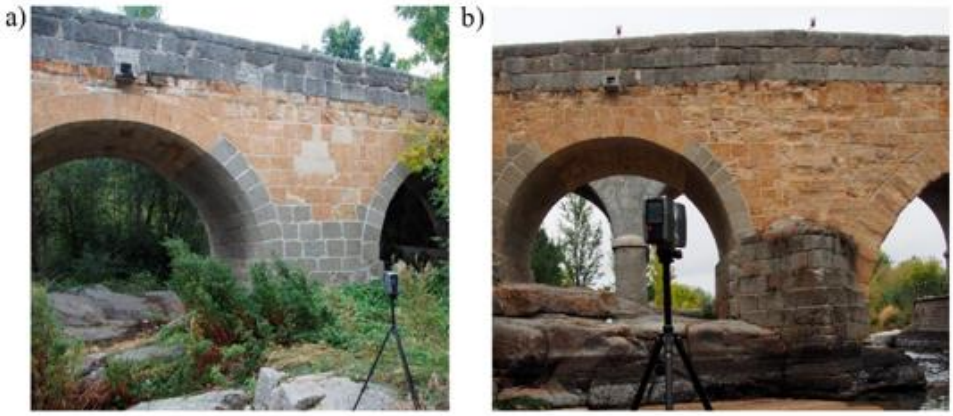

Fig. 8. TLS data acquisition: a) Faro Focus 3D and; b) detail of the registration spheres used to align the different scan stations.

can be attributed to the distinct nature of each kind of granite. While the grey specimen can be considered as an unaltered granite, the ochre granite is a silicified facie with more internal discontinuities [38].

The results of the impact-echo tests yielded an average thickness of 0.57 m in the barrel vaults and an average thickness of 0.47 m in the spandrel walls, being the thickness obtained in the spandrel walls consistent with the data provided by the vertical GPR profiles (Fig. 11) (Table 3).

3.2. Material characterization

3.2.1. Sonic testing

In order to obtain the mechanical properties of the two masonries identified during the visual inspection (Section 2.2), several indirect sonic tests were carried out in different areas of the bridge (Fig. 13). These tests were performed with the same equipment used in the indirect sonic testing carried out on the stone (Section 3.1.3).

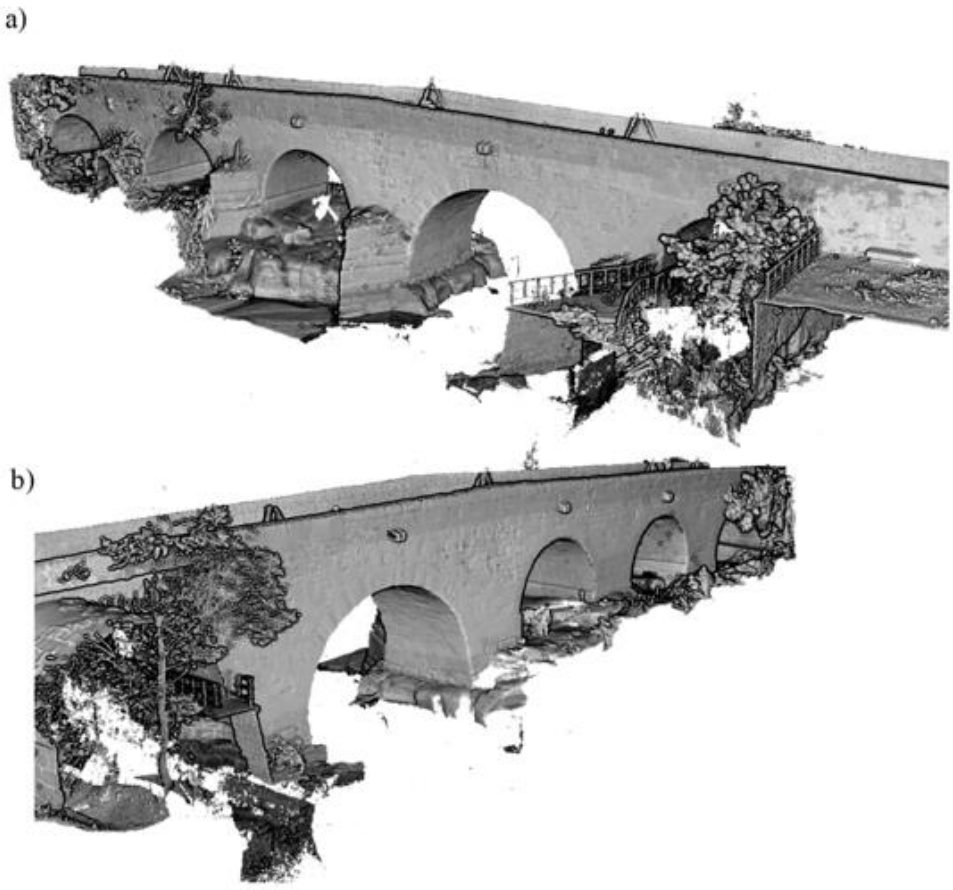

Fig. 9. General view of the bridge's point cloud obtained by the TLS: a) upstream side and; b) downstream side.

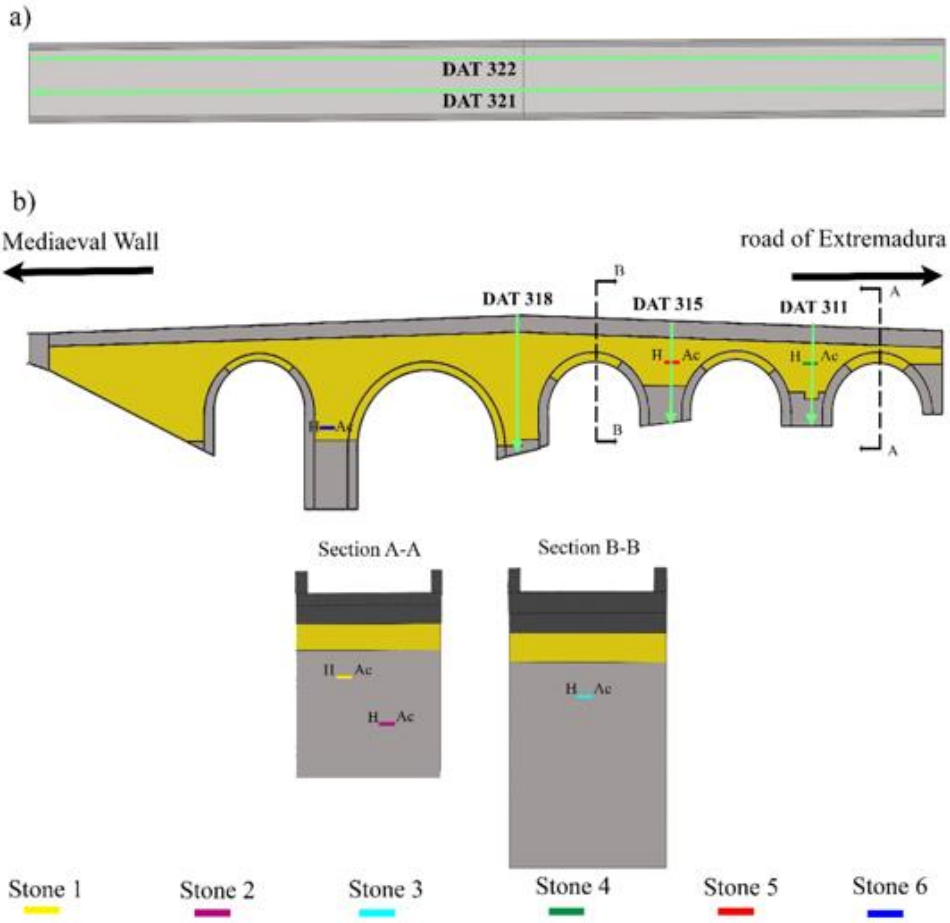

Fig. 10. Positions of the GPR, indirect and impact-echo tests carried out on the bridge: a) plant view and; b) downstream elevation. *H* indicates the position of the hammer and *Ac* indicates the position of the transducer during the indirect sonic tests.

On each evaluated area, the material was excited with the instrumental hammer, promoting the generation of compressional or primary waves (V_p) and surface or Rayleigh waves (V_r). The propagation velocity of these waves was obtained by measuring the time delay between the emission of the signal (impact of the instrumental hammer) and its reception by the transducer. Once the propagation velocity was estimated, it was possible to calculate the mechanical properties of the grey and ochre granite masonries using the following equations (Eqs. (2)–(4)) [42]:

$$V_P = \left(\frac{E(1-\nu)}{\rho(1-\nu)(1-2\nu)}\right)^{1/2} \quad (2)$$

$$V_r = \frac{0.87+1.12\nu}{1+\nu}\left(\frac{E}{2\rho(1+\nu)}\right)^{1/2} \quad (3)$$

$$\frac{V_p}{V_r} = \frac{0.87+1.12\nu}{1+\nu}\left(\frac{(1-2\nu)}{2(1-\nu)}\right)^{1/2} \quad (4)$$

where V_p is the velocity of propagation of the P-waves in m/s; V_r is the velocity of propagation of the R-waves in m/s; E is the Young's Modulus of the material in GPa; ρ is the density of the material in kg/m3 and; ν is the Poisson's coefficient of the material.

While the Poisson's ratio can be directly obtained from the relation between V_p and V_r (Eq. (4)), the masonry's Young's Modulus requires knowing the density (Eqs. (2)–(3)). The density of the grey granite masonry was assumed between 2000 kg/m^3 to 2500 kg/m^3 [19]. Meanwhile, the density of the ochre granite masonry was assumed between 1700 kg/m^3 to 2000 kg/m^3. This assumption was based on the experimental tests carried out by Garcia-Talegon et al. [38] on the ochre granite of Ávila.

Table 4 shows the results of the indirect sonic tests carried out on the masonries. On one hand, the grey masonry showed average propagation velocities values of 1316.56 m/s and 697.78 m/s for the P and R-waves, respectively, yielding a Young Modulus comprised between 2.90 and 3.60 GPa. On the other hand, lower propagation speeds from the ochre masonry were observed (1202.69 m/s for the P-waves and 601.51 m/s for the R-waves) and therefore, a lower Young Modulus, which ranged from 2.05 GPa to 2.41 GPa.

3.2.2. Multichannel analysis of surface waves

The infill material of a masonry arch bridge can be considered as soil inserted within the space delimited by the spandrel walls, vaults, and piers. Under this assumption, Geophysics can offer a wide variety of techniques able to characterize soils from a geometrical, physical and mechanical point of view [43]. Within this context, the multichannel analysis of surface waves (MASW) stands out. This approach allows obtaining a 2D profile, represented by the plane generated between the geophones, the instrumental hammer, and the *z* direction of the phase velocities and frequencies of the waves generated after the excitation of a soil (dispersion curve) [44]. The fundamental mode of the dispersion

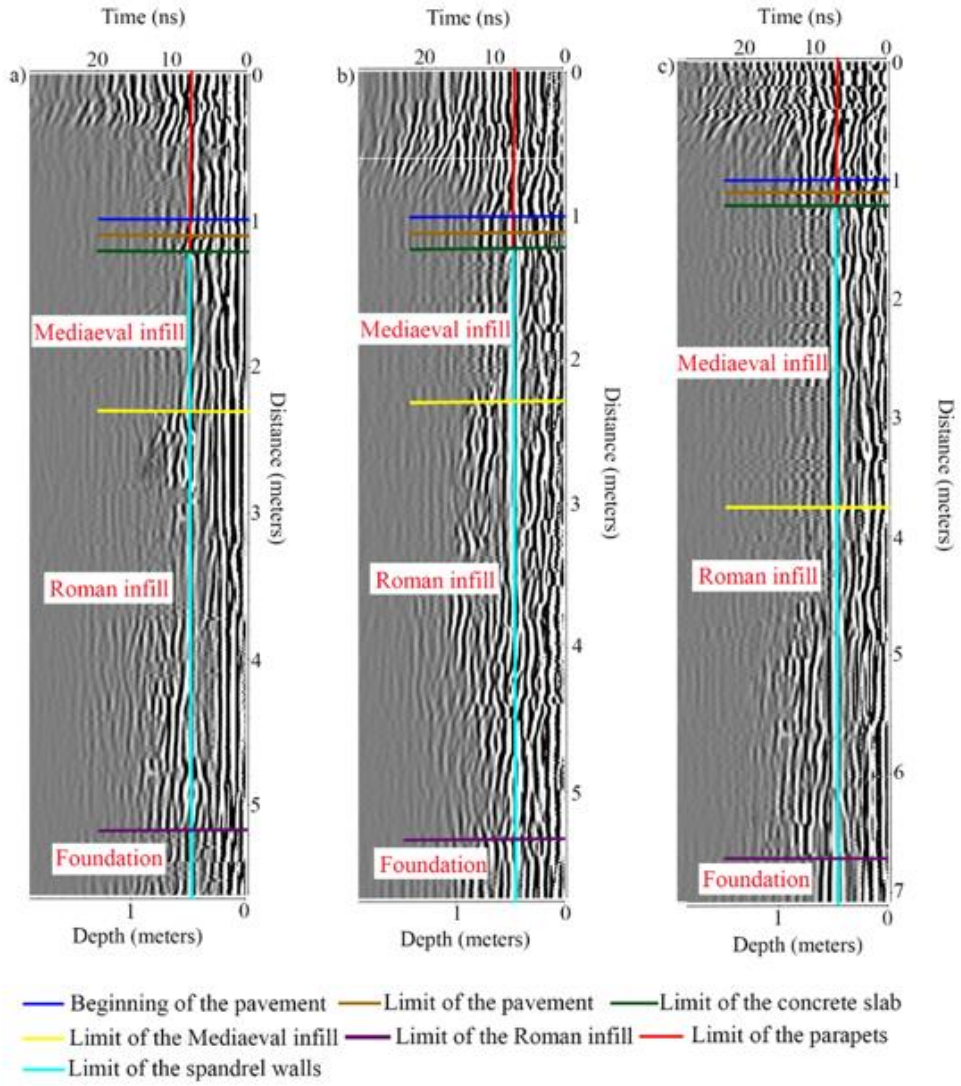

Fig. 11. Results obtained from the vertical GPR profiles: a) radargram DAT-31; b) radargram DAT-315 and; c) radargram DAT-318.

curve is extracted, and an optimization process, also called inversion analysis, is carried out with the aim of obtaining the shear-wave velocities of the soil (V_s) [45]. Additionally, it is possible to capture the primary-wave velocities (V_p) generated during the excitation of the soil [44]. Thus, the MASW method allows obtaining a 2D plot of the average shear and primary-wave velocities of a soil in relation to the position of the linear array of geophones and the z axis. Then, both velocities are linked with the Young Modulus and density of the soil as follows (Eqs. (5)–(6)):

$$\rho = 1.2475 + 0.399\left(V_p/1000\right) - 0.026\left(V_p/1000\right)^2 \quad (5)$$

$$E = \rho V_s^2 \frac{3\left(\frac{V_p}{V_s}\right)^2 - 4}{\left(\frac{V_p}{V_s}\right)^2 - 1} \quad (6)$$

where ρ is the density in kg/m^3; E is the Young's Modulus in GPa; V_p is the primary-wave velocity of the soil in m/s and; V_s is the shear-wave velocity of the soil in m/s.

Taking into account all the above mentioned, a MASW test was carried out on the east part of the bridge (Mediaeval Wall) (Fig. 14a). The excitation of the soil was carried out using a 20.00 kg sledge-hammer connected to a data acquisition unit (Fig. 14b, c). The excitation was captured by a linear array of 20 geophones equally spaced (0.40 between each one of them in a total length of 7.60 m) (Fig. 14a) and connected to the data acquisition unit.

Table 5 shows the results obtained from the MASW test. From the *Vs* values it was possible to obtain a first estimation of the bridge's infill layers (Fig. 15) (Table 5): i) one layer, with a depth of approximately 1.76 m, made up by a compacted material with an average Young's Modulus of 0.43 GPa and; ii) a second infill layer with an average Young's Modulus of 1.03 GPa, ranging from first infill layer's bottom to the foundation of the bridge. These values seem to be consistent with those obtained by the archaeological samples (Section 2.2) as well as with the values found in the existing literature [8,46,47].

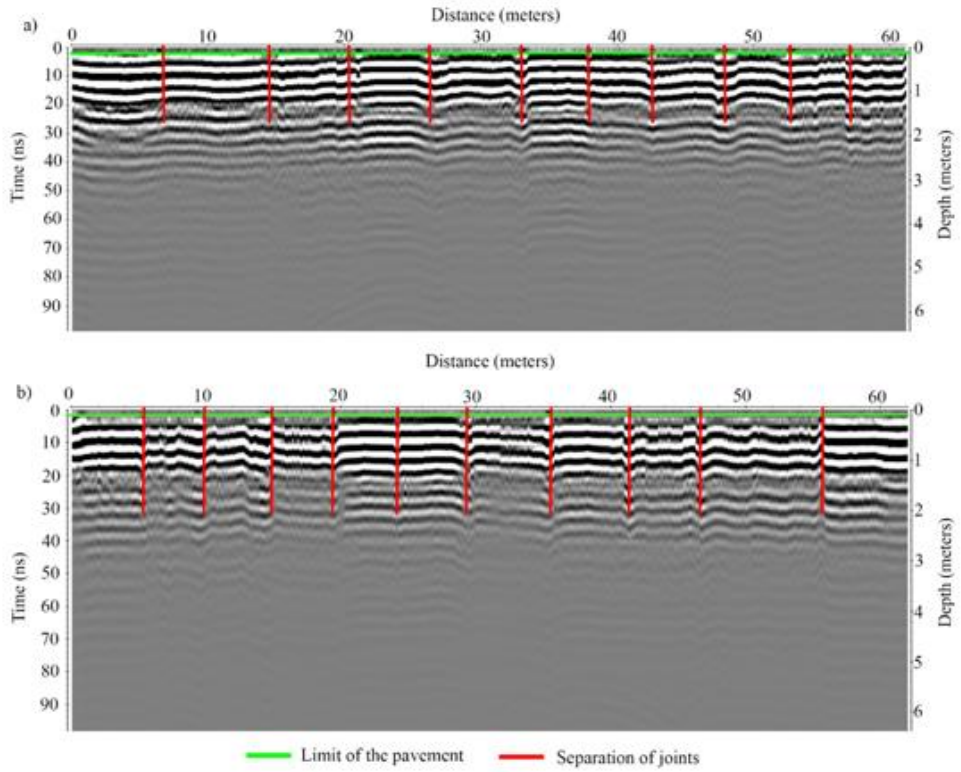

Fig. 12. Results obtained from the horizontal GPR profiles: a) radargram DAT-321 and; b) radargram DAT-322.

Table 2
Propagation velocities obtained during the experimental campaign in each type of granite.

Sample		Propagation speed			
		V_p (m/s)	Cov (%)	V_r (m/s)	Cov (%)
Grey granite	Stone 1	1282.60	1.61	679.78	1.57
	Stone 2	1297.80	1.53	687.73	1.20
	Stone 3	1286.40	1.38	681.79	1.60
Ochre granite	Stone 4	1137.44	1.33	602.84	1.29
	Stone 5	1138.46	1.97	603.38	1.40
	Stone 6	1133.55	1.02	600.78	1.59

Table 3
Results obtained from the impact-echo tests and comparison of the thicknesses data with their counterparts obtained from the vertical GPR profiles. In brackets the covariance, in %, of the frequencies obtained during the impact-echo tests.

Samples		V_p (m/s)	Thickness (m)	
			Impact-echo	GPR
Grey granite (barrel vaults)	Stone 1	1282.60	0.56	–
	Stone 2	1297.80	0.58	–
	Stone 3	1286.40	0.56	–
Ochre granite (spandrel walls)	Stone 4	1137.44	0.51	0.45
	Stone 5	1138.46	0.45	0.45
	Stone 6	1133.55	0.45	0.45

3.3. Dynamic identification

With the aim of identifying the dynamic properties of the bridge (natural frequencies and modal displacements), an ambient vibration test (AVT) was also performed in the last stage of the in-situ non-destructive survey. To achieve reliable results, several numerical simulations, adopting different boundary conditions, were previously performed. This way, it was possible to arrange the most proper configuration for the AVT test as well as the identification of the most appropriate areas to place the accelerometers (Fig. 16).

To determine the dynamic properties of the bridge, the Enhanced Frequency Domain Decomposition algorithm (EFDD), based on the power spectral density, was applied [48]. Consequently, a total of seven mode shapes were successfully identified along with their corresponding frequencies, ranging between 10.29 Hz to 31.90 Hz [8] (Table 6).

For this case study, it is worth mentioning the high frequencies obtained in comparison with similar tests carried out in other masonry bridges (Table 6). These values are suggestive of a structure with a high stiffness/mass ratio which can be explained by the presence of a reinforced concrete slab on the deck, a high-quality infill and the use of a light-weight masonry (ochre granite).

It is worth mentioning that the accelerometers used to capture the dynamic response of the bridge were placed mainly in the z and the y direction in order to capture the weak direction (out-of-plane) as well as the vertical response of the structure. This type of setup is similar to those adopted in other experimental campaigns [8,16].

4. Numerical model

4.1. Point cloud registration

Previous to the generation of the geometrical CAD model, the registration strategy defined by Bautista-De Castro et al. [12] was applied. This approach allows registering the longitudinal axis of the bridge's point cloud with the x-axis of the global coordinate system, and thus the

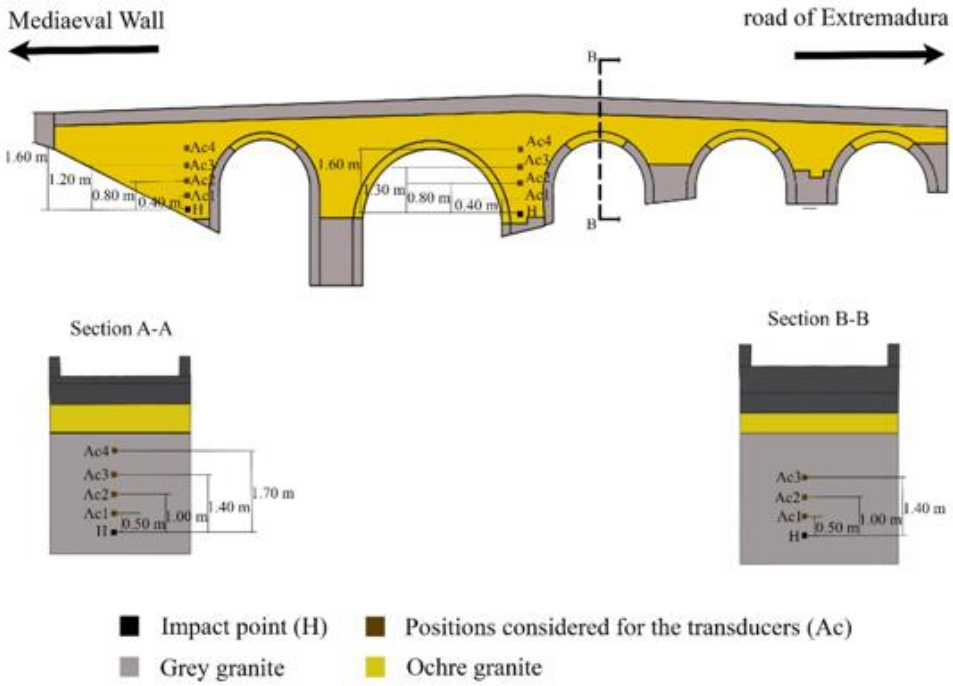

Fig. 13. Layout considered for the sonic testing.

Table 4
Results obtained from the indirect sonic tests.

	Ochre granite		Grey granite	
	P-wave	R-wave	P-wave	R-wave
Average velocity (m/s)	1202.69	601.51	1316.56	697.78
CoV (%)	1.42	1.79	1.48	1.57
Poisson's coefficient	0.26		0.24	
Density (kg/m^3)	1700–2000		2000–2500	
Young's modulus (GPa)	2.05–2.41		2.90–3.60	

correct integration of the different captured data (e.g. AVT). To this end, the following steps were carried out (Fig. 17): i) extraction of the covariance matrix (Eqs. (7)–(80); ii) Eigenvalue analysis of the covariance matrix (Eq. (9)); iii) evaluation of the angle between the Eigenvector associated with the maximum Eigenvalue and the *x*-axis of the global coordinate system and; iv) a *z* rotation of the global point cloud.

$$C = \frac{\sum_{p_i \in P} w_i (p_i - \overline{p})^T (p_i - \overline{p})}{\sum_{i=1}^{n} w_i} \tag{7}$$

$$\overline{p} = \sum_{i=1}^{n} P_i / n \tag{8}$$

$$V^{-1} C V = D \tag{9}$$

where C is the covariance matrix of the point cloud P; w_i is the weight associated to each point p_i; $\overline{p}$ represents the mean of the points; V is an orthogonal matrix that contains the corresponding eigenvectors and; D is the diagonal matrix containing the eigenvalues. For the present case study, the same unit weight was assumed for each point.

4.2. Creation of the as-built CAD model

According to Sánchez-Aparicio et al. [25], the creation of a suitable CAD model for numerical analysis purposes can be carried out by means of the following strategies: i) extraction of orthogonal views and sections over several directions of the point cloud or mesh or; ii) by means of advanced surface representation methods such as the non-uniform b-splines, allowing the representation of complex surfaces. Taking into consideration the out-of-plane deformations observed during the visual inspection (Section 2.3), the second approach was deemed as the most adequate, being carried out through the following workflow (Fig. 18): i) 3D Delaunay triangulation; ii) extraction of sections, spaced 1.00 m, along the *x*-axis; iii) vectorization of each section by means of b-spline curves and; iv) creation of a solid geometrical model based on Loft surfaces, considering the b-splines as its directrix curves [49].

As a result, it was possible to construct a rough solid model of the bridge envelope on which the out-of-plane deformations observed on the spandrel walls were accurately captured. To refine this model, including the barrel vaults and other bridge elements such as the infill layers, several Boolean operations were carried out at a later stage [49], intersecting parametric shapes (e.g., cylinders for the barrel vaults and planes for the definition of the boundaries and materials) with the envelope obtained in the previous stage (Fig. 18). It is worth mentioning that the interface between infills was modeled based on the data provided by the GPR and the MASW tests. Meanwhile, the thickness of the spandrel walls was modeled assuming a fixed average value, estimated in 0.46 m, obtained from the vertical GPR profiles as well as the impact-echo tests (Table 3).

The previously defined reverse engineering procedure allowed obtaining a highly detailed solid CAD model. However, and considering the focus of the present study, the creation of an accurate numerical model of the bridge, the cutwaters were omitted at this stage and later integrated during the generation of the finite element mesh.

4.3. Finite element mesh

With from the previously created geometrical model as a starting point, a finite element mesh was generated using the FEM software TNO Diana® [50] (Fig. 19). This mesh was comprised of 86,418 solid elements and 166,292 degrees of freedom, including two elements along

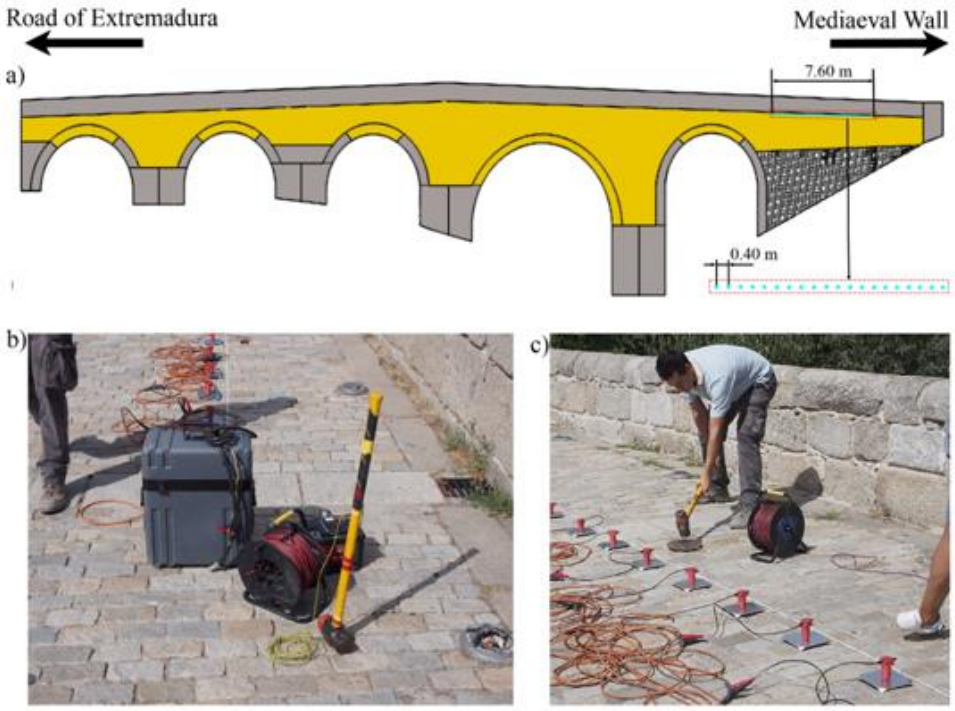

Fig. 14. MASW tests: a) setup; b) detail of the used equipment and; c) moment when the infill is excited. Array of geophones used during this test in blue. (For interpretation of the references to colour in this figure legend, the reader is referred to the web version of this article.)

Table 5
Values obtained for the two infill layers identified on the bridge. UB denotes the upper bound value and LB the lower bound value.

	First layer		Second layer	
	UB	LB	UB	LB
V_p (m/s)	1451.4	1427.3	1705.2	1606.7
V_s (m/s)	316.1	294.7	515.0	419.6
E (GPa)	0.52	0.45	0.84	1.28
ρ (kg/m3)	1771	1764	1852	1821

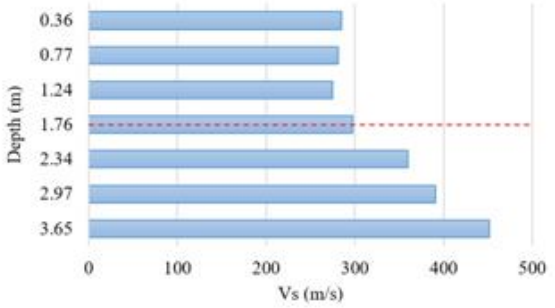

Fig. 15. Graphical representation of the relation between the depth and the V_s speeds. The red line represents the interface between the different bridge's infill layers. (For interpretation of the references to colour in this figure legend, the reader is referred to the web version of this article.)

the thickness of the spandrel walls and barrel vaults in order to correctly capture stress gradients in subsequent non-linear structural analysis. It is worth mentioning that the cutwaters were defined through extrusions, considering a geometry with an equivalent stiffness (Fig. 19). The concrete slab, as well as the granite cobblestone, was included in the model by means of extrusion of the bridge's deck. These extrusions were made without any connection with the spandrel walls as it was observed during the visual inspection.

Concerning the boundary conditions, they were applied in agreement with the surrounding medium of the bridge: pinned supports at the base, abutments, and the spandrel wall covered by the soil added in 1995 (Figs. 4, 5).

As for the material properties of the masonry and infill, they were defined according to the values obtained during the experimental campaign (Tables 7, 8). Meanwhile, the materials of the bridge's deck were defined according to the data provided by the last restoration project (Table 9): a granite cobblestone pavement joined with a cement mortar upon a concrete slab. On one hand, the homogenized Young's Modulus of the granite cobblestone was set according to the equations defined by the Eurocode 6 [51] and the experimental data obtained by Garcia-Talegón et al. [52]. On the other hand, the mechanical and physical properties of the concrete slab were defined according to the Eurocode 2 [53], considering a characteristic compressive strength of 16 N/mm^2 (C 16/20). It is worth mentioning that the steel bars detected by means of the horizontal radargrams were not included in the numerical simulation since they not have a structural function.

5. Evaluation of the discrepancies between the numerical model and the experimental modal data

One of the factors explaining the widespread employment of the FEM method in the analysis of masonry structures is the possibility of simulating complex scenarios such as earthquakes or settlements. However, the quality of the output results obtained from these simulations is strongly influenced by the uncertainties associated with the mechanical properties of the materials, the correct definition of the structure's boundary conditions, and the geometrical simplifications incurred when developing the numerical model. Therefore, these

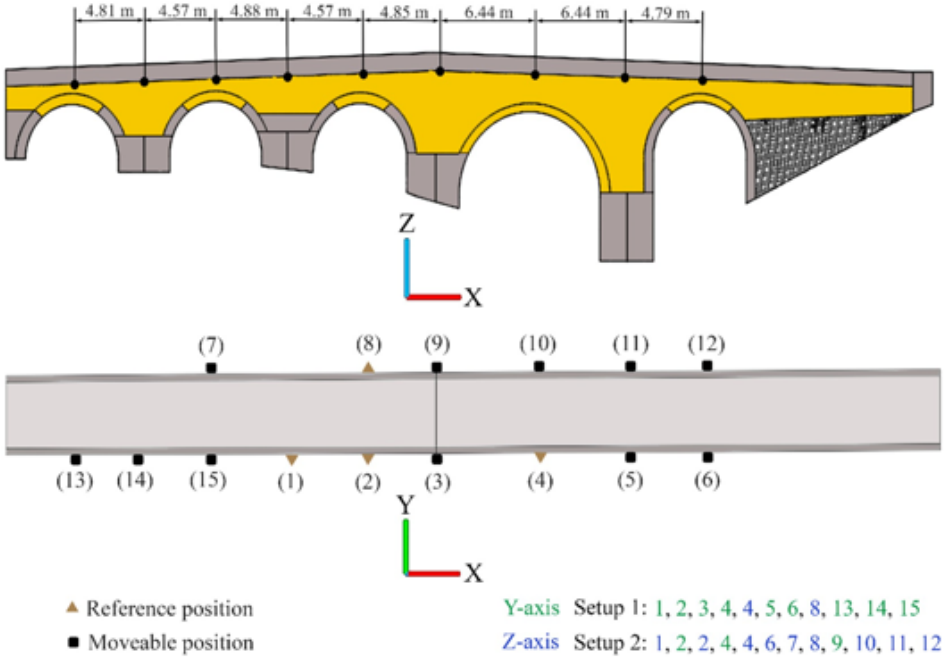

Fig. 16. Schematic representation of the setups carried out during the AVT test.

Table 6
Natural frequencies and mode shapes obtained from the AVT tests.

Mode	Natural frequency (Hz)	Description of the modal shape
1	10.30	Translational mode in the *x* axis
2	14.57	Torsional model in the *x* axis
3	21.09	Translational mode in the *z* axis
4	24.13	Torsional model in the *y* axis
5	26.31	Torsional and translational mode in the *x* and *z* axis respectively
6	29.45	Torsional model in the *x* axis
7	31.90	Torsional model in the *y* and *x* axis

aspects demand the use of suitable strategies able to validate these numerical simulations.

Taking all of this into account, a preliminary numerical simulation (Eigen-value analysis) was carried out with the average values of the different materials present on the structure (Tables 7, 8, 9). In order to evaluate the accuracy of the numerical simulation, the error between frequencies and the modal assurance criterion (MAC) [54] (Table 10) was considered as quality indicators.

The results obtained from this initial numerical simulation showed a more flexible structure in comparison with the real one (with an average error in frequencies of 5.03%), suggesting the need to perform a calibration or model updating procedure to improve the discrepancies (Table 10). As for the MAC values, it was possible to observe a fairly good match at the exception of the 7th mode.

Thereby, manual calibration of the numerical model was carried out by modifying the Young's Modulus of the infill layers and masonries within the possible range of values determined by the upper and lower bounds determined by the experimental campaign (Tables 7, 8). Moreover, to mimic the real response of the structure with greater fidelity, a possible interaction effect between the east part of the bridge and the infill soil added in 1996 was considered. For this particular case, a range of admissible stiffness comprised between 1×10^7 N/m^3 and 1×10^9 N/m^3 according to Bautista-De Castro et al. [12] was defined. As a result, it was possible to obtain a numerical simulation whose dynamic response closely matched the dynamic response captured by the AVT tests (Tables 11, 12) (Fig. 20). Thus, the updated numerical model showed an average error in frequencies of 2.22% and an average modal assurance criterion of 0.91 (Table 12).

It is worth mentioning the asymmetric dynamic response of the bridge in Mode I and II. This phenomenon can be attributed to the structural disposition of the bridge on which the major barrel vault, which is 1.5 times thicker and 3 times longer in terms of span (Table 1), is not in the center of the structure (Fig. 4).

The good quality of masonry as well as the well-shaped ashlars found in the spandrel walls, cutwaters, and vaults are consistent with the values obtained during the sonic tests and the calibration of the numerical model (Fig. 4b, c) (Table 12). As expected, the calibration procedure pointed out a non-negligible interaction effect between the soil added in 1995 and the east part of the bridge (Fig. 1b) (Table 12). Finally, regarding the infill layers, it was possible to corroborate again the presence of a high-quality infill material in most of the structure, which lays in the Roman parts of the bridge, and which is also consistent with the data provided by the archaeological samples taken during 1995.

6. Structural assessment

6.1. Modeling assumptions

In the developed computational model, the non-linear behavior of the masonries (grey and ochre granite) was modeled by adopting the total strain rotating crack model (TSRCM), implemented in the Finite Element software TNO Diana [50]. A post-peak exponential softening for tensile behavior and a parabolic hardening followed by a post-peak parabolic and exponential softening for compression were respectively adopted. To estimate the inelastic parameters describing the masonry nonlinear behavior, the following criteria was considered for both types of masonries: i) the compressive strength value was considered as 1000 times the corresponding Young's Modulus, as proposed by Tomazevic

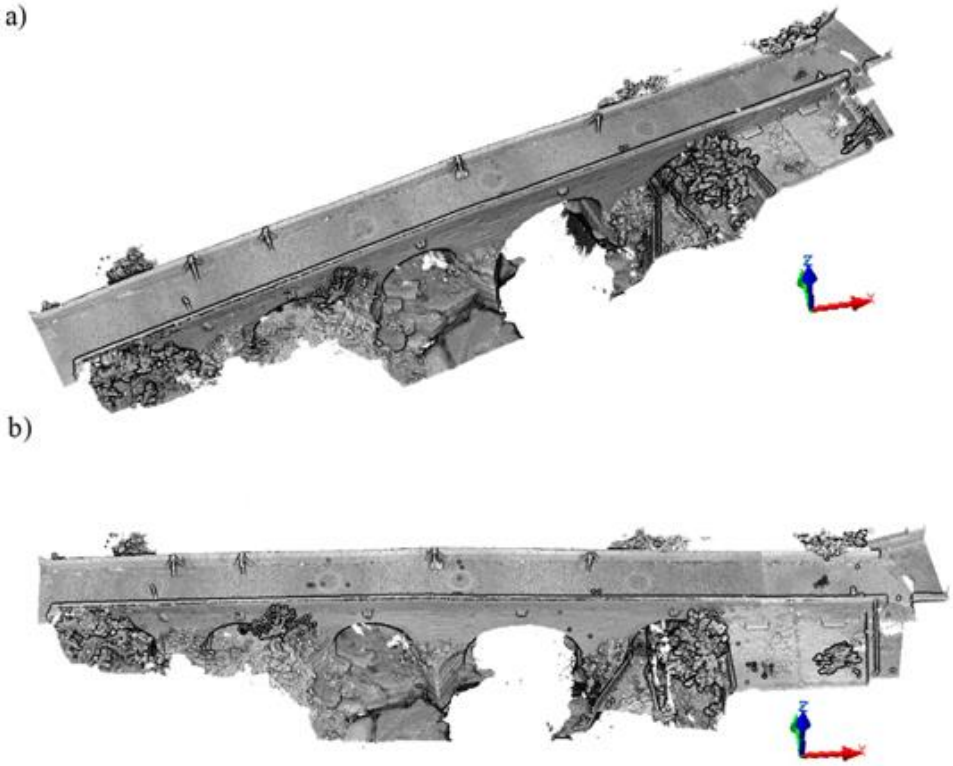

Fig. 17. Point cloud of the bridge: a) before registration and; b) after registration. The longitudinal axis of the bridge after the registration corresponds with the *x*-axis of the global coordinate system.

et al. [55]; ii) for the fracture energy in compression it was adopted a ductility index of 1.60 mm [56]; iii) the tensile strength was taken equal to 5.00% of the compressive strength and; iv) the fracture energy in the tensile regime was assumed as 0.05 N/mm.

The infill layers were modeled obeying to a Mohr-Coulomb failure criterion. For the infill added during the Mediaeval period, it was considered the values proposed by Conde et al. [8], i.e., a friction angle of 30° together with a cohesion of 20 kPa. On the other hand, the *Opus Caementecium* was modeled according to the values proposed by Frunzio et al. [46], i.e., a friction angle of 32° and a cohesion value of 500 kPa.

For the concrete slab added during the last restoration project (see Section 2.1) it was considered a compressive strength of 16.00 N/mm^2 and a tensile strength of 1.90 N/mm^2 according to the Eurocode 2 [57].

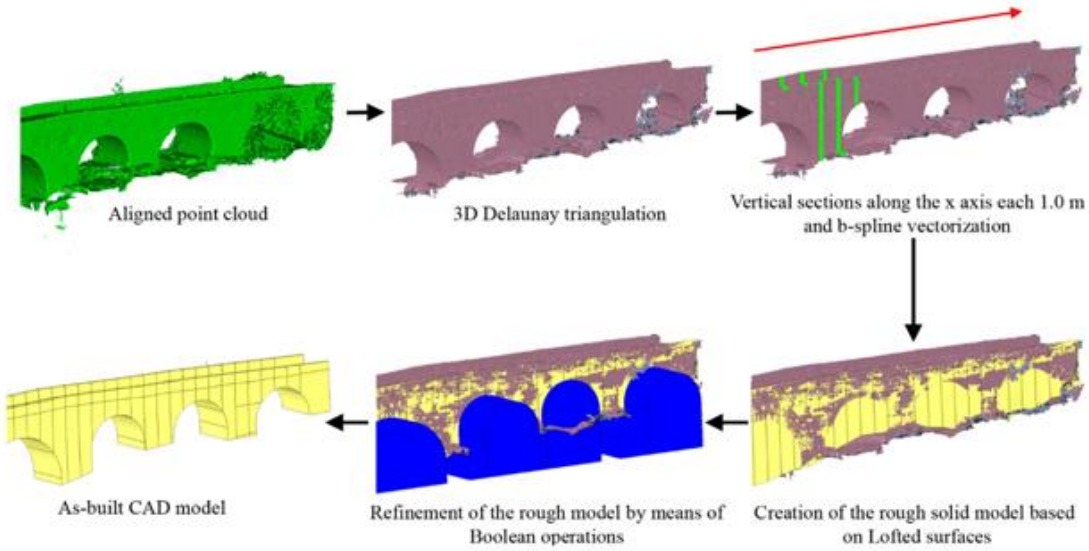

Fig. 18. Proposed workflow for the generation of the as-built CAD model.

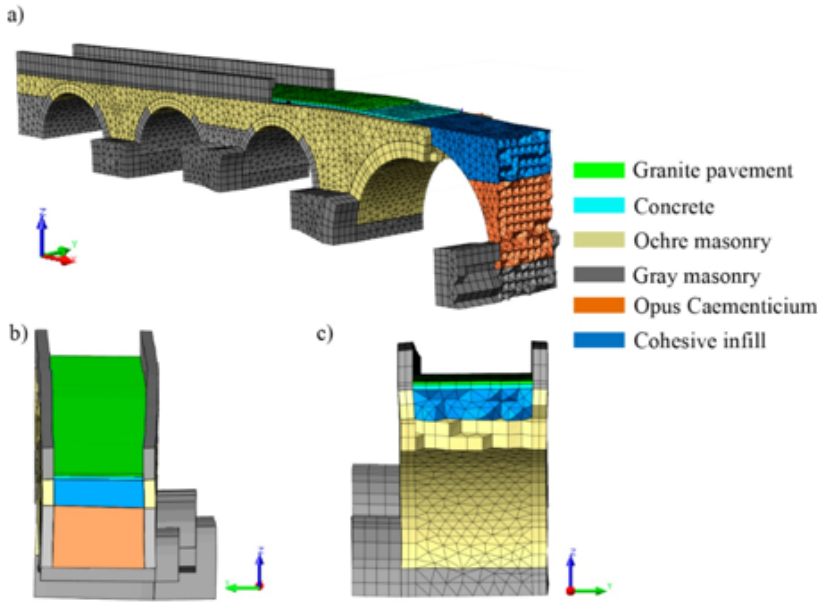

Fig. 19. Finite element mesh: a) general view; b) and c) details of the mesh where it is possible to observe the real captured geometry of the spandrel walls.

Due to the complexity of the model, and the almost null contribution to the overall structural response of the bridge, the granite cobblestone was not explicitly modeled. However, in an attempt to still partially consider it, the mass of this element was added as an external load over the concrete slab. This load had a value of 2.30 kN/m^2.

To obtain the solution of the non-linear problem, the regular (full) Newton-Raphson method, complemented with the line-search technique and the arc-length method in a spherical path, was used. As for the convergence criterion, an energy norm was adopted with a threshold value of 0.001.

6.2. *Safety analysis against vertical loading*

To evaluate the mechanical performance of the bridge, both a non-linear analysis under its self-weight and under an increasing gravitational loading were performed. Both aspects will allow evaluating the current safety condition of the structure against vertical loads. It is noted that the bridge is currently closed to the traffic and in an area with a low seismic hazard. Thus, no analysis under live loads or seismic loading was taken into account within the framework of the present study.

Two different models were used in the numerical simulation procedure, which are categorized as follows: a) Model I: for the analysis of the bridge behavior under its self-weight and; b) Model II: for the evaluation of the performance of the structure under vertical loads. During the numerical simulations, the control node used to track the response of the structure was placed at the mid-line and mid-span of the barrel vault with the higher rise to span ratio (vault number 4).

Thus, concerning the structural behavior of the bridge against its self-weight (Model I), it was observed that the minimum principal (compressive) stresses appeared on an area close to pier number 4, at the springings of the major barrel vault (Fig. 21). The maximum value was around 0.68 MPa, which is pretty far away, 19.00%, of the maximum compressive capacity estimated for the grey granite masonry (around 3.60 MPa). As expected, at this load status the bridge is fundamentally under compression everywhere. Areas with tensile stresses are rather localized, particularly at the upper part of spandrel walls as well as at the mid-span of all barrel vaults. The maximum value for these stresses was approximately 0.10 MPa.

For the case of the Model II, the gravity load was monotonically increased until causing the collapse of the bridge. As a result, the bridge was able to withstand up to seven times its own weight (Fig. 22). This safety factor seems to be related with the high-quality of the different constructive elements (masonry and infill), the weather-tightening concrete placed on the deck (Table 11) and the dimensions of the structure (Table 1). The failure mechanism of the structure is related to the area in between the barrel vaults 3, 4 and 5. In particular, a lateral failure that involves the out-of-plane bending of the spandrel wall between the vaults 3 and 4 is evidenced as a consequence of the high lateral pressures generated by the infill materials. Moreover, significant cracking in the connection between the spandrel wall and the vaults 3–4 can also be observed, as well as longitudinal cracking at the crown of the major barrel vault (number 4) (Fig. 23a). Regarding the compressive stresses status, it is possible to observe some crushing of the masonry in the lower part of the pier that supports the barrel vaults 4 and 5 as well as at the springing of the barrel vault 3 (Fig. 23b).

Table 7
Mechanical properties of the masonries.

Material	Variable	Upper bound	Average value	Lower bound
Grey granite masonry	Young modulus (GPa)	3.60	3.25	2.90
	Poisson ratio (−)	–	0.24	–
	Density (kg/m3)	2500	2250	2000
Ochre granite masonry	Young modulus (GPa)	2.41	2.23	2.05
	Poisson ratio (−)	–	0.26	–
	Density (kg/m3)	2000	1850	1700

Table 8
Mechanical properties of the infill material layers.

Layer	Variable	Upper bound	Average value	Lower bound
1 (cohesive material)	Young modulus (GPa)	0.52	0.48	0.45
	Poisson ratio (−)	–	0.20 [8]	–
	Density (kg/m3)	1771	1768	1764
2 (opus caementicium)	Young modulus (GPa)	1.28	1.03	0.84
	Poisson ratio (−)	–	0.05 [46]	–
	Density (kg/m3)	1852	1837	1821

Table 9
Mechanical properties of the materials of the bridge's deck.

Material	Variable	Upper bound	Average value	Lower bound
Concrete slab	Young modulus (GPa)	–	25.70	–
	Poisson ratio (−)	–	0.20	–
	Density (kg/m3)	–	2400	–
Granite cobblestone	Young modulus (GPa)	–	16.78	–
	Poisson ratio (−)	–	0.20	–
	Density (kg/m3)	–	2318	–

According to these results (and despite the intrinsic uncertainties associated with the accurate determination of the inelastic parameter values), the bridge mechanical performance under vertical loads can be considered fairly satisfactory.

Yet, taking into consideration the focus of the present work: the propose of a multidisciplinary approach able to characterize masonry bridges at the geometrical, material and structural level, a comparative study was also carried out. The aim is confronting the results obtained from the proposed methodology with those that would have been obtained in case of solely considering the values provided by the literature. Accordingly, the values suggested by the Italian code NTC08 [58] were considered. This code provides ranges for the material properties values of different masonry typologies. Herein, both masonries were encapsulated within the class ashlar stone masonry, assuming a Young Modulus of 2.40 GPa for the ochre masonry and 3.20 GPa for the grey masonry. For the infill, it was considered the average values proposed by Conde et al. [8] and Frunzio et al. [46] for the cohesive infill and the *Opus Caementicium*, respectively. Since these values come from the literature a structural knowledge level of LC1 was assumed, with a consequent confidence factor equal to 1.35 [58].

Thereby, with the mechanical properties values provided by the literature, the safety factor of the bridge against vertical loading decreases from 7.3 to 5.5 (25% of reduction) (Fig. 22). Moreover, it is worth mentioning that the failure mechanism shows some discrepancies with respect to the previous model. In this case, the damages associated with the tensile failure of masonry concentrated mainly in vault 4. Indeed, a more intensive cracking at the crown of this element can be appreciated (Fig. 24a). Finally, regarding the compressive stresses status, a similar picture in terms of stress distribution was received (Fig. 24b).

Additionally, several numerical simulations were also carried out with the aim of evaluating the influence of the main structural components, namely masonry and infill, in the global response of the structure. To this end, the mechanical properties of each component were reduced by half (Fig. 22). According to these results, it is possible to observe that both properties have a similar impact in the safety factor; reducing one of them by a half decrease the safety factor of the bridge in about 34%. In spite of this similarity in terms of the safety factor, it was possible to observe that a reduction in the masonry properties leads to a more ductile response in the collapse mechanism development due to the increase of masonry crushing areas (Fig. 22).

6.3. Evaluation of the structural response in case of continuing the material looses

One of the main advantages that can offer an accurate numerical simulation, supported on an extensive experimental campaign, is the

Table 10
Results obtained from the initial numerical simulation.

Mode	Experimental frequency	Numerical frequency	MAC
1	10.30	9.62	0.97
2	14.57	14.39	0.85
3	21.09	20.00	0.97
4	24.13	–	–
5	26.31	24.39	0.94
6	29.45	28.34	0.83
7	31.90	29.95	0.55

Table 11
Updated values obtained after the manual calibration. UB and LB denotes the upper and lower bounds respectively.

	Variable	UB	LB	Update value
Grey granite masonry	Young modulus (GPa)	3.60	2.90	3.60
Ochre granite masonry	Young modulus (GPa)	2.41	2.05	2.41
Cohesive infill	Young modulus (GPa)	0.52	0.45	0.50
Opus Caementicium	Young modulus (GPa)	1.28	0.84	1.28
Interaction soil-bridge	Tangential stiffness in the longitudinal direction (N/m3)	1×10^9	1×10^7	1×10^9
	Tangential stiffness in the transversal direction (N/m3)	1×10^9	1×10^7	1×10^9

Table 12
Results obtained from the updated numerical model.

Mode	Experimental frequency	Numerical frequency	MAC
1	10.30	10.02	0.98
2	14.57	14.95	0.87
3	21.09	20.76	0.96
4	24.13	–	–
5	26.31	25.11	0.95
6	29.45	29.81	0.86
7	31.90	32.11	0.86

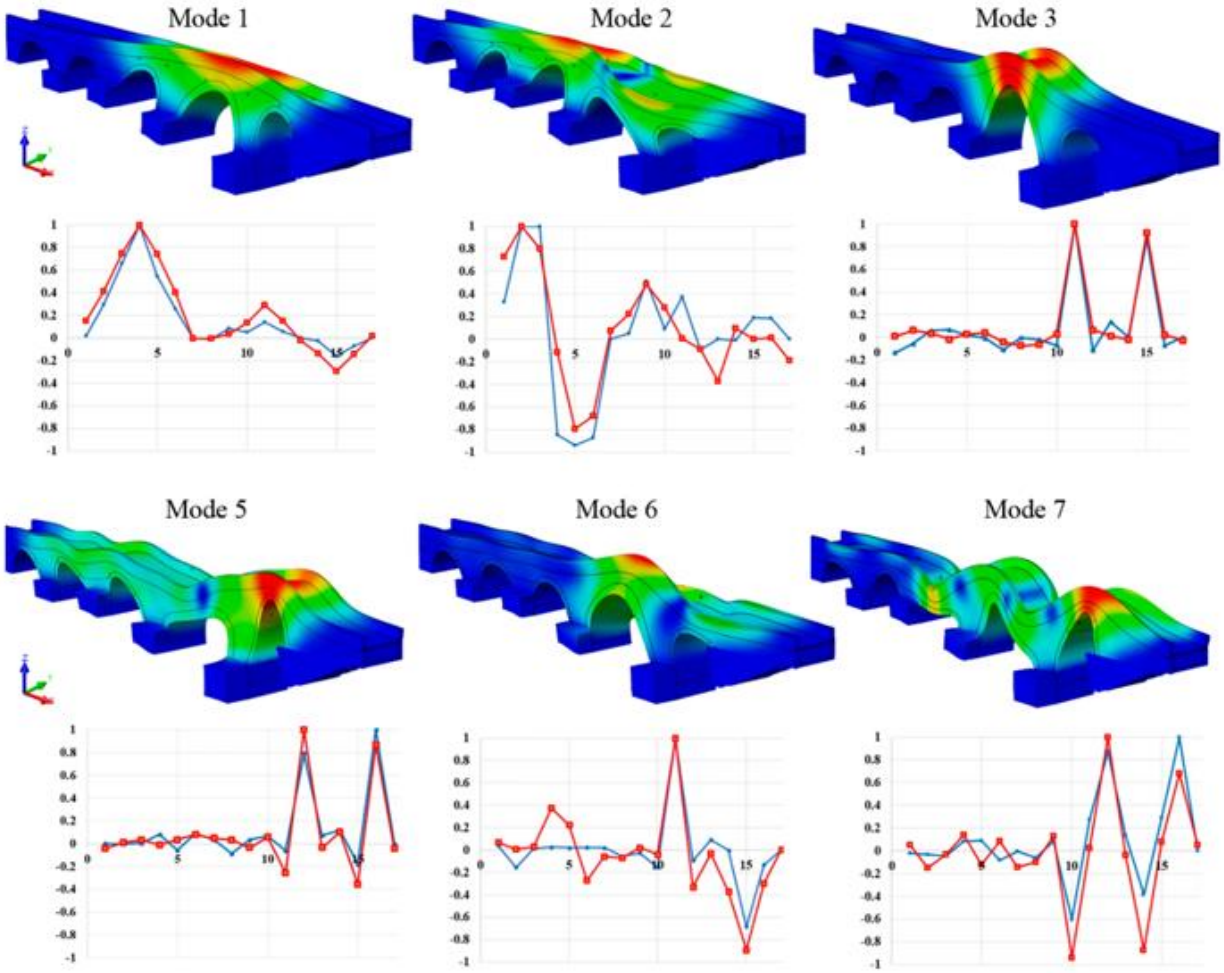

Fig. 20. Results obtained after the manual calibration. The red lines in the graphs represents the numerical normalized modal displacements. The blue lines represent the experimental normalized modal displacements. (For interpretation of the references to colour in this figure legend, the reader is referred to the web version of this article.)

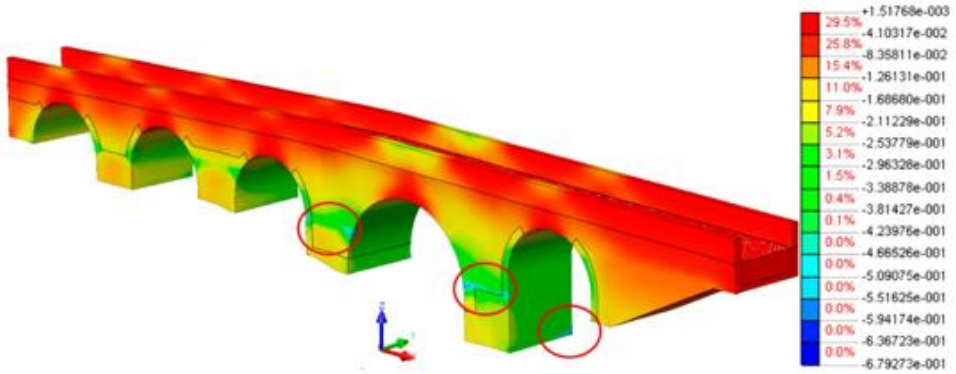

Fig. 21. Contour plot of minimum principal stresses obtained for the Model I (MPa).

possibility of simulating the response of the structure against different hazards such as earthquakes, material losses or pier scours. Therefore, the structure used to validate the proposed multidisciplinary approach was also analyzed against its more probable hazard: the material loses. To this end, the resistance section of both the spandrel walls and vaults were reduced by 25% and 50% (Table 13).

As expected, if the resistance section is reduced, the load-bearing capacity of the bridge is also reduced. On the one hand, if the section is

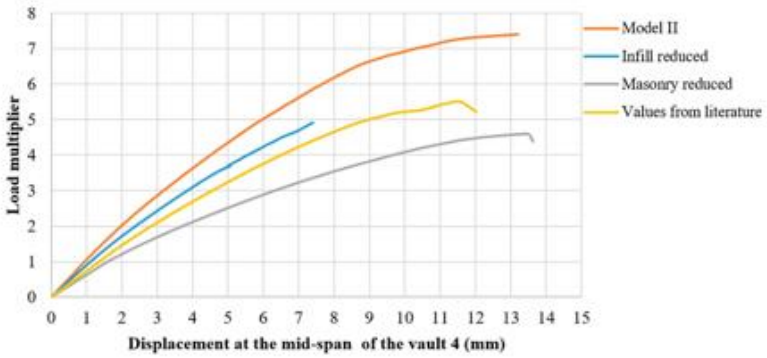

Fig. 22. Load-displacement curves obtained. In orange the response of the bridge in its current configuration. In blue the response of the bridge in case of considering the mechanical properties provided by the literature. In grey and blue the response of the structure in case of reducing by half the masonry and infill properties respectively. (For interpretation of the references to colour in this figure legend, the reader is referred to the web version of this article.)

reduced by 25% the safety factor of the bridge decreases by 13% (from 7.2 to 6.3) (Fig. 25). On the other hand, if the section is reduced by 50% the safety factor decreases by 30% (from 7.2 to 5.2). Thus, based on these results, one might argue that in a medium to a large term the bridge seems to be safe against material losses, mainly due to the high quality of the constituent materials.

As for the collapse mechanism, minor discrepancies were observed with respect to the baseline model (Model II). Thus, for the model that considers a 25% of section reduction, the failure mode is again related to the collapse of the spandrel wall between the barrel vaults 3 and 4, and the tensile cracking of the barrel vault 4 (Fig. 26a). Edge failure of both barrel vaults is again suggested, which is evidenced by the severe concentration of cracks in the form of a staircase pattern going from the springings of the vaults up to ¾ of their rises.

For the model with 50% of section reduction, the collapse mode is mainly related to the consequential and expected weakening of the major barrel vault (vault 4). This way, a severe diagonal crack related to the tensile failure of masonry can be found at the crown (Fig. 26b). Apart from this, a significant bulging of the spandrel wall can also be observed due to the combination of both the high lateral soil pressures generated and the reduction in the section of this element.

7. Conclusions

In this work, a fully non-destructive multidisciplinary approach applied to the structural diagnosis of masonry arch bridges is proposed. This methodology allows a characterization of masonry bridges at different levels: i) geometrical level; ii) material level and; iii) structural

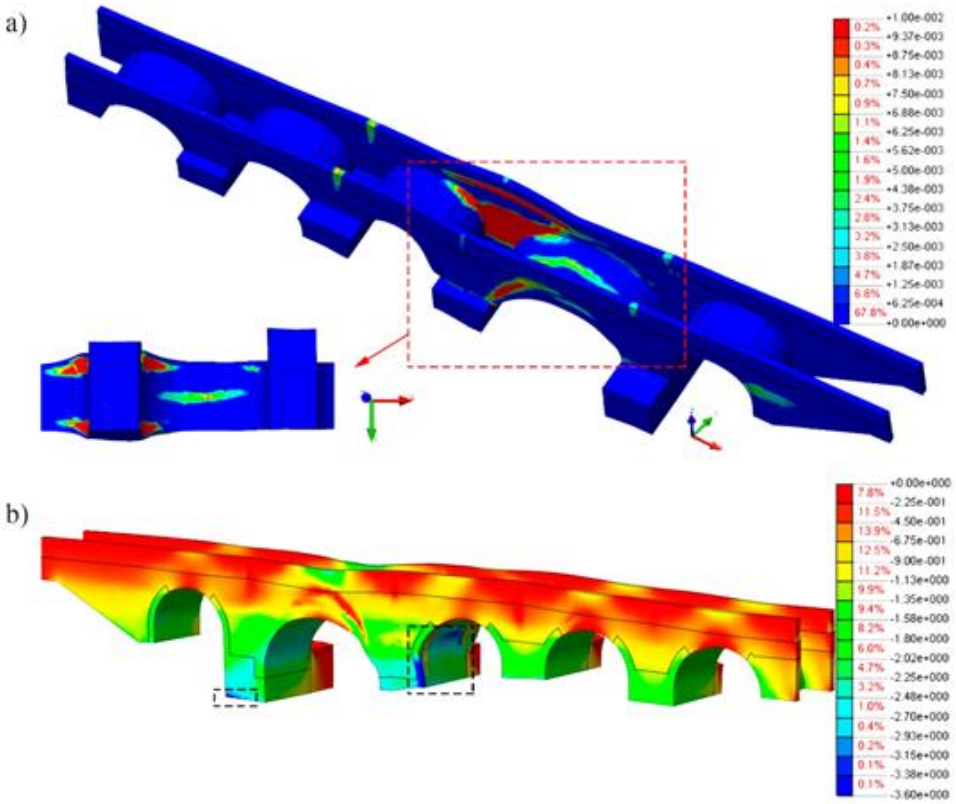

Fig. 23. Deformed shape at failure due to the incremented gravitational loading: a) contour plot of maximum principal strains (indicator of cracking) and; b) contour plot of minimum principal stresses.

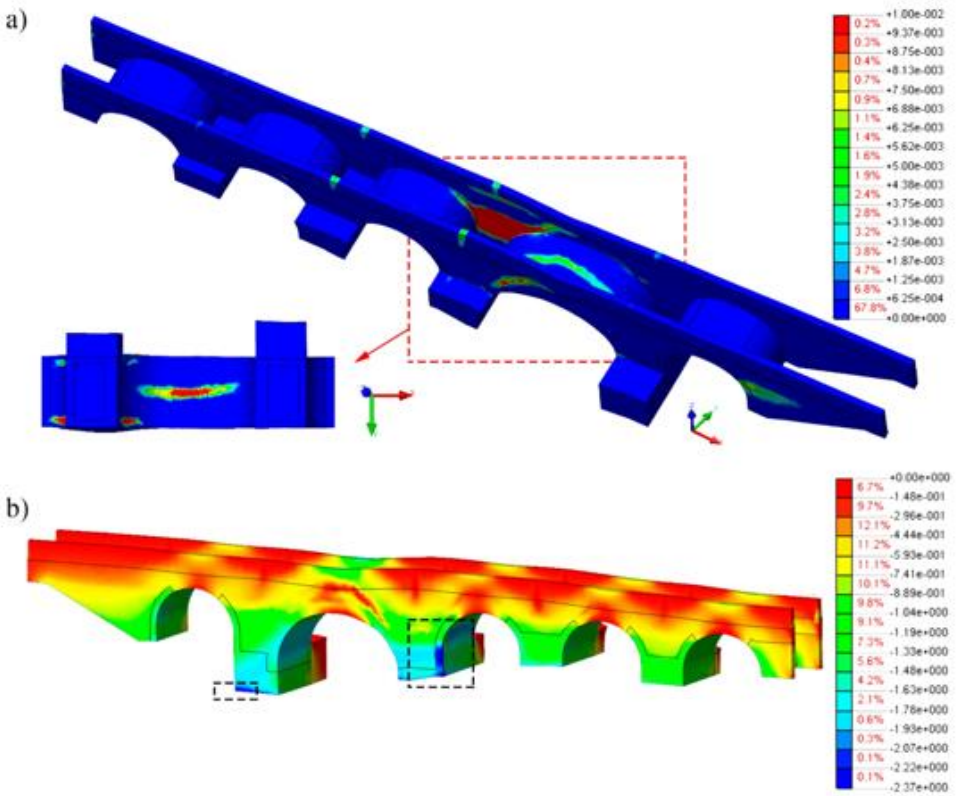

Fig. 24. Results from the numerical model made up by the values provided by the literature [8,46,58]: a) contour plot of maximum principal strains (indicator of cracking) and; b) contour plot of minimum principal stresses.

Table 13
Thicknesses of the spandrell walls and barrel vaults considered.

Element	Original (m)	Reduction of 25%	Reduction of 50%
Vault 1 (West)	0.55	0.41	0.28
Vault 2	0.54	0.41	0.27
Vault 3	0.53	0.40	0.27
Vault 4	0.85	0.64	0.43
Vault 5 (East)	0.55	0.41	0.28
Spandrel wall	0.45	0.34	0.23

level.

From the geometrical point of view, the method uses several well-known approaches such as the terrestrial laser scanner and the ground penetrating radar. These approaches are complemented by several surface waves technologies such as the impact-echo method and the multichannel analysis of surface waves. The former allows evaluating the thickness of the different construction elements (e.g. spandrel walls or vaults). Meanwhile, the latter allows characterizing the inner disposition of the bridge's infill, even in situations in which the ground penetrating radar cannot penetrate. Then, all this data is combined in an as-built CAD model created through the latest means of reverse engineering, i.e. extrusions, boolean operations and Loft surfaces. The combination of these methods allows generating models able to reproduce complex deformations presented in historical constructions.

At the material level, the proposed methodology introduces two surface-waves methodologies. On one hand, the sonic testing for the characterization of the elastic properties of the masonry is proposed. On

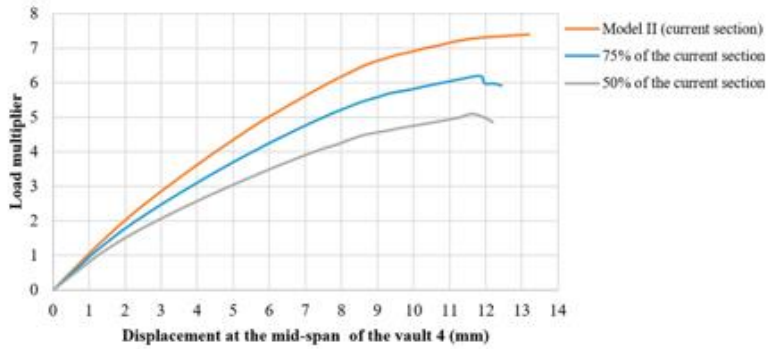

Fig. 25. Load displacement curves obtained during the numerical simulations taking into account possible material loses.

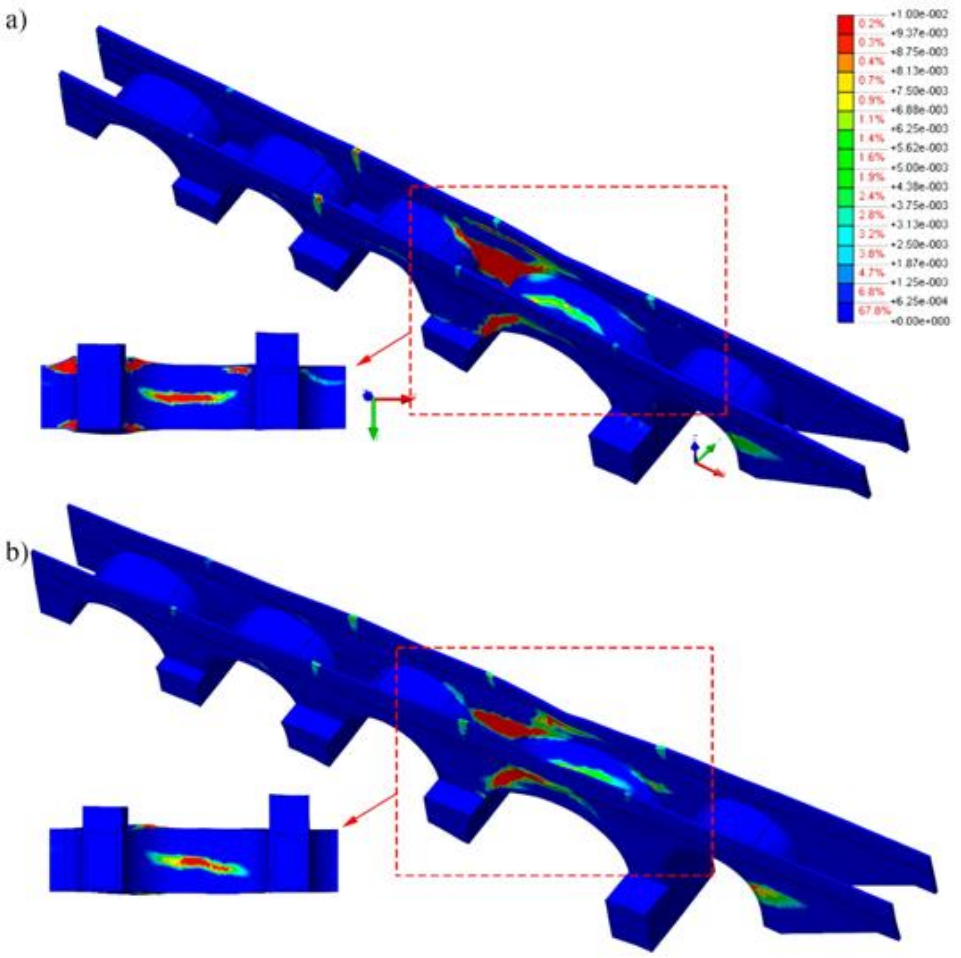

Fig. 26. Results obtained considering a section reduction of the arches and spandrel walls: a) 75% of the original one and; b) 50% of the original one.

the other hand, the multichannel analysis of surface waves is used for the characterization of the Young Modulus and the density of the infill. This method, based on a linear array of geophones, allows creating a 2D profile of the bridge's infill made up by shear-velocities. Both methodologies enable the material characterization of the bridge foregoing the use of invasive techniques.

Finally, the ambient vibration testing was also adopted as a non-destructive technique able to characterize the global response of masonry arch bridges. This technique is used to detect potential mismatches between the real structure behavior and the simulated one.

The combination of all the previously shown methodologies allows generating accurate advanced numerical simulations of masonry arch bridges. In order to evaluate the potentialities and limitations of the proposed methodology, a complex case study was chosen; the Roman bridge over the Adaja River, in Castile and León, Spain. The computational model developed as a result of the proposed methodology was able to capture six of the seven modes detected during the ambient vibration tests. These modes showed an average relative error in frequencies of about 2.22% and an average MAC value of 0.91, corroborating the robustness of the proposed method. Finally, the performance of the structure against vertical loads is evaluated and contrasted with a numerical model created by means of the data obtained in the literature (no experimental data). This comparison highlights the relevance of this methodology, obtaining a discrepancy of 25% in terms of safety factor. Complementary to this evaluation, and taking into consideration the advantages of the finite element method, several numerical simulations were carried out with the aim of evaluating the performance of the bridge in case of ensuing material loses. In all the simulations the results suggest that the bridge has an excellent bearing capacity, being safe in the medium-long term to the material loses that it is suffering.

Futures improvement of the methdodology will be focused on several aspects: i) the use of automatic updating strategies such as those proposed by [8,16,25,27,32] based on genetic and deterministic approaches; ii) further validation of the multichannel analysis of surface waves tests as a potential approach for the analysis of the infill materials and iii) the study of the possible relation between the data provided by the multichannel analysis of surface waves tests and the nonlinear properties of the infill materials.

Acknowledgments

This work was financed by ERDF funds through the V SUDOE INTERREG program within the framework of the HeritageCARE project, Ref. SOE1/P5/P0258 and the research project Patrimonio 5.0 funded by Junta of Castilla y León, Ref. SA075P17. First author would like to thank the University of Salamanca for the program for human resources "Programa II: Contratos Postdoctorales". Authors also wish to thanks to the council of Avila for their support in gathering the historical documentation of the bridge.

References

[1] I. Olofsson, L. Elfgren, B. Bell, B. Paulsson, E. Niederleithinger, J. Sandager Jensen, G. Feltrin, B. Täljsten, C. Cremona, R. Kiviluoma, Assessment of European railway bridges for future traffic demands and longer lives–EC project "sustainable bridges", Struct. Infrastruct. Eng. 1 (2) (2005) 93–100, https://doi.org/10.1080/15732470412331289396.

[2] B. Conde, P. Eguía, G.E. Stavroulakis, E. Granada, Parameter identification for damaged condition investigation on masonry arch bridges using a Bayesian approach, Eng. Struct. 172 (2018) 275–284, https://doi.org/10.1016/j.engstruct.2018.06.040.

[3] C. Modena, G. Tecchio, C. Pellegrino, F. da Porto, M. Donà, P. Zampieri, M.A. Zanini, Reinforced concrete and masonry arch bridges in seismic areas: typical deficiencies and retrofitting strategies, Struct. Infrastruct. Eng. 11 (4) (2015) 415–442, https://doi.org/10.1080/15732479.2014.951859.

[4] V. Sarhosis, S. De Santis, G. de Felice, A review of experimental investigations and assessment methods for masonry arch bridges, Struct. Infrastruct. Eng. 12 (11) (2016) 1439–1464 https://www.tandfonline.com/doi/full/10.1080/15732479.2015.1136655.

[5] P. Zampieri, M.A. Zanini, F. Faleschini, L. Hofer, C. Pellegrino, Failure analysis of masonry arch bridges subject to local pier scour, Eng. Fail. Anal. 79 (2017) 371–384, https://doi.org/10.1016/j.engfailanal.2017.05.028.

[6] A. Arêde, C. Costa, A.T. Gomes, J.E. Menezes, R. Silva, M. Morais, R. Gonçalves, Experimental characterization of the mechanical behaviour of components and materials of stone masonry railway bridges, Constr. Build. Mater. 153 (2017) 663–681, https://doi.org/10.1016/j.conbuildmat.2017.07.069.

[7] A.C. Aydin, S.G. Özkaya, The finite element analysis of collapse loads of single-spanned historic masonry arch bridges (Ordu, Sarpdere Bridge), Eng. Fail. Anal. 84 (2018) 131–138, https://doi.org/10.1016/j.engfailanal.2017.11.002.

[8] B. Conde, L.F. Ramos, D.V. Oliveira, B. Riveiro, M. Solla, Structural assessment of masonry arch bridges by combination of non-destructive testing techniques and three-dimensional numerical modelling: application to Vilanova bridge, Eng. Struct. 148 (2017) 621–638, https://doi.org/10.1016/j.engstruct.2017.07.011.

[9] G. Milani, P.B. Lourenço, 3D non-linear behavior of masonry arch bridges, Comput. Struct. 110 (2012) 133–150, https://doi.org/10.1016/j.compstruc.2012.07.008.

[10] E. Bertolesi, G. Milani, F.D. Lopane, M. Acito, Augustus bridge in Narni (Italy): seismic vulnerability assessment of the still standing part, possible causes of collapse, and importance of the Roman concrete infill in the seismic-resistant behavior, International Journal of Architectural Heritage 11 (5) (2017) 717–746, https://doi.org/10.1080/15583058.2017.1300712.

[11] S. Degli Abbati, A.M. D'Altri, D. Ottonelli, G. Castellazzi, S. Cattari, S. de Miranda, S. Lagomarsino, Seismic assessment of interacting structural units in complex historic masonry constructions by nonlinear static analyses, Comput. Struct. 213 (2019) 51–71, https://doi.org/10.1016/j.compstruc.2018.12.001.

[12] Á. Bautista-De Castro, L.J. Sánchez-Aparicio, L.F. Ramos, J. Sena-Cruz, D. González-Aguilera, Integrating geomatic approaches, operational modal analysis, advanced numerical and updating methods to evaluate the current safety conditions of the historical Bôco Bridge, Constr. Build. Mater. 158 (2018) 961–984, https://doi.org/10.1016/j.conbuildmat.2017.10.084.

[13] J.P.C. Pérez, J.J. de Sanjosé Blasco, A.D. Atkinson, L.M. del Río Pérez, Assessment of the structural integrity of the Roman bridge of Alcántara (Spain) using TLS and GPR, Remote Sens. 10 (3) (2018) 387, https://doi.org/10.3390/rs10030387.

[14] V.N. Moreira, J.C. Matos, D.V. Oliveira, Probabilistic-based assessment of a masonry arch bridge considering inferential procedures, Eng. Struct. 134 (2017) 61–73, https://doi.org/10.1016/j.engstruct.2016.11.067.

[15] M.E. Stavroulaki, B. Riveiro, G.A. Drosopoulos, M. Solla, P. Koutsianitis, G.E. Stavroulakis, Modelling and strength evaluation of masonry bridges using terrestrial photogrammetry and finite elements, Adv. Eng. Softw. 101 (2016) 136–148, https://doi.org/10.1016/j.advengsoft.2015.12.007.

[16] C. Pepi, M. Gioffrè, G. Comanducci, N. Cavalagli, A. Bonaca, F. Ubertini, Dynamic characterization of a severely damaged historic masonry bridge, Procedia engineering 199 (2017) 3398–3403, https://doi.org/10.1016/j.proeng.2017.09.579.

[17] B. Riveiro, J. Caamaño, P. Arias, E. Sanz, Photogrammetric 3D modelling and mechanical analysis of masonry arches: an approach based on a discontinuous model of voussoirs, Autom. Constr. 20 (4) (2011) 380–388, https://doi.org/10.1016/j.autcon.2010.11.008.

[18] B. Riveiro, B. Conde-Carnero, P. Arias-Sánchez, Laser scanning for the evaluation of historic structures, in: M. Khosrow-Pour (Ed.), Laser Scanning for the Evaluation of Historic Structures, Civil and Environmental Engineering: Concepts, Methodologies, Tools, and Applications, IGI Global, Hershey, 2016, pp. 807–835. ISBN-13: 978-1466696198.

[19] B. Conde, L. Díaz-Vilariño, S. Lagüela, P. Arias, Structural analysis of Monforte de Lemos masonry arch bridge considering the influence of the geometry of the arches and fill material on the collapse load estimation, Constr. Build. Mater. 120 (2016) 630–642, https://doi.org/10.1016/j.conbuildmat.2016.05.107.

[20] I. Lubowiecka, P. Arias, B. Riveiro, M. Solla, Multidisciplinary approach to the assessment of historic structures based on the case of a masonry bridge in Galicia (Spain), Comput. Struct. 89 (17) (2011) 1615–1627, https://doi.org/10.1016/j.compstruc.2011.04.016.

[21] B. Riveiro, P. Morer, P. Arias, I. de Arteaga, Terrestrial laser scanning and limit analysis of masonry arch bridges, Constr. Build. Mater. 25 (4) (2011) 1726–1735, https://doi.org/10.1016/j.conbuildmat.2010.11.094.

[22] M. Korumaz, M. Betti, A. Conti, G. Tucci, G. Bartoli, V. Bonora, A.G. Korumaz, L. Fiorini, An integrated Terrestrial Laser Scanner (TLS), Deviation Analysis (DA) and Finite Element (FE) approach for health assessment of historical structures. A minaret case study, Eng. Struct. 153 (2017) 224–238, https://doi.org/10.1016/j.engstruct.2017.10.026.

[23] A.M. D'Altri, G. Milani, S. de Miranda, G. Castellazzi, V. Sarhosis, Stability analysis of leaning historic masonry structures, Autom. Constr. 92 (2018) 199–213, https://doi.org/10.1016/j.autcon.2018.04.003.

[24] S.G. Barsanti, G. Guidi, A geometric processing workflow for transforming reality-based 3D models in volumetric meshes suitable for FEA, The International Archives of Photogrammetry, Remote Sensing and Spatial Information Sciences 42 (2017) 331–338, https://doi.org/10.5194/isprs-archives-XLII-2-W3-331-2017.

[25] L.J. Sánchez-Aparicio, B. Riveiro, D. Gonzalez-Aguilera, L.F. Ramos, The combination of geomatic approaches and operational modal analysis to improve calibration of finite element models: a case of study in Saint Torcato Church (Guimarães, Portugal), Constr. Build. Mater. 70 (2014) 118–129, https://doi.org/10.1016/j.conbuildmat.2014.07.106.

[26] G. Castellazzi, A.M. Altri, G. Bitelli, I. Selvaggi, A. Lambertini, From laser scanning to finite element analysis of complex buildings by using a semi-automatic procedure, Sensors 15 (8) (2015) 18360–18380, https://doi.org/10.3390/s150818360.

[27] E. Bassoli, L. Vincenzi, A.M. D'Altri, S. de Miranda, M. Forghieri, G. Castellazzi, Ambient vibration-based finite element model updating of an earthquake-damaged masonry tower, Struct. Control. Health Monit. 25 (5) (2018) e2150, , https://doi.org/10.1002/stc.2150.

[28] R. Aguilar, M.F. Noel, L.F. Ramos, Integration of reverse engineering and non-linear numerical analysis for the seismic assessment of historical adobe buildings, Autom. Constr. 98 (2019) 1–15, https://doi.org/10.1016/j.autcon.2018.11.010.

[29] M. Solla, R. Asorey-Cacheda, X. Núñez-Nieto, B. Conde-Carnero, Evaluation of historical bridges through recreation of GPR models with the FDTD algorithm, NDT & E International 77 (2016) 19–27, https://doi.org/10.1016/j.ndteint.2015.09.003.

[30] A. Arce, L.F. Ramos, F.M. Fernandes, L.J. Sánchez-Aparicio, P.B. Lourenço, Integrated structural safety analysis of San Francisco master gate in the fortress of Almeida, International Journal of Architectural Heritage 12 (2017) 761–778, https://doi.org/10.1080/15583058.2017.1370507.

[31] C. Costa, A. Arêde, M. Morais, A. Aníbal, Detailed Fe and DE modelling of stone masonry arch bridges for the assessment of load-carrying capacity, Procedia Engineering 114 (2015) 854–861, https://doi.org/10.1016/j.proeng.2015.08.039.

[32] C. Costa, D. Ribeiro, P. Jorge, R. Silva, A. Arêde, R. Calçada, Calibration of the numerical model of a stone masonry railway bridge based on experimentally identified modal parameters, Eng. Struct. 123 (2016) 354–371, https://doi.org/10.1016/j.engstruct.2016.05.044.

[33] The Charter of Krakow: principles for conservation and restoration of built heritage, Available on-line at http://smartheritage.com/wp-content/uploads/2015/03/KRAKOV-CHARTER-2000.pdf , Accessed date: April 2019.

[34] I. Lubowiecka, J. Armesto, P. Arias, H. Lorenzo, Historic bridge modelling using laser scanning, ground penetrating radar and finite element methods in the context of structural dynamics, Eng. Struct. 31 (11) (2009) 2667–2676, https://doi.org/10.1016/j.engstruct.2009.06.018.

[35] A. Blanco Freijeiro, Informes académicos. Puente romano sobre el río Adaja, en Ávila, Boletín de la Real Academia de la Historia 182 (1) (1985) 144–145. Available on-line at: http://www.cervantesvirtual.com/obra/informes-acadmicos-puente-romano-sobre-el-ro-adaja-en-vila-0/ , Accessed date: April 2019.

[36] M.C. Tomás, La manipulación del patrimonio cultural: la Fábrica de Harinas de Ávila, Polit. Soc. 27 (1998) 89–116. Available on-line at: http://revistas.ucm.es/index.php/POSO/article/view/POSO9898130089A , Accessed date: April 2019.

[37] HeritageCARE-Report 1.1: Survey of Construction Systems, Type of Damages and Deterioration Processes within the SUDOE Territory, Available on-line at http://heritagecare.eu/wp-content/uploads/2017/09/HeritageCARE-Report-1.1.pdf , Accessed date: April 2019.

[38] J. García-Talegon, A.C. Iñigo, S. Vicente-Tavera, E. Molina-Ballesteros, Heritage stone 5. Silicified granites (bleeding stone and ochre granite) as global heritage stone resources from Ávila, Central Spain, Geosci. Can. 43 (1) (2016) 53–62, https://doi.org/10.12789/geocanj.2016.43.087.

[39] L.J. Sánchez-Aparicio, S. Del Pozo, L.F. Ramos, A. Arce, F.M. Fernandes, Heritage site preservation with combined radiometric and geometric analysis of TLS data, Autom. Constr. 85 (2018) 24–39, https://doi.org/10.1016/j.autcon.2017.09.023.

[40] M. Franaszek, G.S. Cheok, C. Witzgall, Fast automatic registration of range images from 3D imaging systems using sphere targets, Autom. Constr. 18 (3) (2009) 265–274, https://doi.org/10.1016/j.autcon.2008.08.003.

[41] N.J. Carino, The impact-echo method: An overview, ASCE World Structural Engineering Conference, 2001, pp. 1–18. Available on-line at: https://www.nist.gov/publications/impact-echo-method-overview , Accessed date: April 2019.

[42] L. Miranda, L. Cantini, J. Guedes, A. Costa, Assessment of mechanical properties of full-scale masonry panels through sonic methods. Comparison with mechanical destructive tests, Struct. Control. Health Monit. 23 (3) (2016) 503–516, https://doi.org/10.1002/stc.1783.

[43] G. Grandjean, I. Cousin, M. Seger, J. Thiesson, S. Lambot, B. Van Wesemael, A. Stevens, K. Samyn, A. Bitri, S. Bernardi, From Geophysical Parameters to Soil Characteristics, Available on-line at https://pdfs.semanticscholar.org/832b/3bef86f6889d7bd8dfa268f5bd7d23365bce.pdf?_ga=2.47695463.1384578154.1554894584-921443786.1548157246 , Accessed date: April 2019.

[44] C.B. Park, R.D. Miller, J. Xia, Multichannel analysis of surface waves, Geophysics 64 (3) (1999) 800–808, https://doi.org/10.1190/1.1444590.

[45] L. Knopoff, Observation and inversion of surface-wave dispersion, Tectonophysics 13 (1–4) (1972) 497–519, https://doi.org/10.1016/0040-1951(72)90035-2.

[46] G. Frunzio, M. Monaco, A. Gesualdo, 3D FEM analysis of a roman arch bridge, Historical Constructions, 2001, pp. 591–598. Available on-line at: http://www.csarmento.uminho.pt/docs/ncr/historical_constructions/page%20591-598%20_

69_.pdf , Accessed date: April 2019.
[47] L. Pelà, A. Aprile, A. Benedetti, Comparison of seismic assessment procedures for masonry arch bridges, Constr. Build. Mater. 38 (2013) 381–394, https://doi.org/10.1016/j.conbuildmat.2012.08.046.
[48] R. Brincker, L. Zhang, P. Andersen, Modal identification from ambient responses using frequency domain decomposition, The International Society for Optical Engineering (2000) 625–630. Available on-line at: https://vbn.aau.dk/ws/files/12765845/Modal_Identification_from_Ambient_Responses_using_Frequency_Domain_Decomposition , Accessed date: April 2019.
[49] J. Wang, D. Gu, Z. Yu, C. Tan, L. Zhou, A framework for 3D model reconstruction in reverse engineering, Comput. Ind. Eng. 63 (4) (2012) 1189–1200, https://doi.org/10.1016/j.cie.2012.07.009.
[50] D.I.A.N.A. TNO, DIANA User's Manual, Release 10.2, Available on-line at: https://dianafea.com/manuals/d102/Diana.html, (2017) , Accessed date: April 2019.
[51] EN 1996-1-1, Eurocode 6: Design of Masonry Structures—Part 1-1: General Rules for Reinforced and Unreinforced Masonry Structures, Comité Européen de Normalisation (CEN), Available on-line at https://www.phd.eng.br/wp-content/uploads/2015/02/en.1996.1.1.2005.pdf, (2005) , Accessed date: April 2019.
[52] J. García Talegón, A.C. Iñigo, M. Vicente Hernández, M. Vargas, J.L. Pérez Rodríguez, E. Molina Ballesteros, Granites employed in Ávila-Spain. I. Chemical composition of the different types, Mater. Constr. 44 (233) (1994), https://doi.org/10.3989/mc.1994.v44.i233.594.
[53] EN 1992-1-1, Eurocode 2: Design of Concrete Structures - Part 1–1: General Ruels and Rules for Buildings, Comité Européen de Normalisation (CEN), 2005 Available on-line at: https://www.phd.eng.br/wp-content/uploads/2015/12/en.1992.1.1.2004.pdf , Accessed date: April 2019.
[54] R.J. Allemang, The modal assurance criterion (MAC): twenty years of use and abuse, Sound and vibration 37 (8) (2003) 14–23. Available on-line at: http://www.sandv.com/downloads/0308alle.pdf , Accessed date: April 2019.
[55] M. Tomaževič, Earthquake-Resistant Design of Masonry Buildings, first ed., Imperial College Press, London, 1999 (978-1-84816-083-5).
[56] P. Lourenço, Recent advances in masonry structures: Micromodelling and homogeneization, in: U. Galvanetto, M.H. Ferri Aliabadi (Eds.), Multiscale Modeling in Solid Mechanics: Computational Approaches, Imperial College Press, London, 2009, pp. 251–294. ISBN-13: 978-1848163072.
[57] G. Toniolo, M. di Prisco, Reinforced concrete design to Eurocode 2, first ed., Springer, London, 978-3-319-52033-9, 2017.
[58] Ministerio delle infrastructure e dei trasporti, Norme tecniche per le costruzioni, Decreto Ministeriale del 14, 2008 Available on-line at: http://www.cslp.it/cslp/index.php?option=com_content&task=view&id=66&Itemid=1 , Accessed date: April 2019.

3.3 Un enfoque multidisciplinar para calibrar simulaciones numéricas avanzadas de puentes de arco de mampostería.

El artículo científico publicado en este apartado representa el tercer avance en el desarrollo de la presente Tesis Doctoral. Esta publicación científica describe de forma detallada una nueva metodología multidisciplinar robusta que permite calibrar modelos numéricos avanzados de puentes de arco de mampostería históricos con el fin de poder superar las principales limitaciones que presentan actualmente las simulaciones numéricas de estas infraestructuras.

Esta metodología multidisciplinar propuesta combina procedimientos geomáticos (láser escáner terrestre e ingeniería inversa), técnicas geofísicas (georadar y Análisis Multicanal de Ondas Superficiales), ensayos sónicos indirectos, el método de impacto eco, y ensayos de vibración ambiental con el fin de generar modelos numéricos avanzados de puentes de mampostería. Estos métodos son complementados por un método de calibración de modelos de elementos finitos robusto, basado en la combinación del modelo subrogado PCE (Polynomial Chaos Expansion) con los índices de Sobol para el análisis sensible global y una estrategia de calibración robusta. Con la finalidad de validar esta metodología, se ha utilizado como caso de estudio el puente Arco de Burgohondo (Ávila), donde los resultados obtenidos verifican su viabilidad, obteniendo un error relativo en las frecuencias de un 1.21 % y un valor medio para el MAC de 0.93.

Cabe mencionar que la integración del metamodelo PCE en el análisis sensible global demuestra ser una herramienta eficiente y precisa, ya que requiere llevar a cabo un número menor de iteraciones comparado con el método tradicional de Monte Carlo. En este caso particular, donde han sido consideradas 10 variables de entrada para la construcción del modelo subrogado, ha sido necesario un total de 500 puntos para el DoE (Design of Experiments), lo que supone unas 50 veces el número de variables. De esta forma, el análisis de los índices de Sobol a partir del metamodelo PCE permite evaluar la influencia de cada variable de entrada en la varianza de salida de forma robusta, reemplazando así el uso de análisis sensibles básicos y métodos de correlación (e. g. matriz de correlación de Spearman).

Palabras clave: Puentes de arco de mampostería; Técnicas geomáticas; Técnicas geofísicas; Ensayos de vibración ambiental; Ensayos sónicos; Actualización del modelo de elementos finitos.

Mechanical Systems and Signal Processing 129 (2019) 337–365

Contents lists available at ScienceDirect

Mechanical Systems and Signal Processing

journal homepage: www.elsevier.com/locate/ymssp

A multidisciplinary approach to calibrating advanced numerical simulations of masonry arch bridges

Álvaro Bautista-De Castro [a], Luis Javier Sánchez-Aparicio [a,*], Pedro Carrasco-García [a], Luís F. Ramos [b], Diego González-Aguilera [a]

[a] Department of Cartographic and Land Engineering, University of Salamanca, High Polytechnic School of Ávila, Hornos Caleros, 50, 05003 Ávila, Spain
[b] ISISE, Department of Civil Engineering, University of Minho, Campus de Azurém, 4800-058 Guimarães, Portugal

ARTICLE INFO

Article history:
Received 27 April 2018
Received in revised form 20 February 2019
Accepted 16 April 2019

Keywords:
Masonry arch bridges
Geomatic techniques
Geophysical techniques
Ambient vibration tests
Sonic testing
Finite element model updating

ABSTRACT

This paper proposes a robust multidisciplinary method that combines geomatic procedures (terrestrial laser scanning and reverse engineering), geophysical methods (ground-penetrating radar and multichannel analysis of surface waves), sonic and impact echo tests, and ambient vibration approaches to generate accurate numerical simulations of masonry arch bridges. These methods are complemented by a robust finite element model updating method based on metamodeling global sensitivity analysis and a robust calibration strategy. The results obtained corroborate the feasibility of the proposed methodology with an average relative error in frequencies of 1.21% and an average modal assurance criterion of 0.93.

1. Introduction

Throughout history, masonry arch bridges have been one of the most frequently used constructions in transportation networks. These structures allow overpass of topographic features (such as gullies or rivers) and enable communication and trade between different places. Many of these masonry arch bridges, which were erected during the Roman and Mediaeval periods, are still in use and support new traffic demands for which accurate numerical simulations are necessary [1].

On this topic, accurate structural evaluation of a masonry arch bridge requires extensive knowledge of the different materials and structural systems presented. Within this context, several authors proposed the use of multidisciplinary approaches, with the aim of characterizing the bridge at different levels as follows [1–3]: (i) the geometrical level, (ii) the structural level, and (iii) the material level.

With respect to geometry, certain of these ancient constructions present complex and irregular shapes characterized by a succession of vaults and piers for which photogrammetry and terrestrial laser scanning have been the most suitable solutions [1,2,4]. The product of these procedures, the so-called point cloud, is subsequently used to extract sections or individual measurements for creation of CAD models that do not exploit the advantages offered by the latest advances in reverse engineering [5]. These procedures are able to mimic non-parametric shapes (e.g., existing deformations) using b-spline methods and non-uniform b-spline approaches. Moreover, this type of bridge presents a complex inner composition for which

* Corresponding author.
E-mail addresses: alvarobautistadecastro@usal.es (Á. Bautista-De Castro), luisj@usal.es (L.J. Sánchez-Aparicio), Retep81@usal.es (P. Carrasco-García), lramos@civil.uminho.pt (L.F. Ramos), daguilera@usal.es (D. González-Aguilera).

https://doi.org/10.1016/j.ymssp.2019.04.043
0888-3270/

ground-penetrating radar has been considered the most appropriate solution for characterization, allowing estimates of the thicknesses of spandrel walls, barrel vaults and layering of infill materials.

With respect to material characterization, two main structural components are noted in a masonry arch bridge: (i) masonry and (ii) infill. Masonry is used in the construction of vaults, piers and spandrel walls and can be characterized in situ using sonic tests [1]. These tests allow extraction of the Young's modulus and the Poisson's coefficient via analysis of the waves generated after excitation of the material [6,7]. Infill allows stabilization of the vaults and appropriate transmission of loads from the pavements, and its mechanical and physical properties are a critical issue in structural stability of masonry arch bridges [1,8–10]. Moreover, accurate characterization of the mechanical and physical properties of infill materials is complex, necessitating the use of invasive techniques to extract samples as well as another invasive methods (e.g., Ménard pressuremeter tests) used to locally obtain the infill parameters.

With respect to the structural characterization, many authors propose the use of ambient vibration tests as the most suitable strategy for evaluation of the global behaviour of historical structures [5,11,12]. It is especially useful if numerical simulation of the bridge is conducted using the finite element method, which allows the use of updating methods that enhance the accuracy of the model [1,5]. In these updating strategies, sensitivity approaches are required for evaluation of the influence of each variable in the dynamic response of the bridge. However, the large computational cost of each numerical simulation required in sensitivity analysis leads to the use of a low number of simulations to evaluate the sensitivity of each input via sensitivity methods based on the linear Spearman correlation matrix [5] or basic sensitivity analysis [1,13]. This complexity makes impossible the use of advanced and robust sensitivity methods such as the Sobol's indices [14]. These indices require the use of Monte Carlo simulations to obtain reliable results involving thousands of simulations [15].

Based on this foundation, this article proposes a new fully non-invasive multidisciplinary method that is able to overcome a subset of the main limitations in structural evaluation of historical masonry arch bridges. To this end, the proposed method uses the terrestrial laser scanner, ground-penetrating radar, the impact echo method, and reverse engineering procedures to create as-built CAD models that are able to depict the deformations presented in this type of structure. Moreover, the proposed approach also applies sonic tests for mechanical characterization of the masonry elements, the multichannel analysis of surface waves method for mechanical and physical characterization of infill (without the need for invasive techniques), ambient vibration tests for characterization of the global behaviour of the structure, and the finite element method for advanced numerical simulation of the bridge. Concerning the latter item, the finite element model is enhanced with the use of a robust updating method based on the polynomial chaos expansion meta-modelling strategy for evaluation of the Sobol's indices and the use of a non-linear least squares procedure to minimize the discrepancies between numerical and experimental data.

This methodology is specifically applied to a real case study, the Arco masonry arch bridge, which was erected over the Alberche river and is located in the Avila region of Spain. This ancient construction dates back to the XVIth century according to the description detailed by [16] and was later modified at the beginning of the XXth century to withstand current traffic loads. Thus, this construction presents two different infills, which require accurate mechanical and physical characterization.

This paper is organized as follows. After the Introduction, Section 2 presents the Arco Bridge, followed by Section 3, which describes the experimental campaign performed on this historical construction. Section 4 details the updating process of the numerical model, and finally, Section 5 presents the conclusions.

2. The Arco Bridge (Ávila, Spain)

2.1. Historical background

This historical masonry arch bridge is located on road AV-901, which connects the municipalities of Burgohondo and Villanueva de Avila in the southeast region of Castile and León in Spain. Erected over the Alberche river, this bridge has an origin believed to date back to the 16th century, according to its constructive characteristics [16]: (i) an eurhythmic design, (ii) the use of barrel vaults, (iii) the presence of regular masonry and (iv) a road without variation in width. Throughout its existence, this bridge has experienced modifications due to restoration work after its construction. On 2 October 1920, the rights to construction of a road connecting Avila with the municipality of Casavieja were granted to engineer D. Juan Manuel Torregrosa under a timeframe of completion on 31 March 1923, with this bridge as a component of this road. During this work, the original cambered road of the bridge was removed, a new layer of infill material was added, the spandrel walls were expanded, and the original parapets were replaced by others with larger width (Fig. 1a). However, due to bad weather in this location at the time of the work, the execution time was extended by eight months by order of the Directorate General of Public Works, with completion on 30 November 1923.

Of all of the information supplied on the restoration work performed on this historical construction, it is unknown when the wing wall (Fig. 1b) and the reinforced concrete on the pier (Fig. 1c) were added. However, according to the construction plans of the restoration work finished in 1923, it is known that both components were added after this rehabilitation project (Fig. 1a).

Finally, in 2010, the section of road AV-901 from Burgohondo to Villanueva de Avila was widened, with the exception of the bridge, and the drainage was rehabilitated. As a result, a layer of asphalt was added over the pavement of the bridge without replacement of its parapets.

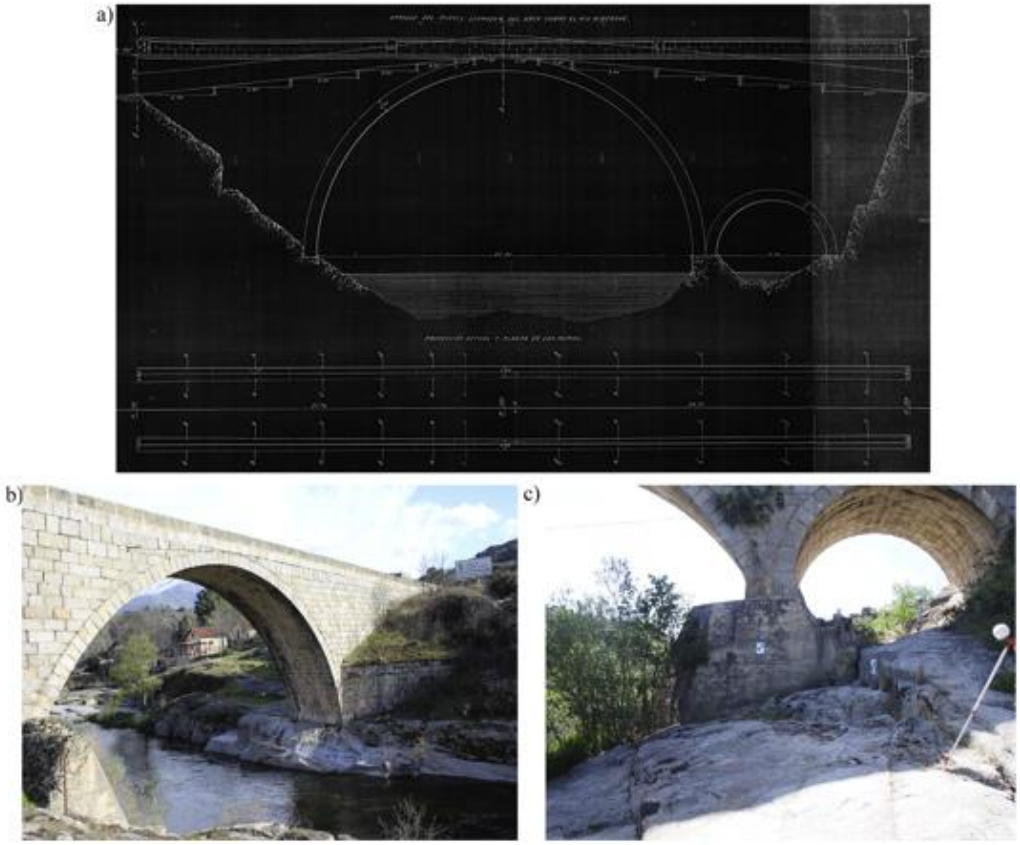

Fig. 1. The Arco Bridge: a) downstream elevation before and after restoration works; b) upstream elevation and; c) reinforced concrete layer added to the pier between vaults.

2.2. Description of the ancient masonry arch bridge

This historical construction presents a total length of approximately 45.91 m, and it contains the following structural components according to the existing drawings (Fig. 2): (i) a main barrel vault with a span of 22.20 m, a rise of 9.05 m and an average thickness of 0.70 m; (ii) a secondary barrel vault with a span of 6.60 m, a rise of 3.15 m and an average thickness of 0.60 m; (iii) spandrel walls with an average thickness of 0.60 m; (iv) a wing wall added after the rehabilitation work of 1923; and (v) a reinforced concrete pier between the two barrel vaults with a height of 4 m. With respect to its inner geometry, the bridge contains the following components: (i) an original infill layer with a maximum depth of 7.11 m, and (ii) an added layer of infill material from the rehabilitation work of 1923 with maximum heights of 2.14 m and 2.30 m at the ends of the bridge.

Complementary to this information, the non-structural elements of the bridge include the following (Fig. 2): (i) asphalt pavement with 150 mm thickness and (ii) two parapets with a height and width of 1000 mm and 400 mm, respectively.

2.3. Damage identification on the bridge: visual inspection

Prior to the experimental campaign on the bridge, visual inspection was conducted to assess its current state and verify the presence of different types of visual indicators of damage (Figs. 3 and 4): (i) out-of-plane deformations and cracks in portions of the spandrel walls, (ii) soiling and white crusts on the barrel vaults due to salts from the mortar used to restore the barrel vaults, (iii) graffiti on the main barrel vault, the wing wall and a parapet, (iv) higher plants on the mortar joints of the spandrel walls and on the mortar joints between the barrel vaults and the spandrel walls, (v) lichens on the wing wall, and (vi) moss. The origin of certain of these damages, such as the out-of-plane deformations and masonry cracks, appear to be related to the current demands of traffic loads as well as unexpected natural events that have occurred in the past.

In addition to the damage indicators previously shown, it was possible to detect two type of masonry (Fig. 4): (i) masonry with material losses in its joints in the spandrel walls and (ii) a masonry without material losses in its joints in the barrel vaults.

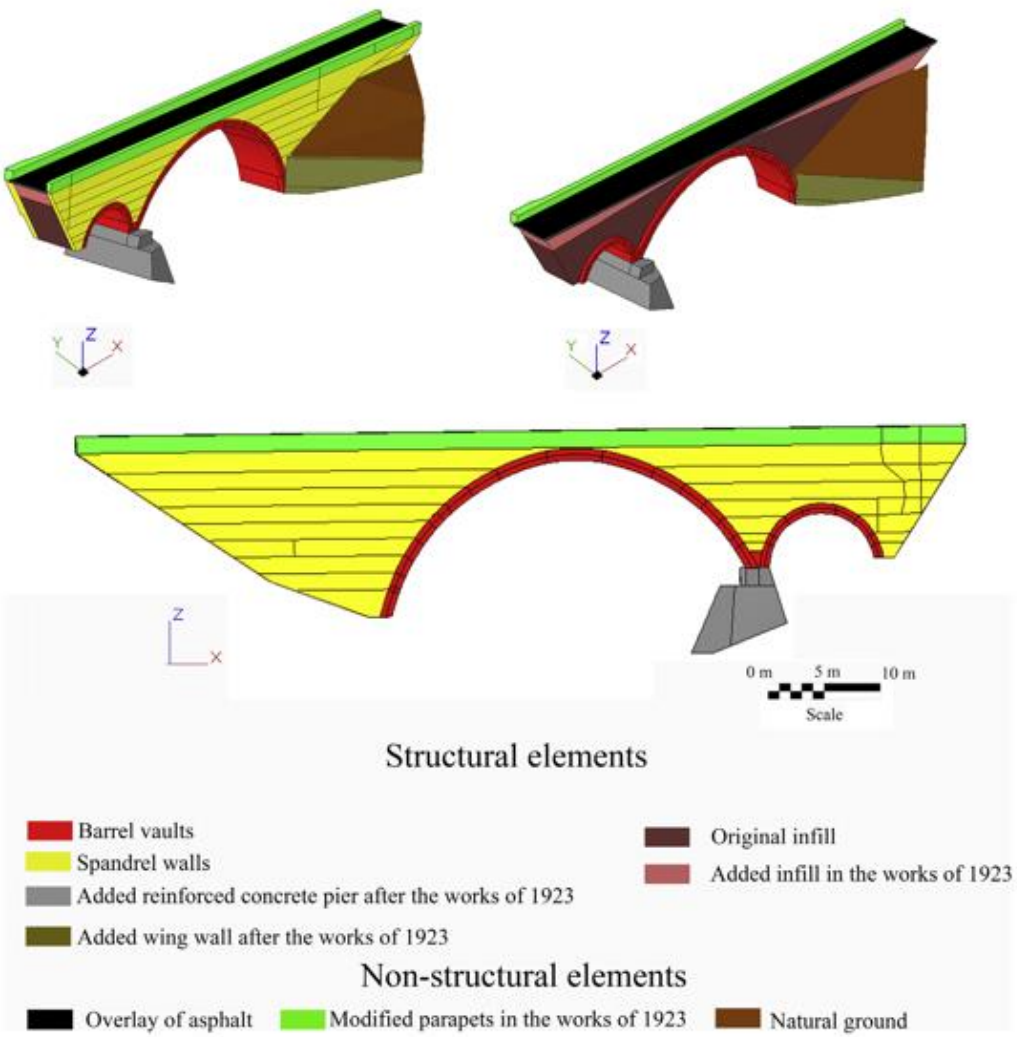

Fig. 2. Structural elements and non-structural elements of the Arco Bridge.

3. Experimental campaign: mechanical, geometrical and dynamical characterization of the Arco Bridge

Accurate numerical simulation of the bridge requires an extensive knowledge of the different structural components of the bridge, and therefore, the below workflow was conducted (Fig. 5).

3.1. Mechanical characterization of materials: multichannel analysis of the surface wave method and sonic tests

Built from masonry, the Arco Bridge is composed of grey granitic spandrel walls and grey granitic barrel vaults originating from the local quarries of Avila. Concerning the inner composition of the structure, historical documentation (Section 2.1) revealed two layers of infill material (Fig. 2). According to this information and considering the relevance of an accurate characterization of the mechanical properties of these structural components, the following non-destructive techniques were used: (i) multichannel analysis of surface waves and (ii) sonic tests.

3.1.1. Multichannel analysis of surface waves

The infill of the bridge can be considered as a soil inserted within the space delimited by its spandrel walls and vaults. Therefore, geophysics can offer a solution for extraction of the mechanical and physical properties of the soils, namely, multichannel analysis of surface waves (MASW) [17,18]. This method allows extraction of the phase velocities and frequencies of the waves created after excitation of a soil. This excitation was performed using a 20.00 kg tenderizer connected to a data

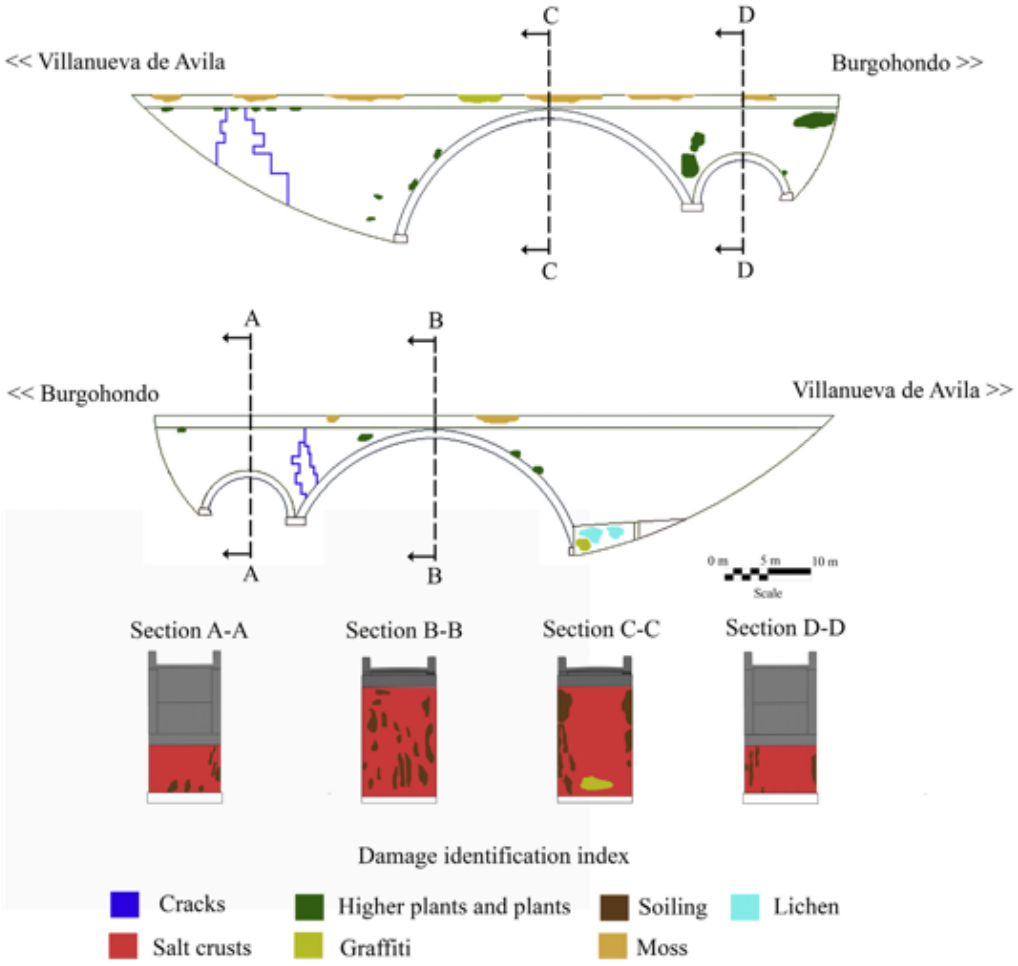

Fig. 3. Damage mapping performed during the visual inspection.

acquisition unit (Fig. 6), and data were captured through a linear array of 24 geophones with a natural frequency of 4.5 Hz. The sensors were placed along the asphalted pavement of the bridge separated by a distance of 0.5 m over a total length of 11.5 m (Fig. 7). To evaluate the reliability of the data acquired, a total of 4 setups were constructed (Fig. 7).

According to the constructive disposition of the bridge and the expected infill distribution (Fig. 2), four setups were installed (Fig. 7). Each setup consisted of a total of 24 geophones with a natural frequency of 4.5 Hz (Fig. 6b) placed along the asphalt pavement of the bridge, separated by a distance of 0.5 m over a total length of 11.5 m (Fig. 7).

From the excitation data captured by the geophones, it was possible to extract the dispersion curve of the soil and its principal model. An optimization procedure known as inversion analysis was performed to obtain the average shear-wave velocities of the soil (*Vs*) with respect to the depth (Fig. 8). Additionally, this method was able to record the primary wave speeds (*Vp*). [17]. The two speeds (*Vs* and *Vp*) are related to the Young's modulus, density, shear modulus and bulk modulus of the soil (Eqs. (1)–(4)).

$$\rho = 1.2475 + 0.399(V_p/1000) - 0.026(V_p/1000)^2 \tag{1}$$

$$E = \rho V_s^2 \frac{3\left(\frac{V_p}{V_s}\right)^2 - 4}{\left(\frac{V_p}{V_s}\right)^2 - 1} \tag{2}$$

$$G = \rho V_s^2 \tag{3}$$

Fig. 4. Current state of conservation of the bridge: a) cracks on the spandrel wall; b) Salt crusts and soiling on the smaller barrel vault; c) Salt crusts, soiling, and graffiti on the bigger barrel vault and d) higher plants on the spandrel wall.

$$K = \rho V_p^2 - \frac{4}{3}G \tag{4}$$

where ρ is the density in kg/m^3, E is the Youngś modulus in GPa, V_p is the primary wave speed of the soil in m/s, G is the shear modulus in GPa, K is the bulk modulus in GPa, and V_s is the shear-wave speed of the soil in m/s.

In addition to these mechanical properties, the N_{spt} (number of blows from the standard penetration tests) of the soil is obtained using Eq. (5).

$$V_s = 85.35N_{spt}^{0.348} \tag{5}$$

As a result, it is possible to characterize the infills of the bridge from a mechanical and physical point of view (Table 1) and estimate the average depths using the V_s obtained during the experimental campaign (Fig. 8).

The large values obtained for the upper bounds of the "original infill layer" (Table 1) can be explained by the presence of selected intrusions of natural soil within the space delimited by the spandrel walls (Figs. 1 and 2).

3.1.2. Sonic testing

In addition to the MASW tests, several indirect sonic tests were conducted in different locations on the bridge with the aim of characterizing the masonry from a mechanical point of view (Fig. 9).

During these tests, an instrumental hammer, a data acquisition unit with 24 bits of resolution and a maximum sampling rate of 100 kHz and several piezoelectric accelerometers (transducers) with a sensitivity of 10 V/g, range of ± 0.5 g and 8 μg rms broadband resolution were used. For each area evaluated, the material was excited with the instrumental hammer, and its excitation (in the form of compressional or primary waves (V_p) and surface or Rayleigh waves (V_r)) was recorded by the

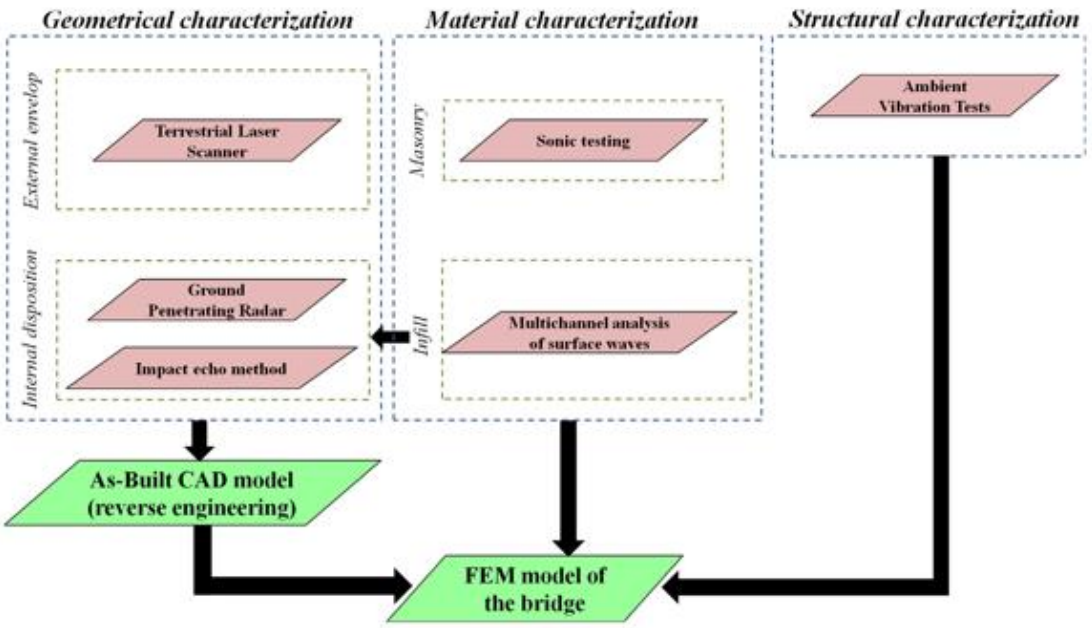

Fig. 5. Workflow of the proposed methodology.

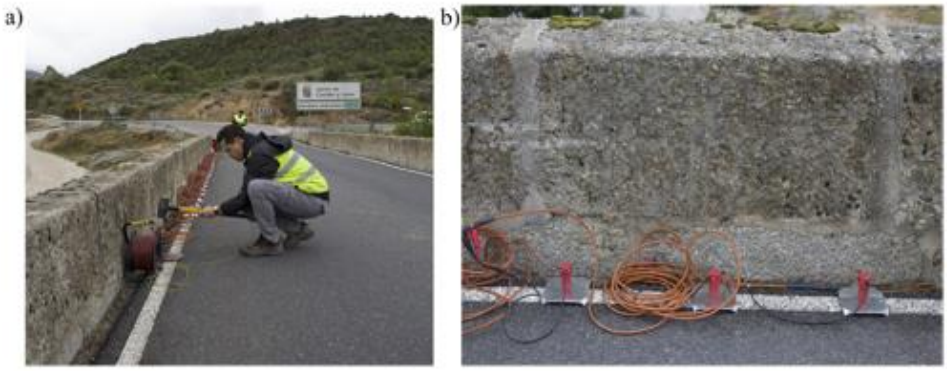

Fig. 6. MASW test carried out on the bridge: a) instrumental hammer and b) geophones with a natural frequency of 4.5 Hz.

transducers. The following equations were applied to evaluate the mechanical properties of the masonry: (Eqs. (6)–(8)) [6,19].

$$V_P = \left(\frac{E(1-\nu)}{\rho(1-\nu)(1-2\nu)}\right)^{1/2} \tag{6}$$

$$V_r = \frac{0.87+1.12\nu}{1+\nu}\left(\frac{E}{2\rho(1+\nu)}\right)^{1/2} \tag{7}$$

$$\frac{V_p}{V_r} = \frac{0.87+1.12\nu}{1+\nu}\left(\frac{(1-2\nu)}{2(1-\nu)}\right)^{1/2} \tag{8}$$

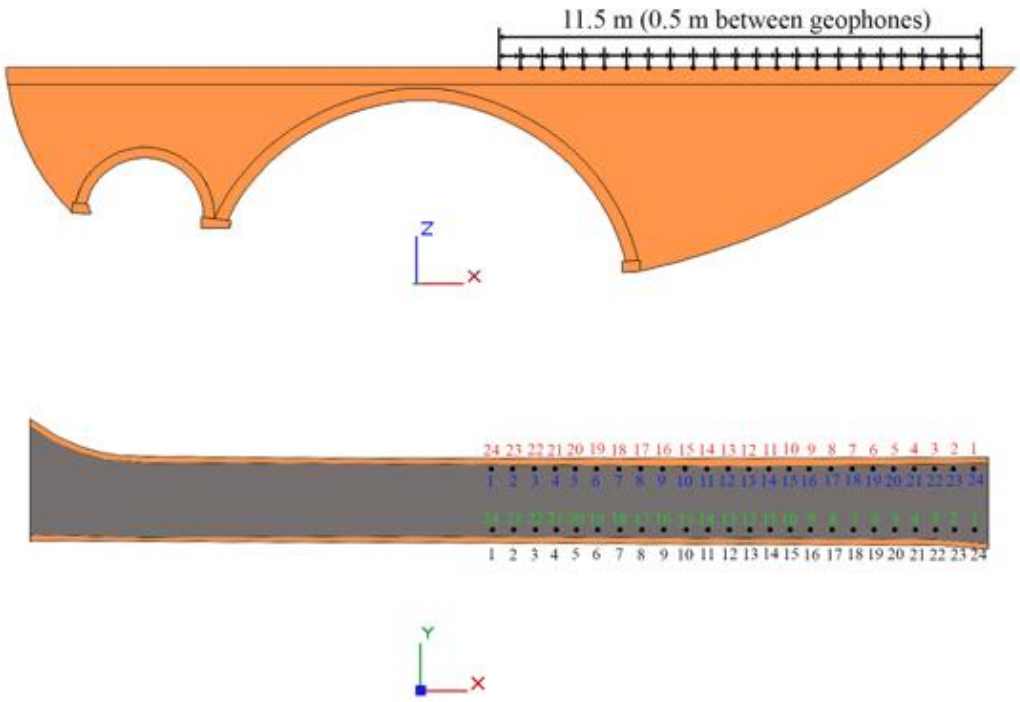

Position 1 of the 24 geophones

Setup 1: 1, 2, 3, 4, 5, 6, 7, 8, 9, 10, 11, 12, 13, 14, 15, 16, 17, 18, 19, 20, 21, 22, 23, 24

Setup 2: 1, 2, 3, 4, 5, 6, 7, 8, 9, 10, 11, 12, 13, 14, 15, 16, 17, 18, 19, 20, 21, 22, 23, 24

Position 2 of the 24 geophones

Setup 3: 1, 2, 3, 4, 5, 6, 7, 8, 9, 10, 11, 12, 13, 14, 15, 16, 17, 18, 19, 20, 21, 22, 23, 24

Setup 4: 1, 2, 3, 4, 5, 6, 7, 8, 9, 10, 11, 12, 13, 14, 15, 16, 17, 18, 19, 20, 21, 22, 23, 24

Fig. 7. Setups and geophones positions used during the mechanical characterization of the two infill layers.

According to the results supplied by the indirect sonic tests (Table 2), two different type of masonry can be considered: (i) the masonry of the spandrel walls, which shows an average Young's modulus of 1.79 GPa, and (ii) the masonry of the barrel vaults with an average Young's modulus of 3.28 GPa. These values are in agreement with the results obtained during the visual inspection (Section 2.3) and appear to be related to the conservation state of the joints because the stones evaluated via indirect tests presented similar velocities (Fig. 9 and Table 3).

3.2. External geometrical characterization: terrestrial laser scanning

Due to difficulty in accessing certain components of the bridge and the extension of the infrastructure, the use of a TLS is the best solution, given its flexibility and rapid data acquisition and processing. To this end, a lightweight TLS Faro Focus 3D 120® instrument was used to digitalize the entire structure. This laser scanner is based on the phase-shift physical principle [20], which applies a significant compromise between data acquisition rate and accuracy (Table 4).

As an addition to the TLS system, several registration spheres with two different diameters (20 cm and 14.5 cm) and several planar targets (Fig. 10b) were used with the purpose to automatically align the different scan stations. To this end, a target-based registration procedure was conducted.

As a consequence, 26 scan stations were needed to conduct 3D digitalization of the entire construction, and these scan stations were distributed as follows: (i) a total of 13 scans on the bridge deck and (ii) a total of 13 scans under the bridge. The alignment error resulting from these scans was 0.009 ± 0.008 m. Considering the goal of the point cloud and the creation of a suitable CAD model for further numerical simulations, additional procedures were required to simplify the large amount of data captured (62,689,274 points). To this end, the procedure proposed in [5] was used. From this process, a more sim-

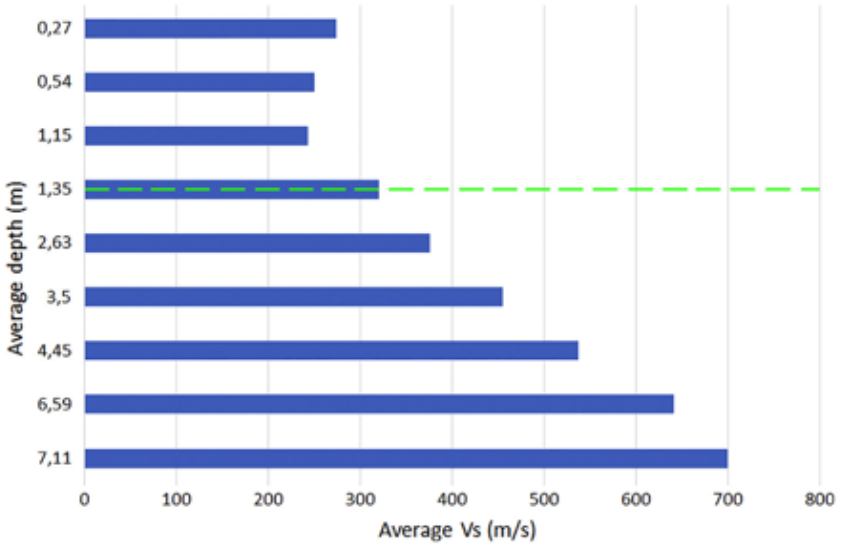

Fig. 8. Estimation of the infill layers through the relation between the average depths and the average V_s speeds. The green line represents the interface between the added and original infill layers.

Table 1
Upper bounds, lower bounds, average values and coefficients of variation (Cov) of the N-SPT, Young Modulus, shear modulus, bulk modulus, Poisson's ratio and density obtained from the MASW tests in the two infill materials. In brackets, the average depths of the added and original infill layers.

		Added infill layer (1.35 m)	Original infill layer (7.11 m)
N-SPT	Upper bound	57.29	581.97
	Lower bound	6.67	52.86
	Average value	29.37	283.54
	Cov (%)	51.02	60.61
Young Modulus (GPa)	Upper bound	0.78	3.18
	Lower bound	0.33	0.56
	Average value	0.41	1.73
	Cov (%)	24.46	41.01
Shear modulus (GPa)	Upper bound	0.19	0.96
	Lower bound	0.11	0.26
	Average value	0.14	0.60
	Cov (%)	34.54	41.85
Bulk modulus (GPa)	Upper bound	4.91	7.08
	Lower bound	3.90	4.88
	Average value	4.44	6.10
	Cov (%)	6.41	11.08
Poisson's ratio	Upper bound	0.50	0.48
	Lower bound	0.48	0.43
	Average value	0.49	0.46
	Cov (%)	0.90	3.02
Density (kg/m^3)	Upper bound	1847.00	1961.00
	Lower bound	1787.00	1848.00
	Average value	1819.00	1909.00
	Cov (%)	0.95	1.80

plified 3D representation of the bridge was obtained with a total of 18,233,172 points (29.08% of the points of the original point cloud) (Fig. 11).

3.3. Internal geometrical characterization: ground-penetrating radar and the impact echo method

3.3.1. Ground-penetrating radar

The ground-penetrating radar (GPR) technique was chosen to characterize the distribution of the inner composition of the bridge from a geometrical point of view as well as the thicknesses of the barrel vaults and spandrel walls. The equipment

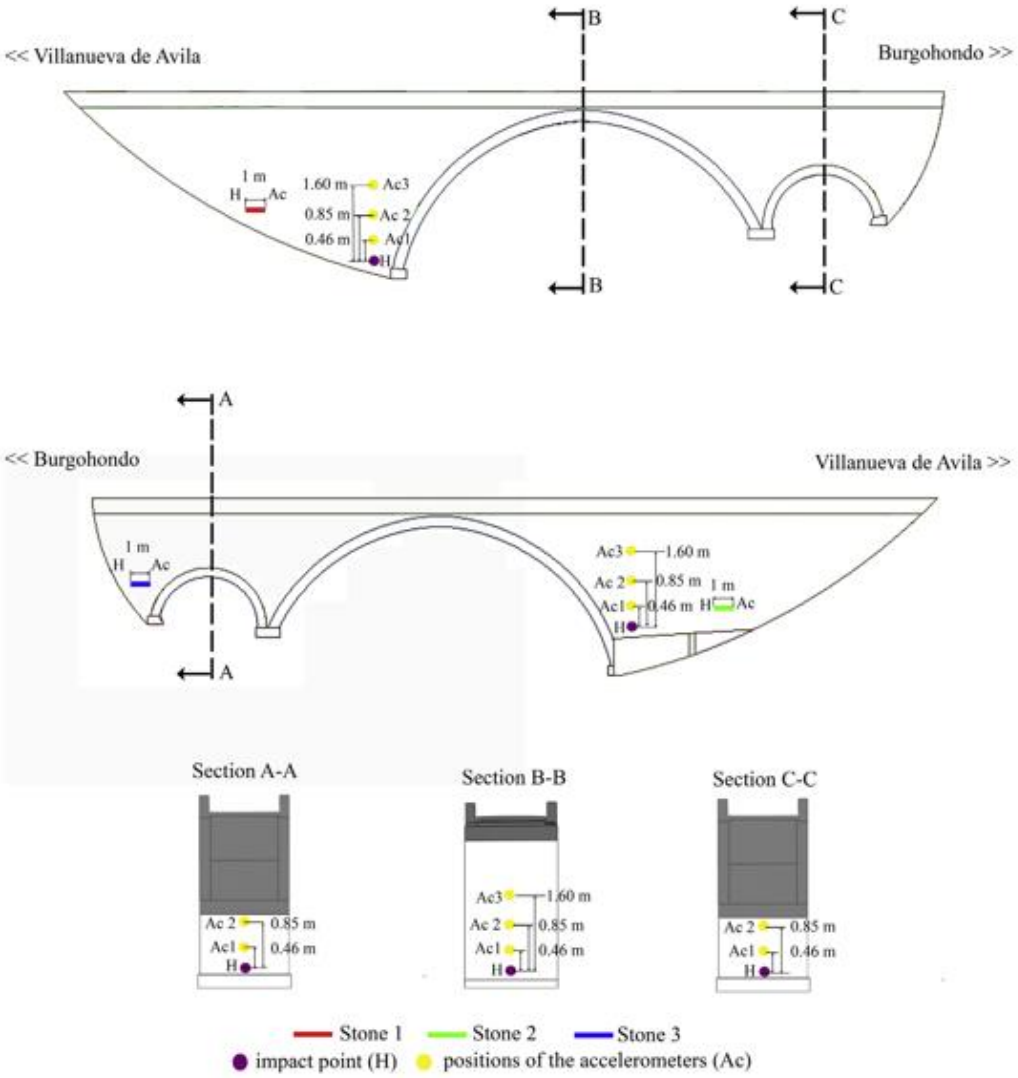

Fig. 9. Places considered for the indirect sonic testing.

Table 2
Results obtained from the indirect sonic tests carried out on the bridge. It is worth mentioning, that a range of densities between 2000 and 2500 kg/m^3, were considered with the aim of obtaining a confidence range of admissible values for the different mechanical properties.

	Spandrel walls		Barrel vaults	
	P-wave	R-wave	P-wave	R-wave
Average velocity (m/s)	1110.00	588.00	1240.00	657.00
Cov (%)	1.56	1.75	0.68	0.55
Poisson's coefficient	0.26		0.24	
Density (kg/m^3)	2000–2500		2000–2500	
Youngs modulus (GPa)	1.00–2.57		2.56–4.00	

applied for this purpose included a X3M® GPR system from MALA Geoscience, which was used to capture a total of six profiles (Fig. 12): (i) two longitudinal profiles in opposite directions to obtain additional information on the homogeneity and stratification of the infill materials, in addition to the thicknesses of the barrel vaults, with a central frequency of 250 MHz

Table 3
Results obtained from the indirect tests carried out on the stones.

	Stone 1		Stone 2		Stone 3	
	P-wave	R-wave	P-wave	R-wave	P-wave	R-wave
Average velocity (m/s)	1113.14	589.96	1146.56	607.68	1113.80	590.31
Cov (%)	0.10	0.08	1.12	1.08	0.06	0.04
Poisson's coefficient	0.26		0.26		0.26	
Density (kg/m^3)	2000–2500		2000–2500		2000–2500	
Young's modulus (GPa)	2.02–2.53		2.15–2.68		2.03–2.53	

Table 4
Technical specifications of the TLS Faro Focus 3D 120®.

Faro Focus 3D 120®	
Measurement principle	Phase shift
Wavelength	905 nm
Measurement range	0.6–120 m
Accuracy nominal value	2 mm to 25 m in normal conditions of illumination and reflectivity
Field of view	360° Horizontal 305° Vertical
Capture rate	122,000/976,000 points
Beam divergence	0.19 mrad

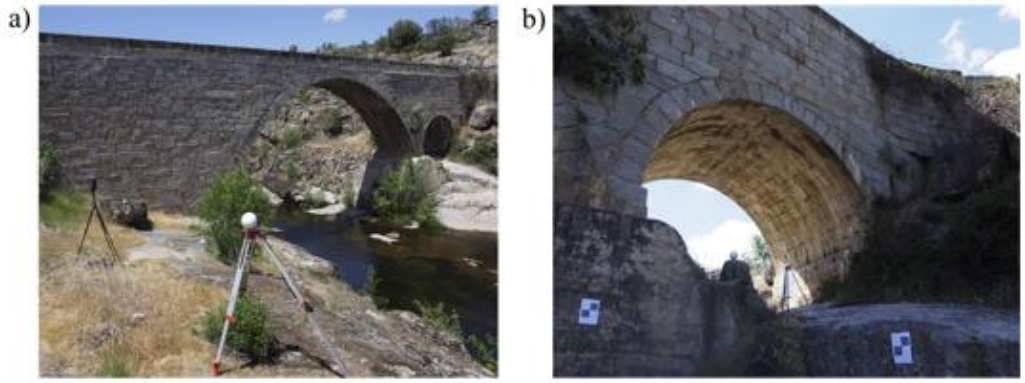

Fig. 10. TLS data acquisition: a) TLS Faro Focus 3D 120® and registration spheres used for scanning the bridge; b) registration spheres and planar targets at the lower part of the bridge.

and a total time-window of 28 ns; and (ii) four profiles in the vertical direction with the aim of characterizing the thickness of the spandrel walls with a central frequency of 800 MHz and a total time-window of 104 ns.

Each horizontal profile (Figs. 12c and 13a) was used to identify two different infill layers (Fig. 2) through the reflection produced between its interfaces until a maximum of 42 ns (2.15 m), whereas the pavement (Fig. 2) was identified by the paving-infill interface at 2 ns (0.20 m). These measurements were obtained with a pre-calibrated velocity of 0.1 m/ns [21]. Moreover, these horizontal profiles were used to estimate the thicknesses of the barrel vaults at an average travel-time distance of 12 ns, corresponding to a thickness value of 0.70 m for the larger barrel vault, whereas the smaller barrel vault did not appear in the horizontal profiles (Fig. 13a) due to the limited depth of penetration of the system. For this reason, a thickness of 0.70 m was assumed for the smaller barrel vault according to the drawings of the bridge (Fig. 1a). Furthermore, the thickness measurement of the larger barrel vault was obtained by the time distance travelled between the reflections of the arch-air interface and the masonry-infill interface, with a pre-calibrated velocity of 0.1 m/ns for granitic ashlar [21]. It is worth mentioning that the thickness values of the asphalt and the major barrel vaults were compared with the data supplied by the most recent restoration project due to the amount of geometrical uncertainty obtained by the 250 MHz GPR antenna.

Additionally, the vertical profiles (Figs. 12a, b and 13b, c) were used to identify the thickness of the spandrel walls via the reflection produced in the masonry-infill interface due to the dielectric contrast between media and the reflections patterns of the infill. Therefore, with the difference between this reflection and the direct-wave reflection at the surface level (air-masonry interface), the thickness of the spandrel walls was estimated at 10 ns (0.60 m) with a pre-calibrated velocity of 0.13 m/ns [21].

Fig. 11. 3D representation of the optimized point cloud of the bridge.

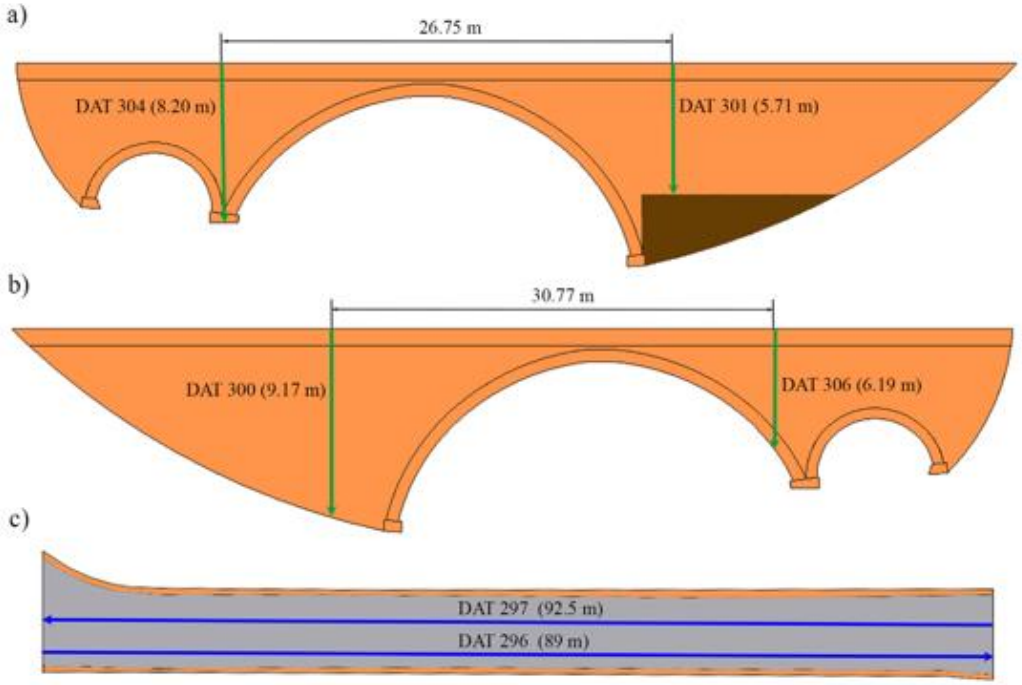

Fig. 12. Positions of the GPR tests considered to characterize the inner distribution of the bridge: a) upstream elevation; b) downstream elevation and; c) plant view. In green the vertical profiles and in blue the horizontal profiles.

It was also possible to observe a high amount of reflections in the area of the masonry, suggesting the presence of holes on the interface between the masonry and the infill as well as in the masonry joints, which was in accordance with the visual inspection and the mechanical values obtained during the sonic tests (Fig. 3 and Table 2).

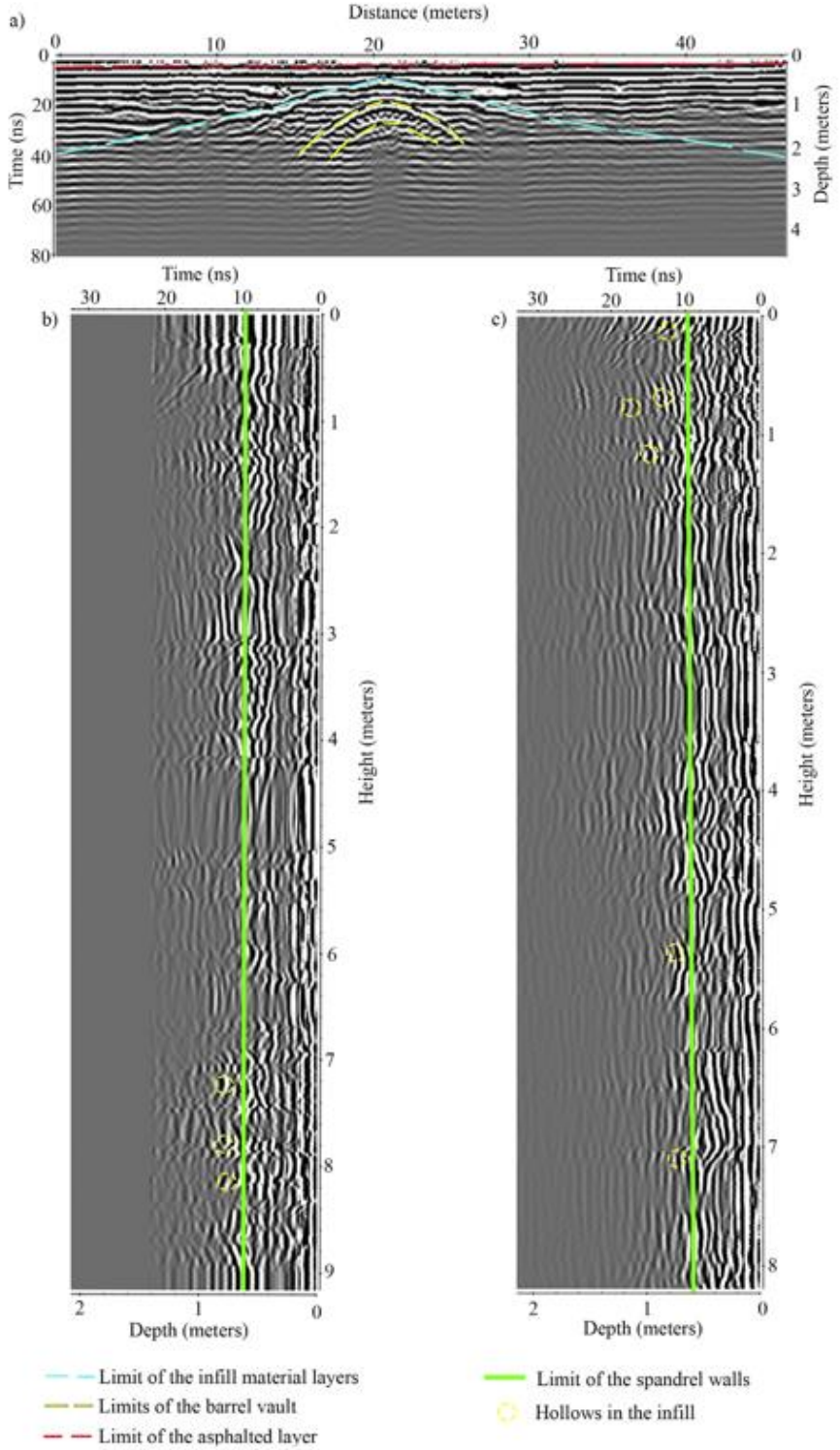

Fig. 13. Results obtained by the ground penetrating radar: a) asphalted layer, infill material layers and barrel vault thickness (DAT 296); b) and c) thickness of the spandrel walls and hollows in the infill layers (DAT 300 and DAT 304).

3.3.2. Impact echo method

The impact echo method was used to ensure and compare the thicknesses of the spandrel walls obtained from the vertical profiles by the GPR (Figs. 12a, b and 13b, c). This test was used to determine the changes in the inner composition of solids (e.g., cracks into elements made by concrete) via Fourier analysis of the wave generated during excitation of the material [22]. During these tests, the same instruments as those used in indirect sonic testing were applied. In this case, the instrumental hammer and the transducers were placed in the same positions (Fig. 14a) considering the starting and ending point as the same point. The excitation captured by the transducer was later transformed into a frequency spectrum via the fast Fourier transform (FFT) (Fig. 14b). The peaks of this spectrum denote the presence of inhomogeneities inside the material and thus indicate the interfaces between the masonry and the infill.

According to this information, 3 impact echo tests were conducted at different points of the bridge (Fig. 9). To obtain reliable results, a total of 10 impacts were performed on each point. The FFT and Eq. (4) were used to obtain the thickness of the spandrel walls (Table 5). It is worth mentioning that this equation requires knowledge of the velocity of the material, using the velocity (V_p) of the stone obtained during sonic testing (Table 3).

$$V_P = 2df \tag{9}$$

where V_p is the velocity of the P-wave in m/s of the stone; d is the thickness of the material in m; and f corresponds to the frequency of the peak in Hz.

As a result, an average spandrel wall thickness of 0.59 m was obtained, with a difference of 1.67% with respect to the average spandrel wall thickness obtained by the GPR (0.60 m) (Table 5).

3.4. Dynamic identification: ambient vibration tests (AVT)

Based on the operational modal analysis (OMA) approach, a dynamic identification campaign was conducted to identify the dynamic properties of the masonry arch bridge: (i) frequencies, (ii) modal displacements and (iii) damping ratios. With the aim of obtaining better results, several numerical evaluations (eigenvalues analysis) were performed. In this context, the results obtained by the tests and the previously shown procedures were considered (CAD model and mechanical properties of the different structural components) as well as the different boundary conditions (with all degrees of freedom fixed and all degrees of freedom fixed except for the Y-axis translation). These previous dynamic simulations were used to establish the most suitable configuration for the OMA tests (such as acquisition time and sampling rate) in addition to placement of the accelerometers in the proper areas of the bridge.

Considering the results obtained from these previous simulations, three setups were used with an acquisition time of 20 min and a sampling rate of 256 Hz. For each setup, a total of 12 uniaxial piezoelectric accelerometers with a sensitivity of 10 V/g, range of ±0.5 g and 8 μg rms broadband resolution were placed along the bridge pavement. Of the 12 accelerometers used during the tests, 7 were considered as references (fixed positions) in the following directions (Fig. 15): (i) accelerometers (3), (4), (5) and (10) in the Z-direction and (ii) accelerometers (2), (4) and (6) in the Y-direction.

Finally, based on raw time series, the stochastic subspace identification principal component algorithm (SSI-PC) was used to determine the frequencies, damping ratios and modal shapes and to obtain the dynamic properties of the bridge [23]. As a result, a total of 5 modes were identified, with frequencies ranging from 5.56 Hz to 18.09 Hz (Table 6 and Fig. 16). The low coefficients of variation (Cov) for the frequencies and damping ratios revealed the quality of the obtained modal properties. For the damping ratio, an average value of 3.48% was obtained.

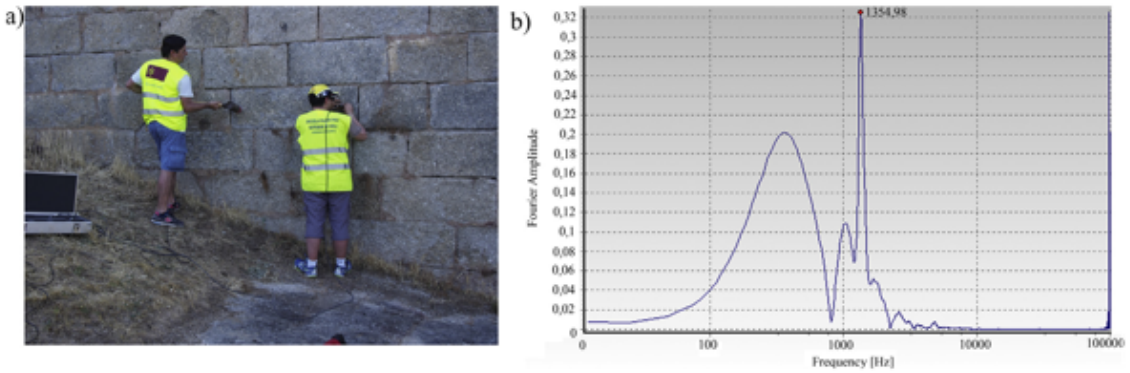

Fig. 14. Impact echo tests carried out on the bridge: a) instrumented hammer and accelerometer and; b) identified peak from the frequencies obtained by the Fourieŕs spectrum.

Table 5
Comparison between the spandrel walls thicknesses obtained by the impact echo tests regarding average spandrel walls thickness obtained by the GPR.

Number of stone	Average velocity of the P-waves (m/s)	Average frequency (Hz)	Thickness (m)	Average thickness (GPR)	Difference (%)
Stone 1	1113.14	915.53	0.61	0.60	1.67
Stone 2	1146.56	791.63	0.72	0.60	20.00
Stone 3	1113.80	1298.83	0.43	0.60	28.33

4. Numerical model of the current state of the bridge

Robust structural evaluation of masonry arch bridges requires the development of an extensive experimental campaign with the aim of characterizing the structure from different points of view and accurate design of numerical models able to reproduce the structural behaviour against different causes, such as static or seismic loads. In this sense, the use of the finite element method (FEM) is one of the most frequently used solutions for the structural evaluation of bridges [1,5,13].

4.1. From the point cloud to the numerical model

Considering all of the data supplied by the experimental campaign, an as-built CAD model was constructed. This CAD model was created with the external envelope from the TLS (Fig. 11) and the inner distribution of the different infills and thickness of the masonry from the GPR and impact-echo tests (Figs. 12 and 13) (Section 3.3.2).

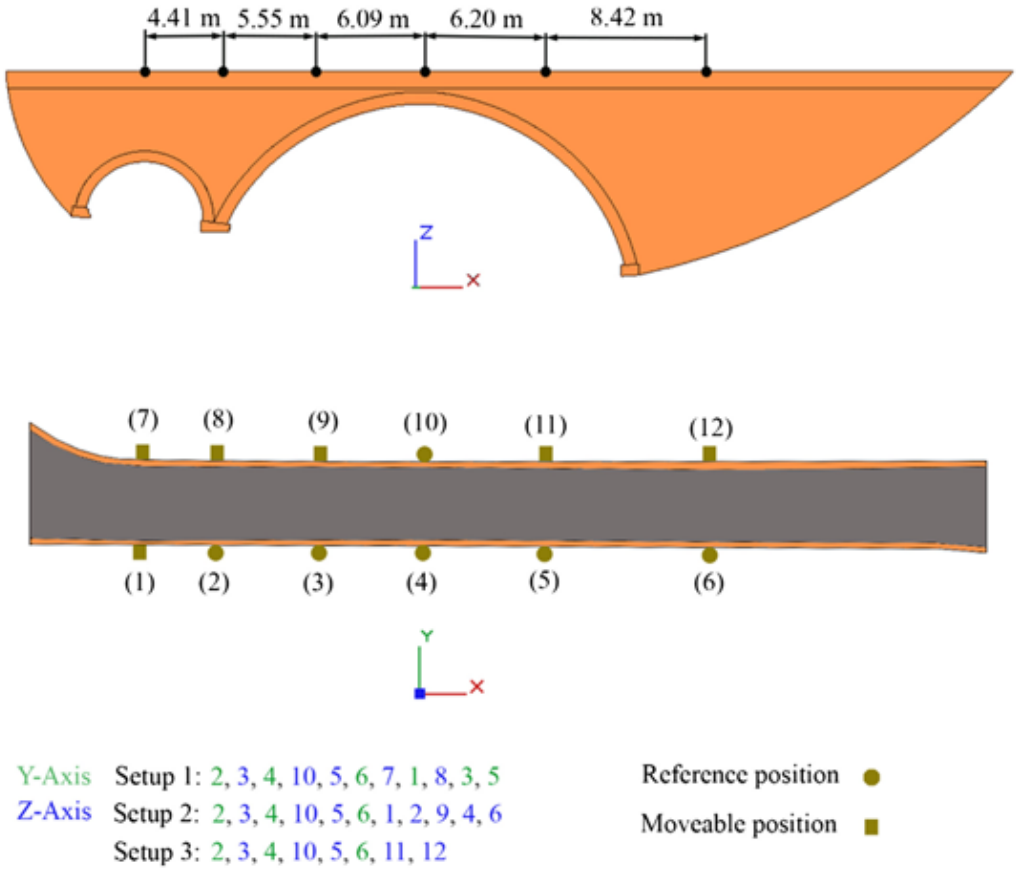

Fig. 15. Setups and positions of the accelerometers used during the dynamical identification campaign.

Table 6
Natural frequencies and damping ratios obtained from the AVT.

Mode shape	Frequencies (Hz)	CoV (%)	Damping ratios (%)	CoV (%)	Description
1	5.56	0.02	2.53	1.60	1st asymmetrical translational (Y-axis)
2	8.22	<0.01	2.29	2.50	2nd asymmetrical translational (Y-axis) 1st asymmetrical torsional (X-axis)
3	9.31	0.02	4.30	1.83	3rd asymmetrical translational (Y-axis) 1st asymmetrical vertical bending (Z-axis)
4	11.47	0.04	3.63	2.47	2nd asymmetrical vertical bending (Z-axis)
5	18.09	0.03	4.65	2.87	4th asymmetrical translational (Y-axis) 2nd asymmetrical torsional (X-axis)

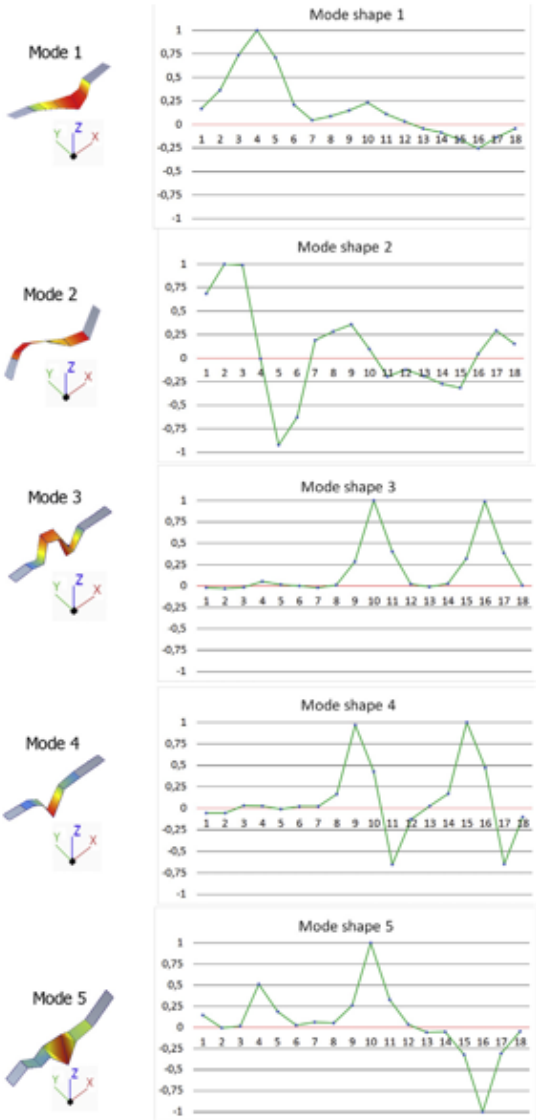

Fig. 16. Graphical representation of the vibrational modes obtained by the SSI-PC algorithm. The green line are the experimental modal displacements. The horizontal axis and the vertical axis of the graphs represent the degree of freedoms and the normalized modal displacements, respectively.

The as-built CAD model was analysed using the methodology defined by [5]. This methodology includes the following stages: (i) alignment of the point cloud according to the main axis of the bridge (Fig. 17) and (ii) construction of the CAD model via reverse engineering procedures.

For the first stage, principal component analysis was applied over the entire point cloud with the use of the following equations (Eqs. (10) and (11)). This evaluation produced the maximum dispersion direction (third eigenvector), which corresponds to the longitudinal axis of the bridge. A rotation along the z-axis was performed with the aim of aligning the x-axis of the point cloud with the longitudinal axis of the bridge (Fig. 17).

$$V_i = \frac{1}{n-1}\sum_{m=1}^{n}\left(X_{im} - \overline{X}_i\right)^2 \tag{10}$$

$$C_{ij} = \frac{1}{n-1}\sum_{m=1}^{n}\left(X_{im} - \overline{X}_i\right)^2\left(X_{jm} - \overline{X}_j\right)^2 \tag{11}$$

where V_i and C_{ij} are the variance and the covariance of each variable i and j; n is the number of points of the data matrix from the point cloud, $\sum_{m=1}^{n}$ is the sum over all n points; X_{im} is the value of each variable i; X_{jm} is the value of each variable j; $\overline{X}_i$ is the mean of the variable i and; $\overline{X}_j$ is the mean of the variable j.

In the second step, the multistep geometrical modelling method proposed by [24] was used. This methodology is based on the following stages: (i) Delaunay triangulation of the aligned point cloud, (ii) hole filling based on radial basis functions [25], (iii) topological noise removal via local re-triangulation [26], (iv) segmentation of the different structural components, and (v) adjustment of the segmented elements into basic primitives based on linear and non-linear (b-splines) extrusions. As a result, a mesh composed of a total of 9,567,843 triangles was transformed into a suitable and accurate CAD model of the bridge for subsequent numerical simulations (Fig. 18).

Finally, the FEM method was applied in the CAD model to perform further numerical simulations using the software TNO Diana® [27]. As a result, a mesh composed of a total of 128,884 elements was obtained (Fig. 19) including (i) 127,089 solid elements for the structural components and (ii) 1,795 interface elements for simulating the interaction of the bridge with the soil. This mesh was built assuming the following criteria: (i) maximum size of the element = 1 m, (ii) minimum size = 0.3 m to better represent the geometry of the as-built CAD model, and (iii) a minimum of 2 elements in the thickness direction of the barrel vaults to identify possible non-linearities in further non-linear assessments.

However, although the numerical model is detailed from the point of view of each structural element in the best possible way, certain simplifications were assumed considering the feasibility of the model development and computational cost reduction in subsequent numerical simulations. Thus, the thicknesses of the spandrel walls and barrel vaults was assumed to be constant over the entire height and width, respectively. Furthermore, the wing wall and the reinforced concrete pier were not included in the final model because they can be considered as perfect fixed structures (Figs. 19 and 20).

4.2. First results from the numerical model of the Arco Bridge

Considering the mean values of the mechanical parameters obtained during the experimental campaign (Tables 1, 2 and 7) and assuming boundary conditions in agreement with the bridgés surrounding medium (all degrees of freedom fixed with infinite normal and shear stiffnesses in all interface elements), an initial assessment was performed (Fig. 19). To evaluate the accuracy of the numerical model, two quality indices were considered: (i) the relative error between the numerical and experimental frequencies and (ii) analysis of the discrepancies between modal displacements via the modal assurance criterion (MAC) [28]. The results obtained from the evaluation of the different quality indices revealed a rigid structure (high relative error between frequencies, especially in mode 1) as well as moderate discrepancies in modes 2 and 3 (transversal modes) with respect to the modal displacements (Table 8 and Fig. 20).

According to the previous results (Table 8 and Fig. 20), it was possible to observe selected discrepancies in the first frequency and lower MAC values in the 2nd and 3rd eigenmodes, suggesting the necessity of using an updating method to enhance the results.

For more in-depth evaluation of the origin of the discrepancies in the 2nd and 3rd eigenmodes, the coordinate modal assurance criterion (COMAC) [28] was used. As a result, it was possible to observe a concentration of discrepancies in the following degrees of freedom (Fig. 21): (i) the first degree of freedom in the Y- axis direction and (ii) the fourth and tenth degrees of freedom in the Z-axis direction. These discrepancies correspond with the mid-span of the larger barrel vault as well as an iteration in the soil-bridge (see Section 3.3).

4.3. Numerical model updating strategy

Considering the results obtained in the previous section (Table 8) (Figs. 20 and 21), an updating procedure was conducted. During this procedure, the following stages were considered: (i) global sensitivity analysis and (ii) minimization of the cost function.

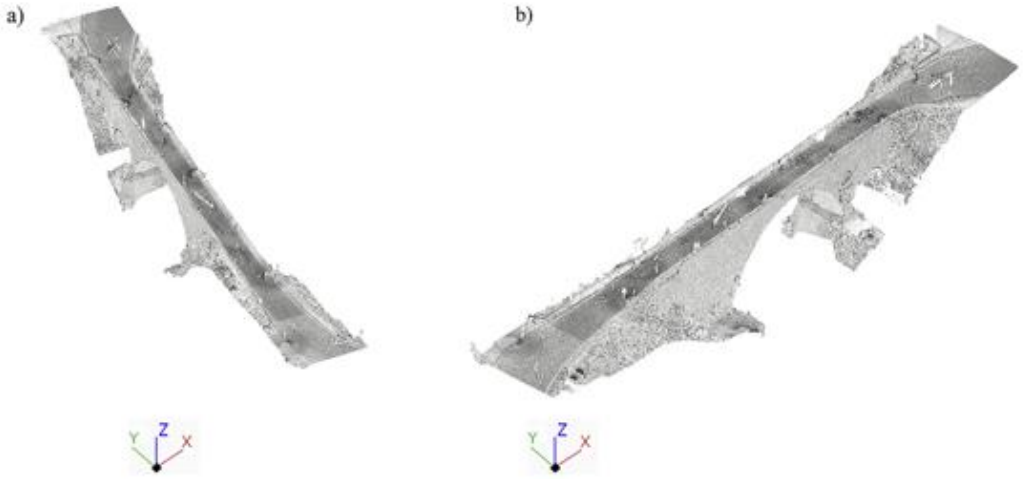

Fig. 17. Results applying the methodology proposed by [5]: a) original point cloud; b) rotated point cloud.

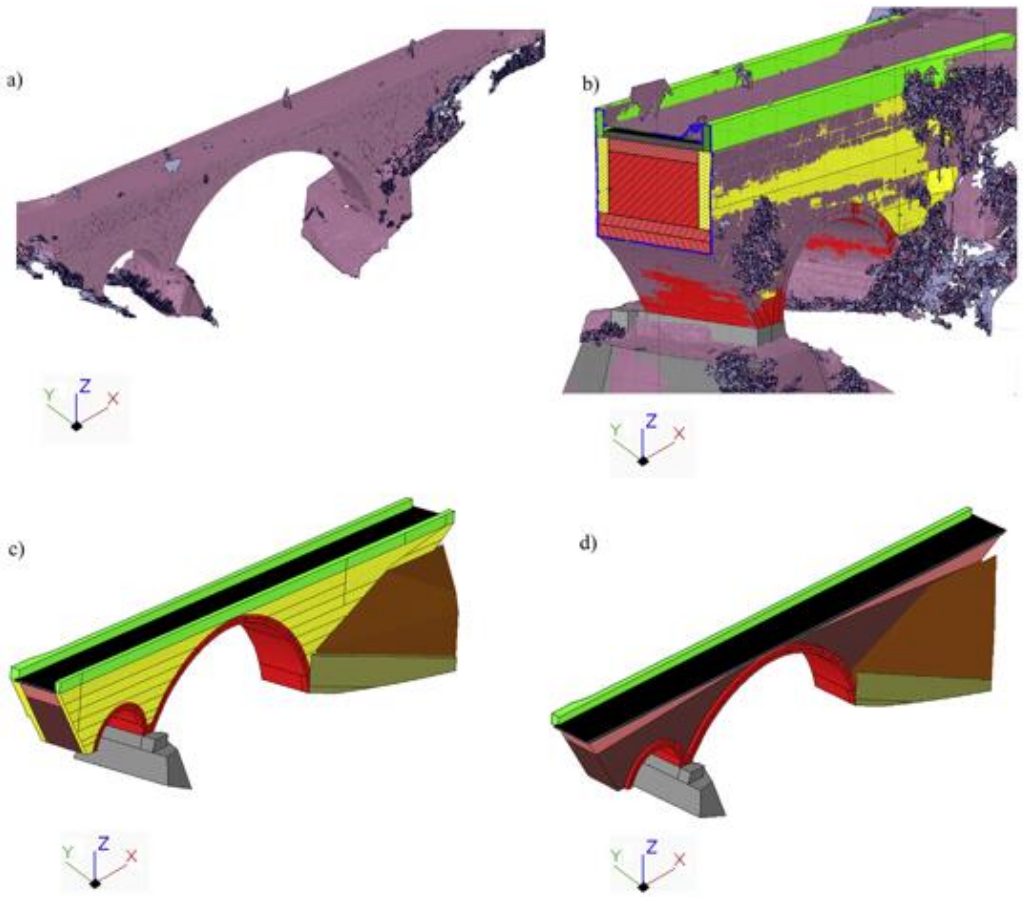

Fig. 18. As-built CAD model obtained: a) isometric view of the mesh obtained from the rotated point cloud; b) detail of the accuracy between the CAD model and the mesh c) isometric view of the as-built CAD model and d) isometric view of the infill material layers.

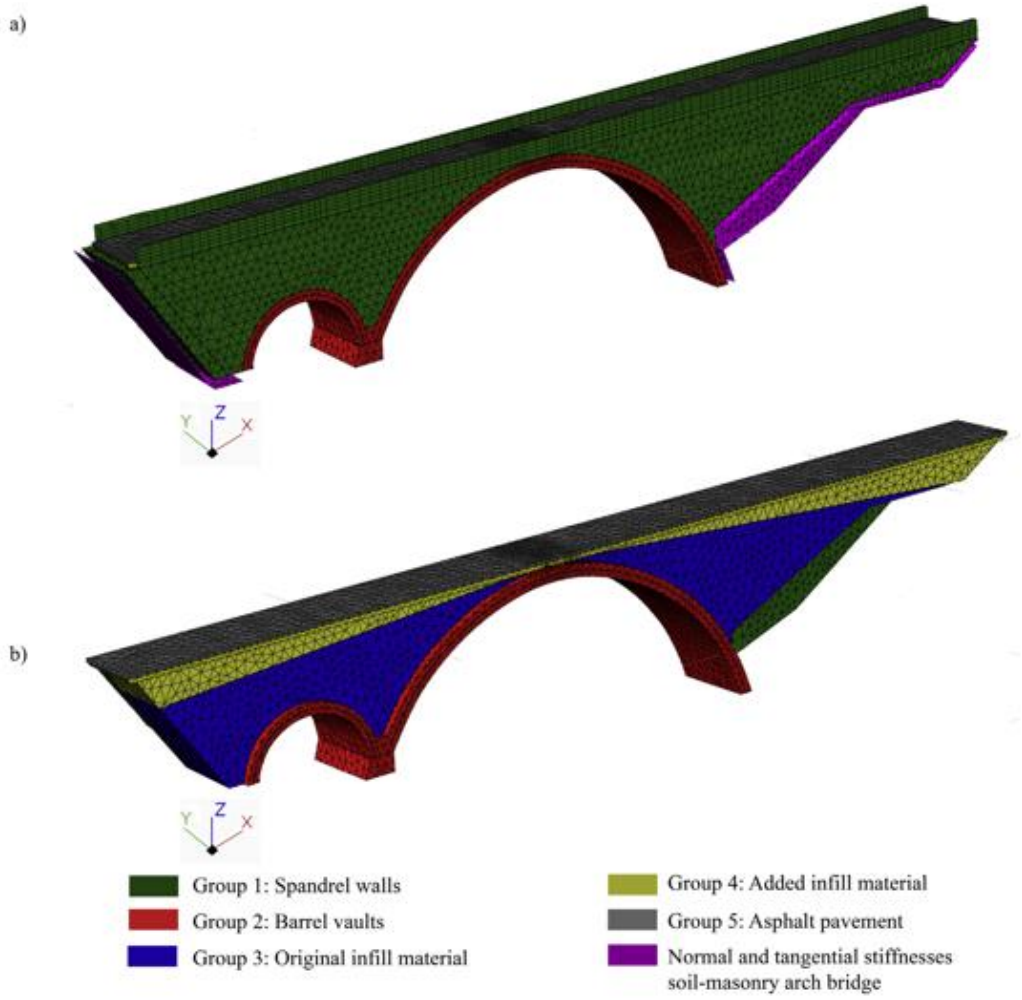

Fig. 19. Mesh model used for the numerical simulations: a) bridgés envelop and b) inner distribution of the bridge.

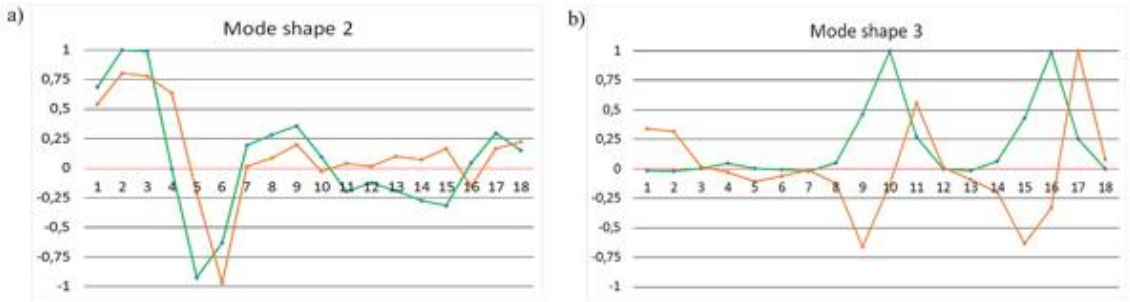

Fig. 20. Comparison between experimental and numerical modal displacements of the mode shape 2 and the mode shape 3. In green the experimental modal displacements and in orange the numerical ones. The vertical axis of the graphs represent the normalized modal displacements and the horizontal axis the degree of freedoms. (For interpretation of the references to colour in this figure legend, the reader is referred to the web version of this article.)

Table 7
Average values of the Youngs modulus and densities calculated from the values obtained during the sonic tests (Groups 1 and 2) and MASW tests (Groups 3 and 4). With respect to the asphalt pavement (Group 5), the average values proposed by Von Quintos [29] were assumed.

Group	Elastic modulus (GPa)	Density (kg/m^3)
Group 1	1.78	2250
Group 2	3.29	2250
Group 3	1.73	1909
Group 4	0.41	1819
Group 5	2.41	2237

4.3.1. A global sensitivity analysis based on the combination of polynomial chaos expansion and Sobol's indices

Global sensitivity analysis is used to determine how the variability of the model response (frequencies and modal displacements) is affected by the value of the input parameters (variables of the model). A common and robust technique is based on the decomposition of the response variance as a sum of contributions that can be associated with each input, i.e., the so-called Sobol's indices [14]. Commonly, these indices are evaluated using Monte Carlo simulations, which require thousands of simulations to obtain reliable results. Therefore, this strategy is non-viable for those cases in which the computational costs of the numerical model are high [15].

As such, a reliable alternative is the use of the so-called surrogate models. These models are compact and scalable analytical models that approximate the input output response of a complex system, i.e., in this case, advanced numerical simulation approximations of the original computational model requiring only a limited number of runs to obtain accurate results (Eq. (12)).

$$x \epsilon D_x \subset R^d \rightarrow y = f(x) \tag{12}$$

where $\times$ are the input parameters; D_x the space of these parameters, y the output of the subrogate and $f(x)$ the subrrogate model.

Of the wide variety of metamodels that are currently available, from Kriging metamodels to radial basis functions [30], the polynomial chaos expansion (PCE) is one of the most used options. This approach evaluates the sensitivity indices and their iterations [30] and assumes that the numerical simulation can be represented as a finite variance model $M(X)$ whose inputs x are a random vector of independent constrained variables $X \in \square^M$. Each of these inputs is described as a joint probability density function (PDF) fx, and therefore, the computational model can be represented by the following equation (Eq. (13)).

$$Y \approx f(X) = \sum_{\alpha \in N^M} y_\alpha \psi_\alpha(X) \tag{13}$$

where Y is the computational model, $\psi_\alpha(X)$ is the multivariate orthonormal polynomial with respect to $fx(x)$, $\alpha \in \mathbb{N}^M$ is a multi-index that locates the components of the multivariate polynomials ψ_α and the $y_\alpha \in \mathbb{R}$ are the respective coefficients (coordinates) and; M is the number of input variables.

From a practical point of view, the sum of Eq. (13) must be truncated to a finite sum of the truncated polynomial chaos expansion (Eq. (14)) [31]:

$$Y \approx \tilde{f}^{PCE}(X) = \sum_{\alpha \in A} y_\alpha \psi_\alpha(X) \tag{14}$$

where $M^{PCE}(X)$ is the polynomial chaos expansion surrogate model; $\alpha = \{\alpha_1 \ldots \alpha_d\}$ are the indexes of the polynomial chaos expansion; $A \in \mathbb{N}^M$ is the set of indexes α corresponding to the truncation scheme; $X = (X_1, X_2, \ldots, X_d)$ is the multivariate vector of the input parameters considered and $\psi_\alpha$is the multivariate polynomial.

Table 8
MAC values and numerical frequencies obtained from the initial model compared with the experimental frequencies obtained from the AVT.

Vibration modes	*fexp* (Hz)	*fnum* (Hz)	Relative error (%)	MAC
1	5.56	5.31	4.45	0.95
2	8.22	8.11	1.37	0.80
3	9.31	9.48	1.81	0.82
4	11.47	11.36	0.95	0.96
5	18.09	18.02	0.40	0.87

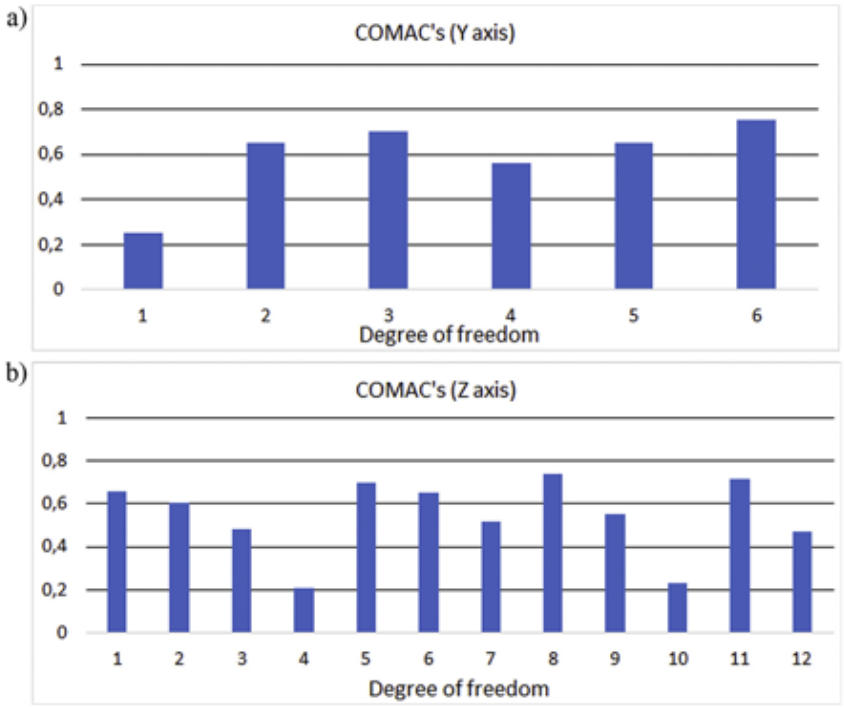

Fig. 21. COMAC values obtained from the first simulation: a) COMAC values in Y axis and b) COMAC values in Z axis.

Moreover, the multivariate polynomials (ψ_α) that include the PCE basis are obtained through the tensorization of suitable univariate polynomials. It is worth mentioning that each univariate polynomial was constructed using the classical families of polynomial proposed by [32]. Legendre polynomials were applied for those inputs with uniform PDFs, and Hermite polynomials were chosen for inputs with Gaussian PDFs. Multivariate polynomials $(\psi_\alpha)(\chi)$ are assembled as the tensor product of their univariate polynomials. For calculation of the coefficients, we used a non-intrusively strategy based on the least-square minimization proposed by [33].

The set of multi-indices A of Eq. (14) is obtained using a suitable truncation scheme, which consists of selection of multivariate polynomials up to a total degree p^t, i.e., $\{\psi_\alpha, \alpha \in \mathbb{N}^{M:} \sum_{i=1}^{M} \alpha_i \leq p^t\}$. Therefore, the corresponding number of terms in the truncated series is defined as shown (Eq. (15)):

$$cardA = \binom{M+p^t}{p^t} = \frac{(M+p^t)!}{M!p^t!} \tag{15}$$

where M are the input variables of the polynomial; and p the degree of the polynomials.

It is important to highlight that the truncated polynomial chaos expansion shown in (Eq. (13)) can be decomposed into summands of increasing order, similar to the definition of the Sobol's indices. For any non-empty set $u \subset \{1, \ldots, M\}$ and any finite truncation set $A \subset \mathbb{N}^M$, it can be stated that $A_u = \{\alpha \in A : k \in u \Leftrightarrow \alpha_k \neq 0, k = 1,\ldots M\}$. This statement means that A_u encompasses all multi-indices within the truncation set A that have non-zero components $\alpha_k \neq 0$ if and only if $k \in u$. Moreover, the sum of the associated terms from the PCE creates a function that depends only on the input variables x_u. Due to the orthonormality of the PCE, the variance of the truncated model can be expressed as shown (Eqs. (16) and (17)):

$$Var[Y_A] = \sum_{\substack{\alpha \in A \\ \alpha \neq 0}} \hat{y}_\alpha^2 \tag{16}$$

$$Var[f_v(X_v)] = \sum_{\substack{\alpha \in A \\ \alpha \neq 0}} \hat{y}_\alpha^2 \tag{17}$$

where Y_A is the truncated model; and $f_v(x_v)$ is the expresion of each summand for the polynomial chaos expansion.

Considering the expressions previously shown, the Sobol's indices can be expressed as follows (Eqs. (18) and (19)):

$$\widehat{S}_i = \frac{\sum_{\alpha \in A_i} \widehat{y}_\alpha^2}{\sum_{\alpha \in A, \alpha \neq 0} \widehat{y}_\alpha^2} \quad \text{where } A_i = \{\alpha \in A : \alpha_i > 0, \alpha_{j \neq i} = 0\} \tag{18}$$

$$\widehat{S}_i^T = \frac{\sum_{\alpha \in A^T} \widehat{y}_\alpha^2}{\sum_{\alpha \in A, \alpha \neq 0} \widehat{y}_\alpha^2} \quad \text{where } A_i^T = \{\alpha \in A : \alpha_i > 0\} \tag{19}$$

where $\hat{S}_i$ and $\hat{S}_i^T$ are the first-order and total Sobol's indices of the output variable i; $\hat{y}$ and α are the coefficients and indices of the polynomial chaos expansion, respectively; and A is the subset of input variables. The first-order Sobol's indices $\hat{S}$ i represent the effect of each input variable alone in the model variance. Additionally, the total Sobol's indices represent the full effect of each input variable (alone and in combination with other input variables) in the output model variance.

According to the previously defined approach, a total of 100 metamodels were built to evaluate the first five frequencies and the associated modal displacements (90 for each mode). Furthermore, validation of these metamodels was conducted using the leave-one-out error (LOO error) (Eq. (20)) [34,35].

$$LOO\ error = \frac{1}{N} \sum_{i=1}^{N} \left(\frac{Y\left(X^{(i)}\right) - \tilde{f}^{PCE}\left(X^{(i)}\right)}{1 - h_i} \right)^2 \tag{20}$$

where $Y\left(X^{(i)}\right)$ is the computational model; $\tilde{f}^{PCE}\left(X^{(i)}\right)$ is the subrogate model obtained from a specific DoE with N samples and; h_i is the i–th diagonal term of matrix $A(A^TA)^{-1}A^T$; and A the experimental matrix.

The relative LOO error (err_{LOO}) is obtained from the normalization of the *LOO error* (Eq. (20)) with the empirical variance of the set of model evaluations at the experimental design $Y = \{Y\left(X^{(i)}\right), \cdots, Y\left(X^{(N)}\right)\}$. Considering that the estimate of this error may be too optimistic, a corrected estimate proposed by [36] was used (Eq. (21)).

$$errLOO^* = errLOO\left(1 - \frac{cardA}{N}\right)^{-1}\left(1 + tr\left(\psi^T\psi\right)^{-1}\right) \tag{21}$$

where *card A* is the number of terms in the truncated series; and $\psi = \{\psi_{ij} = \psi_j(x^{(i)}),\ i = 1, \cdots, N; j = 1, \cdots, cardA\}$.

This metric of error offers a good compromise between fair error estimation and affordable computational cost.

4.3.2. The minimization strategy

Once the most sensitive variables were obtained, the subsequent step minimized the discrepancies between the numerical and the experimental data. To this end, the following cost function was considered (Eq. (22)).

$$\pi = \frac{1}{2}\left[W_f \sum_{i=1}^{n} \left(\frac{f_{i,num}^2 - f_{i,exp}^2}{f_{i,exp}^2} \right)^2 + W \sum_{j=1}^{m} (1 - MAC)^2 \right] \tag{22}$$

where π is the cost function to be minimized, which is composed of the residuals of the relative error between the numerical $f_{i,num}$ and experimental frequencies $f_{i,exp}$ as well as the MAC values. The terms n and m of this cost function represent the number of frequencies and mode shapes assumed in the calibration of the numerical model, respectively, whereas W_f is the frequency weight, and W is the MAC weight. To balance the contributions of the frequencies and MAC of the residuals of the objective function, the values for the W_f and the W were assumed to be three and one, respectively.

Considering the possible non-linear relationship between the residuals of the cost function and the input variables, the minimization problem was formulated as a non-linear least-squares problem using the iterative Gauss-Newton method to minimize the cost function (LS). This method was complemented by the trust region reflective algorithm, as previously proposed [13]. Within this iterative minimization problem, the gradient and the Hessian of the objective function were calculated as follows (Eqs. (23) and (24)):

$$\nabla\pi(\theta) = J(\theta)^T r(\theta) \tag{23}$$

$$\nabla^2(\theta) = J(\theta)^T J(\theta) + \sum_{i=1}^{k} r_i(\theta)\nabla^2 r_i(\theta) \cong J(\theta)^T J(\theta) \tag{24}$$

where r is the k -dimensional vector of the frequency and mode shape residuals, θ represents the vector of input variables, and J indicates the Jacobian or sensitivity matrix containing the first partial derivatives of the residuals with respect to the input variables. These derivatives were calculated via the finite difference strategy.

Considering that the previously shown optimization strategy is a local minimization method, and with the aim of finding the global minimum of the cost function, a multi-start approach was chosen. This approach runs several optimization prob-

Table 9
Upper and lower bounds considered during the updating stage. The upper and lower bounds of the supports stiffnesses, the Young Modulus (*E5*) and the density (*d5*) of the asphalt pavement were extracted from Chen & Bathurst [39] and Von Quintus [29], respectively.

Parameter	Upper bounds	Lower bounds
E1 (GPa)	2.56	1.00
E2 (Gpa)	4.00	2.57
E3 (Gpa)	3.18	0.56
E4 (Gpa)	0.78	0.33
d1 (kg/m^3)	2500	2000
d2 (kg/m^3)	2500	2000
Kn1 (N/m^3)	1.00×10^8	1.00×10^6
$Kt1_x$ (N/m^3)	1.00×10^8	1.00×10^6
$Kt1_y$ (N/m^3)	1.00×10^8	1.00×10^6
Kn2 (N/m^3)	1.00×10^8	1.00×10^6
$Kt2_x$ (N/m^3)	1.00×10^8	1.00×10^6
$Kt2_y$ (N/m^3)	1.00×10^8	1.00×10^6

lems, beginning each from a different initial point. These initial points were created with the Latin hypercube sampling method (LHS) [37].

4.4. Calibrated model

With the workflow proposed in the previous section, an updating process for the previously defined numerical model was conducted (Fig. 19). To this end, an initial set of variables was considered: (i) four Young's modulus (*E1–E4*) values corresponding to the groups of masonry and infill materials (Table 7); (ii) two densities (*d1* and *d2*) corresponding to the masonry of the spandrel walls and barrel vaults and; (iii) two normal stiffnesses (*Kn1* and *Kn2*) and four shear stiffnesses in the X-direction and Y-direction ($Kt1_x$, $Kt1_y$ and $Kt2_x$, $Kt2_y$) at the extremes of the bridge to simulate the possible interaction between the bridge and the soil. The inputs *d3* (density of the added infill layer), *d4* (density of the original infill layer), *E5*, *d5* (the Young Modulus and density of the pavement) were not considered during the sensitivity analysis with the aim of reducing the complexity of the surrogate model. Additionally, *d3* and *d4* were not considered due to their low variance compared with the remainder of variables (Table 1). However, *d5* and *E5* were not included because it is expected that their contribution is low compared with the variables previously cited.

With this set of variables and under the premises defined in Section 4.3.1, different PCE-metamodels were built to evaluate the Sobol's indices of each output variable (5 frequencies and 90 modal displacements). In these evaluations, different sample sizes were considered to generate the optimum metamodel of each output (best relationship between the number of evaluations and the accuracy of the model). The samples of the DoE were extracted in a sequential manner using the sequential Latin hypercube sampling (LHS) methodology, as proposed by [38]. This stage used the constriction of the upper and lower bounds of the variables obtained during the experimental campaign (Table 9).

According to Table 10, it was possible to conclude that the optimum design of experiment (DoE) value of the metamodel is 500, showing an average LOO error of 2.19×10^{-3}. This DoE corresponds to 50 times the number of input variables used as inputs to represent the response of the numerical model. Therefore, PCE metamodels built with 500 samples were considered for calculation of the Sobol's indices (Fig. 22).

Table 10
LOO error in frequencies output variables and average LOO error in modal displacements output variables for different sizes of the DoE. Dm_i is the average value of the modal displacements for the mode *i*.

	Number of samples obtained with the LHS					
Output variable	100	200	300	400	500	600
f1	5.27×10^2	1.80×10^{-2}	7.48×10^{-3}	1.06×10^{-5}	3.17×10^{-6}	1.14×10^{-6}
f2	3.06×10^2	2.16×10^{-2}	1.38×10^{-2}	1.73×10^{-5}	6.76×10^{-6}	8.21×10^{-6}
f3	1.90×10^{-1}	1.02×10^{0}	1.01×10^{0}	1.01×10^{-1}	8.90×10^{-5}	8.12×10^{-5}
f4	3.93×10^3	2.37×10^{-2}	2.25×10^{-2}	3.32×10^{-4}	1.37×10^{-5}	1.43×10^{-5}
f5	1.69×10^{-2}	4.26×10^{-1}	4.12×10^{-1}	3.71×10^{-3}	2.57×10^{-5}	1.36×10^{-5}
dm1	2.18×10^3	1.65×10^{-1}	1.09×10^{-1}	9.08×10^{-4}	5.78×10^{-5}	4.17×10^{-5}
dm2	3.83×10^2	4.94×10^{-1}	4.99×10^{-1}	4.53×10^{-4}	3.30×10^{-4}	3.71×10^{-4}
dm3	3.08×10^3	4.71×10^{-1}	4.59×10^{-1}	3.85×10^{-1}	5.04×10^{-3}	4.76×10^{-3}
dm4	6.10×10^5	8.63×10^{-1}	8.09×10^{-1}	7.76×10^{-3}	7.84×10^{-3}	7.57×10^{-3}
dm5	3.77×10^4	9.96×10^{-1}	8.75×10^{-1}	9.34×10^{-3}	8.46×10^{-3}	8.60×10^{-3}

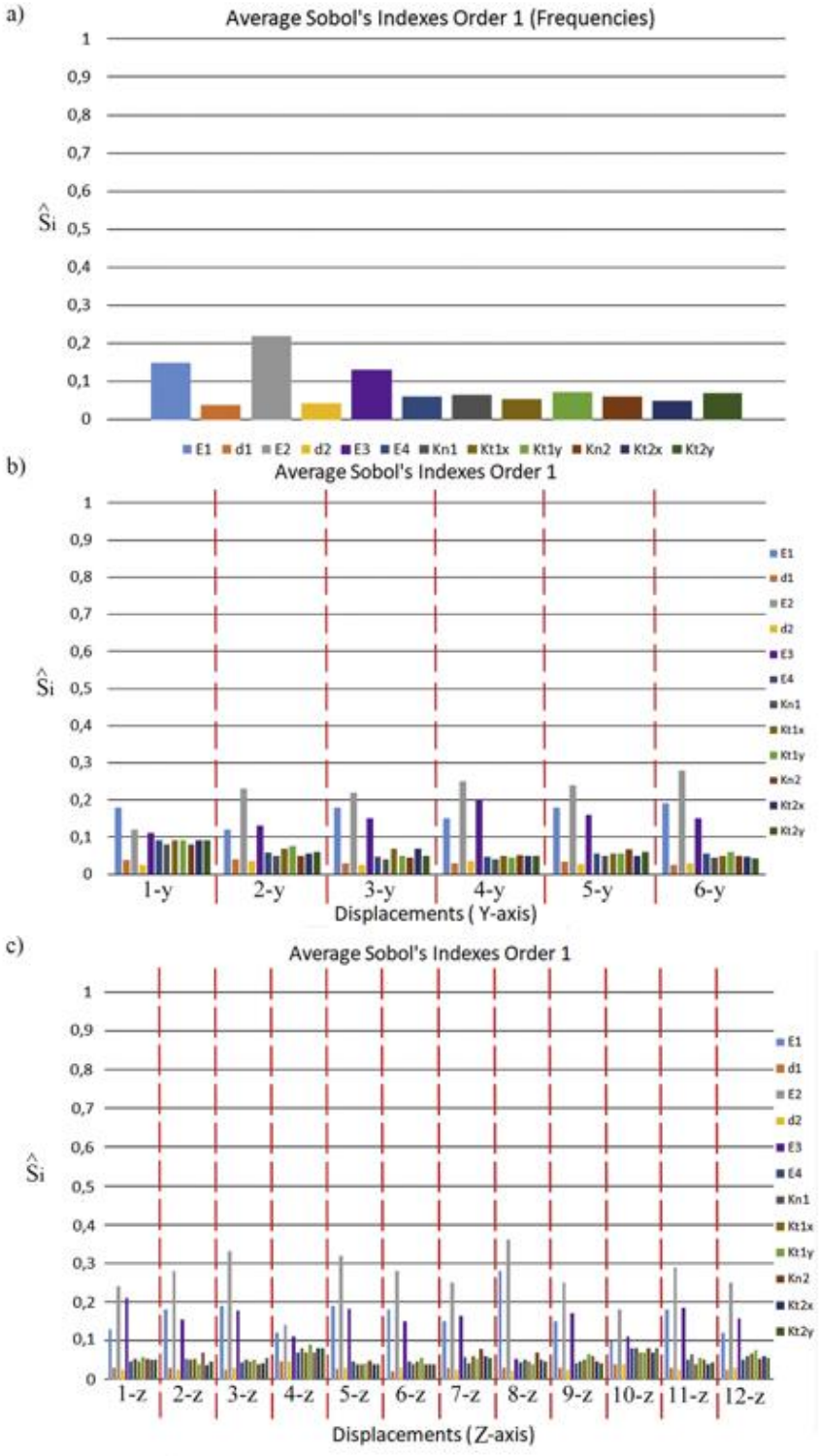

Fig. 22. Average first order Sobol's indexes ($\hat{S}_i$) obtained during the global sensitivity analysis of the numerical model: a) Average first order Sobol's indexes of the first five eigenfrequencies; b) Average first order Sobol's indexes of the Y-axis modal displacements and c) Average first order Sobol's indexes of the Z-axis modal displacements.

Table 11
Values of each one of the 20 samples coming from the LHS method obtained for the sensitive parameters. These values were used as starting points during the calibration of the numerical model of the bridge.

Sample	*E1* (GPa)	*E2* (GPa)	*E3* (GPa)	*E4* (GPa)	*Kn1* (N/m^3)	$Kt1_x$ (N/m^3)	$Kt1_y$ (N/m^3)	*Kn2* (N/m^3)	$Kt2_x$ (N/m^3)	$Kt2_y$ (N/m^3)
1	2.03	3.32	1.23	0.42	5.27×10^7	6.54×10^7	6.54×10^7	3.28×10^7	2.26×10^7	2.26×10^7
2	2.54	2.24	1.81	0.32	4.31×10^7	2.31×10^7	2.31×10^7	5.21×10^7	1.45×10^7	1.45×10^7
3	1.47	3.93	1.98	0.39	2.13×10^7	1.37×10^7	1.37×10^7	4.31×10^7	3.51×10^7	3.51×10^7
4	2.45	3.17	1.65	0.47	3.71×10^7	5.76×10^7	5.76×10^7	2.56×10^7	2.29×10^7	2.29×10^7
5	1.81	2.61	1.49	0.34	1.82×10^7	2.67×10^7	2.67×10^7	1.38×10^7	1.15×10^7	1.15×10^7
6	1.07	3.41	1.70	0.53	6.31×10^7	5.83×10^7	5.83×10^7	3.17×10^7	2.62×10^7	2.62×10^7
7	1.30	3.16	1.33	0.36	7.11×10^7	4.41×10^7	4.41×10^7	5.21×10^7	3.45×10^7	3.45×10^7
8	1.67	3.57	1.03	0.56	4.38×10^7	3.16×10^7	3.16×10^7	2.68×10^7	1.93×10^7	1.93×10^7
9	2.39	3.26	1.85	0.37	2.94×10^7	2.77×10^7	2.77×10^7	1.81×10^7	1.35×10^7	1.35×10^7
10	2.17	3.78	1.63	0.53	3.55×10^7	2.91×10^7	2.91×10^7	2.64×10^7	2.12×10^7	2.12×10^7
11	2.09	3.69	1.20	0.34	1.71×10^7	1.28×10^7	1.28×10^7	2.96×10^7	1.73×10^7	1.73×10^7
12	1.65	3.89	1.07	0.38	2.94×10^7	2.33×10^7	2.33×10^7	3.52×10^7	2.51×10^7	2.51×10^7
13	1.29	2.82	1.15	0.31	4.21×10^7	3.27×10^7	3.27×10^7	5.13×10^7	3.47×10^7	3.47×10^7
14	1.80	3.11	1.61	0.45	5.16×10^7	4.71×10^7	4.71×10^7	4.67×10^7	2.95×10^7	2.95×10^7
15	1.41	2.72	1.23	0.51	2.73×10^7	1.56×10^7	1.56×10^7	3.21×10^7	2.67×10^7	2.67×10^7
16	1.97	3.86	1.74	0.44	3.51×10^7	2.73×10^7	2.73×10^7	4.15×10^7	2.38×10^7	2.38×10^7
17	1.58	3.25	1.29	0.41	2.19×10^7	1.91×10^7	1.91×10^7	3.67×10^7	2.14×10^7	2.14×10^7
18	1.38	3.09	1.78	0.47	1.87×10^7	1.76×10^7	1.76×10^7	2.44×10^7	1.65×10^7	1.65×10^7
19	1.51	3.13	1.81	0.49	3.61×10^7	2.73×10^7	2.73×10^7	4.10×10^7	2.42×10^7	2.42×10^7
20	1.31	3.77	1.54	0.56	2.54×10^7	2.21×10^7	2.21×10^7	3.59×10^7	2.67×10^7	2.67×10^7

Table 12
Discrepancies obtained from the second calibration in terms of relative error in frequencies (*f*) and MAC values. In brackets, values obtained from the initial model.

Vibration modes	*fexp* (Hz)	*fnum* (Hz)	Relative error (%)	MAC
1	5.56	5.45	2.03	0.96
		(5.31)	(4.48)	(0.95)
2	8.22	8.27	0.72	0.92
		(8.11)	(1.37)	(0.80)
3	9.31	9.23	0.87	0.90
		(9.48)	(1.81)	(0.82)
4	11.47	11.53	0.56	0.97
		(11.36)	(0.95)	(0.96)
5	18.09	17.76	1.86	0.91
		(18.02)	(0.41)	(0.87)

From the sensitivity analysis, it was possible to conclude that the variance of the output model is strongly influenced by the variance of each input alone because the first-order Sobol's indices are similar to the total Sobol's indices. The frequencies are strongly influenced by the inputs *E1*, *E2* and *E3*, showing average first-order Sobol's indices of 0.15, 0.21 and 0.13, respectively. This result means that 15 %, 21 % and 13 % of the output variance is caused by the variance of these inputs. For the modal displacements, it was possible to observe that the inputs *E1*, *E2* and *E3* are the most sensitive variables, with average first-order Sobol's indices of 0.18, 0.26 and 0.17, respectively. For the remaining inputs, it was possible to observe that the different variables that define the interaction bridge-soil have a similar impact on the output variance. The densities (*d1* and *d2)* are the inputs with less impact in the output variance, especially in the frequencies of the model.

Higher average first-order Sobol's indices were obtained in the frequencies (Fig. 22a) for the Young's modulus *E1*, *E2*, and *E3* corresponding to the Group 1 (spandrel walls), Group 2 (barrel vaults) and Group 3 (original infill material), respectively, as the most initially sensitive parameters. With the aim of identifying more parameters with high sensitivity, the degrees of freedom (DOF) with lower COMAC values from the initial model were associated with the corresponding DOF of the average first-order Sobol's indices of the displacements (the first DOF in the Y-axis direction and the fourth and tenth DOF in the Z-axis direction) (Figs. 21 and 22b, c). This approach identified the Young's modulus *E4* corresponding to the Group 4 (added infill material) and all stiffnesses that represent the interaction between the bridge and the soil ($Kn1$, $Kt1_x$, $Kt1_y$, $Kn2$, $Kt2_x$ *and* $Kt2_y$) as the most sensitive parameters together with *E1*, *E2* and *E3*. Therefore, a total of 10 parameters were considered for the subsequent updating process. During this stage, we used the average values of the inputs *d1*, *d2*, *d3*, *d4*, *d5* and *E5* to calibrate the model (Tables 1 and 7).

Finally, minimization of the cost function was performed via the optimization strategy defined in Section 4.3.2 (LHS + LS). In this case, a total of 20 samples from the LHS method were considered as starting points for the minimization problem (Table 11). As a result of these 20 minimizations, it was possible to find a minimum for which the numerical model showed an average relative error in frequencies of 1.21% and an average MAC value of 0.93 (Table 12). The updated values of the

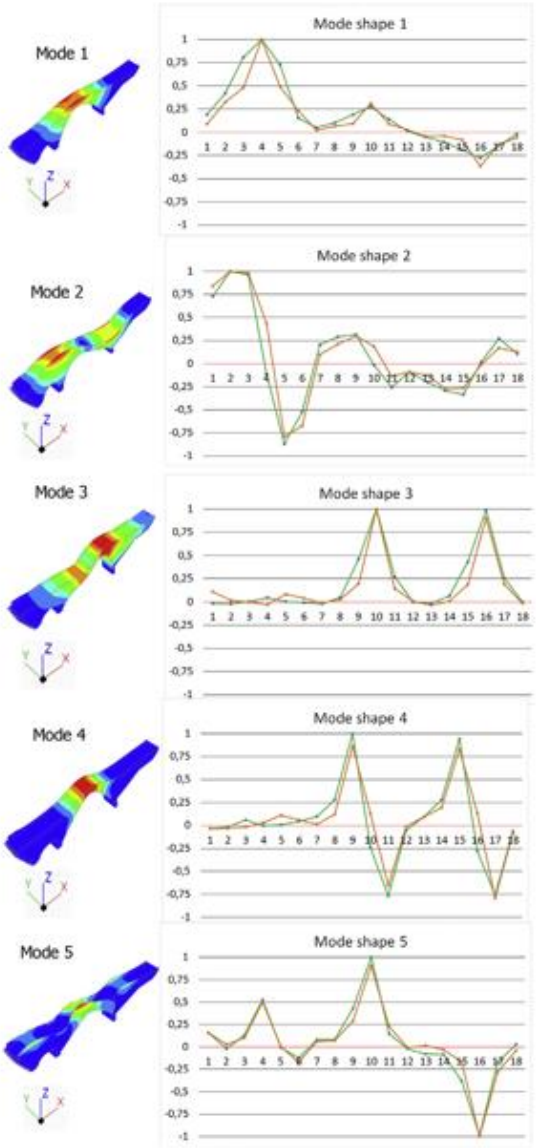

Fig. 23. Graphical comparison between experimental (green) and numerical (orange) modal shapes obtained from the updated numerical model. The horizontal axis of the graphs represent the degree of freedoms and the vertical axis the normalized modal displacements. (For interpretation of the references to colour in this figure legend, the reader is referred to the web version of this article.)

masonry structural elements and the infill materials of the numerical model (Table 12) are approximated with respect to the average values obtained from the experimental campaign (Tables 1 and 2), corroborating the robustness of the calibrated numerical model and the experimental tests conducted on the bridge (MASW and sonic tests).

Finally, Fig. 23 reveals a comparison between the experimental and numerical mode shapes from a graphic point of view (Fig. 16). Finally, (Table 13) (Fig. 16), the results obtained from the updated numerical model present a better correlation for the experimental results obtained from the AVT, especially with respect to the discrepancies observed in the 2nd and 3rd vibrational modes, which improved their MAC values from an initial value of 0.80 and 0.82 for the 2nd and 3rd modes to 0.92 and 0.90, respectively. This result re-affirmed the importance of the influence of the boundary conditions on the dynamic behaviour of the bridge.

Table 13
Comparison between the initial numerical model and the updated numerical model.

Parameter	Upper bounds	Lower bounds	Initial numerical model	Updated numerical model
E1 (GPa)	2.56	1.00	1.79	1.91
E2 (GPa)	4.00	2.57	3.28	3.62
E3 (GPa)	3.18	0.56	1.73	0.97
E4 (GPa)	0.78	0.33	0.41	0.51
$Kn1$ (N/m^3)	1.00×10^8	1.00×10^6	–	1.88×10^7
$Kt1_x$ (N/m^3)	1.00×10^8	1.00×10^6	–	1.83×10^7
$Kt1_y$ (N/m^3)	1.00×10^8	1.00×10^6	–	1.83×10^7
$Kn2$ (N/m^3)	1.00×10^8	1.00×10^6	–	3.34×10^7
$Kt2_x$ (N/m^3)	1.00×10^8	1.00×10^6	–	1.01×10^7
$Kt2_y$ (N/m^3)	1.00×10^8	1.00×10^6	–	1.01×10^7

5. Conclusions

This paper proposes a robust multidisciplinary approach used to obtain accurate numerical simulations of masonry arch bridges via the finite element method. This methodology, which is fully based on non-destructive methods, enhances the current multidisciplinary methods for structural assessment of masonry bridges at different levels.

At the material and geometrical levels, the proposed methodology considers the use of several wave-based approaches, such as multichannel analysis of surface waves or sonic testing, with the aim of accurately characterizing the different materials presented in the bridge compared with the traditional multidisciplinary methodology. It is worth mentioning that the values obtained for the "original infill layer" can be justified by the presence of selected intrusions of natural soil within the space delimited by the spandrel walls. The combination of the terrestrial laser scanner and ground-penetrating radar with reverse engineering procedures allowed creation of as-built CAD models of masonry bridges. This methodology is able to reproduce possible non-parametric shapes presented in this type of structure in contrast with other methodologies in which the CAD model is created via extraction of a section from the point cloud. Additionally, the proposed methodology was able to characterize the mechanical and physical properties of the infill without requiring the use of values from the literature or the application of invasive methods based on extraction of samples, as in other multidisciplinary approaches.

For the numerical field, the finite element model derived from the proposed methodology shows good correlation with respect to the ground truth (ambient vibration tests). This model shows an error in frequencies of approximately 1.80% and an average MAC value of 0.88, demonstrating the robustness of the multidisciplinary approach. This correlation was enhanced due to the use of an updating method based on the combination of a polynomial chaos expansion metamodel and Sobol's indices for the sensitivity analysis as well as a non-linear least squares optimization approach. The great efficiency and accuracy of the polynomial chaos expansion metamodel for the sensitivity analysis lies in the requirement of a low number of iterations compared with the classical Monte Carlo approach. In our case, considering that 10 input variables were used to build the surrogate model, we needed a total of 500 points for the DoE (approximately 50 times the number of variables). Additionally, the ability to analyse the Sobol's indices from the polynomial chaos expansion allow us to evaluate the influence of each input in the output variance in a robust manner, instead of using basic sensitivity analysis or correlation methods (e.g., the Spearman matrix).

This updating approach created a numerical model with a relative error in frequencies of 1.21% and an average MAC value of 0.93. During this stage, and considering the nature of the optimization algorithm used, which is prone to becoming trapped in local optima, a total of 20 optimization runs were conducted with the aim of exploring the search space and obtaining a possible global minimum. The starting point of each run was obtained via the LHS method. Each run required 4836 seconds to reach the minimum and thus, a total of 109,320 seconds was spent during the updating stage: i) 12,600 seconds for the sensitivity analysis (PCE + Sobol) and ii) 96,720 seconds for the optimization (non-linear squares + Gauss-Newton) on a system with a Intel® XEON E3-1240 v3 processor running at 3.4 GHz with 8 GB RAM DDRII.

Finally, we offer several options for future work in several fields. Different numerical analyses will be conducted with the aim of evaluating the current structural performance against static (traffic loads) and dynamic (such as earthquakes) situations as well as the use of adaptive sampling strategies, such as those proposed by [40] based on the LOLA-VORONOI algorithm. Additionally, further research will be focused on an in-depth evaluation of the MASW method with the aim of characterizing the non-linear properties of the infill, i.e., the (i) cohesion and (ii) friction angle, as well as the use of additional methods such as electric resistivity tomography to obtain an in-depth evaluation of the bridge infill topology. Additionally, considering the uncertainty associated with the data obtained by the 250 MHz GPR antenna, several impact-echo tests will be performed on the barrel vaults and asphalt with the aim of corroborating the thicknesses supplied by GPR and historical drawings. Finally, several radiometric classifications based on the data acquired from the TLS system will be performed to complete damage evaluation of the construction using pixel-based classification methods.

Acknowledgments

This work was financed by ERDF funds through the V Sudoe Interreg program within the framework of the HeritageCARE project, Ref. SOE1/P5/P0258. This research has been also partially supported by Patrimonio 5.0 funded by Junta of Catilla y León, Ref. SA075P17. Second author would like to thank the University of Salamanca for the program for human resources "Programa II: Contratos Postdoctorales".

References

[1] B. Conde, L.F. Ramos, D.V. Oliveira, B. Riveiro, M. Solla, Structural assessment of masonry arch bridges by combination of non-destructive testing techniques and three-dimensional numerical modelling: application to Vilanova bridge, Eng. Struct. 148 (2017) 621–638, https://doi.org/10.1016/j.engstruct.2017.07.011.
[2] B. Riveiro, J. Caamaño, P. Arias, E. Sanz, Photogrammetric 3D modelling and mechanical analysis of masonry arches: an approach based on a discontinuous model of voussoirs, Autom. Constr. 20 (2011) 380–388, https://doi.org/10.1016/j.autcon.2010.11.008.
[3] D. Ribeiro, R. Calçada, R. Delgado, M. Brehm, V. Zabel, Finite element model updating of a bowstring-arch railway bridge based on experimental modal parameters, Eng. Struct. 40 (2012) 413–435, https://doi.org/10.1016/j.engstruct.2012.03.013.
[4] M. Stavroulaki, B. Riveiro, G. Drosopoulos, M. Solla, P. Koutsianitis, G.E. Stavroulakis, Modelling and strength evaluation of masonry bridges using terrestrial photogrammetry and finite elements, Adv. Eng. Softw. 101 (2016) 136–148, https://doi.org/10.1016/j.advengsoft.2015.12.007.
[5] , Constr. Build. Mater. 158 (2018) 961–984, https://doi.org/10.1016/j.conbuildmat.2017.10.084.
[6] L.F. Miranda, J. Rio, J.M. Guedes, A. Costa, Sonic Impact Method–A new technique for characterization of stone masonry walls, Constr. Build. Mater. 36 (2012) 27–35, https://doi.org/10.1016/j.conbuildmat.2012.04.018.
[7] S. Russo, Integrated assessment of monumental structures through ambient vibrations and ND tests: the case of Rialto Bridge, J. Cult. Heritage 19 (2016) 402–414, https://doi.org/10.1016/j.culher.2016.01.008.
[8] A.S. Gago, J. Alfaiate, A. Lamas, The effect of the infill in arched structures: Analytical and numerical modelling, Eng. Struct. 33 (2011) 1450–1458, https://doi.org/10.1016/j.engstruct.2010.12.037.
[9] B. Conde, L. Díaz-Vilariño, S. Lagüela, P. Arias, Structural analysis of Monforte de Lemos masonry arch bridge considering the influence of the geometry of the arches and fill material on the collapse load estimation, Constr. Build. Mater. 120 (2016) 630–642, https://doi.org/10.1016/j.conbuildmat.2016.05.107.
[10] B. Conde, G. Drosopoulos, G. Stavroulakis, B. Riveiro, M. Stavroulaki, Inverse analysis of masonry arch bridges for damaged condition investigation: application on Kakodiki bridge, Eng. Struct. 127 (2016) 388–401, https://doi.org/10.1016/j.engstruct.2016.08.060.
[11] V. Compan, P. Pachón, M. Cámara, Ambient vibration testing and dynamic identification of a historical building. Basilica of the Fourteen Holy Helpers (Germany), Procedia Engineering 199 (2017) 3392–3397, https://doi.org/10.1016/j.proeng.2017.09.572.
[12] L.J. Sánchez-Aparicio, B. Riveiro, D. Gonzalez-Aguilera, L.F. Ramos, The combination of geomatic approaches and operational modal analysis to improve calibration of finite element models: a case of study in Saint Torcato Church (Guimarães, Portugal), Constr. Build. Mater. 70 (2014) 118–129, https://doi.org/10.1016/j.conbuildmat.2014.07.106.
[13] L.J. Sánchez-Aparicio, L.F. Ramos, J. Sena-Cruz, J.O. Barros, B. Riveiro, Experimental and numerical approaches for structural assessment in new footbridge designs (SFRSCC–GFPR hybrid structure), Compos. Struct. 134 (2015) 95–105, https://doi.org/10.1016/j.compstruct.2015.07.041.
[14] I.M. Sobol, Sensitivity estimates for nonlinear mathematical models, Math. Modell. Comput. Exp. 1 (1993) 407–414.
[15] B. Sudret, Global sensitivity analysis using polynomial chaos expansions, Reliab. Eng. Syst. Saf. 93 (2008) 964–979, https://doi.org/10.1016/j.ress.2007.04.002.
[16] E.R. Almeida, Puentes históricos de la provincia de Ávila, Institución Gran Duque de Alba, 2015.
[17] C.B. Park, R.D. Miller, J. Xia, Multichannel analysis of surface waves, Geophysics 64 (1999) 800–808, https://doi.org/10.1190/1.1444590.
[18] C.S. Blázquez, A.F. Martín, P.C. García, D. González-Aguilera, Thermal conductivity characterization of three geological formations by the implementation of geophysical methods, Geothermics 72 (2018) 101–111, https://doi.org/10.1016/j.geothermics.2017.11.003.
[19] L. Miranda, L. Cantini, J. Guedes, A. Costa, Assessment of mechanical properties of full-scale masonry panels through sonic methods. Comparison with mechanical destructive tests, Struct. Control Health Monit. 23 (2016) 503–516, https://doi.org/10.1002/stc.1783.
[20] H. Yoon, H. Song, K. Park, A phase-shift laser scanner based on a time-counting method for high linearity performance, Rev. Sci. Instrum. 82 (2011), https://doi.org/10.1063/1.3600456 075108.
[21] M. Solla, J. Caamaño, B. Riveiro, P. Arias, A novel methodology for the structural assessment of stone arches based on geometric data by integration of photogrammetry and ground-penetrating radar, Eng. Struct. 35 (2012) 296–306, https://doi.org/10.1016/j.engstruct.2011.11.004.
[22] N.J. Carino, The impact-echo method: an overview, Structures, A Struct. Eng. Odyssey 2001 (2001) 1–18, https://doi.org/10.1061/40558(2001) 15.
[23] H. Herlufsen, P. Andersen, S. Gade, N. Møller, Identification techniques for operational modal analysis–an overview and practical experiences, Proceedings of the 1st International Operational Modal Analysis Conference, Copenhagen, 2005.
[24] M. Herrero-Huerta, D. González-Aguilera, P. Rodriguez-Gonzalvez, D. Hernández-López, Vineyard yield estimation by automatic 3D bunch modelling in field conditions, Comput. Electron. Agric. 110 (2015) 17–26, https://doi.org/10.1016/j.compag.2014.10.003.
[25] D. Branch, L.C. Dang, N. Hall, W. Ketchum, M. Melakayil, J. Parrent, M. Troxel, D. Casebeer, D.J. Jeffery, E. Baron, Comparative direct analysis of type Ia supernova spectra. II. Maximum light, Publ. Astron. Soc. Pac. 118 (2006) 560.
[26] I. Guskov, Z.J. Wood, Topological noise removal, 2001 Graphics Interface Proceedings: Ottawa, Canada 2001 (2001) 19.
[27] T. Diana, DIANA finite element analysis, The Netherlands, (2005).
[28] R.J. Allemang, The modal assurance criterion–twenty years of use and abuse, Sound Vib. 37 (2003) 14–23.
[29] H.L. Von Quintus, Asphalt-aggregate Mixture Analysis System, AAMAS, Transportation Research Board, 1991.
[30] M. Asher, B. Croke, A. Jakeman, L. Peeters, A review of surrogate models and their application to groundwater modeling, Water Resour. Res. 51 (2015) 5957–5973, https://doi.org/10.1002/2015WR016967.
[31] R. Ghanem, P. Spanos, Stochastic Finite Elements: A Spectral Approach, Revisited ed., Dover Publications, INC, New York, 2003.
[32] D. Xiu, G.E. Karniadakis, The Wiener-Askey polynomial chaos for stochastic differential equations, SIAM J. Sci. Comput. 24 (2002) 619–644, https://doi.org/10.1016/j.jcp.2010.12.021.
[33] G. Blatman, B. Sudret, Adaptive sparse polynomial chaos expansion based on least angle regression, J. Comput. Phys. 230 (2011) 2345–2367, https://doi.org/10.1137/S1064827501387826.
[34] M. Stone, Cross-validatory choice and assessment of statistical predictions, J. Roy. Stat. Soc.: Ser. B (Methodol.) (1974) 111–147.
[35] S. Geisser, The predictive sample reuse method with applications, J. Am. Stat. Assoc. 70 (1975) 320–328.
[36] G. Deman, K. Konakli, B. Sudret, J. Kerrou, P. Perrochet, H. Benabderrahmane, Using sparse polynomial chaos expansions for the global sensitivity analysis of groundwater lifetime expectancy in a multi-layered hydrogeological model, Reliab. Eng. Syst. Saf. 147 (2016) 156–169.
[37] M.D. McKay, R.J. Beckman, W.J. Conover, Comparison of three methods for selecting values of input variables in the analysis of output from a computer code, Technometrics 21 (1979) 239–245, https://doi.org/10.1080/00401706.1979.10489755.
[38] Z. Liu, M. Yang, W. Li, A Sequential Latin Hypercube Sampling Method for Metamodeling, Theory, Methodology, Tools and Applications for Modeling and Simulation of Complex Systems, Springer (2016) 176–185, https://doi.org/10.1007/978-981-10-2663-8_19.

[39] J. Chen, R. Bathurst, Investigation of interface toe sliding of reinforced soil block face walls using FLAC, Proceedings of Continuum and Distinct Element Numerical Modeling in Geomechanics, Itasca International, Shanghi, China, 2013.
[40] T. Van Steenkiste, J. van der Herten, I. Couckuyt, T. Dhaene, Data-Efficient Sensitivity Analysis with Surrogate Modeling, Uncertainty Modeling for Engineering Applications, Springer, 2019, pp. 55–69.

CAPÍTULO IV

CONCLUSIONES Y PERSPECTIVAS FUTURAS

Las investigaciones que se han llevado a cabo durante el desarrollo de esta Tesis Doctoral han sido capaces de alcanzar el objetivo principal planteado, aportando soluciones innovadoras que han permitido superar los obstáculos que actualmente presentan las evaluaciones del comportamiento estructural de puentes históricos. Las aportaciones que ofrecen estas soluciones innovadoras se muestran en los artículos publicados en revistas científicas internacionales con alto factor de impacto donde se exponen metodologías multidisciplinares y resultados exitosos, representando así un gran avance que es producto de las investigaciones realizadas. En este capítulo se revela con detalle las principales conclusiones, teniendo en cuenta los objetivos específicos establecidos en el Capítulo II, así como futuros trabajos que permitirán seguir desarrollando la línea de investigación aquí iniciada.

4.1 Conclusiones

- **Evaluar las ventajas del uso de sensores geomáticos (láser escáner terrestre) en puentes históricos para caracterizar la geometría de sus componentes estructurales.**

- El uso del sensor geomático láser escáner terrestre ha demostrado ser una herramienta potencial para caracterizar de forma precisa la geometría externa de los elementos estructurales de puentes históricos.

- **Desarrollar metodologías que permitan hacer coincidir la nube de puntos obtenida mediante técnicas de escaneado láser con los ejes longitudinal y transversal de puentes de arco históricos, con el fin de integrar de forma correcta los datos obtenidos de la campaña experimental (Ensayos de Vibración Ambiental).**

- El análisis de componentes principales (PCA) aplicado en la nube de puntos obtenida por medio del láser escáner terrestre permite extraer su matriz de covarianza, analizar los autovalores de esta matriz de covarianza, y obtener el ángulo entre el autovector asociado con el autovalor máximo y el eje en la dirección *X* del sistema global de coordenadas, demostrando así su capacidad de alinear la nube de puntos a los ejes longitudinal y transversal de estos puentes mediante una rotación en la dirección *Z*.

- **Desarrollar metodologías que permitan construir modelos CAD precisos a partir de la nube de puntos obtenida mediante sensores geomáticos (láser escáner terrestre) con el fin de que sean adecuados para realizar simulaciones numéricas avanzadas.**

- Para obtener modelos CAD de puentes históricos a partir de la nube de puntos obtenida por el láser escáner terrestre es necesario el uso de estrategias de modelado basadas en la combinación de triangulaciones de Delaunay, el llenado de orificios por medio de funciones radiales, la eliminación del ruido topológico usando una re-triangulación local, la segmentación de sus elementos estructurales, y el ajuste de sus elementos estructurales segmentados a primitivas básicas por medio de extrusiones lineales y no lineales (b-splines). Por lo tanto, estas estrategias de modelado permiten obtener mallas que son transformadas posteriormente en modelos CAD precisos que son adecuados para realizar simulaciones numéricas avanzadas.

- El uso de métodos de representación superficial avanzada tales como las b-splines no uniformes permiten obtener con precisión superficies complejas, como por ejemplo deformaciones fuera del plano que presentan los tímpanos de varios puentes históricos de mampostería.

- **Evaluar las ventajas e inconvenientes de la aplicación de diferentes enfoques geofísicos (georradar y análisis multicanal de ondas superficiales) para la caracterización del relleno en puentes de arco de mampostería.**

- El georradar es una herramienta muy útil que permite caracterizar la distribución de los estratos de materiales de relleno que presentan muchos de estos puentes históricos de mampostería, así como los espesores de sus tímpanos y de sus bóvedas.

- Permite identificar nuevos materiales que han sido añadidos posteriormente, tales como losas de hormigón armado añadidas en algunas cubiertas de estos puentes históricos con el fin de evitar filtraciones de agua en sus materiales de relleno. La presencia de estas losas de hormigón armado es corroborada por medio de la visualización del mismo patrón repetido indefinidamente en los radargramas, debido a que sus barras de acero impiden la penetración de los pulsos electromagnéticos.

- Dificultad de la interpretación de los datos obtenidos en los radargramas en algunas ocasiones debido a ruido, atenuación de la señal o movimientos bruscos de la antena (en los perfiles verticales) por la presencia de viento.

- Generación de reflexión continua que hace imposible la interpretación de los radargramas en algunos casos, debido a la presencia de barras de acero de losas de hormigón reforzado añadidas en la cubierta de algunos de estos puentes durante trabajos de restauración.

- La penetración de los pulsos electromagnéticos del georradar está limitada a determinadas profundidades dependiendo de la banda de la frecuencia de la antena seleccionada.

- El análisis multicanal de ondas superficiales (MASW) permite obtener con precisión los parámetros mecánicos (Módulo de Young, módulo de corte, coeficiente de Poisson, entre otos) y físicos (densidad) de los materiales de relleno de puentes de arco de mampostería, así como un perfil de su distribución en 2D por medio de las velocidades de corte (V_s), reemplazando así el uso de técnicas invasivas.

- **Analizar la aplicabilidad de métodos no-destructivos basados en ondas (ensayos sónicos e impacto-eco) para la caracterización de los materiales que constituyen los tímpanos y las bóvedas de puentes de arco de mampostería, así como sus espesores.**

- Los ensayos sónicos demuestran ser una herramienta efectiva que es capaz de caracterizar de forma precisa los parámetros mecánicos (Módulo de Young y coeficiente de Poisson) de la fábrica pétrea de los puentes de arco de mampostería, evitando así el uso de técnicas destructivas que puedan perjudicar el estado de conservación de estas construcciones históricas.

- El método de Impacto-Eco ha demostrado ser una herramienta eficaz para caracterizar de forma precisa los espesores de los tímpanos y de las bóvedas de los puentes históricos de mampostería.

- Este método permite comparar los espesores obtenidos con los espesores identificados en los radargramas, permitiendo así corroborar estos últimos.

- **Aplicar técnicas basadas en ensayos de vibración ambiental (AVT) para evaluar el comportamiento dinámico de los puentes de arco históricos en función de su estado actual de conservación.**

- Los ensayos de vibración ambiental (AVT) han demostrado que son capaces de caracterizar de forma precisa el comportamiento dinámico estructural de puentes históricos de hormigón armado y de mampostería en función de su estado actual de conservación.

- El algoritmo EFDD (Enhanced Frequency Domain Decomposition) y el algoritmo SSI-PC (Stochastic Subspace Identification Principal Component) permiten extraer las formas modales, las frecuencias naturales y los coeficientes de amortiguamiento de forma simple y efectiva.

- La precisión de modelos numéricos avanzados de puentes de arco históricos puede ser evaluada comparando las frecuencias naturales obtenidas por los AVT con las frecuencias naturales de las simulaciones numéricas (error relativo), así como las discrepancias entre los desplazamientos modales experimentales y los desplazamientos modales de las simulaciones numéricas por medio del indicador MAC (Modal Assurance Criterion).

- El origen de las discrepancias entre los desplazamientos modales experimentales y los desplazamientos modales de las simulaciones numéricas puede ser identificado por medio del indicador COMAC (Coordinate Modal Assurance Criterion).

- **Desarrollar estrategias de calibración robusta de modelos numéricos de puentes de arco históricos que permitan reducir las discrepancias entre los resultados experimentales y los resultados obtenidos mediante simulaciones numéricas.**

- La metodología de coste optimizado que parte de un método basto (Douglas-Reid) a un método fino (mínimos cuadrados no-lineales) permite reducir el error relativo de las frecuencias naturales e incrementar los valores MAC.

- La metodología basada en la combinación del metamodelo PCE (Polynomial Chaos Expansion) y los índices de Sobol para el análisis sensible global (que optimiza el proceso de calibración) y el método de mínimos cuadrados no lineales, es capaz de reducir considerablemente el error relativo de las frecuencias naturales y de aumentar los valores MAC.

- El metamodelo PCE y los índices de Sobol para el análisis sensible global requiere un coste computacional más bajo en comparación con el método clásico de Monte Carlo.

4.2 Perspectivas futuras

Las metodologías propuestas que han sido utilizadas para generar modelos numéricos avanzados de puentes de arco históricos han demostrado ser capaces de superar los problemas planteados antes y durante su desarrollo. Sin embargo, cabe señalar el rápido progreso de técnicas y métodos innovadores implementados en las evaluaciones del comportamiento global estructural de puentes históricos, lo cual hace necesario plantear nuevos desafíos que permitan abrir puertas para poder llevar a cabo futuras investigaciones.

Teniendo esto en cuenta, se plantean los siguientes futuros trabajos:

- Aplicación de métodos no destructivos, tales como los ensayos sónicos y ultrasónicos en puentes históricos de hormigón armado y en puentes históricos de acero con el fin de caracterizar con precisión los parámetros mecánicos y físicos de estos materiales, evitando así la extracción de muestras que posteriormente se ensayan en laboratorio, lo que supone un gran ahorro de coste de tiempo.

- El uso de fotogrametría aérea de corto alcance con drones para complementar la digitalización obtenida por el TLS con el propósito de digitalizar las áreas no accesibles en puentes históricos.

- Realización de varias clasificaciones radiométricas basadas en los datos adquiridos por el sistema TLS con el fin de realizar una evaluación completa de la presencia de daños en puentes históricos por medio del uso de métodos de clasificación supervisados y no supervisados basados en estrategias de machine learning.

- Introducción de más metodologías no invasivas, tales como la tomografía eléctrica con el fin de caracterizar con precisión el terreno sobre el que están construidos puentes históricos, así como la distribución interna de los materiales de relleno en puentes históricos de mampostería con el fin de corroborarla con respecto al georradar y con su perfil 2D de las velocidades de corte del análisis multicanal de ondas superficiales.

- Combinación de sensores, utilizando cámaras termográficas y la dinámica de estructuras con el fin de ver cómo influye la temperatura en el comportamiento estructural dinámico de puentes históricos.

- Realización de ensayos estáticos con diferentes configuraciones de carga en puentes históricos con el propósito de agregarlos en conjunto con los datos dinámicos en metodologías de calibración robustas de modelos numéricos avanzados para llevar a cabo diagnósticos estructurales más precisos.

- Desarrollo de métodos de calibración robustos basados en modelos subrogados, análisis sensibles y estrategias de optimización, tales como los algoritmos genéticos u optimizaciones basadas en procedimientos del tipo Gauss-Newton que permitan calibrar modelos numéricos avanzados de puentes históricos, con el fin de reducir discrepancias entre los datos experimentales y numéricos para poder llevar a cabo diagnósticos estructurales.

REFERENCIAS

1. González Capitel, A., *Metamorfosis de monumentos y teorías de la restauración*. 1988: Alianza Editorial.
2. Lemaire, R. and H. Stovel, *Documento de Nara en Autenticidad*. 1994, Nara (Japón). http://ipce. mcu. es/pdfs/1994_Documento_Nara. pdf.
3. de Cracovia, C. *Principios para la conservación y restauración del patrimonio construido*. in *Preámbulo. La Carta de Cracovia fue elaborada por los participantes de la conferencia internacional Cracovia*. 2000.
4. Solla, M., et al., *Structural analysis of the Roman Bibei bridge (Spain) based on GPR data and numerical modelling.* 2012. **22**: p. 334-339.
5. Pérez, J., et al., *Assessment of the Structural Integrity of the Roman Bridge of Alcántara (Spain) Using TLS and GPR.* 2018. **10**(3): p. 387.
6. Melbourne, C., J. Wang, and A.K. Tomor. *A new masonry arch bridge assessment strategy (SMART)*. in *Proceedings of the Institution of Civil Engineers-Bridge Engineering*. 2007. London:[Thomas Telford], c2003-.
7. Melbourne, C., A.K. Tomor, and J. Wang. *Cyclic load capacity and endurance limit of multi-ring masonry arches*. in *Arch bridges IV conference proceedings*. 2004.
8. Fanale, L., D. Galeota, and A. Pietrucci, *Case Study: Assessment of the Load-Carrying Capacity of Multi-span Masonry Ancient Roman Arch Bridge Situated in "Campana", Near L'Aquila City (IT)*, in *Structural Analysis of Historical Constructions*. 2019, Springer. p. 1027-1035.
9. Sena-Cruz, J., et al., *Luiz Bandeira bridge: assessment of a historical reinforced concrete (RC) bridge.* 2013. **7**(6): p. 628-652.
10. Conde, B., et al., *Structural assessment of masonry arch bridges by combination of non-destructive testing techniques and three-dimensional numerical modelling: Application to Vilanova bridge.* 2017. **148**: p. 621-638.
11. Balasubramanian, A., *Bridges and their Types*. 2017.
12. Magalhães, F., et al., *Ambient and free vibration tests of the Millau Viaduct: Evaluation of alternative processing strategies.* 2012. **45**: p. 372-384.
13. Wilson, J.C., W.J.E.E. Gravelle, and S. Dynamics, *Modelling of a cable-stayed bridge for dynamic analysis.* 1991. **20**(8): p. 707-721.
14. ASTUDILLO PASTOR, R.J.H.y.A., *DYNAMIC TEST OF STAYED GIRDER BRIDGES.* 1994(190).
15. Brownjohn, J., et al., *Ambient vibration re-testing and operational modal analysis of the Humber Bridge.* 2010. **32**(8): p. 2003-2018.
16. Game, T., et al. *Full dynamic model of Golden Gate Bridge*. in *AIP Conference Proceedings*. 2016. AIP Publishing.
17. Imai, K. and D.M.J.J.o.B.E. Frangopol, *Reliability-based assessment of suspension bridges: Application to the Innoshima Bridge.* 2001. **6**(6): p. 398-411.
18. Matos, J., et al., *Structural assessment of a RC Bridge over Sororó river along the Carajás railway.* 2015. **8**(2): p. 140-163.
19. Figueiras, J., et al. *An integrated system for structural health monitoring–application to the Sorraia River Bridge*. in *Numerical Modelling of Discrete Materials in Geotechnical Engineering, Civil Engineering and Earth Sciences: Proceedings of the First International UDEC/3DEC Symposium, Bochum, Germany, 29 September-1 October 2004*. 2004. CRC Press.
20. Conde, B., et al., *Structural analysis of Monforte de Lemos masonry arch bridge considering the influence of the geometry of the arches and fill material on the collapse load estimation.* 2016. **120**: p. 630-642.
21. Slawomir, K., N.-T.J.A.J.o.C.E. Tuan, and Architecture, *The World's Oldest Bridges-Mycenaean Bridges.* 2017. **5**(6): p. 237-244.
22. Blanco, S.A., M.D. Fuentes, and C.N. Ortiz, *Puentes históricos de Galicia*. 1990: Colegio Oficial de Ingenieros de Caminos, Canales y Puertos, Xunta de ….

23. Morer, P., et al., *Comparative structural analyses of masonry bridges: An application to the Cernadela Bridge.* 2011. **12**(3): p. 300-309.
24. Solla, M., et al., *Non-destructive methodologies in the assessment of the masonry arch bridge of Traba, Spain.* 2011. **18**(3): p. 828-835.
25. Cossons, N. and B.S. Trinder, *The iron bridge: Symbol of the Industrial Revolution*. 2002: Phillimore & Company.
26. Bolton, A.J.N.C.E., *Strength on a plate.* 1992(1020).
27. Jaques, J.A.L. and D.R. Bragado. *Rehabilitación del puente-viaducto de Requejo (Puente de Pino)*. in *Resúmenes de comunicaciones*. 2014. Asociación Científico-técnica del Hormigón Estructural.
28. Grima López, R., A. Aguado de Cea, and J.J.I.J.o.A.H. Gómez Serrano, *Gaudí and reinforced concrete in construction.* 2013. **7**(4): p. 375-402.
29. Carreres Rodríguez, M., *LA CARRETERA DEL ALTO DE LAS ATALAYAS-MURCIA. UN RECORRIDO HISTÓRICO.*
30. McBeth, D. *Francois Hennebique (1842-1921), reinforced concrete pioneer*. in *Proceedings of the Institution of Civil Engineers: Civil Engineering*. 1998.
31. Bosc, J.-L., et al., *Joseph Monier et la naissance du ciment armé*. 2001: Ed. du Linteau.
32. O.Calvo, *Consideraciones técnicas de la Dirección General de Carreteras para la conservación, reparación y refuerzo del patrimonio estructural.* Nuevas técnicas de evaluación estructural, rehabilitación y refuerzo de estructuras, 1999.
33. WP. A. Yáñez, L.O., *Puentes de Fábrica: Situación actual.* Jomada sobre puentes de bóvedas de fábrica. AIPCR-CEDEX 2000, 2000.
34. Proske, D. and P. Van Gelder, *Safety of historical stone arch bridges*. 2009: Springer Science & Business Media.
35. Boothby, T.E.J.M.I., *Collapse modes of masonry arch bridges.* 1995. **9**(2): p. 62-69.
36. https://www.geoengineer.org/news-center/news/item/2293-collapse-of-the-keritis-historic-bridge-in-crete-greece. *Collapse of the Keritis historic bridge in Crete, Greece*. 2019.
37. Simos, N., et al., *On the Assessment of the Plaka Bridge Collapse using Non-linear Analysis Preventable or Doomed?* 2017: p. 423-40.
38. Wang, J. and C. Melbourne. *Finite element analyses of soil-structure interaction in masonry arch bridges*. in *Proceedings of the 5th international conference on arch bridges ARCH*. 2007.
39. Douglas, B.M. and W.H.J.J.o.t.S.D. Reid, *Dynamic tests and system identification of bridges.* 1982. **108**(ST10).
40. Solla, M., et al., *Ancient stone bridge surveying by ground-penetrating radar and numerical modeling methods.* 2013. **19**(1): p. 110-119.
41. Frunzio, G., M. Monaco, and A.J.H.c. Gesualdo, *3D FEM analysis of a Roman arch bridge.* 2001: p. 591-598.
42. Costa, C., et al., *Calibration of the numerical model of a short-span masonry railway bridge based on experimental modal parameters.* 2015. **114**: p. 846-853.
43. Connolly, D., et al., *Assessment of railway vibrations using an efficient scoping model.* 2014. **58**: p. 37-47.
44. Costa, C., et al., *Updating numerical models of masonry arch bridges by operational modal analysis.* 2015. **9**(7): p. 760-774.
45. Costa, C., et al., *Calibration of the numerical model of a stone masonry railway bridge based on experimentally identified modal parameters.* 2016. **123**: p. 354-371.
46. Sánchez-Aparicio, L.J., et al., *Experimental and numerical approaches for structural assessment in new footbridge designs (SFRSCC–GFPR hybrid structure).* 2015. **134**: p. 95-105.
47. Almeida, E.R., *Puentes históricos de la provincia de Ávila.* Institución Gran Duque de Alba 2015.

ANEXO I

INDEXACIÓN Y FACTOR DE IMPACTO DE LOS ARTÍCULOS PUBLICADOS

1. Primer artículo publicado

Á. Bautista-De Castro, L.J. Sánchez-Aparicio, L.F. Ramos, J. Sena-Cruz, D. González-Aguilera, Integrating geomatic approaches, Operational Modal Analysis, advanced numerical and updating methods to evaluate the current safety conditions of the historical Bôco Bridge, *Construction and Building Materials* 158 (2018) 961-984 DOI: https://doi.org/10.1016/j.conbuildmat.2017.10.084.

- **CITAS RECIBIDAS POR EL ARTÍCULO**

- WOS: 4
- SCOPUS: 4
- GS: 4

- **REVISTA**

- TÍTULO: Construction and building materials
- EDITOR: Michael C.Forde
- ISSN: 0950-0618

- **INDICADORES DE CALIDAD DE LA REVISTA**

- WOS
- SJR
- GSM

- **WOS. WEB OF SCIENCE (2017)**

- IMPACT FACTOR: 3,485
- RANK: 10/62 (CONSTRUCTION AND BUILDING TECHNOLOGY)
- Q1, Categorie CONSTRUCTION AND BUILDING TECHNOLOGY (**PRIMER CUARTIL)**
- Q1, Categorie ENGINEERING, CIVIL (**PRIMER DECIL Y PRIMER CUARTIL**)
- JIF PERCENTILE: 83,796

CONSTRUCTION AND BUILDING MATERIALS

ISSN: 0950-0618

ELSEVIER SCI LTD
THE BOULEVARD, LANGFORD LANE, KIDLINGTON, OXFORD OX5 1GB, OXON, ENGLAND
ENGLAND

Go to Journal Table of Contents Go to Ulrich's

Titles
ISO: Constr. Build. Mater.
JCR Abbrev: CONSTR BUILD MATER

Categories
CONSTRUCTION & BUILDING TECHNOLOGY - SCIE;
ENGINEERING, CIVIL - SCIE;
MATERIALS SCIENCE, MULTIDISCIPLINARY - SCIE;

Languages
English

8 Issues/Year;

Key Indicators

Year	Total Cites Graph	Journal Impact Factor Graph	Impact Factor Without Journal Self Cites Graph	5 Year Impact Factor Graph	Immediacy Index Graph	Citable Items Graph	Cited Half-Life Graph	Citing Half-Life Graph	Eigenfacto Score Graph	Article Influence Score Graph	% Articles in Citable Items Graph	Normalizec Eigenfacto Graph	Average JIF Percentile Graph
2017	39,162	3.485	2.271	4.039	0.600	2,105	4.3	7.9	0.05...	0.661	96.77	6.92...	83.796
2016	28,963	3.169	2.068	3.703	0.521	1,878	4.2	8.2	0.04...	0.654	97.02	5.57...	85.526
2015	18,061	2.421	1.599	2.883	0.367	1,323	3.9	8.3	0.04...	0.659	96.30	4.73...	82.356
2014	13,430	2.296	1.419	2.710	0.381	1,250	3.9	8.4	0.03...	0.592	96.96	3.53...	83.797
2013	10,338	2.265	1.382	2.769	0.345	1,098	4.2	8.5	0.02...	0.644	96.63	2.99...	85.006
2012	7,337	2.293	1.319	2.818	0.391	960	3.9	8.8	0.02...	0.680	96.46	Not ...	83.199
2011	4,396	1.834	1.358	2.134	0.269	532	4.0	9.2	0.01...	0.663	97.74	Not ...	78.110
2010	2,791	1.366	1.053	1.570	0.163	325	3.7	8.6	0.01...	0.538	97.23	Not ...	73.312
2009	2,113	1.456	1.114	1.515	0.289	440	3.9	9.2	0.00...	0.539	96.82	Not ...	73.624
2008	1,255	0.947	0.795	1.168	0.156	276	5.2	>10.0	0.00...	0.492	97.46	Not ...	61.095
2007	912	0.841	0.748	1.158	0.141	241	5.4	>10.0	0.00...	0.734	99.59	Not ...	64.149
2006	562	0.506	0.442	Not ...	0.155	116	5.5	9.3	Not ...	Not ...	100.00	Not ...	39.915
2005	363	0.343	0.335	Not ...	0.033	91	5.9	>10.0	Not ...	Not ...	100.00	Not ...	26.626
2004	288	0.565	0.513	Not ...	0.036	83	5.7	9.0	Not ...	Not ...	98.80	Not ...	57.818
2003	204	0.330	0.298	Not ...	0.050	60	6.6	7.6	Not ...	Not ...	100.00	Not ...	37.006

Source Data
Rank
Cited Journal Data
Citing Journal Data
Box Plot
Journal Relationships
Metric Trend

Metric Trend

View All Years

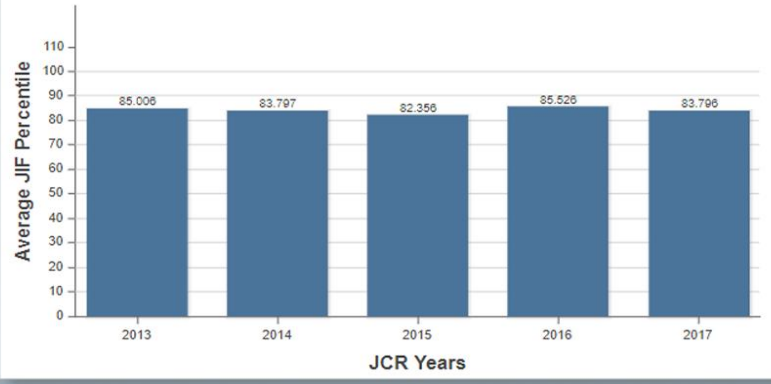

Source Data
Rank
Cited Journal Data
Citing Journal Data
Box Plot
Journal Relationships

JCR Impact Factor

JCR Year	CONSTRUCTION & BUILDING TECHNOLOGY			ENGINEERING, CIVIL		
	Rank	Quartile	JIF Percentile	Rank	Quartile	JIF Percentile
2017	10/62	Q1	84.677	11/128	Q1	91.797
2016	8/61	Q1	87.705	11/125	Q1	91.600
2015	9/61	Q1	86.066	15/126	Q1	88.492
2014	7/59	Q1	88.983	16/125	Q1	87.600
2013	7/58	Q1	88.793	12/124	Q1	90.726
2012	7/57	Q1	88.596	NA	undefined	
2011	8/56	Q1	86.607	NA	undefined	
2010	7/53	Q1	87.736	NA	undefined	
2009	7/49	Q1	86.735	NA	undefined	
2008	8/38	Q1	80.263	NA	undefined	
2007	6/34	Q1	83.824	NA	undefined	
2006	17/33	Q3	50.000	NA	undefined	
2005	21/31	Q3	33.871	NA	undefined	
2004	8/31	Q2	75.806	NA	undefined	
2003	15/29	Q3	50.000	NA	undefined	
2002	19/29	Q3	36.207	NA	undefined	

- **SJR. SCIMAGO JOURNAL & CONTRY RANK (2017)**

- SJR: 1.61
- Q1 Categorie BULIDING AND CONSTRUCTION
- Q1 Categorie CIVIL AND STRUCTURAL ENGINEERING
- Q1 Categorie MATERIALS SCIENCE (MISCELLANEOUS)

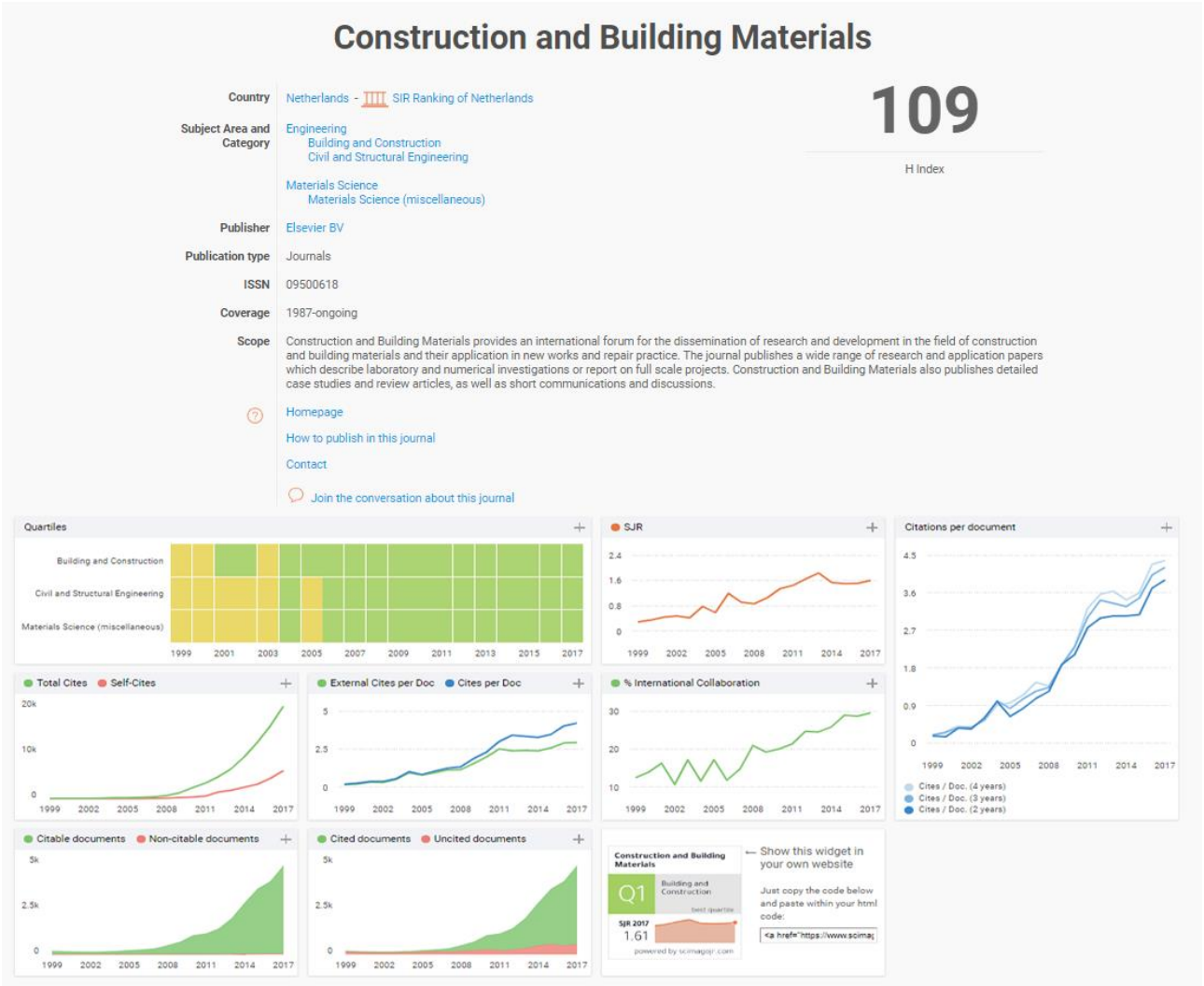

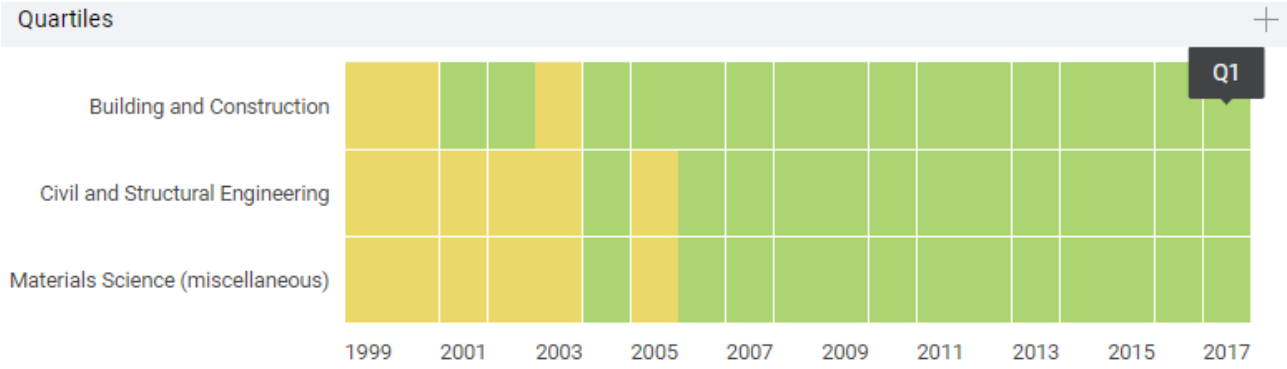

- **GOOGLE SCHOLAR METRICS**

- H5 GSM: 81

- H5 MEDIAN: 98

Publications matching *construction and building materials*

	Publication	h5-index	h5-median
1.	Construction and Building Materials	81	98

Dates and citation counts are estimated and are determined automatically by a computer program.

2. Segundo artículo publicado

L.J. Sánchez-Aparicio, Á. Bautista-De Castro, Borja-Conde, P. Carrasco-García, L.F. Ramos, Non-destructive means and methods for structural diagnosis of masonry arch bridges, *Automation in Construction* 104 (2019) 360-382 DOI: https://doi.org/10.1016/j.autcon.2019.04.021.

- **CITAS RECIBIDAS POR EL ARTÍCULO**

- WOS: 0
- SCOPUS: 0
- GS: 0

- **REVISTA**

- TÍTULO: Automation in Construction
- EDITOR: Miroslaw J.Skibniewski
- ISSN: 0926-5805

- **INDICADORES DE CALIDAD DE LA REVISTA**

- WOS
- SJR
- GSM

- **WOS. WEB OF SCIENCE (2017)**

- IMPACT FACTOR: 4,032
- RANK: 6/128 (ENGINEERING, CIVIL)
- RANK: 7/62 (CONSTRUCTION AND BUILDING TECHNOLOGY)
- Q1, Categorie ENGINEERING, CIVIL (**PRIMER DECIL Y PRIMER CUARTIL**)
- Q1, Categorie CONSTRUCTION AND BUILDING TECHNOLOGY
- JIF PERCENTILE: 92,610

AUTOMATION IN CONSTRUCTION

ISSN: 0926-5805

ELSEVIER SCIENCE BV
PO BOX 211, 1000 AE AMSTERDAM, NETHERLANDS
NETHERLANDS

Go to Journal Table of Contents Go to Ulrich's

Titles
ISO: Autom. Constr.
JCR Abbrev: AUTOMAT CONSTR

Categories
CONSTRUCTION & BUILDING TECHNOLOGY - SCIE;
ENGINEERING, CIVIL - SCIE;

Languages
English

8 Issues/Year;

Key Indicators

Year	Total Cites Graph	Journal Impact Factor Graph	Impact Factor Without Journal Self Cites Graph	5 Year Impact Factor Graph	Immediacy Index Graph	Citable Items Graph	Cited Half-Life Graph	Citing Half-Life Graph	Eigenfacto Score Graph	Article Influence Score Graph	% Articles in Citable Items Graph	Normalizec Eigenfacto Graph	Average JIF Percentile Graph
2017	6,520	4.032	3.332	4.437	0.741	185	4.9	7.0	0.00…	0.676	93.51	0.93…	92.610
2016	4,781	2.919	2.375	3.432	0.323	189	5.2	7.7	0.00…	0.589	93.65	0.76…	85.593
2015	3,543	2.442	1.914	2.827	0.199	151	5.1	7.2	0.00…	0.629	97.35	0.80…	89.289
2014	2,637	1.812	1.324	2.414	0.281	171	4.9	7.5	0.00…	0.633	95.32	0.74…	84.197
2013	2,130	1.822	1.134	2.217	0.361	191	4.8	7.7	0.00…	0.484	97.91	0.50…	85.213
2012	1,692	1.820	1.179	2.038	0.181	160	4.9	8.2	0.00…	0.449	96.25	Not …	85.782
2011	1,147	1.500	0.984	1.702	0.103	116	4.6	7.7	0.00…	0.449	97.41	Not …	82.786
2010	996	1.311	0.978	1.454	0.238	101	4.8	7.3	0.00…	0.350	92.08	Not …	83.142
2009	870	1.372	1.105	1.510	0.124	97	4.6	7.9	0.00…	0.356	93.81	Not …	83.149
2008	844	1.664	1.230	1.569	0.430	93	4.1	7.6	0.00211	0.285	95.70	Not …	94.455
2007	391	0.609	0.398	0.776	0.092	87	5.2	7.4	0.00…	0.231	98.85	Not …	63.706
2006	341	0.792	0.558	Not A…	0.046	65	4.7	7.1	Not A…	Not …	98.46	Not …	84.465
2005	181	0.387	0.184	Not A…	0.000	63	4.0	6.9	Not A…	Not …	98.41	Not …	34.486
2004	148	0.360	0.166	Not A…	0.018	57	4.5	6.7	Not A…	Not …	96.49	Not …	46.488
2003	93	0.320	0.206	Not A…	0.016	62	Not A…	6.2	Not A…	Not …	96.77	Not …	43.481
2002	69	0.312	0.260	Not A…	0.019	52	Not A…	7.0	Not A…	Not …	96.15	Not …	43.735

Source Data
Rank
Cited Journal Data
Citing Journal Data
Box Plot
Journal Relationships
Metric Trend

Metric Trend

View All Years

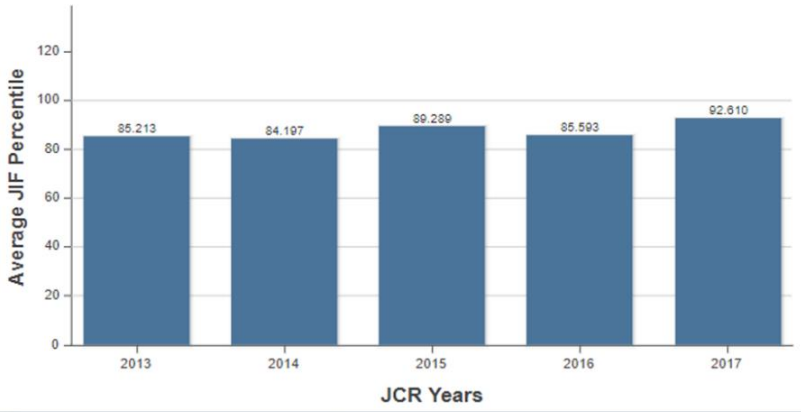

Source Data
Rank
Cited Journal Data
Citing Journal Data
Box Plot
Journal Relationships

JCR Impact Factor

JCR Year	CONSTRUCTION & BUILDING TECHNOLOGY			ENGINEERING, CIVIL		
	Rank	Quartile	JIF Percentile	Rank	Quartile	JIF Percentile
2017	7/62	Q1	89.516	6/128	Q1	95.703
2016	11/61	Q1	82.787	15/125	Q1	88.400
2015	8/61	Q1	87.705	12/126	Q1	90.873
2014	9/59	Q1	85.593	22/125	Q1	82.800
2013	9/58	Q1	85.345	19/124	Q1	85.081
2012	9/57	Q1	85.088	17/122	Q1	86.475
2011	11/56	Q1	81.250	19/118	Q1	84.322
2010	8/53	Q1	85.849	23/115	Q1	80.435
2009	8/49	Q1	84.694	20/106	Q1	81.604
2008	2/38	Q1	96.053	7/91	Q1	92.857
2007	12/34	Q2	66.176	35/89	Q2	61.236
2006	3/33	Q1	92.424	20/83	Q1	76.506
2005	20/31	Q3	37.097	55/80	Q3	31.875
2004	17/31	Q3	46.774	43/79	Q3	46.203
2003	16/29	Q3	46.552	44/73	Q3	40.411
2002	17/29	Q3	43.103	40/71	Q3	44.366

- **SJR. SCIMAGO JOURNAL & CONTRY RANK (2017)**

- SJR: 1.61
- Q1 Categorie BUILDING AND CONSTRUCTION
- Q1 Categorie CIVIL AND STRUCTURAL ENGINEERING
- Q1 Categorie CONTROL AND SYSTEMS ENGINEERING

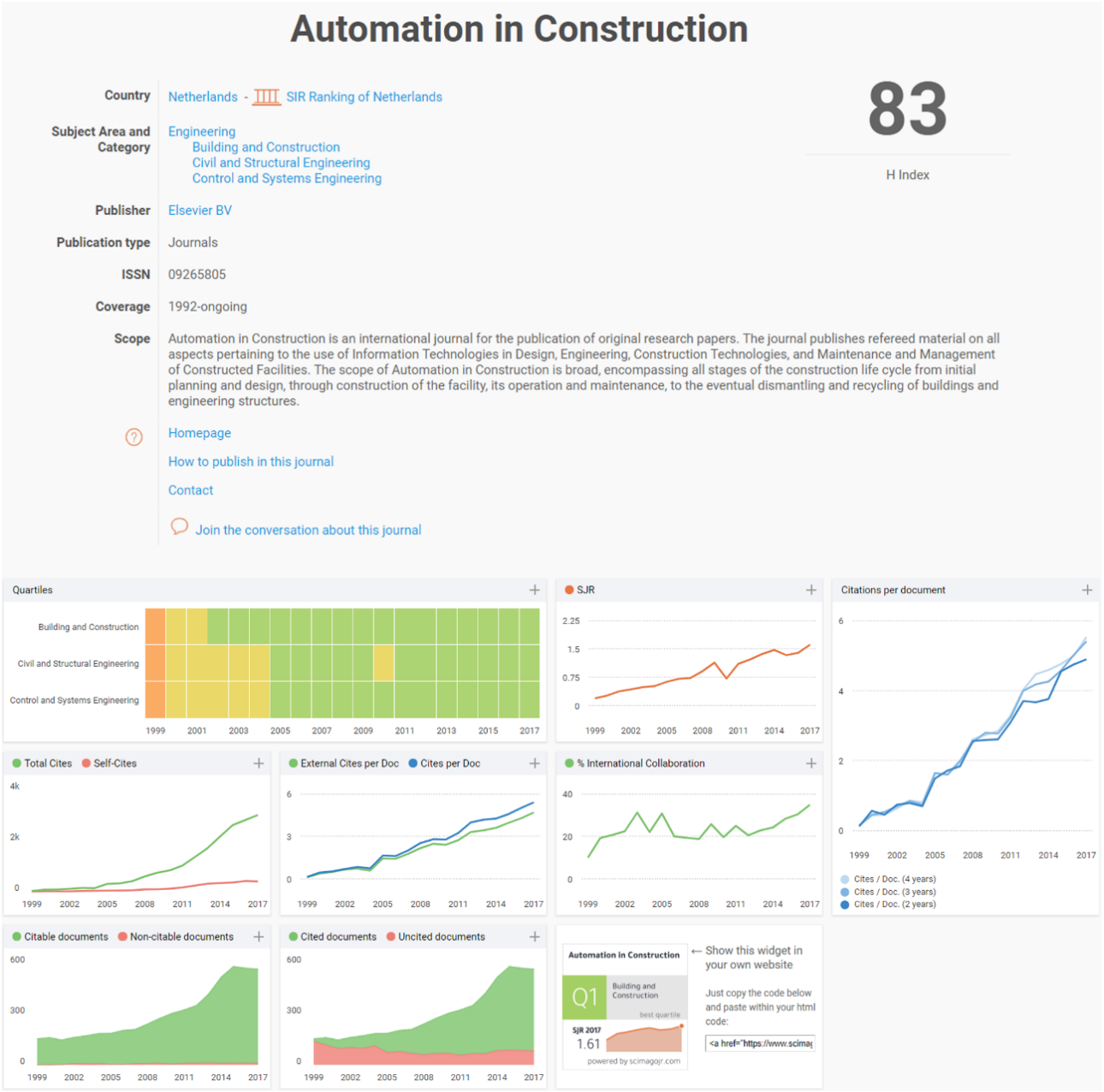

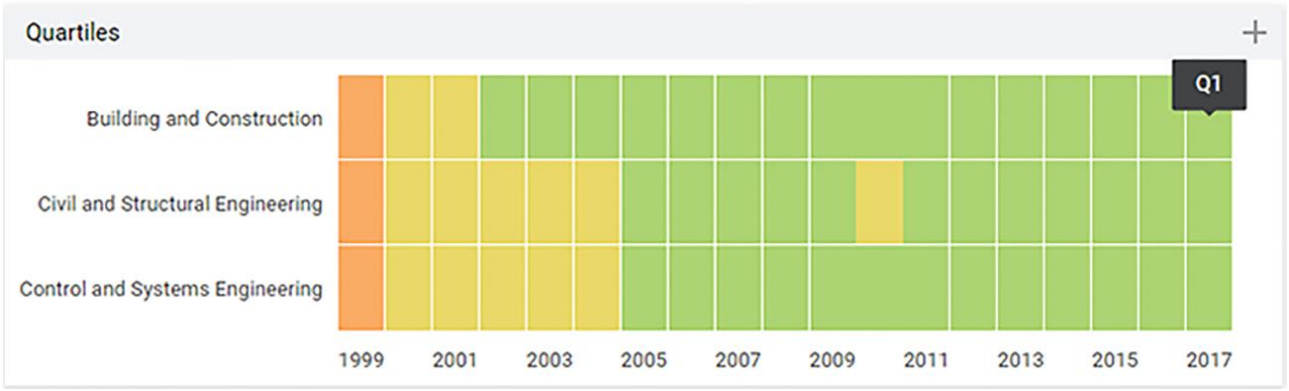

- **GOOGLE SCHOLAR METRICS**

- H5 GSM: 63

- H5 MEDIAN: 92

Publications matching *automation in construction*

	Publication	h5-index	h5-median
1.	Automation in Construction	63	92

Dates and citation counts are estimated and are determined automatically by a computer program.

3. Tercer artículo publicado

Á. Bautista-De Castro, L.J. Sánchez-Aparicio, P. Carrasco-García, L.F. Ramos, D. González-Aguilera, A multidisciplinary approach to calibrating advanced numerical simulations of masonry arch bridges, *Mechanical Systems and Signal Processing* 129 (2019) 337-365 DOI: https://doi.org/10.1016/j.ymssp.2019.04.043.

- **CITAS RECIBIDAS POR EL ARTÍCULO**

- WOS: 0
- SCOPUS: 0
- GS: 0

- **REVISTA**

- TÍTULO: Mechanical systems and signal processing
- EDITOR: J.E. Mottershead
- ISSN: 0888-3270

- **INDICADORES DE CALIDAD DE LA REVISTA**

- WOS
- SJR
- GSM

- **WOS. WEB OF SCIENCE (2017)**

- IMPACT FACTOR: 4,370
- RANK: 7/128 (ENGINEERING, MECHANICAL)
- Q1, Categorie ENGINEERING, MECHANICAL (**PRIMER DECIL Y PRIMER CUARTIL**)
- JIF PERCENTILE: 94,922

MECHANICAL SYSTEMS AND SIGNAL PROCESSING

ISSN: 0888-3270

ACADEMIC PRESS LTD- ELSEVIER SCIENCE LTD
24-28 OVAL RD, LONDON NW1 7DX, ENGLAND
ENGLAND

Go to Journal Table of Contents Go to Ulrich's

Titles
ISO: Mech. Syst. Signal Proc.
JCR Abbrev: MECH SYST SIGNAL PR

Categories
ENGINEERING, MECHANICAL - SCIE

Languages
English

8 Issues/Year;

Key Indicators

Year	Total Cites	Journal Impact Factor	Impact Factor Without Journal Self Cites	5 Year Impact Factor	Immediacy Index	Citable Items	Cited Half-Life	Citing Half-Life	Eigenfacto Score	Article Influence Score	% Articles In Citable Items	Normalized Eigenfacto	Average JIF Percentile
	Graph	Graph	Graph	Graph	Graph	Graph	Graph	Graph	Graph	Graph	Graph	Graph	Graph
2017	14,814	4.370	3.629	4.525	1.408	517	6.0	8.9	0.02...	1.004	98.26	2.36...	94.922
2016	12,930	4.116	3.459	4.874	1.234	432	5.9	9.1	0.01...	1.068	98.84	2.17...	97.308
2015	8,451	2.771	2.317	3.418	0.789	308	6.3	9.2	0.01...	0.952	97.08	1.80...	90.530
2014	6,646	2.256	1.952	2.870	0.487	193	6.2	9.8	0.01...	0.879	96.89	1.71...	89.615
2013	5,731	2.465	1.902	2.903	0.356	292	6.1	9.3	0.01...	0.826	97.60	1.40...	89.453
2012	4,408	1.913	1.582	2.623	0.276	239	5.7	9.5	0.01...	0.835	98.74	Not ...	87.600
2011	3,552	1.824	1.396	2.471	0.279	204	5.4	9.8	0.01...	0.841	94.12	Not ...	88.115
2010	2,779	1.762	1.389	2.212	0.310	174	4.9	9.1	0.01...	0.777	98.85	Not ...	89.754
2009	2,766	2.075	1.601	2.472	0.365	189	5.3	9.3	0.00...	0.740	98.41	Not ...	95.259
2008	2,136	1.984	1.668	1.981	0.344	122	5.3	8.7	0.00...	0.576	98.36	Not ...	93.810
2007	1,476	1.333	0.757	1.631	0.362	199	5.6	9.2	0.00...	0.573	98.99	Not ...	91.121
2006	1,042	1.180	0.832	Not ...	0.186	118	6.1	8.7	Not ...	Not ...	95.76	Not ...	88.208
2005	771	0.826	0.702	Not ...	0.125	80	5.7	8.8	Not ...	Not ...	100.00	Not ...	77.404
2004	715	0.828	0.674	Not ...	0.173	81	5.5	8.3	Not ...	Not ...	98.77	Not ...	82.039
2003	520	0.809	0.588	Not ...	0.103	97	5.5	8.6	Not ...	Not ...	100.00	Not ...	79.717
2002	439	0.556	0.407	Not ...	0.030	66	5.6	7.9	Not ...	Not ...	98.48	Not ...	62.255
2001	473	0.806	0.756	Not ...	0.081	62	5.2	8.7	Not ...	Not ...	100.00	Not ...	75.000

Source Data
Rank
Cited Journal Data
Citing Journal Data
Box Plot
Journal Relationships
Metric Trend

Metric Trend

View All Years

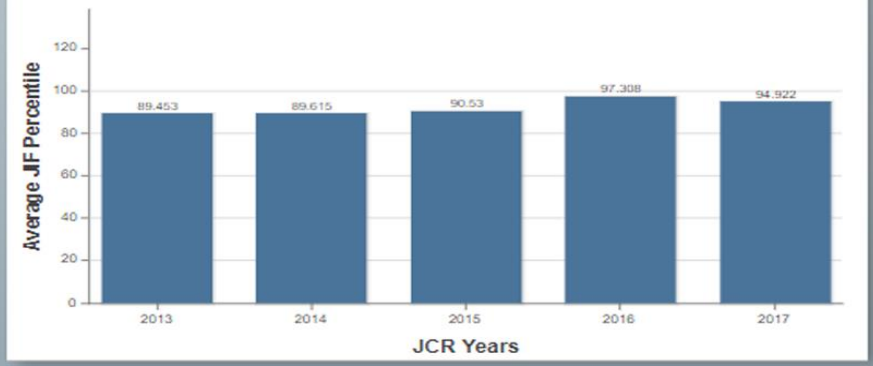

InCites Journal Citation Reports dataset updated Sep 20, 2018

Source Data
Rank
Cited Journal Data
Citing Journal Data
Box Plot
Journal Relationships

JCR Impact Factor

JCR Year	ENGINEERING, MECHANICAL Rank	Quartile	JIF Percentile
2017	7/128	Q1	94.922
2016	4/130	Q1	97.308
2015	13/132	Q1	90.530
2014	14/130	Q1	89.615
2013	14/128	Q1	89.453
2012	16/125	Q1	87.600
2011	15/122	Q1	88.115
2010	13/122	Q1	89.754
2009	6/116	Q1	95.259
2008	7/105	Q1	93.810
2007	10/107	Q1	91.121
2006	13/106	Q1	88.208
2005	24/104	Q1	77.404
2004	19/103	Q1	82.039
2003	22/106	Q1	79.717
2002	39/102	Q2	62.255
2001	26/102	Q2	75.000
2000	22/102	Q1	78.922

- **SJR. SCIMAGO JOURNAL & CONTRY RANK (2017)**

- SJR: 1.80
- Q1 Categorie AEROSPACE ENGINEERING
- Q1 Categorie CIVIL AND STRUCTURAL ENGINEERING
- Q1 Categorie COMPUTER SCIENCE APPLICATIONS
- Q1 Categorie CONTROL AND SYSTEMS ENGINEERING
- Q1 Categorie MECHANICAL ENGINEERING
- Q1 Categorie SIGNAL PROCESSING

Mechanical Systems and Signal Processing

Country	United States - SJR Ranking of United States
Subject Area and Category	Computer Science Computer Science Applications Signal Processing Engineering Aerospace Engineering Civil and Structural Engineering Control and Systems Engineering Mechanical Engineering
Publisher	Elsevier Inc.
Publication type	Journals
ISSN	10961216, 08883270
Coverage	1987-ongoing
Scope	Ongoing developments in Mechanical, Aeronautical and Civil Engineering and major changes brought about by advances in instrumentation and associated computing power, necessitate the application and integration of techniques involving systems theory, signal processing, control theory and statistics. Mechanical Systems and Signal Processing provides a forum for the discussion of research findings related to applications utilizing these disciplines, while maintaining a healthy balance between fundamental and experimental topics.
	Homepage
	Join the conversation about this journal

121

H Index

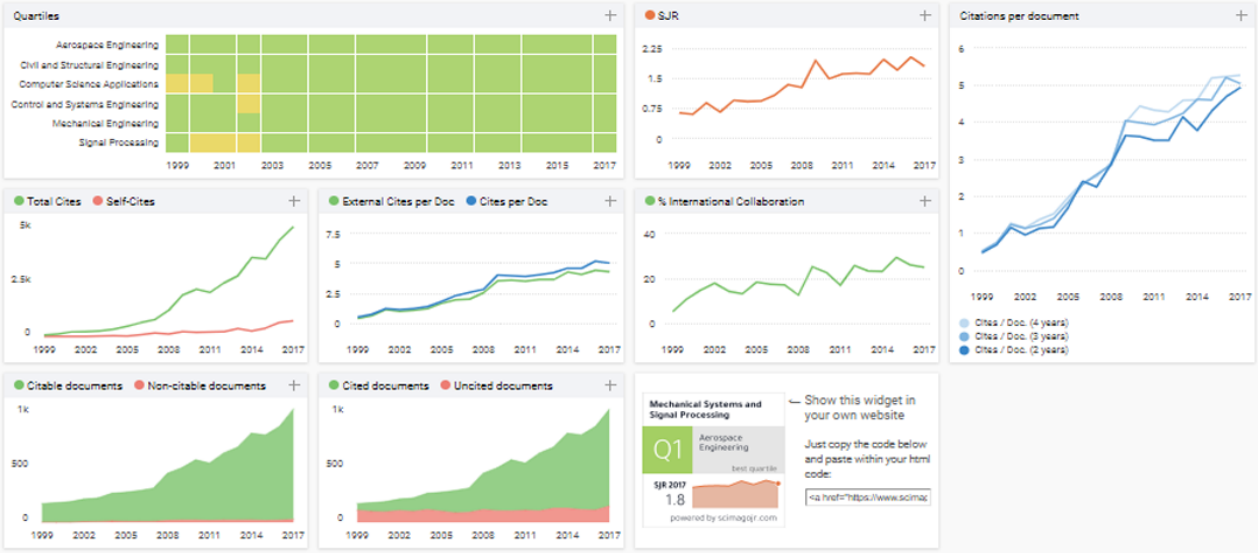

Quartiles

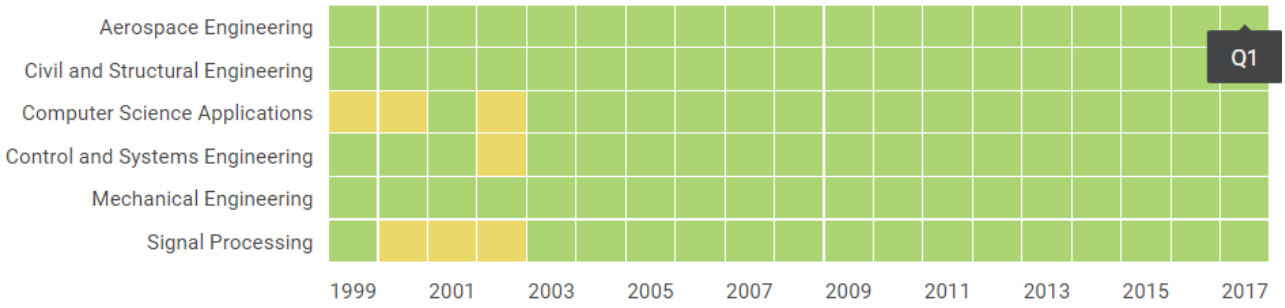

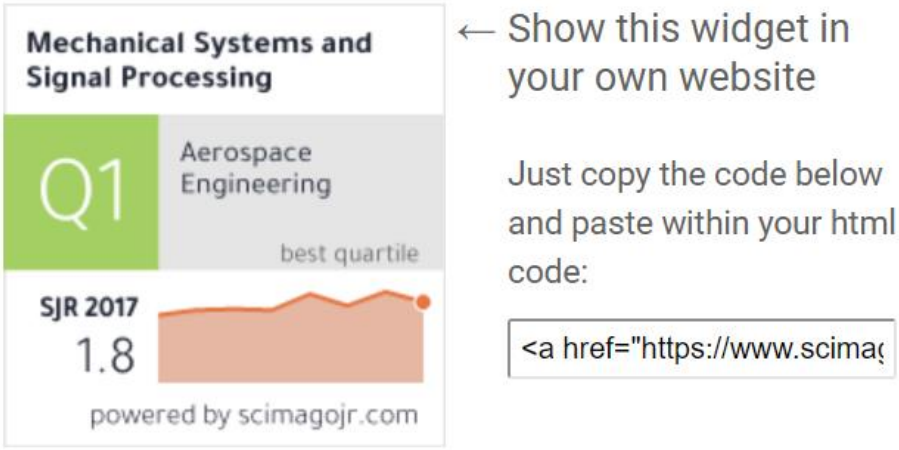

- **GOOGLE SCHOLAR METRICS**

- H5 GSM: 59

- H5 MEDIAN: 81

Publications matching *mechanical systems and signal processing*

	Publication	h5-index	h5-median
1.	Mechanical Systems and Signal Processing	59	81

Dates and citation counts are estimated and are determined automatically by a computer program.